

Synthesis and Application of [2.2]Paracyclophane Derivatives in Supramolecular Systems

Zur Erlangung des akademischen Grades eines

DOKTORS DER NATURWISSENSCHAFTEN

(Dr. rer. nat.)

von der KIT-Fakultät für Chemie und Biowissenschaften

des Karlsruher Instituts für Technologie (KIT)

genehmigte

DISSERTATION

von

M.Sc. Yichuan Wang

aus Baoding

Dekan: Prof. Dr. Hans-Achim Wagenknecht

Referent: Prof. Dr. Stefan Bräse

Korreferent: Prof. Dr. Michael Meier

Tag der mündlichen Prüfung: 27.10.2022



This document is licensed under a Creative Commons
Attribution-ShareAlike 4.0 International License (CC BY-SA 4.0):
<https://creativecommons.org/licenses/by-sa/4.0/deed.en>

Industry is good at diligence, waste in play; action in thinking, destroyed in following.

业精于勤荒于嬉，行成于思毁于随

– *Yu Han A.D. 813*

Honesty Declaration

This work was carried out from October 05th 2018 through September 03rd 2022, at the Institute of Organic Chemistry, Faculty of Chemistry and Biosciences at the Karlsruhe Institute of Technology (KIT) under the supervision of Prof. Dr. STEFAN BRÄSE.

Die vorliegende Arbeit wurde im Zeitraum vom 05. Oktober 2018 bis 03. September 2022 am Institut für Organische Chemie (IOC) der Fakultät für Chemie und Biowissenschaften am Karlsruher Institut für Technologie (KIT) unter der Leitung von Prof. Dr. STEFAN BRÄSE angefertigt.

Hiermit versichere ich, YICHUAN WANG, die vorliegende Arbeit selbstständig verfasst und keine anderen als die angegebenen Hilfsmittel verwendet, sowie Zitate kenntlich gemacht zu haben. Die Dissertation wurde bisher an keiner anderen Hochschule oder Universität eingereicht.

Hereby I, YICHUAN WANG, declare that I completed the work independently, without any improper help and that all material published by others is cited properly. This thesis has not been submitted to any other university before.

German Title of this Thesis

**Synthese und Anwendung von
[2.2]Paracyclophanderivaten in
Supramolekularen Systemen**

Table of Contents

Honesty Declaration	I
German Title of this Thesis	III
Kurzzusammenfassung	1
Abstract	3
1 Introduction	5
1.1 [2.2]Paracyclophane	6
1.1.1 Structure of [2.2]Paracyclophane	6
1.1.2 Character of [2.2]Paracyclophane	7
1.1.3 Applications of [2.2]Paracyclophanes	10
1.2 Supramolecular Chemistry	14
1.2.1 Cucurbit[<i>n</i>]uril in Host-Guest System	14
1.2.2 Cucurbit[<i>n</i>]uril in Supramolecular Chemosensors	19
1.2.3 Supramolecular Skeleton and Cage based on [2.2]paracyclophanes	24
2 Objective	26
3 Main Section	28
3.1 Exploration of Affinity Study Using Functional [2.2]Paracyclophane Derivatives	28
3.1.1 Molecular Design and Synthesis.	28
3.1.2 Basic Affinity Analysis.	32
3.1.3 Binding Constants K_a Determination	37
3.1.4 ITC Measurements and Discussion.	42
3.1.5 Chiral Application of (<i>S_p</i>)-MVCP (50)	46
3.1.6 Conclusion	48
3.2 Exploration of Affinity New Cyclophanyl-derived Extended and Functionalized Chromophores 49	
3.2.1 Exploration of Affinity on Extended [2.2]Paracyclophane Derivatives	49
3.2.2 Exploration of other [2.2]Paracyclophane Derivatives	57
3.2.3 Exploration of Affinity on Azo-functionalized [2.2]Paracyclophane Derivatives	63
3.2.4 Conclusion	68
3.3 Supramolecular Skeleton and Cage based on [2.2]Paracyclophane	69
3.3.1 Molecules design and Synthesis.	69
3.3.2 Characteristic Analysis.	72
3.3.3 Other PCP compounds	75
4 Summary and Outlook	77

4.1	Exploration of Affinity on Foundational [2.2]Paracyclophane Derivatives	77
4.2	Exploration of Affinity on Extended and Functionalized [2.2]Paracyclophane Derivatives	78
4.3	Supramolecular Skeleton and Cage based on [2.2]Paracyclophane	79
5	Experimental Section	80
5.1	General Remarks	80
5.2	Exploration of Affinity on Functional [2.2]Paracyclophane Derivatives	85
5.3	Exploration of Affinity on Extended and Functionalized [2.2]Paracyclophane Derivatives	107
5.4	Supramolecular Skeleton and Cage based on [2.2]Paracyclophane derivatives	137
5.5	Crystallographic Data	155
5.5.1	Crystallographic Data solved by Dr. Martin Nieger	155
5.5.2	Crystallographic Data solved by Dr. Olaf Fuhr	159
5.6	Additional data	162
6	List of Abbreviations	164
7	Bibliography	169
8	Acknowledgments	177

Kurzzusammenfassung

[2.2]Paracyclophan (PCP) ist ein einzigartiges kofacial gestapeltes prochirales Molekülgerüst, das aus zwei koplanaren Phenylringen besteht, die durch zwei Ethylenbrücken in para-Orientierung verbunden sind und im letzten Jahrhundert entdeckt und synthetisiert wurden. Starrheit, Stabilität, Planarität, π -Stapelung und elektronische Kommunikation über Pfade durch den Raum und durch Bindungen innerhalb des PCP sind interessante Aspekte, die bei der Materialherstellung berücksichtigt werden sollten. [2.2]Paracyclophan wurde bisher intensiv in der asymmetrischen Katalyse als chiraler Ligand untersucht, hat aber auch einen Platz in der Materialwissenschaft, etwa für Leuchtstoffe, Polymere oder Gerüstmaterialien.

Nach der bahnbrechenden Forschung zum Nachweis von Struktur- und Reaktivitätsbeziehungen und zum Verständnis ihrer Eigenschaften hat sich die [2.2]Paracyclophanchemie von der synthetischen Kuriosität zu neuen Materialanwendungen, einschließlich verschiedener supramolekularer Systeme, entwickelt. Auch die supramolekulare Chemie ist zu einem beliebten Gegenstand umfangreicher Forschung geworden. Supramolekulare Chemie ist ein Konzept kovalent gebundener Anordnungen, begleitet von dynamischen nicht-kovalenten Bindungen, um supramolekulare Strukturen zu bilden, einschließlich Wasserstoffbrücken, Van-der-Waals-Kräfte, hydrophobe Wechselwirkung, Metallkoordination, π - π -Stapelung und elektrostatische Effekte usw. Eines der modernsten Klassen der supramolekularen Chemie ist die Wirt-Gast-Chemie, die aus kleinen molekularen Gästen und großen makrocyclischen Wirten zusammensetzt, die nicht kovalent gebunden sind. Das [2.2]Paracyclophan kann als Gast in Kombination mit dem makrocyclischen Wirt Cucurbit[8]uril (CB8) verwendet werden und hat sich als nützlicher Kandidat für die Chemosensorik erwiesen. Das Ziel dieser Dissertation war es, eine neue Klasse von [2.2]Paracyclophan-Derivaten zu entwerfen und zu synthetisieren und ihren Bindungsstatus an CBs als supramolekulares CB_n -Wirt-Gast-System zur Modulation supramolekularer Assays und anderer supramolekularer Anwendungen zu untersuchen.

Unter Verwendung sorgfältig ausgewählter Reaktionsparameter und Transformationsschritte wurden funktionalisierte Paracyclophanderivate aus mono- und dibromiertem [2.2]Paracyclophan über Kupplungsreaktionen, nämlich Suzuki-Miyaura- und Mizoroki-Heck-Kreuzkupplung, synthetisiert und anschließend umgewandelt, um fähig zu sein der Bindung an CB. Die Fähigkeit dieser [2.2]Paracyclophan-Derivate, fest an CB8 zu binden, wurde durch eine Reihe von Tests demonstriert und durch verschiedene Techniken charakterisiert, darunter NMR und Massenspektrometrie sowie Spektroskopie. Computergestützte Methoden und theoretische Modelle wurden verwendet, um unsere detaillierten experimentellen Beobachtungen zu rationalisieren oder besser zu verstehen. Die Bindungsaffinität dieser PCP-Derivate zu CB7 und CB8 wurde dann durch zwei Hauptmethoden, NMR und Spektroskopie, untersucht, um ihre Bindungskonstanten K_a zu bestimmen. Darüber hinaus wurde die Bindungsenergie an CB8 durch isotherme Titrationskalorimetrie (ITC) analysiert, und durch Vergleich mit früherer Literatur wurde der Schluss gezogen, dass **DMPCP** der einzelne stärkste Gast ist, der bisher gefunden wurde, um CB8 zu binden.

Die Bindung von tri- und tetrasubstituierten PCPs an CB8 wurde ebenfalls demonstriert, während ihre Bindungskonstanten K_a an CB8 ebenfalls berechnet wurden. Durch den Vergleich der Ergebnisse dieser [2.2]Paracyclophan-Derivate wurde der Schluss gezogen, dass **DMPCP** immer noch das stärkste Bindungsmittel für CB8 war. Außerdem wurde festgestellt, dass ihre Fähigkeit, CB8 zu binden, und die Anzahl der positiven Ladungen bis auch zu einem gewissen Grad von der spezifischen Struktur des modifizierenden [2.2]Paracyclophans abhängt. Darüber hinaus wurden auch andere *para*- und pseudo-*para*-Dimethylamino substituierte [2.2]Paracyclophane und apophenisch modifizierte synthetisiert und ihre Bindung an CB8 durch einfache Analyse abgeleitet. Das Substitutionsmuster der PCPs beeinflusst nicht nur die Natur und die molekularen Eigenschaften des PCP-Gerüsts selbst stark, sondern die Komplexierung mit CB kann sich in den Fluoreszenzsensoreigenschaften als geringfügige Änderungen der Chromophor-Konjugation, der relativen Orientierung und der Substitutionsmuster der Cyclophanyl-Gerüste widerspiegeln können die Fluoreszenzsensoreigenschaften des supramolekularen CB_n -Wirt-Gast-Systems erheblich verändern. Die CB_n -basierte Komplexierung und hochaffine Bindungen wurden mit Direktbindungsassays (DBA), Indikatorverdrängungsassays (IDA) und Gastverdrängungsassays (GDA) untersucht, die eine hohe Empfindlichkeit, schnelle Reaktionszeit und technische Einfachheit aufweisen.

Während der Untersuchung unter Verwendung verschiedener Herstellungstechniken wurden maßgeschneiderte [2.2]Paracyclophanderivate untersucht, um andere ehrgeizigere supramolekulare Multitasking-Systeme zu entwickeln, einschließlich koordinationsgesteuerter metallorganischer Käfige und nicht-koordinativer, mehrfach gestapelter Cyclophanboxen.

Abstract

[2.2]Paracyclophane (PCP) is a unique co-facially stacked prochiral molecular scaffold consisting of two coplanar phenyl rings linked by two ethylene bridges in a *para* orientation, which was discovered and synthesized in the last century. Rigidity, stability, planarity, π -stacking, and electronic communication via through-space and through-bond pathways within the PCP are interesting aspects for consideration in material fabrication. To date, [2.2]paracyclophane has been intensively investigated in asymmetric catalysis as chiral ligands, but also has a place in materials science, for instance, luminescent materials, polymers or framework materials.

After the pioneering research on the structure and reactivity relationship and understanding of their properties, [2.2]paracyclophane chemistry has evolved from synthetic curiosity to emerging materials applications including diverse supramolecular systems. Supramolecular chemistry has also become a popular subject for extensive research. Supramolecular chemistry is a concept of covalently bonded assemblies accompanied by dynamic non-covalent bonds to form supramolecular structures, including hydrogen bonding, van der Waals forces, hydrophobic interaction, metal coordination, π - π stacking, electrostatic effects *etc.* One of the most fashionable classes of supramolecular chemistry is host-guest chemistry, composed of small molecular guests and large macrocyclic hosts that are non-covalently bonded. The [2.2]paracyclophane can be used as a guest combined with the macrocyclic host cucurbit[8]uril (CB8) and has been shown to have potential as a useful chemosensing candidate. This thesis aimed to design and synthesize a new class of [2.2]paracyclophane derivatives and to investigate their binding statuses to CBs as CB n host-guest supramolecular system for modulating supramolecular assays and other supramolecular applications.

Using carefully chosen reaction parameters and transformation steps, functionalized paracyclophane derivatives were synthesized from mono- and di-brominated [2.2]paracyclophane via coupling reactions. Namely, Suzuki-Miyaura, and Mizoroki-Heck cross-coupling were transformed to be capable of binding to CB. The ability of these [2.2]paracyclophane derivatives to bind tightly to CB8 was demonstrated by a series of tests and was characterized by various techniques including NMR and mass spectrometry, and spectroscopy. Computer-aided methods and theoretical models were used to rationalize or better understand our detailed experimental observations. The binding affinity of these PCP derivatives to CB7 and CB8 was then investigated by two main methods, NMR and spectroscopy, to determine their binding constants K_a . In addition, the energy of binding to CB8 was analyzed by isothermal titration calorimetry (ITC), and by comparison with previous literature, it was concluded that **DMPCP** is the single most powerful guest found to date to bind CB8.

The binding of tri- and tetrasubstituted PCPs to CB8 was also demonstrated, while their binding constants K_a to CB8 were also calculated. Comparing the results of these [2.2]paracyclophane derivatives, it was concluded that **DMPCP** was still the strongest binding agent to CB8. Moreover, it was concluded that their ability to bind CB8 and the number of positive charges depended, to a certain extent on the specific structure

of the [2.2]paracyclophane being modified. In addition, another *para*- and pseudo-*para*-dimethylamino substituted [2.2]paracyclophane and apophenic-modified were also synthesized, and their binding to CB8 was derived by simple analysis. Substitution pattern of the PCPs heavily influences not only the nature and molecular features of the PCP scaffold itself, but complexing with CB can be reflected in fluorescent sensing properties as minor changes in the chromophore conjugation, relative orientation, and substitution patterns of the cyclophanyl-scaffolds can alter fluorescent sensing properties of the CB n host-guest supramolecular system significantly. The CB n -based complexation and high-affinity bindings were investigated by direct-binding assays (DBA), indicator displacement assays (IDA), and guest displacement assay (GDA) that exhibit high sensitivity, fast response time, and technical simplicity.

During the investigation employing different fabrication techniques, bespoke [2.2]paracyclophane derivatives were investigated in developing other more ambitious multi-tasking supramolecular systems, including coordination-driven organo-metallic cages, and non-coordinative multi-stacked cyclophane-boxes.

1 Introduction

“Despite the fabulous advances in science and engineering over the past century, manifested most clearly by modern aircraft, we are nevertheless humbled by the realization that we still cannot synthesize a bird, a single cell of the bird or even one of its complex biological machines.”^[1] was told by Ben L. Feringa in his Nobel Lecture in 2017 to indicate that synthesis is important for our life and still has a long way to go.

As two broad hydrocarbon classes, cycloalkanes and aromatics were the interest being investigated all this time. And attracted by their charms of structural diversity, as early as the 1940s, scientists have already made various attempts at the π complex which was presumed to be a “molecular sandwich” held together by attraction between face-to-face, partially anionic, partially cationic π systems^[2]. Donald J. Cram^[2] and Henning Hopf^[3] systematically studied this π complex and pioneered the structural class of acronym **cyclophanes**, which contains a **cyclic** arrangement of at least one aromatic or **phenyl** ring bridged by an alkane (**Figure 1**, general structures **1**).

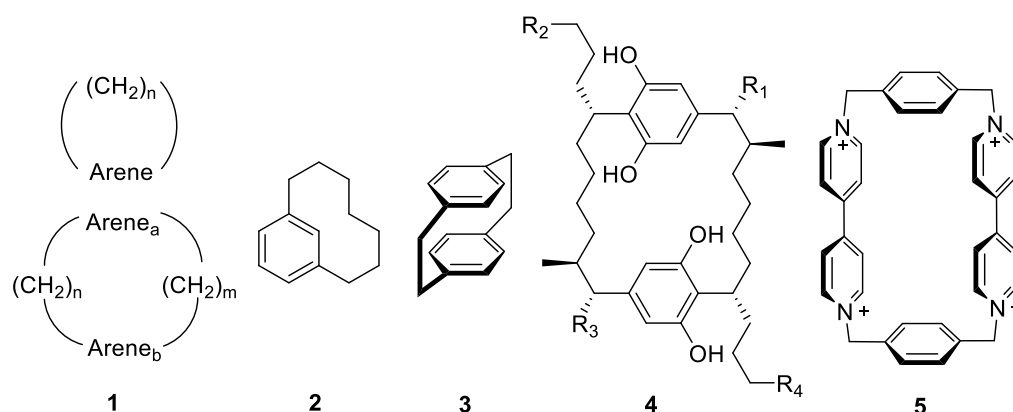


Figure 1. examples of cyclophane: general structures (1), [7]metacyclophane (2), [2.2]paracyclophane (3), cylindrocyclophanes (4), “blue box” (5).

Thus, a noteworthy and intriguing structure systems were exhibited in the chemistry family. With “*bent and battered benzene rings*”,^[2] [2.2]cyclophane are the most distinctive and the earliest synthesized by Brown and Farthing.^[4] Due to the impact of the transannular electronic effects, the substitution reactions on one aromatic ring are not independent but as a whole object on both aligned aromatic rings, giving an alternative possibility of intramolecular charge-transfer-complexes.^[5] Investigating the unique structural and chemical properties have led scientists to keep exploring this exciting field. In **Figure 1**, [2.2]Paracyclophane **3** (PCP) is the main structure we discussed later, apart from which, [7]metacyclophane **2** is a monoaromatic ring synthesized by Hopf et al. in 1978.^[6] Cylindrocyclophanes **4** are the first cyclophanes found in nature, isolated from a species of cyanobacteria, and have proven to be an interesting group of compounds to study due to their unusual molecular structure and intriguing biological possibilities, especially their cytotoxicity to some cancer cell lines.^[7] “Blue box”, reported by Stoddart in 1988, is constructed from organic and inorganic ions, frequently used in supramolecular chemistry and gradually developed into its molecular machine system.^[8]

Strictly speaking, the fact that “blue box” was not classified as a cyclophane. Rather than being an extension of cyclophanes, it transcends them, since “blue box” possesses many unique properties. Consequently, this thesis is focused exclusively on discovering emerging structures and novel properties in supramolecular chemistry by employing customized molecular building blocks of [2.2]paracyclophane.

1.1 [2.2]Paracyclophane

1.1.1 Structure of [2.2]Paracyclophane

Brown and Farthing reported [2.2]paracyclophane in 1949 as one of the products obtained by the gas-phase pyrolysis of *p*-xylene under low pressure.^[4] With two short ethyl bridges attached at the *para* position, two benzene rings (also called “decks”) are face-to-face stacked but out of the expected aromatic planarity forced to bend out at the bridgehead carbon atom by 12.6° out of the benzene plane, and leads to strain energy of about 31 kcal per mole.^[9] This strained system is due to the interaction of the π -electrons of the two proximal benzene rings with 3.09 \AA .^[10] In the meantime, to further compensate for the transannular steric and electronic interactions, the $\text{CH}_2\text{-CH}_2$ bond length of the bridge is considerably larger than usual up to 1.69 \AA , which also causes the originally planar of sp^2 hybrid orbits to bend at an angle of 11.2° .^[11] The forced boat-shaped structure results in a reduced overlap of the p-orbitals and leads to diminished aromaticity, thus, with an overlap of the π -electrons, a single over rings extended π -system formed. These special properties can be detected by $^1\text{H NMR}$, where the aromatic protons are shifted upfield to $\delta = 6.50$ ppm, while in benzene they are observed at $\delta = 7.26$ ppm.^[5] This strained structure and conformational stability is the result that leads to reduced aromatic character, which allows peculiar chemical properties; this is increased reactivity of [2.2]paracyclophane towards electrophilic substitution reactions. Different from independent benzene, a further substitution reaction is laborious not only for the already substituted benzene ring but also the second, the whole system.^[9, 12]

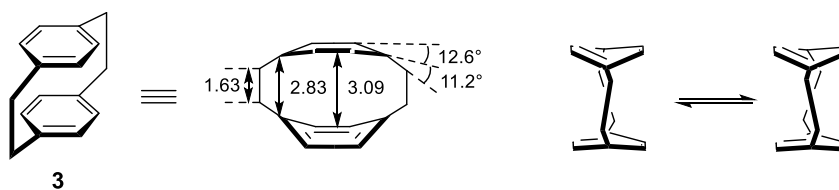
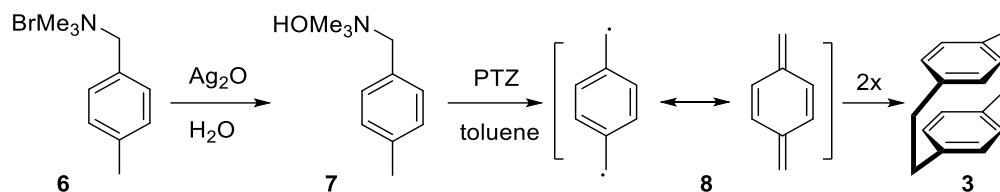


Figure 2. Structural parameters of [2.2]paracyclophane. Distances are given in Ångström (Å)

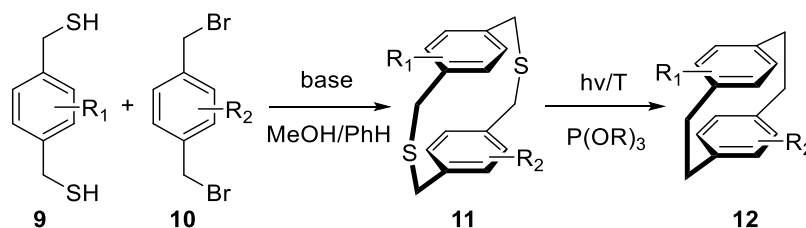
[2.2]Paracyclophane was synthesized in 1948 by Szwarc,^[13] and subsequently Brown and Farthing synthesized and reported it.^[4] Then Cram and Steinberg reported the synthesis of this novel compound by intramolecular Wurtz reaction two years later.^[5] This is the beginning of the blooming time of research on aromatic anomalies; after that, the cyclophanes family entered formal to the chemistry stage. In 1960, Winberg *et al.* used ammonium salt **6** as a precursor generating quinodimethane intermediate **8** to yield 17% of the desired [2.2]paracyclophane *via* 1,6-Hofmann elimination (**Scheme 1**).^[14] The ammonium hydroxide intermediate, by adding silver(I) oxide to the precursor, formed the reactive species *p*-xylylene **8** under

heating which undergoes dimerization where phenothiazine (PTZ) is a polymerization inhibitor. This method is still the basement of the current method to produce [2.2]paracyclophane on an industrial scale.^[15]



Scheme 1. 1,6-Hofmann elimination access to [2.2]paracyclophane (**3**) by Winberg *et al.* PTZ = phenothiazine.

In 1969, another synthetic approach was developed, which allows the dithia[3.3]paracyclophane **11** as the intermediate *via* photolytic sulfur extrusion or sulfone pyrolysis to compression into the ring scaffold.^[16] The intermediate can be easily prepared from the corresponding dithiol **9** and the dibromide **10** under alkaline conditions (**Scheme 2**). This method is particularly extraordinarily suitable to access more functional groups modified [2.2]paracyclophane, Stevens^[17] or pummerer^[18] rearrangements have been reported can be the key to accessing disparately substituted phane decks.



Scheme 2. General access to unsymmetrically substituted [2.2]paracyclophanes **24** *via* photolytic sulfur extrusion.

1.1.2 Character of [2.2]Paracyclophane

1.1.2.1 Nomenclature and chirality

Since the official IUPAC nomenclature for cyclic compounds is rather difficult, Vögtle *et al.* developed a specific cyclophane nomenclature, based on a core-substituent ranking.^[19] The core structure is named according to the length of the aliphatic bridges in square brackets (e.g. [n.m]) and the benzene substitution patterns (*ortho*, *meta* or *para*). As for [2.2]paracyclophane, the impeded rotation of the rings alongside the bridges is one remarkable feature at room temperature. Therefore, introducing a substituent other than hydrogen at any carbon atom renders these molecules chiral (**Figure 3**). To determine the sequence of name, the substituted arene is set to the chiral plane, and the first atom of the cycloalkane structure that is out of the plane and closest to the chiral center is defined as the “pilot atom”, *i.e.*, carbon 1. The stereo descriptor is determined by the sense of rotation viewed from the pilot atom, and a subscripted *p* is added to indicate the planarity of chiral center’ planarity (*S_p* or *R_p*). Typically, when the bridges are substituted, the central chirality is observed.^[20]

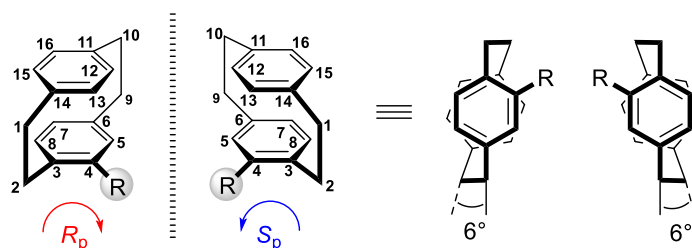


Figure 3. Planar chirality of monosubstituted [2.2]paracyclophane

When the same group substitutes both arenes, a total of seven regioisomers are observed (**Figure 4** top), then priority is given to the higher prioritized substituent according to the Cahn-Ingold-Prelog (CIP) nomenclature.^[20-21] But for other substitution patterns, the substituent at the other arene, a preferred common rule is that adding the prefix “pseudo” is easier to avoid detailed descriptions. On the other hand, with different substituents, it is obvious that disubstituted [2.2]paracyclophane are all chiral.

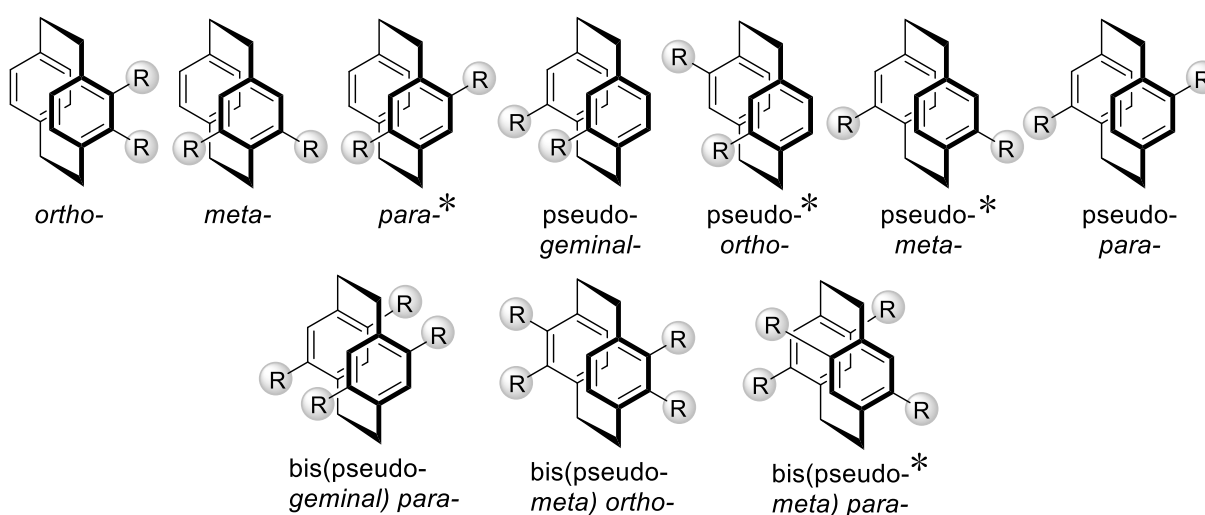
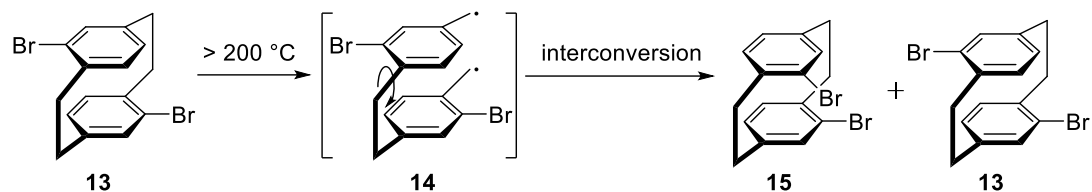


Figure 4. Top: substitution pattern of disubstituted [2.2]paracyclophane. Bottom: available known substitution pattern of tetrasubstituted [2.2]paracyclophane. Compounds marked with an asterisk are chiral with the same substitution.

Tetrasubstituted [2.2]paracyclophane, the most thoroughly investigated known precursors, can be accessed by multiple electrophilic substitution reactions (**Figure 4** bottom).^[22] Herein, both nomenclatures are available; two determinations of the substituted positions are required if in the traditional nomenclature. And the same, with different substituted groups, all the tetrasubstituted [2.2]paracyclophane are chiral, especially, apart from bis(pseudo-*meta*) *para* structure, others with the same substituent are achiral.

Notably, the conformational stability of basic substituted [2.2]paracyclophane can be changed, and racemization is observed, when the temperature is up to 200 °C. The racemization occurs due to the homolytic cleavage of bonds between the bridge carbon atoms, thereby allowing the benzene ring to free from the rotational hindrance of the decks, thus producing a statistical distribution of both recombination products.^[23] And in this way, disubstituted [2.2]paracyclophanes such as pseudo-*para* structure **13** can be isomerized to the pseudo-*ortho* derivative **14**, which leads to a 1:1 mixture of both isomers, where

isomerization ratios can be controlled by different condition.(**Scheme 3**) This phenomenon of interconversion occurs in some basic simple structures, which is uncommon when the substituents are large enough on the arene, as the energy required for rotation is larger or even inclined to breakage the bridge bonds.^[24]



Scheme 3. Interconversion of [2.2]paracyclophane above 200 °C. Racemization when monosubstituted.

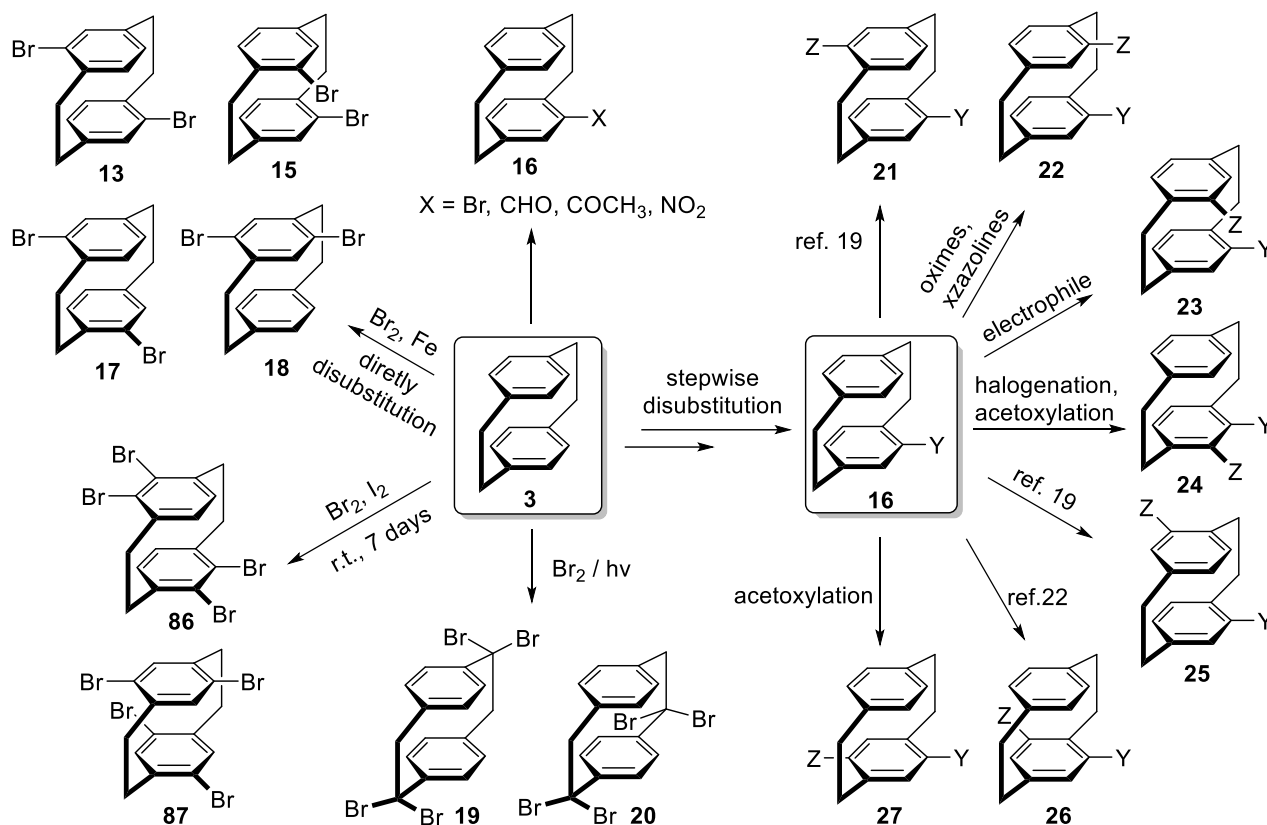
1.1.2.2 Functionalization

As an aromatic compound, [2.2]paracyclophane is susceptible to functionalization by usual electrophilic aromatic substitution reactions, except a few examples need *de novo* syntheses to obtain the derivatives. Mono-functionalization by highly selective methods can give good yields of initially functionalized derivatives such as formyl, bromine, nitro and acylated products.^[25]

Compared to mono-functionalization, di-functionalization has two approaches that are more complex and challenging (**Scheme 4**). One is direct bromination, which gives a mixture of different pseudo-dibromo isomers at the same time. The different products can be separated depending on their solubility, or the conditions can be optimized to obtain as single a product as possible before conversion.

Another approach is the further functionalization of already monosubstituted precursors; Cram and Reich have investigated the distribution of regioisomers in the re-monofunctionalized of electrophilic aromatic substitutions. For substituents with electron-donating structures pseudo-*meta* and pseudo-*geminal* are the main products, whereas the electron-absorbing substituent, mainly pseudo-*ortho* and pseudo-*para*, can be achieved by lithiation reaction.^[26] This regioselectivity is well explained by the transannular directing effect, described in detail by Cram *et al.*^[27]

Furthermore, De Meijere *et al.* reported that photochemically initiated bromination gives access to the functionalization of aliphatic ethyl bridges, which produced the mixtures of 1,1,9,9- and 1,1,10,10-tetrabromo[2.2]paracyclophane.^[28]



Scheme 4. A variety of functionalization of [2.2]paracyclophane derivatives.^[29]

1.1.3 Applications of [2.2]Paracyclophanes

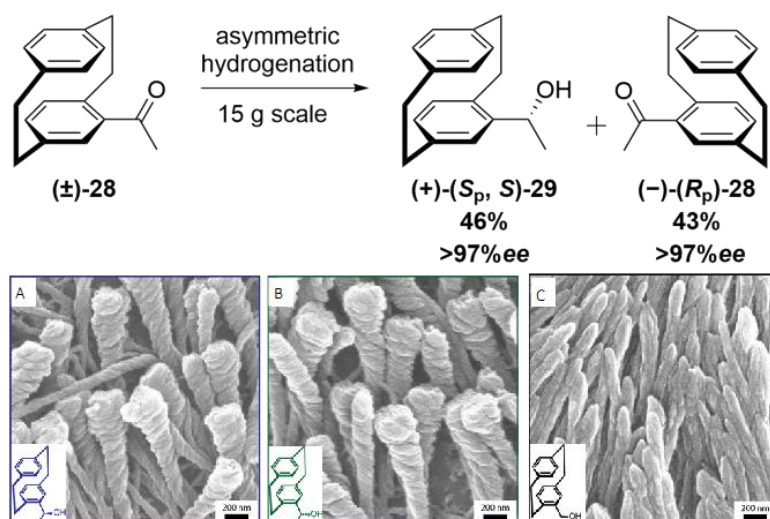
As the unique structure of [2.2]paracyclophane, considerable progress has been made in the chiral resolution and selective functionalization, engaging a characteristic position in numerous applications. The planar chirality has been widely used in asymmetric synthesis^[30] and various materials such as various coatings,^[30c, 31] and has also been extensively investigated in macrocycle topological strategy^[32] because of the rigidity skeleton property.^[33] In addition, recently it has been discovered that it combines well with the macrocycle cucurbit[8]uril (CB8), which opens up a new application in the supramolecular field.^[34] Here only the aspect of applications will be considered by the properties of the structure itself, other additional properties due to the characteristic substituents will not, such as the metal-ligand compounds.^[35]

1.1.3.1 [2.2]Paracyclophane in Asymmetric Synthesis and Materials

Enantioselective synthesis has long been an important topic of research, as chirality is an essential property that affects the characteristics of compounds in nature and many biologically active molecules, including the occurring amino acids (the building blocks of proteins) and sugars. As for a structure with a chiral plane, the planar chiral element of PCP has played an important role in the developing modern ligand systems. It certainly holds promise for stereoselective synthesis due to its conformational stability up to 200 °C, its stability to acids/bases and its ease of functionalization.^[30a, 30b, 36] Whereas kinetic splitting is a prerequisite for the study of chirality, pure enantiomers are significant intermediates in catalytic systems and functional chiral materials.^[37] Our group has dedicated efforts, for example a simple method was developed using only

catalytic amounts of N,O-ligand without additional central metal (other than zinc itself) based on PCP derivatives.^[38] Also a novel method was reported that an enantiomeric acetyl derivative **28** with the plane and central chirality was proceeded on a multigram scale which are useful intermediates for the synthesis of cyclophane-based ligand/catalyst system (**Scheme 5** top). This method employed kinetic resolution of compounds by a ruthenium-catalyzed enantioselective hydrogenation process, resulting in pure enantiomers with *ee* value up 97%.^[39]

As a readily available chiral precursor, PCP has been applied to prepare chiral polymeric materials by recently reported chemical vapor deposition (CVD) polymerization.^[39] Lahann *et al.* reported that polymerization of PCP derivatives into liquid crystalline templates to construct long-range polymer fibers arrays with unprecedented interfacial properties which were not possible with other techniques (**Scheme 5** bottom).^[40]



Scheme 5. Top: advanced method of asymmetric synthesis. Bottom: Chiral polymerization by CVD.
Copyright © 2021 Wiley-VCH Verlag GmbH & Co. KGaA.^[40]

1.1.3.2 Macromolecular

Over the past couple of years, [2.2]paracyclophane was applied as a rigid backbone for polymers^[41] besides CVD and metalorganic frameworks (MOFs)^[42] in general. Since polymers were first reported in 1990,^[43] have penetrated daily life and are widely used in polymer-based electronic and photonic devices.^[44] By incorporating aromatic compounds into the backbone of conjugated polymers, physical properties they exhibited have been extensively investigated. PCP has also been applied to polymers as a representative of intramolecular opposite conjugated systems because of their unique structure and electronic properties derived from the interaction between cofacial electron systems.^[45] Chujo and co-workers *et al.* have carried out detailed research in this area.^[41a, 41b]

MOFs (3D) and surface-mounted MOFs (SURMOF, 2D) are an emerging category of directionally prepared crystalline solid materials, mainly investigated for application in catalysis, sorption, gas storage and separation. Macgilivray *et al.* designed 2D MOF with square and hexagon cavities using a template-

directed solid-state organic synthesis (**Figure 5 30**).^[42a] With more research into MOF, [2.2]paracyclophane, the rigid π -stacked system, with the ability to carry out multiple functionalization sites, has led to a new wave of research in building functional materials. Liu (**Figure 5 31**), Farha (**Figure 5 32, 33**) and their co-workers have explored novel PCP-based organic linkers, using different substituents and modified PCP with carboxylic acid as the terminal.^[42b, 42c]

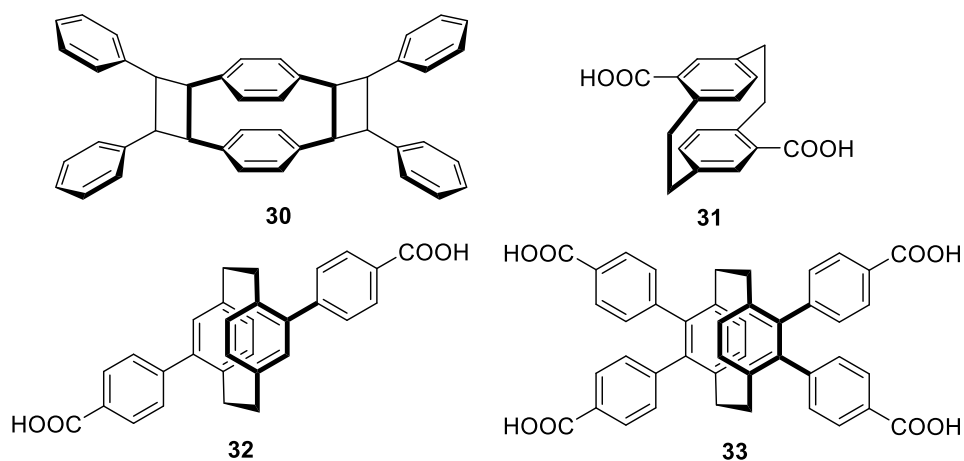


Figure 5. Monomer of [2.2]paracyclophane used as linkers in MOFs.

1.1.3.3 Topological Macrocycle

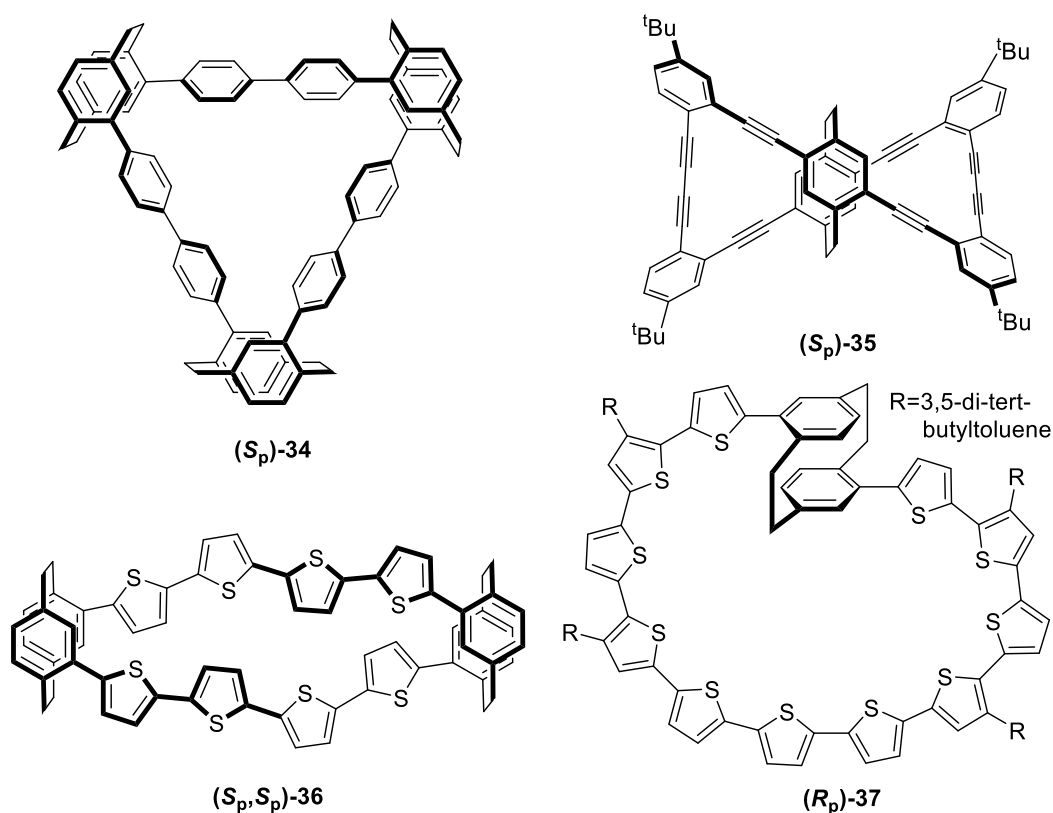


Figure 6. Macrocycle based on [2.2]paracyclophane

Synthesizing aesthetically pleasing structures is always challenging which can be seen as an art of chemistry in the eyes of chemists. These structures with the conjugated group also have special physical properties,

like circularly polarized luminescence (CPL). Chujo, Morisaki, and co-workers reported a series of optically active macrocycles based on tetrasubstituted [2.2]paracyclophane core that afforded luminescent materials with excellent chiroptical properties in both the ground and excited states (**Figure 6 34, 35**). PCP derivatives offer optically active high-order structures, such as the propeller-shaped cyclic structure, that are promising scaffolds for obtaining CPL.^[46] Another macrocyclic structure that has been reported several times is the PCP with a pseudo substitution of oligothiophene attached.^[33f, 47] The synthetic tenability of PCP provide additional possibilities for multiple regioselective halogenation and cross-coupling reactions. The cores also introduce a three-dimensional perturbation to these nearly planar macrocycles, which subsequently cause helical chirality (**Figure 6 36, 37**).

1.1.3.4 Host-Guest Chemistry

The size of [2.2]paracyclophane skeleton had been measured early in the synthesis, Frank Biebermann's group first noticed that PCP was just the right-sized scaffold to be accommodated within the cavity of cucurbit[8]uril and can be a novel candidate for developing assays.^[34] CBs, one of the main host macrocycles, commonly used in the supramolecular, have been extensively studied. In supramolecular sensing, CB8, with a relatively larger cavity up to 8.8 Å, among many subject dyes that were studied, no suitable dye can be employed as a sensor for binding adamantyl-species (*e.g.*, memantine) with CB8. A large number of CB8 guests showed that typical aromatic components (*e.g.*, typical chromophores) and cyclic and acyclic aliphatic species (*e.g.*, terpenes, steroids) do not exceed K_a values of 10^9 M^{-1} . However, PCP is a promising subject for this purpose, a sphere-like compound with a conjugated structure, as it is functionalized with positively charged pyridinium moiety to improve water solubility and a stronger affinity for CB8. The molecular model of density functional theory (DFT) indicated an ideal packing coefficient (PC) of 57% which is spot-on in the ideal packing regime of $(55 \pm 9)\%$ for supramolecular host-guest complexes (**Figure 7**). Fluorescence spectra of MPCP in water with increasing CB8 concentrations showed a very strong binding ($\log K_a \geq 9$), which has proven to be a novitiat guest candidate in application to CB-based systems for blood-serum sensing assay.

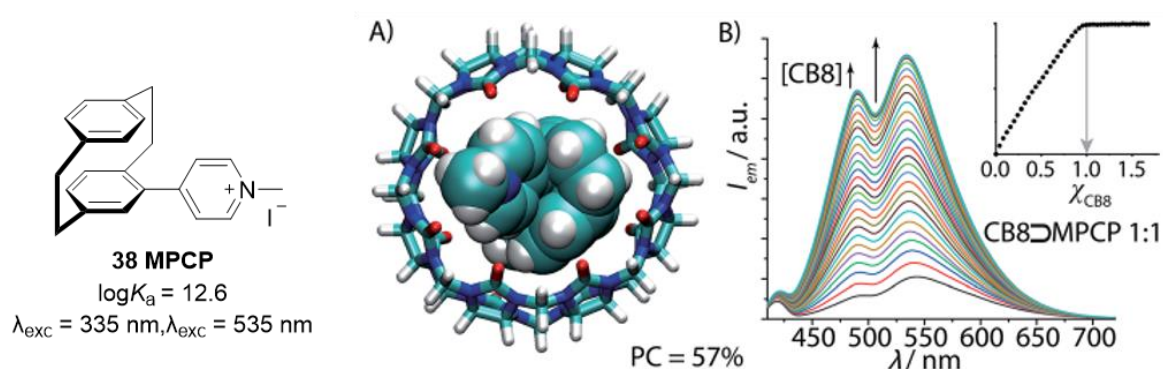


Figure 7. DFT model and Fluorescence spectra of the affinity of CB8 and MPCP. Copyright © 2019 Royal Society of Chemistry.

The study on the binding characterizations of various [2.2]paracyclophane derivatives with CB8 is exactly the main content of this thesis.

1.2 Supramolecular Chemistry

Supramolecular chemistry became widely acknowledged in 1987 when the Nobel Prize in Chemistry was awarded to Charles J. Pedersen, Jean-Marie Lehn and Donald J. Cram in recognition of their extraordinary contributions to the world of chemistry.^[48] The concept of supramolecules (*i.e.*, “Übermoleküle”) was introduced in the 1930s and defined by the “entities of the higher organization resulting from the association of coordinatively saturated species”.^[48c, 49] And this was preceded by many scientists who made outstanding contributions to this end; as Issac Newton famously put it, “*If I have seen further it is by standing on the shoulders of giants.*” For example, the invention of van der Waals forces, first postulated by Johannes Diderik van der Waals, laid the theoretical foundations for supramolecular chemistry, which include attraction and repulsions between atoms, molecules, and surfaces, as well as other intermolecular forces.^[50] Supramolecules are formed based on weak and reversible non-covalent interactions between molecules, which include hydrogen bonding, van der Waals forces, hydrophobic interaction, metal coordination, π - π stacking, electrostatic effects, *etc.*^[51]

Supramolecular chemistry has now evolved from concept to novel applications, from the original study of biological processes to current improvements, to more and broader interdisciplinary disciplines.^[52] The 2016’s Nobel Prize, shared by Jean-Pierre Sauvage, J. Fraser Stoddart, and Bernard L. Feringa, once again elevated supramolecular chemistry to a certain height from macroscopic to microscopic, recognizing the synthesis of a series of molecular machines that symbolize a milestone in the exploration of the nanoworld.^[1, 53] At the moment, more outstanding scientists in a variety of fields continue to produce results, *e.g.*, D. Leigh^[54] in molecular knots and motor, E. W. Meijer^[55] and T. Aida^[56] in supramolecular polymer chemistry, M. Fujita^[57] in supramolecular coordination chemistry, *etc.*

1.2.1 Cucurbit[n]uril in Host-Guest System

Host-guest chemistry, a branch of supramolecular chemistry, describes the complexes consisting of two or more molecules or ions in unique structural relationships by forces other than covalent bonds.^[51b, 58] Host-guest chemistry has made impressive developments driven by almost limitless possible applications. The host molecule as an important component has completely different characteristics in various fields, such as drug delivery,^[59] environmental monitoring,^[60] detection and sensing,^[61] functional materials.^[62] For example, in drug delivery in biology, the host needs water solubility, non-toxicity *etc.*, features, while selective binding of specific guest is required in environmental monitoring. Macrocyclic structures are popular as the guest molecules, and gained vast favors owing to their dynamic reversible complexing ability with numerous guest components, which are commonly cyclodextrin, cucurbit[n]uril, pillar[n]arene, calix[n]arene, *etc.* They all exhibit the ability to compound dynamically reversible for various guest components. Cucurbit[n]uril is the one used in this thesis.

1.2.1.1 Synthesis and Properties of Cucurbit[n]urils

Eberhard. Meyer first reported the accidental synthesis of CB6 in 1905 in the condensation reaction of glycoluril and formaldehyde.^[63] It was not until 1981 that the structure of CB6 was revealed by X-ray crystal data to be glycoluril units linked by six methylene-bridge pairs and referred to by the name cucurbituril.^[64] Then in the 21st century, Kim, Day, and coworkers isolated and characterized the structures of other homologs, including five, seven, eight, and ten glycoluril units (**Figure 8**).^[65] By now, more homologs of CB have been reported, such as CB14,^[66] *nor-seco-CBn*^[67], and others, and as further research into their properties is conducted, more applications will be employed.

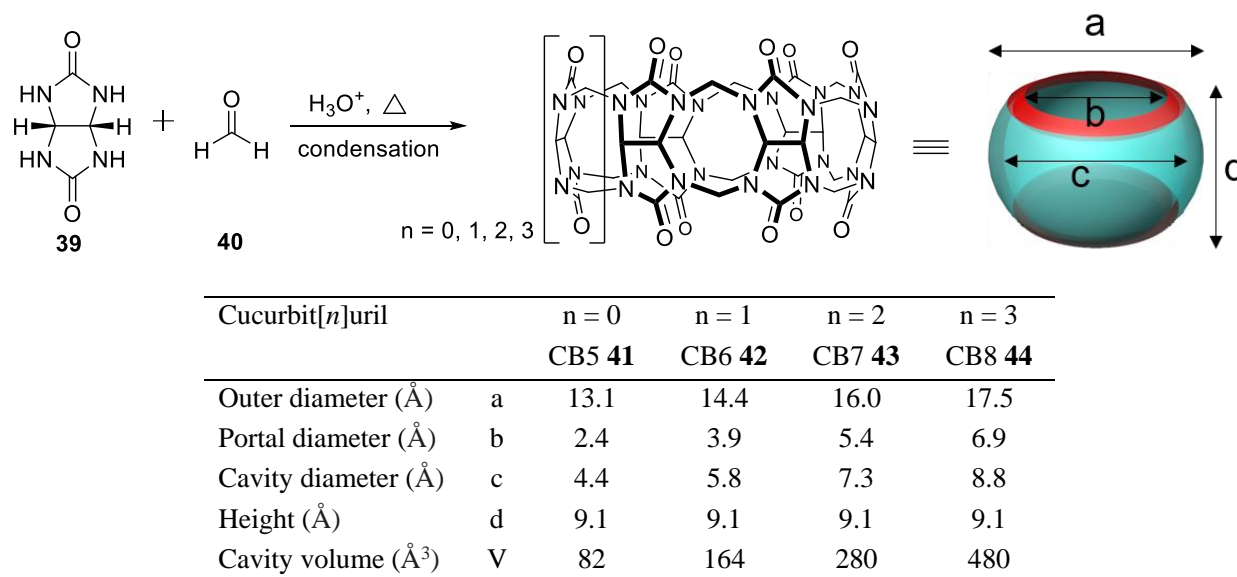


Figure 8. Chemical structure and structural parameters of CB5 to CB8

Kim and Day's early research shown that the production of common homologs could be controlled by adjusting the reaction conditions, *i.e.*, reaction temperature, substrate, acid concentration, *etc.* For instance, the yields of CB7 and CB8 were greatly reduced under high dilution experimental conditions.^[65] In the case where the reaction has been established, the means of separation is also an influential factor in the final yield. Many researchers gave more detailed separation protocols, generally batch elution depending on their solubility and addition, column chromatography depending on polarity.^[68]

Unlike cyclodextrins, which are naturally occurring, CBs can only be synthesized and are relatively homologous in size. Considering the conditions of its synthesis, CBs are characterized by solubility in acidic water and an aqueous solution of alkali metal ions, aqueous solutions and low solubility in pure water, with the highest CB7 being also. Moreover, CBs, especially CB6, have excellent thermal stability and chemical inertness. The decomposition starts at around 370 °C and remains stable in the presence of strong oxidizing or reducing agents.^[69]

The highly symmetrical structure determines the properties of CB_n family. Neither functional groups nor electron pairs are pointing to the interior of the cavity, and therefore hydrogen bonds cannot be formed, thus leading to the formation of high hydrophobicity in the cavity.^[70] Several solvatochromic dyes have been reported to confirm this conclusion, such as rhodamine binds to CB7 with a significant change in the

absorption spectrum thus demonstrating it is in a less polar environment.^[71] Another property is the high electron density of the carbonyl group at the entrance to the barrel structure of CB_n , which provide the positively charged guests a higher affinity than other neutral guests. As shown in the electrostatic potential map (**Figure 9**), the CB_n family has a similar, but not identical, distribution diagram.^[72] CB_8 has a larger cavity and an internal negative potential. Combined with the structure, the entrance diameter is 2 Å smaller than the maximum diameter of the cavity, which contributes to a structural barrier to binding and dissociation between host and guest.^[73] As a result, CB_n has a higher affinity and selectivity for specific classes of guest molecules than other macrocycles, for example, protonated hydrophobic amino acids, alkylated ammonium, and imidazolium, additionally different selective guests for homologues.^[68c, 74]

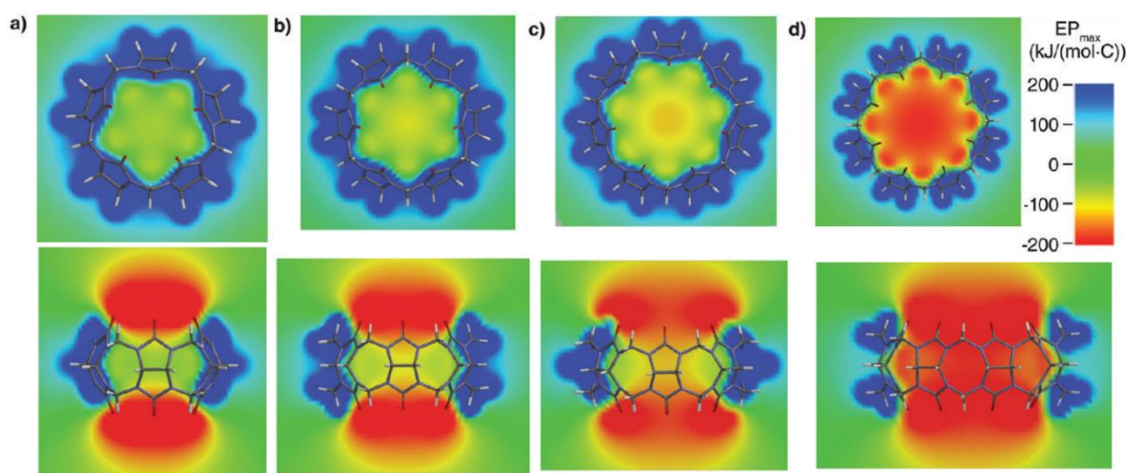


Figure 9. Calculated electrostatic potential (EP) for (a) CB_5 , (b) CB_6 , (c) CB_7 , and (d) CB_8 . Reprinted by permission from ref.72. Copyright © 2012 American Chemical Society.

Another helpful characteristic is the packing coefficient (PC), a concept Rebek and Mecozzi introduced as the guest size ratio to the host cavity's volume. Although this value was originally used to describe the capsule as a host, it was later found to be still used for the main guest compound.^[75] This value was considered the best for evaluating the superiority of the spatial fit of the host-guest complex, with 55% being regarded to produce the best affinity between the host and guest. However larger or smaller would result in a reduced affinity. Nau and coworkers reported that the analysis of PC value for known guests with hydrophobic binding motifs revealed average values are well in line with the rules (55% solution), which are 47% for CB_5 , 58% for CB_6 , 52% for CB_7 , and 53 for CB_8 .^[76] 55% is the natural coefficient of water molecules in water, which can be empirically estimated for synthetic substances, and is in the range of 46-64% to indicate a stable complex.

In addition, hydrophobic effects and ion-dipole interactions are the main influences leading to the strong binding affinity observed in CB_n . The first guest molecule initially demonstrated experimentally was the water molecule in CB_6 .^[65a] In aqueous solutions, water molecules in CB cavities have high energies because of their very limited hydrogen bonding and weak dispersion interactions with weakly polarized CB cavity walls. When the guest and CB are complexed, releasing high-energy water from the cavity gives rise to a large enthalpy gain, which is an important driving force for guest binding.^[77] The discharged water

participates in a stronger H-bond network in the water column, which plays an essential role in the overall hydrophobic effect (**Figure 10**). Biedermann *et al.* used MD simulations to calculate the relative potential energy of removing all water molecules from the CB cavity, showing that CB7 gains the largest calculated potential energy and that the cavity is not large enough for the water molecules inside to form a structurally stable H-bond network.^[77b] However, for CB5 and CB6, although the internal water molecules are the most energetic, the cavities are small and very few in number, so the total energy is still greatest for CB7. CB8 has a larger cavity, allowing the internal water molecules to form a structurally optimized network similar to that of bulk water, with the consequence that the potential energy of CB8 is also less than that of CB7. This is also in line with the high binding guest now found, with the tested CB7 currently having the highest binding affinity. Kim also reports evidence that water molecules also influence the ion-dipole interactions between host and guest mainly in the gas phase.^[78] It was concluded that ion-dipole interactions are the main driving force for complexation in the absence of solvent, while in solution, hydrophobic interactions are dominant.

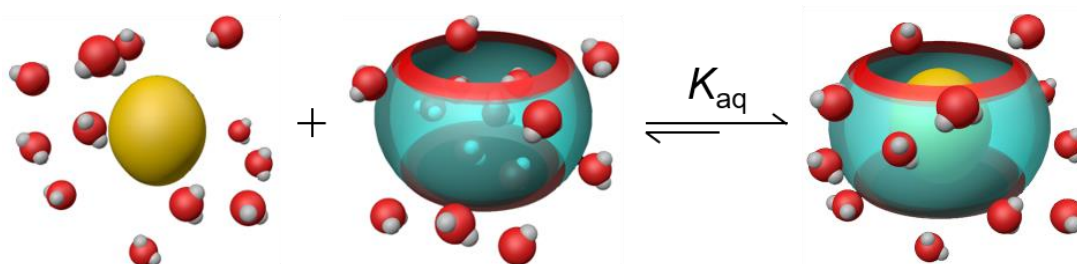


Figure 10. Schematic illustration of the release of high-energy water molecules upon guest-binding.

1.2.1.2 Applications of Cucurbit[*n*]urils

As widely known host, CB n can be accessible on a kilo scale, and combined with a diversity of guests thanks to its conditional adaptability, allowing for applications in various fields such as chemical sensing,^[79] biological applications,^[80] catalysis in reactions and fluorescence,^[74b] skeletons in MOFs and polymers,^[81] surface functional materials^[82] *etc.* Since CB n hosts are spectrally silent in the visible electromagnetic spectrum, the optical signal of CB n -based chemosensing ensembles is typically performed by indicator displacement analysis (IDA), which is depressed and applicable to aliphatic and aromatic analytes. CB n -based chemosensors have been successfully reported by Biedermann *et al.* for real-time monitoring with unlabeled analytes or substrates. The details are given in the next section.

CB n is fully adaptable to the entire pH range, and several researchers have conducted biocompatibility evaluation in mice and blood cells, showing excellent profiles and no significant direct damage to the cells.^[83] Park and coworkers reported the synthesis of stable complexes CB7-Cy3 and adamantylamine-cyanine 5 conjugate (Ada-Cy5) and displaying different organelles and fusion processes in living cells by functionalized modifications of CB n . The time-dependent increase in Fluorescence resonance energy transfer (FRET) signal was applied to the image and detected particular cellular processes as supramolecular donors and acceptors transferred to mitochondria and fusion media, respectively, fusion

was observed to occur.^[84] In addition, the targeted delivery of chemotherapy drugs combined with CB_n to cancer cells is one of the most practical applications and has been widely and intensively studied. For example, the combination of clinical antitumor drug biotin and CB7 was reported to show an order of magnitude higher intracellular bioactivity than oxaliplatin alone.^[85] Isaacs and coworkers reported self-assembly of functionalized CB7 into vesicles encapsulating drugs doxorubicin (DOX), and release of drugs not only by dual pH-chemical stimulation of adamantane carboxylates in different protonated states, but also by dual pH-photochemical stimulation of stilbene derivatives in different photoisomerization states.^[86] Wang and coworkers proposed a “Lego-like” Functionalization strategy on the surface of nanoparticles by binding CB7 to its corresponding guest labelled with functional units (*e.g.*, folic acid, polyvinyl alcohol) and loading the drug into the cavity of CB, offering further possibilities for combination drug therapy.^[87]

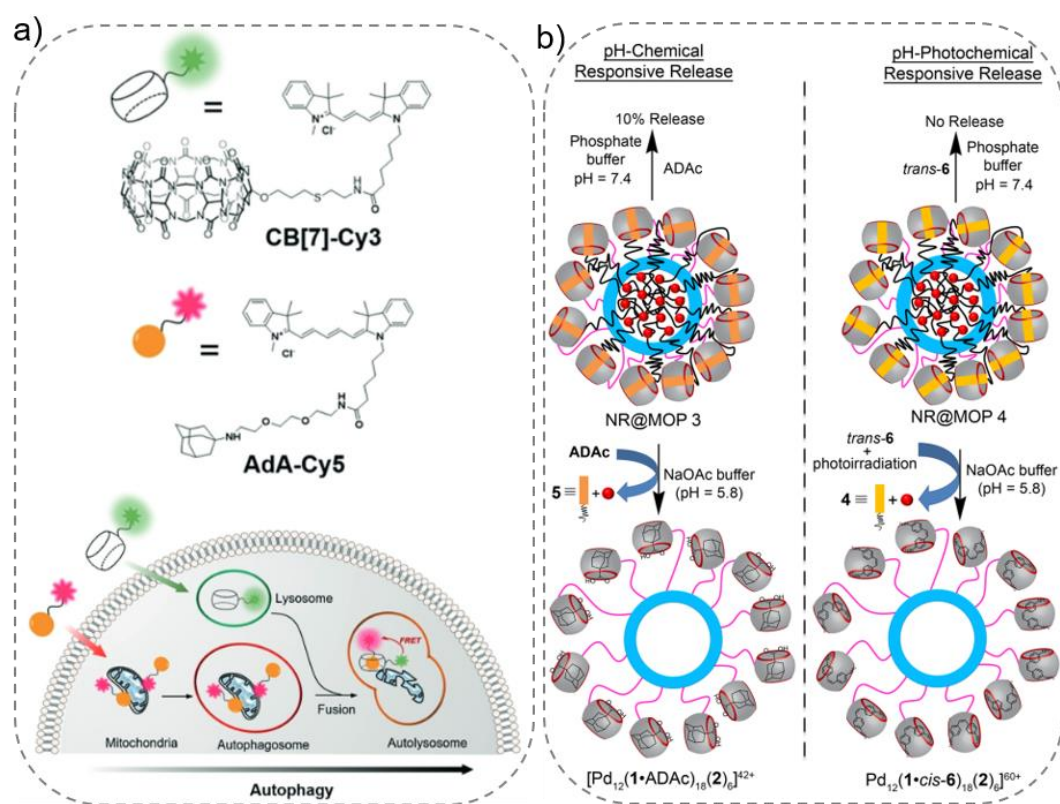
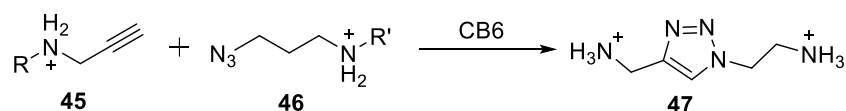


Figure 11. (a) Organelles imaging and fusion process monitoring of FRET signal via the binding of CB7-Cy3 and AdA-Cy5. Reprinted by permission from ref. 84. Copyright © 2018, Wiley-VCH Verlag GmbH & Co. KGaA. (b) Schematic representation of pH-chemistry and pH- Photochemical response release of hydrophobic cargoes. Reprinted by permission from ref. 86. Copyright © 2017, American Chemical Society.

The ability of CB_n to encapsulate a variety of guest molecules and the hydrophobic effect of the cavity gave the possibility and optimized performance for a vast of chemical reactions for catalysis and templating. Mock and coworkers reported the first examples of CB catalysis in 1989, where a [3+2] cycloaddition of alkynes and azides was shown in the CB6 cavity (**Scheme 6**). In a 40 °C aqueous formic acid solution, the slow cycloaddition reaction and substituted triazoles were formed. However, after the addition of a catalytic amount of CB6, the reaction increased by 6×10^5 with only isomer triazole.^[88] Reddy reported on the

catalytic action of a series of reactions involving halogen-CB6-H₂O complexes, formed by CB6 in iodine or bromine vapors. The halogen-involved oxidation reactions were carried out under such complexes of halogen with CB6, and all the reactions tested showed an increase in final yield compared to those without CB involvement. The largest increase was in the iodine-catalyzed Prins cyclization, with a 7% increase over that reported in the literature.^[89] Kim also reported examples of the application of the hydrophobic cavity of CB for photoreaction promotion. The photodimerization of CD-anthracene was investigated by adjusting the bulky attachment of the external object to control the stereospecific photoreaction occurring within the cavity. CB8 macrocyclic additions resulted in a 99% combined yield of photodimers with otherwise low *ee* value and head-to-head selective inversion of the structures from head-to-tail.^[90]



Scheme 6. Schematic of azide-alkyne click reaction mediated by CB6

In summary, the many successful cases of CB n prove that it has broad application prospects in various aspects, such as functional applications and materials, which are beyond the mandate of this work and will not be described in detail here.

1.2.2 Cucurbit[n]uril in Supramolecular Chemosensors

Traditionally, chemical sensors combine signal emission and recognition, which interact at the molecular level to detect certain matrices, such as solutions, blood, waste water, *etc.* In general, once the analyte is bound to the receptor, the indicator emits a detectable signal for detection. In most cases, however, the guests are spectrally silent and their corresponding complexes do not have the typical absorbance or emission signals. In the case of CB, it does not absorb or emit electromagnetic waves in the visible range and is limited to sensing inherently photophysical transparent analytes. Depending on the other excellent properties of CB, researchers are using various means to expand its range of applications.^[79b, 91]

1.2.2.1 Strategies for Sensing Assay

The unmodified CB n molecule is not redox active and neither absorbs nor emits light in the visible range of the electromagnetic spectrum. Therefore the macrocycles are usually only used for analytes that are intrinsically spectrally active or redox active, *i.e.*, direct binding assay (DBA, **Figure 11 a**). This approach is more restrictive than the others, but the signal can be readout easily, absorption (ABS), fluorescence (FL), circular dichroism (CD), NMR/MRI, mass spectrometry (MS) *etc.*^[92]

For “spectroscopically silent” host-guest complexes, this can be addressed by using spectrally active indicator dyes as auxiliary additives employed in indicator displacement assay (IDA, **Figure 12 b**). This strategy requires the indicator to have a sufficiently high affinity for the host and to exhibit significantly different photophysical properties. Typically, the affinity of the indicator dye for the host should be similar to that of the analyte in such a way that high complexation of the indicator dye in the absence of the analyte

and presence of the analyte is sufficient for the dye to displace to maintain a balance.^[93] For instance, Nau and coworkers reported how CB6 and a putrescine-anchored 1-naphthylamine-5-sulfonate indicator dye could be used to detect hydrocarbon gases.^[94] In contrast, CB7 and Cb8 can be utilized as detection hosts for larger analytes, like terpenes and adamantanes.^[95] Even Cb8 can be detect fluorescent proteins with a modified gene-bound N-terminal Phe-Gly-Gly portion as the recognition sequence for CB8.^[96]

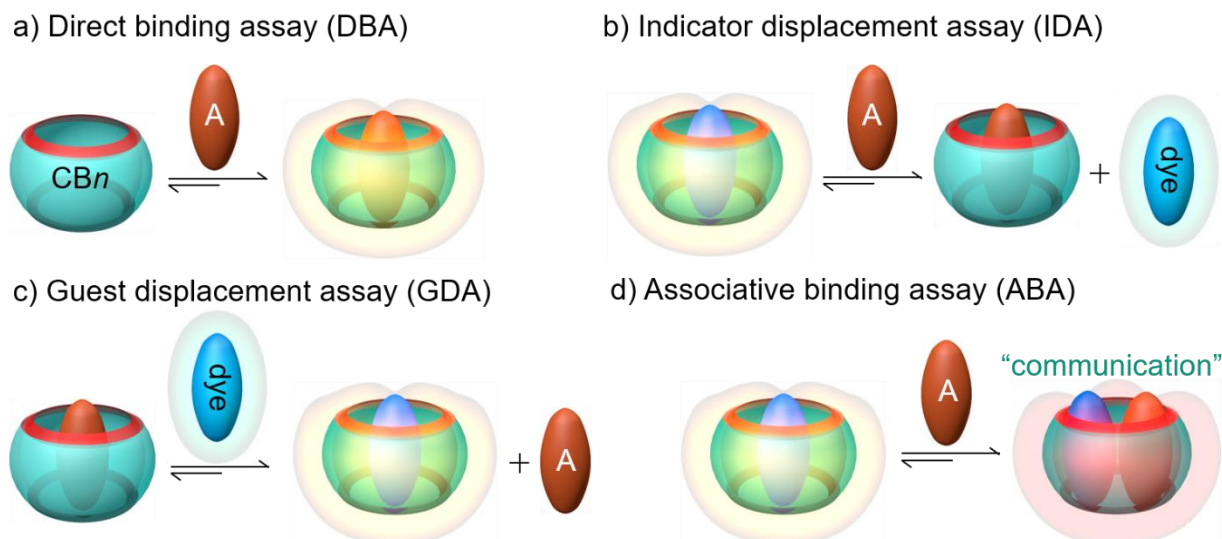


Figure 12. a) Schematic illustration of a direct binding assay (DBA). b) Schematic illustration of an indicator displacement assay (IDA). c) Schematic illustration of guest displacement assay (GDA). d) Schematic illustration of the associative binding assay (ABA). A = analyte.

Biedermann and coworkers reported a new strategy of guest displacement assay (GDA) as a complementary method to IDA, capable of determining the binding affinity of spectrally silenced host-guest and protein-ligand pairs (**Figure 12 c**). In contrast to IDA, the GDA method, involves replacing the analyte with a dye to re-equilibrate and thereby detect signal enhancement changes.^[97] It has the advantage of permitting the application to insoluble guests, typically hydrophobic and weakly bound guests.

A distinctive detection method is associative binding assay (ABA), where CB8 forms a 1:1:1 triple complex with the guests to carry out the association by circumventing some problems (**Figure 12 d**). In the absence of CB8, there is no signal change since the two aromatic guests are far apart. When CB8 is present, the two guests are strictly controlled by the cavity at a close distance, resulting in a charge-transfer (CT) interaction between the two guests and a chromogenic change.^[98] In many cases of ABA, it is more sensitive to analyte sensing in terms of energy than IDA and is, therefore, more suitable for small molecule guests at low concentrations.

1.2.2.2 Experimental Techniques for Binding Affinities

Common methods for studying host-guest interactions in terms of binding affinity are nuclear magnetic resonance (NMR) spectroscopy,^[99] spectrometer-based titration methods^[79b, 93a, 93b] and isothermal titration calorimetry (ITC).^[100]

	$H + D \rightleftharpoons HD$	Eq. 1	
	$K_a^{HD} = \frac{[HD]}{[H][D]}$	Eq. 2	
DBA	$[H]_0 = [HD] + [H]$	Eq. 3	
	$[D]_0 = [HD] + [D]$	Eq. 4	
	$I_t = I^0 + I^{HD}[HD] + I^D[D]$	Eq. 5	
	$HD + G \rightleftharpoons HG + D$	Eq. 6	
	$K_{rel} = \frac{[HG][D]}{[HD][G]}$	Eq. 7	
	$H + D \rightleftharpoons HD$	Eq. 8	
	$H + G \rightleftharpoons HG$	Eq. 8	
IDA	$K_a^{HD} = \frac{[HD]}{[H][D]}$	$K_a^{HG} = \frac{[HG]}{[H][G]}$	Eq. 9
or			
GDA	$K_{rel} = \frac{K_a^{HG}}{K_a^{HD}}$		Eq. 10
	$[H]_0 = [HD] + [H] + [HG]$	Eq. 11	
	$[D]_0 = [HD] + [D]$	$[G]_0 = [HD] + [G]$	Eq. 12
	$[HD] = \frac{K_a^{HD}}{1 + K_a^{HD}[H]} [D]_0$	$[HG] = \frac{K_a^{HG}}{1 + K_a^{HG}[H]} [G]_0$	Eq. 13
	$I_t = I^0 + I^{HD}[HD] + I^D[D]$	Eq. 14	

NMR spectroscopy is an important tool for studying host-guest complexes, identifying the different nuclei in a molecule by measuring the chemical shifts of the molecule. The binding activity of two molecules leads to considerable changes in their electron density and local magnetic field, which generate changes in chemical shifts and signal intensity in NMR. NMR allows for qualitative and quantitative analysis of complexes, and the detection on a time scale when the host and guest binding equilibrium is slow.^[99d, 101] However, because the measurement time of NMR is on the millisecond scale, when the equilibrium time reached by the binding process is too fast, an average signal of the equilibrium state is detected while the equilibrium process cannot be monitored. A common strategy used to compensate was investigated as DBA and IDA for complexes with different affinities. DBA is the preferred option for guests with weak binding *i.e.*, small binding constant K_a (**Equations 1 and 2**). For the high-affinity host-guest complexes, competition

experiments are the most commonly used means and involve a reference guest of known K_a^{HD} and a second guest of unknown K_a^{HG} . If two guests did not have a large gap in the K_a values, they could be determined by **Equation 6** to **Equation 10**, which defines the binding constant K_{rel} .^[102]

The main limitations are that NMR requires a rather high concentration range and that only spectrally simple molecular binding processes can be studied, whereas their processes cannot be accurately detected for complex molecules with many spectrally active nuclei.

Ultraviolet–visible (UV-Vis) and emission spectroscopy are rapid methods for studying molecular binding affinity. The absorption of UV light occurs on picosecond time scales and is based on a transition from the ground state to the excited state induced by a photon. Therefore, the wavelength of the absorbed photons depends on the energy gap between them, which is determined by the molecule's characteristics. Since the total energy is directly related to the substance's mass, the absorption intensity is directly related to the concentration of the substance.^[103] According to Beer-Lambert's law, the concentration of a dilute homogeneous solution can be related to the absorbance of the sample and the absorbance of the substance. The law states that the absorbance is directly proportional to the concentration (c) of the absorbing species, ϵ as the molar attenuation coefficient or absorptivity of the attenuating species, l as optical path length, $I_{\text{Abs-0}}$ as the intensity of the irradiated light, and I_{Abs} as the intensity of the transmitted light (**Equation 15**).^[104]

$$\text{Abs} = \epsilon c l = \log \frac{I_{\text{Abs-0}}}{I_{\text{Abs}}} \quad \text{Eq. 15}$$

The absorbance of the complex formed by the titration of one substance to another is measured and the absorbance curve obtained by fitting can be used to determine the host-guest binding affinity. Absorption is the radiative leap of a molecule from a lower to a higher electronic state, whereby most molecules in the population are at the lowest energy level of the ground state at room temperature. When a molecule absorbs a photon, it is raised from S_0 to one of the vibrational energy levels of the singly excited state and cannot be excited directly to the triplet excited state due to the conservation of angular momentum. Molecules in the excited state still have different multiplicities and tend to dissipate the energy gained back to the ground state owing to the higher energy, which can occur in several different ways. Molecules with the same spin multiplicity may undergo non-radiative transitions, namely vibrational relaxation (VR) and internal conversion (IC), or radiative transitions to produce fluorescence (FI). For molecules with different spin multiplicities, intersystem crossing (ISC) from S_1 to T_1 and possibly from T_1 to S_0 occurs, which is phosphorescence (P) with a longer lifetime than fluorescence.^[105] Similar to absorbance-based titrations, fluorescence-based titrations can be used to determine binding affinities. The formation of a host-guest complex leads to changes in the microenvironment of the host-guest molecule. A variety of reasons make the binding of the host and guest to fluorescence enhancement or extinction.^[103, 106] Depending on the properties of the different dyes, both DBA and IDA can be used equally well for titration curve plotting and fitted with **Equation 3** to **Equation 5** for DBA or **Equation 11** to **Equation 14** for an IDA or GDA.^{[93b,}

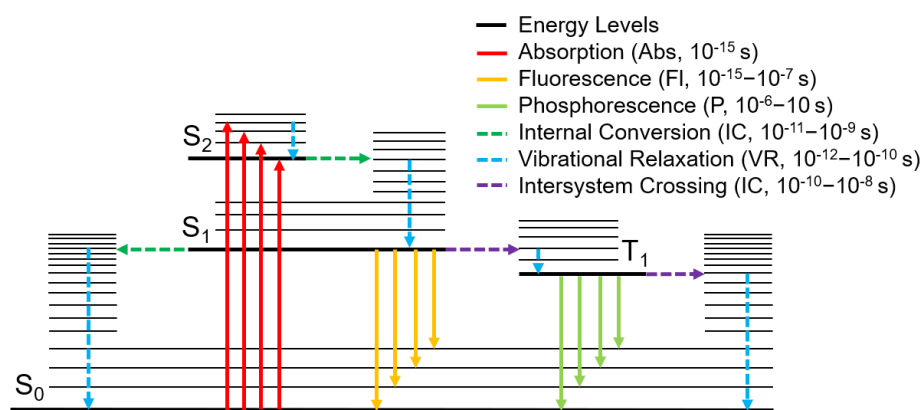


Figure 13. A typical Jablonski diagram was amended.

Parameters for **Equation 1** to **Equation 14** were assigned as follows: $[H]$ – host concentration at equilibrium, $[H]_0$ – initial host concentration, $[D]$ – dye concentration at equilibrium, $[D]_0$ – initial dye concentration, $[G]$ – guest concentration at equilibrium, $[G]_0$ – initial guest concentration, $[HD]$ – host⊃dye concentration at equilibrium, $[HG]$ – host⊃guest concentration at equilibrium, K_a^{HD} – binding constant for the association of the host⊃dye (HD) complex, K_a^{HG} – binding constant for the association of the host⊃guest (HG) complex, I^0 – background signal; I^{HD} – signal from the host⊃dye (HD) complex; I^D – signal from the free dye (D); I_t – observable signal as a function of time.

ITC is a physical method of measuring molecular binding based on the thermal change resulting from the interaction between two or more molecules in a solution. ITC calorimetry consists of two identical unit cells, a sample cell and a reference cell, encased in an adiabatic jacket (**Figure 14 a**).^[100b] The reference cell contains a refrigerated buffer solution to the reference temperature. The sample cell is filled with a solution of the first component whose temperature difference is monitored in real-time by a sensitive thermopile automatically adjusted to reduce the temperature difference. The solution of the second component is titrated into the cell in precisely known aliquots until its concentration is multiplied by that of the first component. As the aliquots are injected, the feedback regulator adjusts to maintain the same temperature as the two components combine to produce a temperature change. The current changes generated by this process are recorded and the raw data consists of a series of heat flow (power) spikes, each spike corresponding to a single injection. The titration curve is generated by integrating the result concerning time and normalizing the concentration (**Figure 14 b**).^[108]

$$\Delta G = -RT \ln K_a = \Delta H - T\Delta S \quad \text{Eq. 16}$$

The experiment is carried out under isothermal conditions and the procedure is similar to the conventional titration process, where the host solution is added to the guest solution and compared to a blank solution to measure the heat absorbed or given off. Based on the resulting base data, a non-linear regression analysis pair is applied to the equation to obtain the desired data, binding affinity ($K_d = 1/K_a$), stoichiometry/molar ratio (N), and the molar reaction enthalpy (ΔH). The relevant results, association constant (K_a) standard free

energy (ΔG) and entropy (ΔS), are then obtained from the Gibbs-Helmholtz equation (**Equation 16**), where R is the gas constant ($R = 8.314 \text{ J mol}^{-1} \text{ K}^{-1}$) and T is the absolute temperature.^[109]

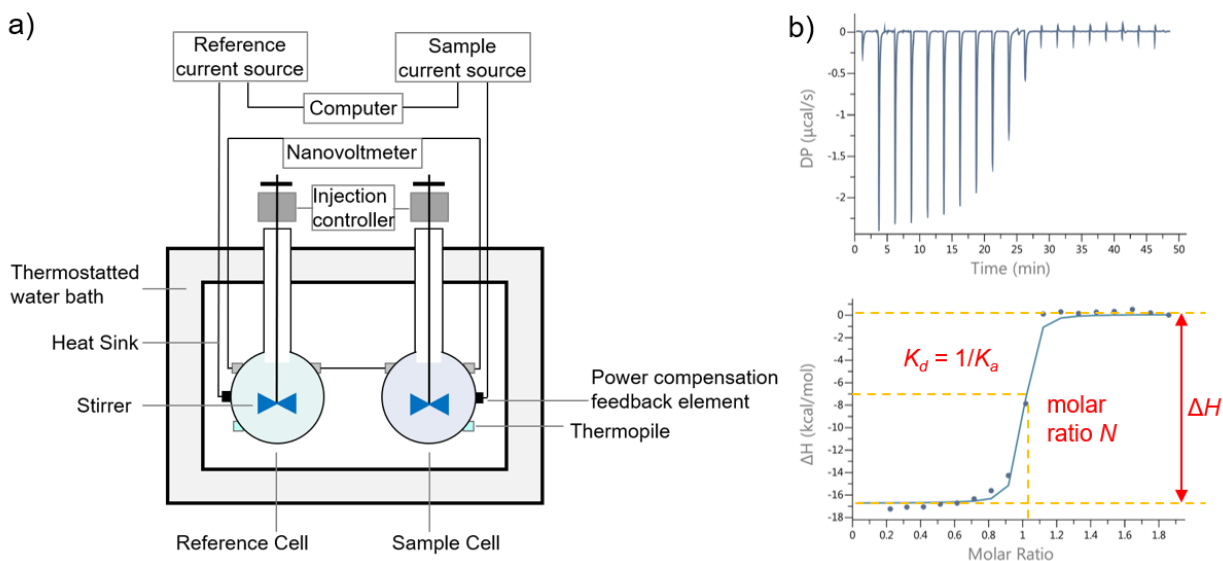


Figure 14. a) Schematic depiction of ITC. b) ITC thermogram depiction of the titration and analysis results.

1.2.3 Supramolecular Skeleton and Cage based on [2.2]paracyclophanes

Supramolecules are quite a large concept and have sprung up in various complex structures and cages. In addition to the host and guest, this thesis deals with metal coordination assemblies and non-covalent cages. The Nobel Prize winners, Jean-Pierre Sauvage^[53a] and J. Fraser Stoddart^[53b] were awarded for their pioneering work in these areas. Coordinated cages are usually self-assembled by metal coordination. Makoto Fujita *et al.* have contributed much work on metal-liganded cages that support catalytic reactions.^[110] Haibo Yang *et al.* have also conducted studies on supramolecular radical cages, offering prospects for reactions containing radicals.^[111] In addition to metallic cages,^[112] non-covalently self-assembled cages have also been reported for use in encapsulation and controlled release.^[113] The mechanically interlocking covalent bond cage pioneered by Stoddart is also a highlight, consisting of π - π interactions, which are then encapsulated. These structures are widely used in synthesis to form states where non-contact connections can be made, with charge interactions replacing the hydrophobic-hydrophilic effects of the host and guest.^[114]

Similarly, multi-locus modification of [2.2]paracyclophane as a rigid backbone has been reported in the skeleton and the cages. Arne Lützen and coworkers reported that the PdL_2 , Pd_2L_4 and Fe_4L_6 cage structures, competed by complexing palladium with pseudo-*meta* PCP termination in pyridine and an amino group, respectively (**Figure 15 a, b, c**).^[115] Eli Zysman-Colman and coworkers reported a palladium-centered PCP cage with deep-blue light emission (**Figure 15 d**).^[116]

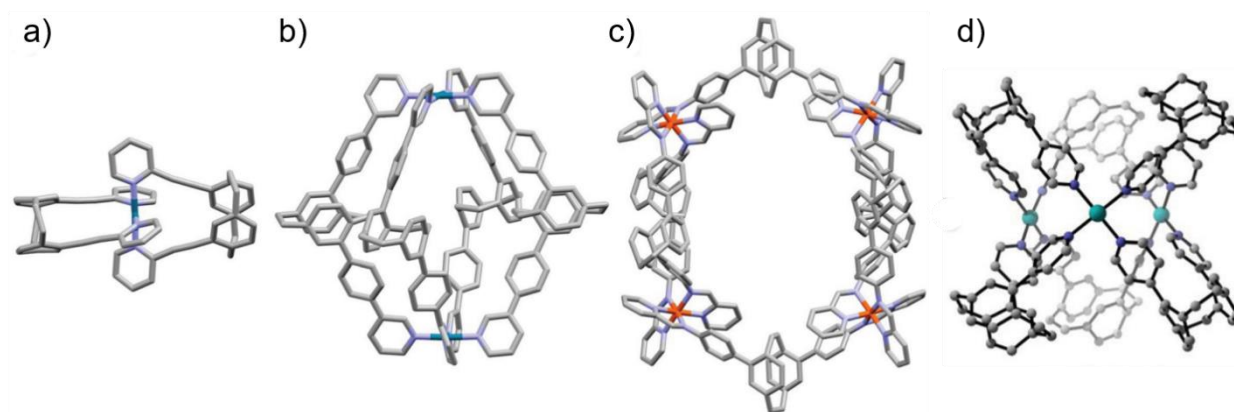


Figure 15. Illustration of the X-ray crystal structures of (a) Pd₂L₂ macrocyclic structure, (b) Pd₂L₄ cage structure, (c) Fe₄L₆ helicate incorporating PCP compounds and (d) Pd₃L₆ supramolecular cage structure. Copyright © 2020, Royal Society of Chemistry.

2 Objective

Among many scientists, Cram started by studying the structure and synthesis of PCP and gradually went deeper, interestingly, he won the Nobel Prize for the definition of supramolecules at a later stage.^[48a] It is all fantasy, from the covalently bonded molecule PCP to the non-covalently bonded supramolecule, with a seemingly unbridgeable gap and a coupled connection. Supramolecules, now defined as existing beyond molecules, have also become an entirely new field and have developed various applications in materials and biology. Cram's research has transcended from molecules to supramolecules, completing its achievements and laying the foundations for future generations, which fully demonstrates the fascination of chemistry, both in terms of transcending all that is shown to the world.

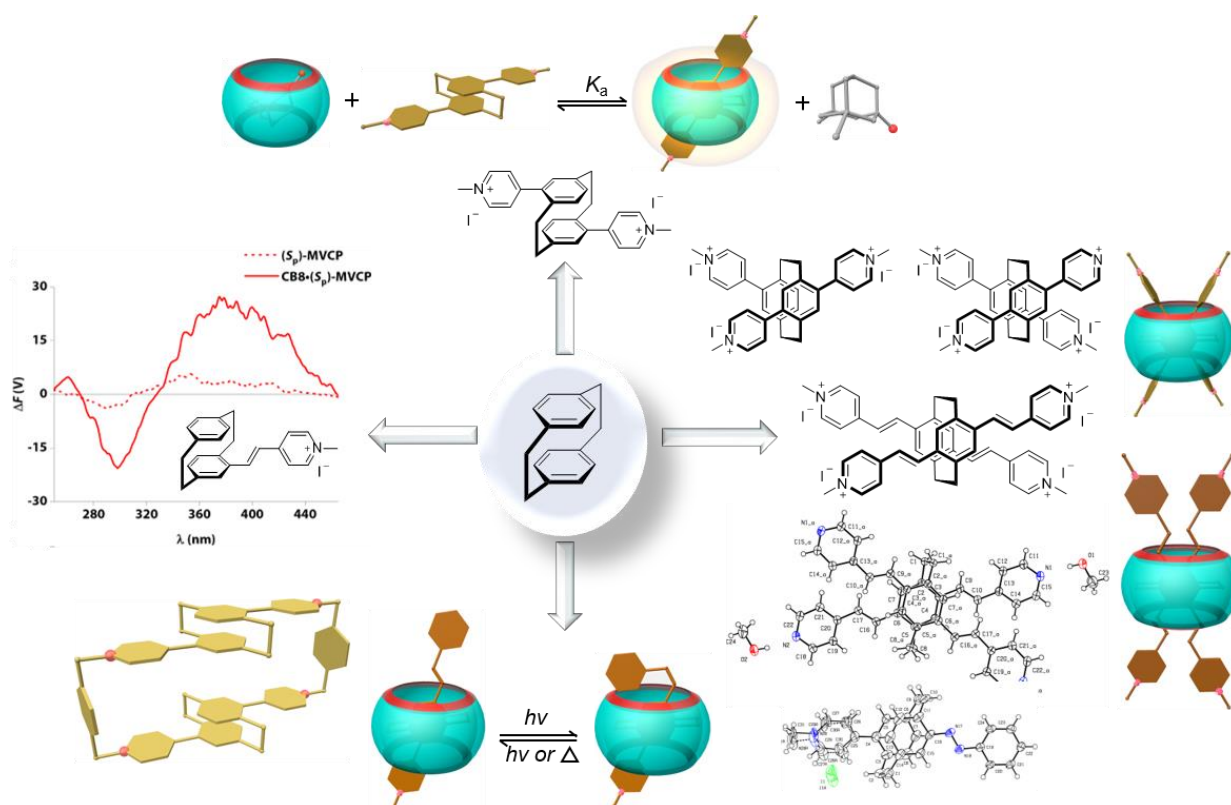


Figure 16. Projects of this thesis for the investigation of supramolecular arts based on [2.2]paracyclophane.

This thesis begins with the modular synthesis of customized PCP derivatives and their potential application in the field of supramolecular systems. PCP, thanks to its suitable molecular conformation, was reported that exhibits excellent binding properties when combined with the macrocyclic subject CB8.^[34] At the same time, because of the variety of substitution patterns, PCP can be used to obtain different regular structures or *p*-asymmetric derivatives, which have the potential to lead to function-inspired supramolecular structures.

In this study, a series of guests capable of binding to CB8 were synthesized, taking full advantage of the multi-location modifiability of the PCP. The project showed a high level of binding ability to CB8. The symmetry of the PCP structures and the planar chirality of the substituents also influenced their binding affinity to CB8, making PCP a promising guest for the host-guest supramolecular systems. The goal is to

conclude a theory for optimizing the PCP structure by studying the binding state of the various derivatives of PCP to CB8. Another aspect of chirality and preparing enantiomerically pure supramolecular systems was aimed at chirality recognition and sensing applications.

Moreover, due to the distinctive structures of PCP, more characteristic compounds have been synthesized for supramolecular applications. The study of a wider variety of supramolecular assemblies will contribute to a better in-depth understanding of the interplay of intermolecular non-covalent interactions as controlling forces in molecular engineering that might find applications in developing technologically sound systems.

3 Main Section

3.1 Exploration of Affinity Study Using Functional [2.2]Paracyclophane Derivatives

Supramolecular sensing aims to find cost-effective and rapid detection methods in medicine. Regular monitoring of drug levels in a patient's blood during drug therapy can be of great help to medical staff in assessing the condition. Therefore, various sensing systems must be tested to adapt to the detection of body fluids in different environments in the human, which places great demands on the choice of artificial receptors.^[58, 117] For the Alzheimer's disease drug memantine (Mem), the relevant plasma concentrations range between 0.03 and 1 mM, which means that the worker receptor has to have a binding K_a to the analyte to be tested in serum of at least 10^6 M^{-1} .^[118] Within the many hosts that have been reported, CB7 and CB8 are among those known to bind strongly to memantine. Only for CB8, few single molecules show strong binding because of its large cavity, Mem has shown considerable affinity, and its $\log K_a$ is up to 12.9.^[119] In contrast, **MPCP (38)**, the member of the PCP family, has been shown for the first time to bind strongly to CB8 and to have utility for memantine sensing in serum (**Figure 7**).

This subchapter, therefore, intends to synthesize PCP-derived dyes and to determine their binding state to CB8.

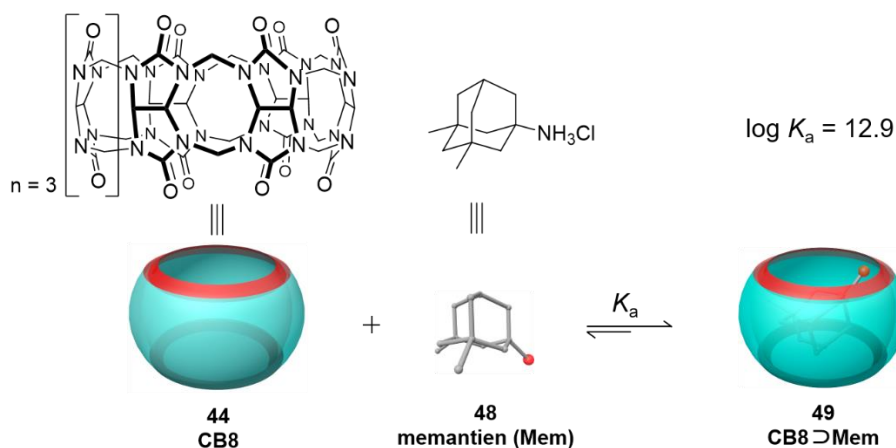


Figure 17. Schematic diagram of the generation of CB8⊃Mem

3.1.1 Molecular Design and Synthesis.

Since **MPCP** is an *N*-methyl pyridyl substituted PCP, the charged pyridyl has a stronger affinity to the oxygen atoms when bound to the CB8, while the PCP core remains in the cavity of the CB8. Therefore, two groups of molecules were designed employing various synthesis methods (**Figure 18**), one with the *N*-methyl pyridyl directly attached to the PCP substitution like **MPCP** and the other with an alkene bond between the pyridine and the PCP, which maintains conjugated electron transfer and allows for an increased

distance between the charge and the PCP core. Both molecules contain one-fold and two-fold charge structures detect the link between the number of charges and the bonding force.

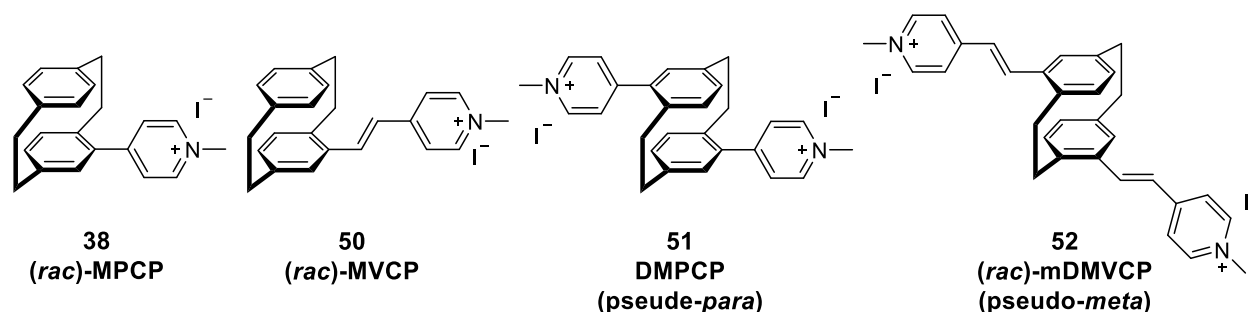
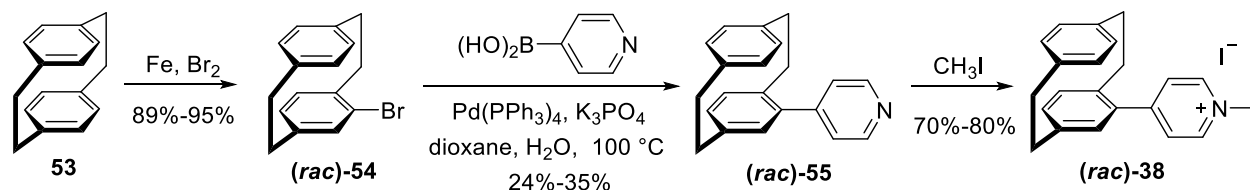


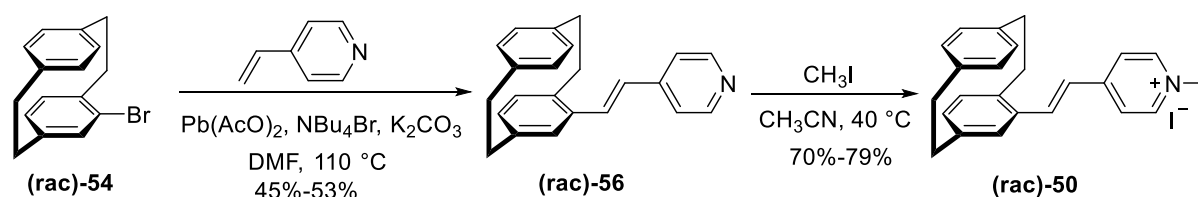
Figure 18. Chemical structures of **MPCP (38)**, **MVCP (50)**, **DMPCP (51)**, and **mDMVCP (52)**. (Hereafter this section will be referred to as **DMVCP (52)**).

The first compound was published by our group in a previous research paper and described as the first demonstration of a PCP derivative combined with CB8. Toward this end the iron-catalyzed bromination of [2.2]paracyclophane (**53**) gives monosubstituted 4-bromo[2.2]paracyclophane (**54**), then the palladium-catalyzed Suzuki-Miyaura cross-coupling reaction gives 4-pyridinyl[2.2]paracyclophane (**55**), and finally on reaction with iodomethane gives the corresponding final product **MPCP (Scheme 7)**. The product of each step of this reaction is racemic, and obtaining the enantiomerically pure isomer requires chiral HPLC for separation.^[34]



Scheme 7. Synthetic route for (*rac*)-4-(*N*-methyl-4'-pyridinium)[2.2]paracyclophane iodide (**MPCP 38**).

The second monosubstituted compound **MVCP (50)** was obtained starting from 4-bromo[2.2]paracyclophane as the primary material, followed by a palladium-catalyzed Heck reaction to give the vinyl pyridine substituted PCP, and finally the addition of methyl group to *N*-pyridine (**Scheme 8**). Product **56** was confirmed by single crystal X-ray analysis (**Figure 19**). This product remains racemic and one method of accessing the pure enantiomer is using chiral HPLC, introducing an alternative method of obtaining the chiral precursor directly.



Scheme 8. Synthetic route for (*rac*)-4-(*N*-methyl-4'-pyridinium-(*E*)-vinyl)[2.2]paracyclophane iodide (**MVCP 50**).

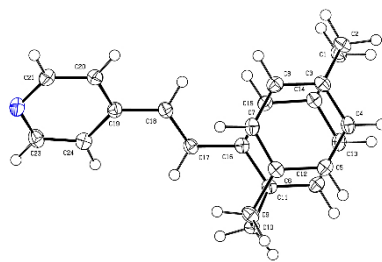
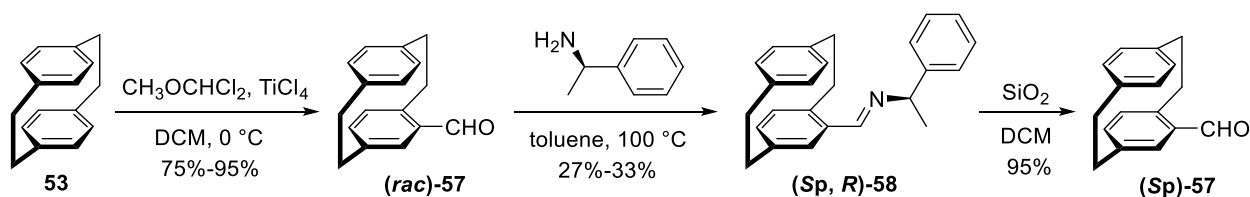


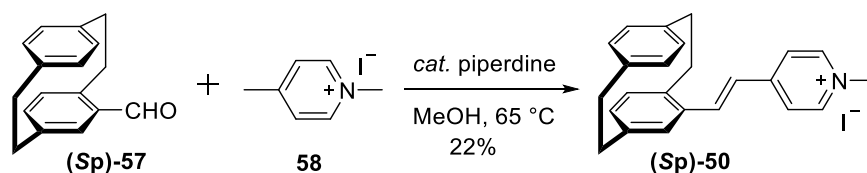
Figure 19. Single Crystal X-rays molecular structure of 56 drawn at 50% probability level. Dr. Martin Nieger provided the result.

First [2.2]paracyclophane was acylated with dichloromethoxymethane under titanium tetrachloride, a strong Lewis acid, to form (*rac*)-4-formyl[2.2]cyclophane ((*rac*)-**57**). It was then reacted with the chiral reagent *R*-(+)-phenylethylamine to produce a chiral intermediate which was separated from the pure enantiomer by fractional crystallization and then reduced to (*Sp*)-**57** in a weakly acidic environment (**Scheme 9**). This method has been reported previously by Bräse *et al.*,^[120] and recently Zippel and colleagues in our laboratory have developed new separation methods that can be performed on a multigram-scale; two separate isomers can be easily obtained.^[39]



Scheme 9. Synthetic route for (*S_p*)-4-formyl[2.2]paracyclophane (**57**)

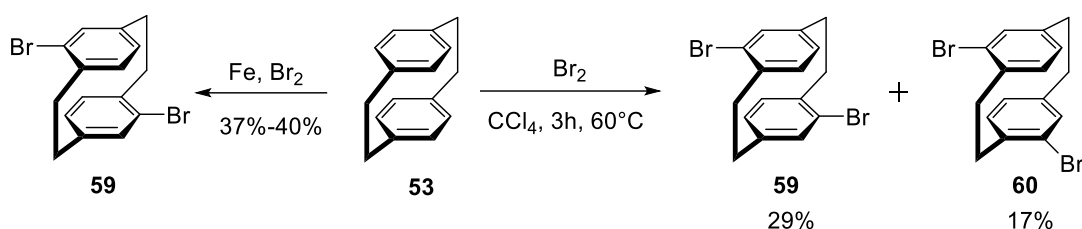
The (*S_p*)-MVCP was thus obtained in one more step, since the precursor was enantiomerically pure, and the product was still enantiomerically pure after the Knoevenagel condensation with piperidine as catalyst in methanol (**Scheme 10**). Because this reaction produced a small number of by-products, it required further purification by column (silica, dichloromethane/methane, 20/1). This nucleophilic addition reaction occurred readily and in high yield, but due to the more polar product, a large polar solvent is required to elute the product out and product loss remained a synthetic challenge.



Scheme 10. Synthesis of (*S_p*)-MVCP **50**.

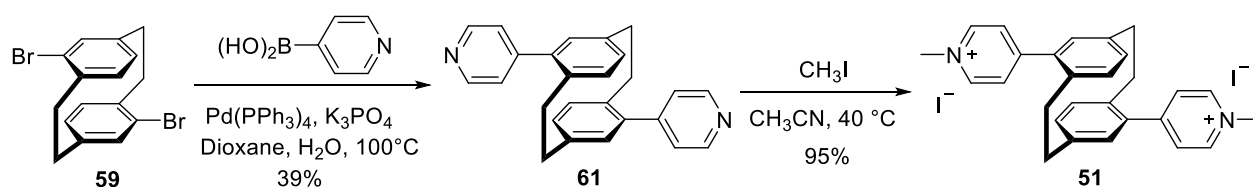
The dibromo substituted PCP product differed depending on the conditions and results; here, the pseudo-para and pseudo-meta isomers were required. The reaction of PCP and bromine in carbon tetrachloride solution produced two main products, which could be obtained by stepwise washing and crystallization.^[121]

The method is similar to monosubstituted PCP, also using iron as a catalyst, with the difference that the reaction time has increased. This gave a more homogeneous product mainly, which has been reported.



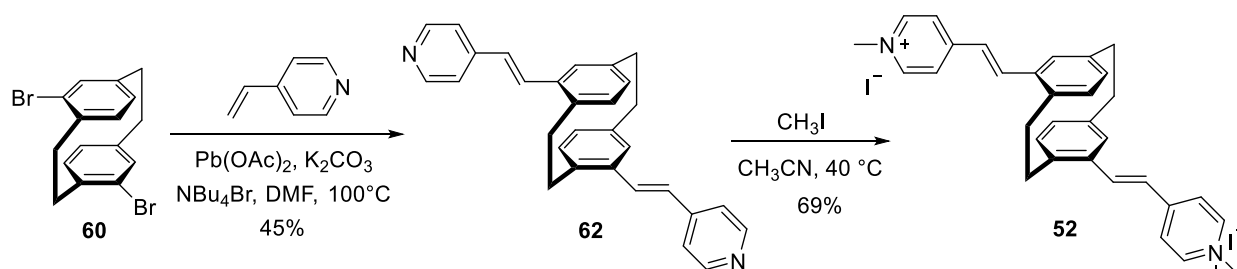
Scheme 11. Synthesis of disubstituted PCP by bromine, 4,16-dibromo[2.2]paracyclophane (**59**) and (*rac*)-4,15-dibromo[2.2]paracyclophane (**60**).

The third compound was derived from dibromo[2.2]paracyclophane by Suzuki coupling reaction and the intermediate 4,16-dipyridyl[2.2]paracyclophane (**61**).^[122] Braun tested several Suzuki coupling reactions with palladium catalysts and different bases in various solvents and tried the Stille, and Kumada coupling conditions to synthesize various pyridine substituted structures. The target compound **51** was obtained by *N*-methylation as racemic mixture.



Scheme 12. Synthesis route for 4,16-Di(*N*-methyl-4'-pyridinium)[2.2]paracyclophane iodide (**DMPCP 51**).

The Heck reaction produced the fourth compound, followed by the *N*-methylation of 4,15-dibromo[2.2]paracyclophane as the starting material. Because the initial brominated PCP was racemic, the end product obtained was also racemic. They were not further separated here because there was no significant difference in the binding constants of the assay with CB8.



Scheme 13. Synthesis route for (*rac*)-4,15-Di(*N*-Methyl-4'-pyridinium-(*E*)-vinyl)[2.2]paracyclophane iodide (**DMVCP 52**).

3.1.2 Basic Affinity Analysis.

3.1.2.1 DFT Calculation and Chemical Characterization

DFT calculations were carried out utilizing the hybrid functional B3LYP with the standard valence basis set 6-31G(d,p) for C,H,N and O. DFT model showed all PCP cores in CB8 cavities with branched chains extending at an angle to the outside (**Figure 20**).

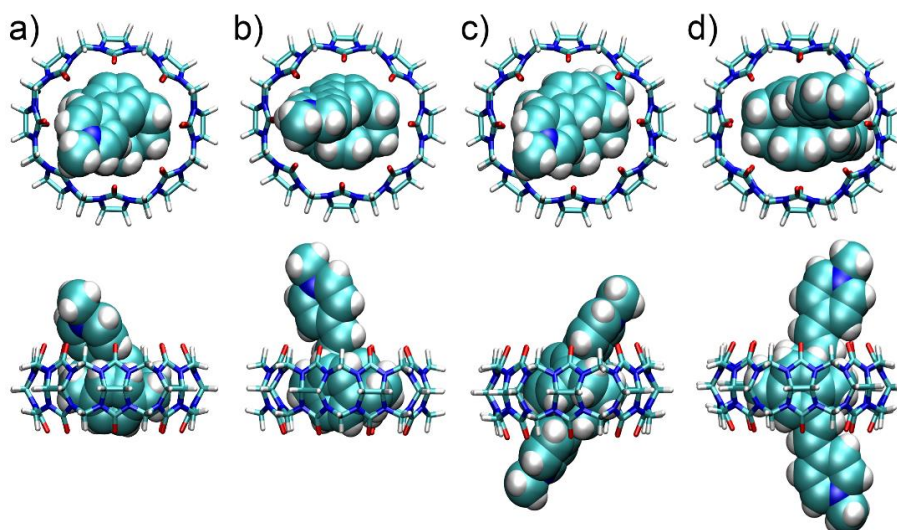


Figure 20. DFT calculations of top and side of the complex structures: (a) **CB8**⊃**MPCP** (**63**), (b) **CB8**⊃**MVCP** (**64**), (c) **CB8**⊃**DMPCP** (**65**) and (d) **CB8**⊃**DMVCP** (**66**). Sebastian Spicher provided these results in the frame of our ongoing research cooperation.

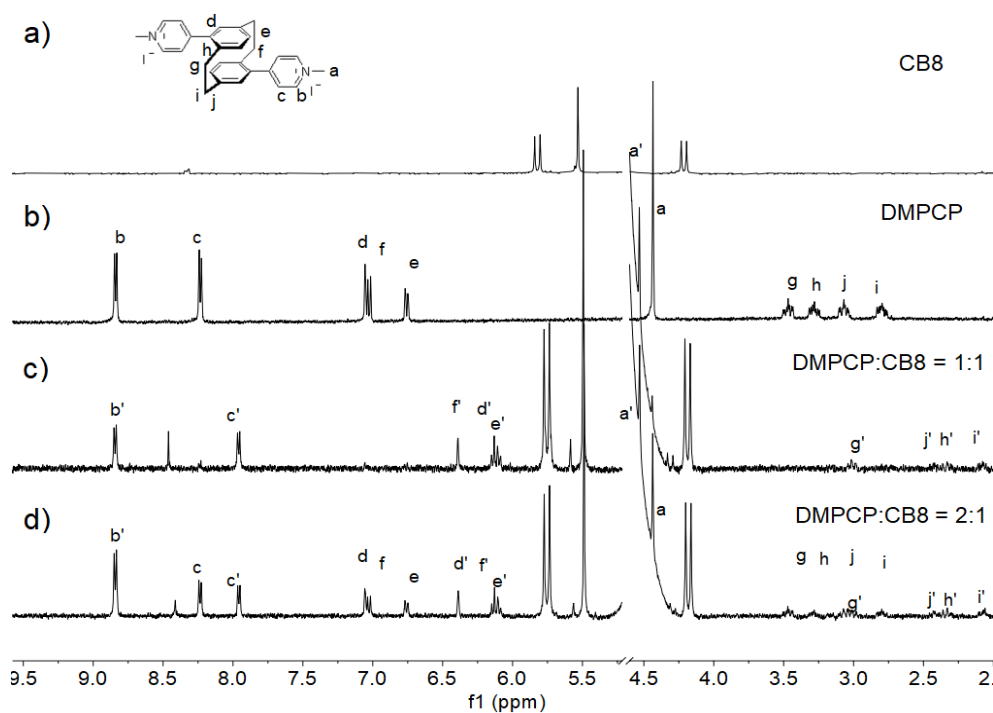


Figure 21. ^1H NMR spectra recorded (400 MHz, D_2O , r.t.) for (a) **CB8** (50 μM) (b) **DMPCP** (400 μM), (c) a mixture of **CB8** (125 μM) and **DMPCP** (125 μM), (d) a mixture of **CB8** (125 μM) and **DMPCP** (250 μM). Primed (') resonances arise from the **CB8**⊃**DMPCP** complex.

When the guest and host are combined, the corresponding ^1H NMR changes significantly, thanks to the special structure of CB consisting of the polar molecules of O and N hetero atoms. The CB resembles the distribution of benzene rings in terms of magnetic anisotropy. Inside the cavity, the induced magnetic field causes the hydrogen nucleus resonance peaks to move in the direction of the higher magnetic field, leading to a shielding effect and a decrease in chemical shift. Conversely, a magnetic field when hydrogen nuclei are located outside the CB or at the edge, the magnetic field creates a deshielding effect and an increase in chemical shift.

In the case of **DMPCP**, when **DMPCP** and CB8 are combined, varying degrees of shifts of protons H^c to H^j are observed towards the up field (**Figure 21**). The protons H^d to H^j in the core of **DMPCP** are shifted by about 0.6 ppm to the center of the CB8 cavity, while smaller 0.2 ppm shifts the proton H^c . In contrast, the proton H^b of the pyridyl group is not significantly shifted, while the proton H^a of methyl group is shifted to the lower field, indicating that it is in the deshielded region of the CB8. Combined with the DFT model (**Figure 20 c**), it can be verified that the **DMPCP** is at an angle to the CB8 axis, thus causing the pyridyl group to be right at the edge of the CB8 macrocycle; meanwhile, such change in proton H^b and H^c , while the methyl is further away from the CB8 central axis.

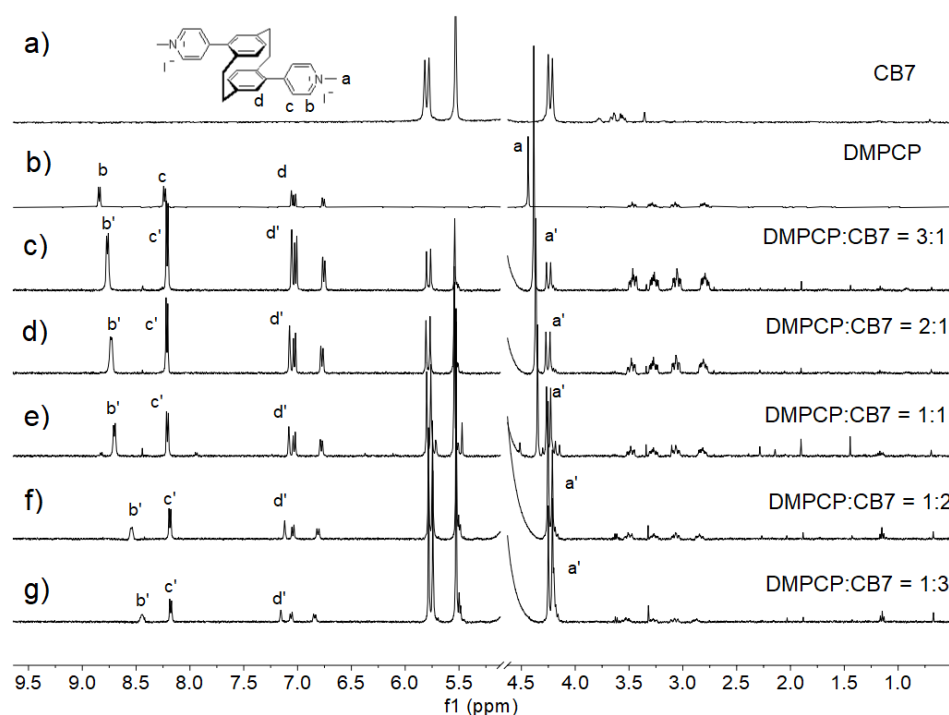


Figure 22. ^1H NMR spectra recorded (400 MHz, D_2O , r.t.) for (a) CB7 (200 μM), (b) **DMPCP** (250 μM), (c) a mixture of **DMPCP** (180 μM) and CB7 (60 μM) = 3:1, (d) a mixture of **DMPCP** (160 μM) and CB7 (80 μM) = 2:1, (e) a mixture of **DMPCP** (125 μM) and CB7 (125 μM) = 1:1, (f) a mixture of **DMPCP** (80 μM) and CB7 (160 μM) = 1:2, (g) a mixture of **DMPCP** (60 μM) and CB7 (180 μM) = 1:3. Primed (') resonances arise from **CB7** \rightarrow **DMPCP** complex.

When the concentration of **DMPCP** is twice to that of CB8, it can be observed that the macroscopic presentation is half bound guest and half free at the NMR scale. This binding process is dynamic, but for

DMPCP, the macroscopic result is entirely statistical. It is also evident in the NMR analysis tests that their binding process is very rapid and can reach equilibrium in a short time.

When combined with CB7, **DMPCP** shows a marked difference. As evidence of the absence of significant binding, the ^1H NMR shows that only protons H^a and H^b shift towards the upfield, while the other protons gradually shift towards the downfield (**Figure 22**). This is fully consistent with the **MPCP** pattern already reported, where only the protons H^a and H^b tend to move closer to the central axis of CB7, but cannot fully enter the cavity, while the other protons are in the deshielded region of CB7. As the concentration of CB7 increases, the dynamic shift is more clearly manifested.

As supporting data, the mass spectra were also applied as evidence of the binding of PCP with CB8; here, only **DMPCP** is shown as an example; see 5.2 for additional data analysis. HRMS-ESI (m/z): $[\text{M}-2\text{I}]^{2+}$, calc. for $\text{C}_{76}\text{H}_{76}\text{N}_{34}\text{O}_{16}$, 860.3084/ 860.8101/ 861.3118 (100/82/33); found: 860.3081/ 860.8091/ 861.3102 (100/97/48) (**Figure 23**).

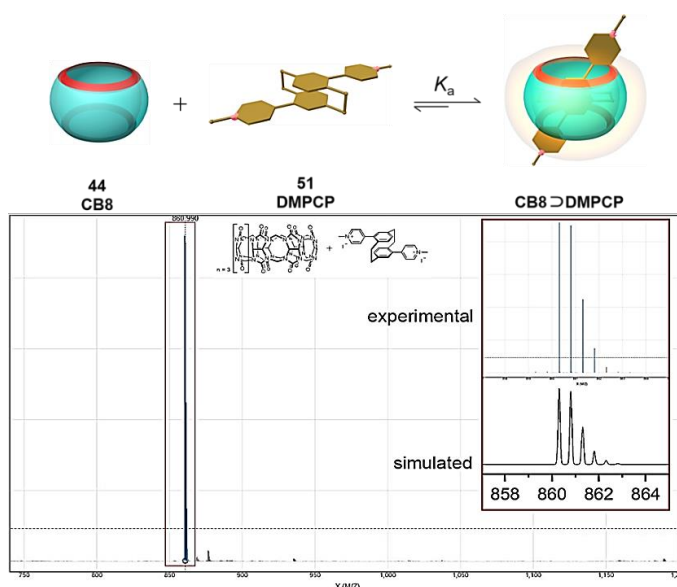


Figure 23. Schematic diagram and mass spectra of **CB8⊃DMPCP**.

DMVCP, an extended structure with longer alkenyl “arms”, shows a marked reduction in the rate of binding rate to CB8, about 48 h required, which is somewhat different from **DMPCP**. This is probably because the longer “arms” is not completely rigid and will wobble to some extent, with some spatial barriers present as the PCP core enters the cavity. As can be seen from the final ^1H NMR, the binding results are complex, leading to confusion of peaks in the aromatic region and the inability to identify proton peaks attribution from the integration (**Figure 24**). It is possible to discern that the protons from the range of alkenyl positions shift to upfield, and the pyridyl protons have shown down field shift, including the methyl ones. These results are also consistent with the DFT model, where the long “arms” of the pseudo-meta substitution are in the *E* configuration while biased in the same direction towards the central axis.

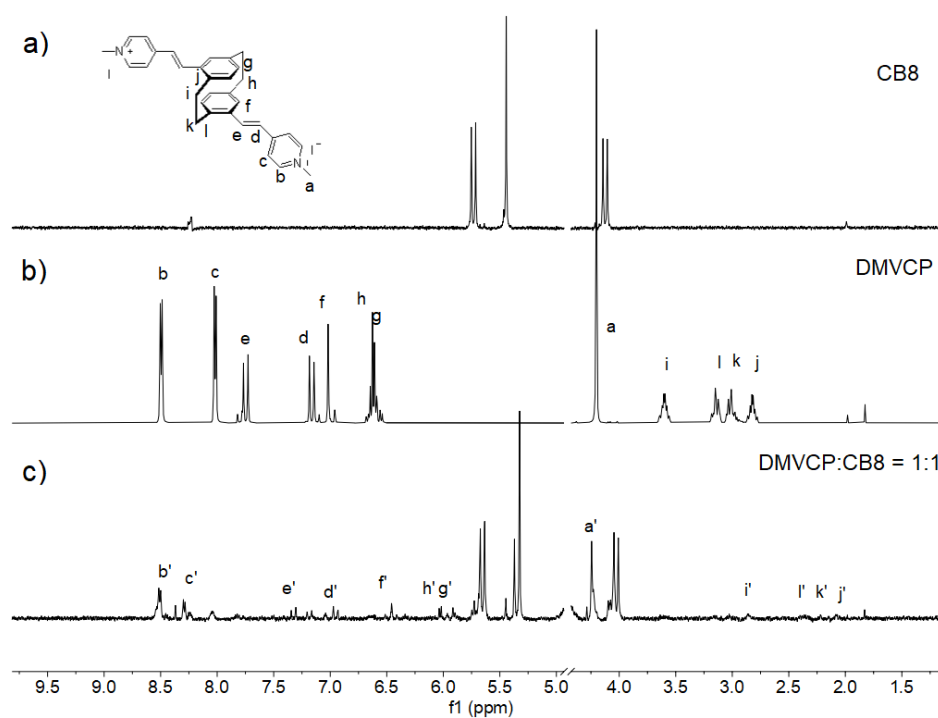


Figure 24. ^1H NMR spectra recorded (400 MHz, D_2O , r.t.) for (a) **CB8** (50 μM), (b) **DMVCP** (400 μM), (c) a mixture of **CB8** (100 μM) and **DMVCP** (100 μM) = 1:1. Primed (') resonances arise from **CB8**⊃**DMVCP** complex.

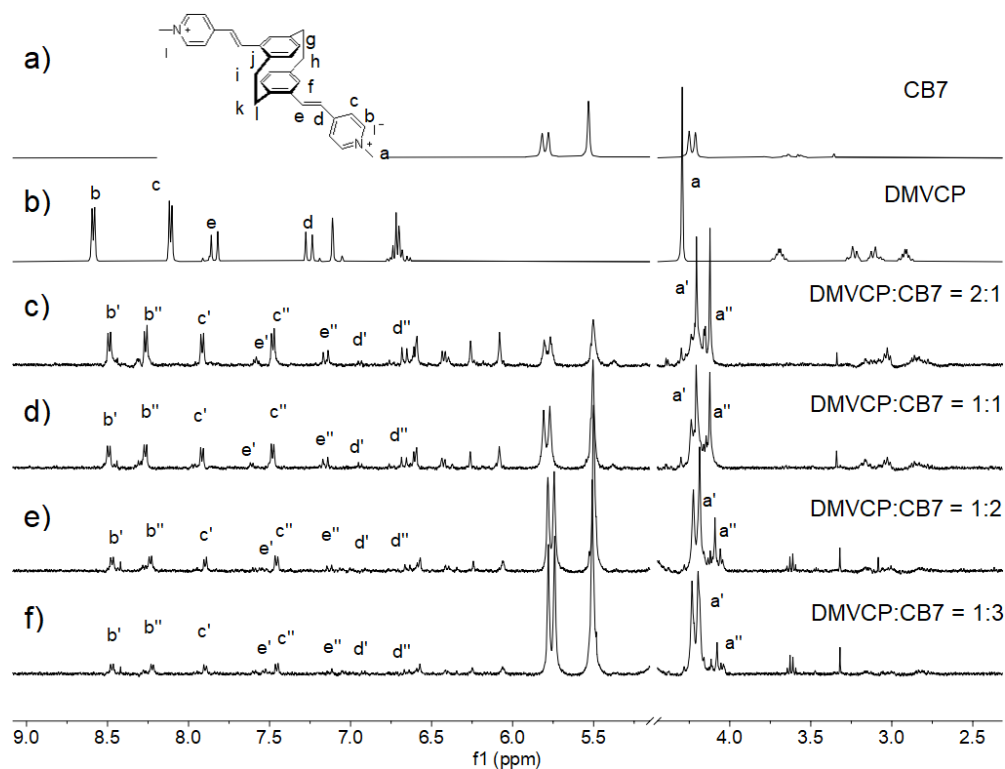


Figure 25. ^1H NMR spectra recorded (400 MHz, D_2O , r.t.) for (a) **CB7** (200 μM), (b) **DMVCP** (250 μM), (c) a mixture of **DMVCP** (160 μM) and **CB7** (80 μM) = 2:1 (d) a mixture of **DMVCP** (125 μM) and **CB7** (125 μM) = 1:1, (e) a mixture of **DMVCP** (80 μM) and **CB7** (160 μM) = 1:2, (f) a mixture of **DMVCP** (60 μM) and **CB7** (180 μM) = 1:3. Primed (') resonances arise from **CB7**⊃**DMVCP** complex.

In contrast, **DMVCP** binds CB7 at a higher relative rate and behaves differently from **DMPCP**. Since the positive charges in the long “arms” are at a longer distance from the PCP core, they exhibit relative stability when bound to CB7, while the protons shifts are fixed and do not drift with increasing CB7 concentration (**Figure 25**). However, the ^1H NMR still presents a complex spectrum that the peaks show an inappropriate degree of splitting. A more convincing explanation is that the two “arms” are in different dynamic binding states to CB7, leading to a splitting of the proton peaks. The PCP core is still not as far into the CB7 cavity as it could be, but the “arms” affects on the protons at the edge of CB7 at 4.1 ppm, and a split has also occurred. Further evidence of the combination is described in the next section.

The available data cannot determine whether two CB7 are bound on the two “arms” of the same **DMVCP**. Single crystal analysis, as it is to be developed, could reveal this mystery.

Other analytical data, also for **MPCP** and **MVCP**, are given at **5.2**.

3.1.2.2 Photophysical Characterization

After the chemical NMR method, then we turned to photophysical studies. Firstly the molar absorption coefficients of PCP dyes were determined in water. The disubstitued PCP (**DMPCP** and **DMVCP**) obtained higher values, respectively, $3.8 \cdot 10^4$, $1.7 \cdot 10^4 \text{ M}^{-1} \text{ cm}^{-1}$, correspondingly the **MPCP** and **MVCP** are $1.2 \cdot 10^4$, $7.3 \cdot 10^3 \text{ M}^{-1} \text{ cm}^{-1}$ (**5.2 Figure 74**). Absorption spectra in aqueous solution showed that these PCP dyes have considerable Stokes shifts. The monosubstituted **MPCP** and **MVCP** have Stokes shifts 200 nm, and the disubstituted, although relatively small, exceed 180 nm. Another result shows that the alkenyl group of **DMVCP** and **MVCP** give molecular larger conjugate components than **DMPCP** and **MPCP**; as a result, the maximum absorption and emission wavelength red shift (**Table 1**). Additional spectral data are detailed in **5.2 (Figure 75 a, Figure 76 a)**.

Table 1. Photophysical characters data of PCP dyes before and after binding with CB8

PCP Dyes	Absorbance maximum		Emission maximum		Enhancement factor
	wavelength (nm)		wavelength (nm)		
	Before binding	After binding	Before binding	After binding	
MPCP	333	341	563	545	4.25
MVCP	385	404	606	556	6.01
DMPCP	321	321	508	486	0.72
DMVCP	388	401	574	536	2.12

The next step is for the state to combine CB with **DMPCP**. The aqueous solution was emissive in the visible area of the electromagnetic spectrum, when 1 *eq.* CB8 was added to the solution changes in absorbance

(0.027 to 0.035) and fluorescence (to I_{max} 508 nm). After 2 eq. CB8 was added, the no more significant change in results (**Figure 26 a**).

Despite the four PCP dyes substituted with similar groups (pyridinium and vinyl pyridinium), they exhibit different spectroscopic properties, even more in combination with CB8. Different dyes show different absorbance, emission and enhancement factor after binding with CB8 (**Table 1**). As we can see, **DMPCP** presents different results from the other three PCP dyes; there is no change in the maximum absorbance. The other three appeared more or less redshifted after binding with CB8. And for fluorescence, **DMPCP** also appeared to be different from the others in that the fluorescence became lower, that is, CB8 can result in fluorescence quenching. Meanwhile it can be seen from the emission enhancement factor that **DMPCP** is 0.72; the others are 4.25, 6.01, and 2.12, respectively. This special nature makes it even more interesting to investigate their combination with CB.

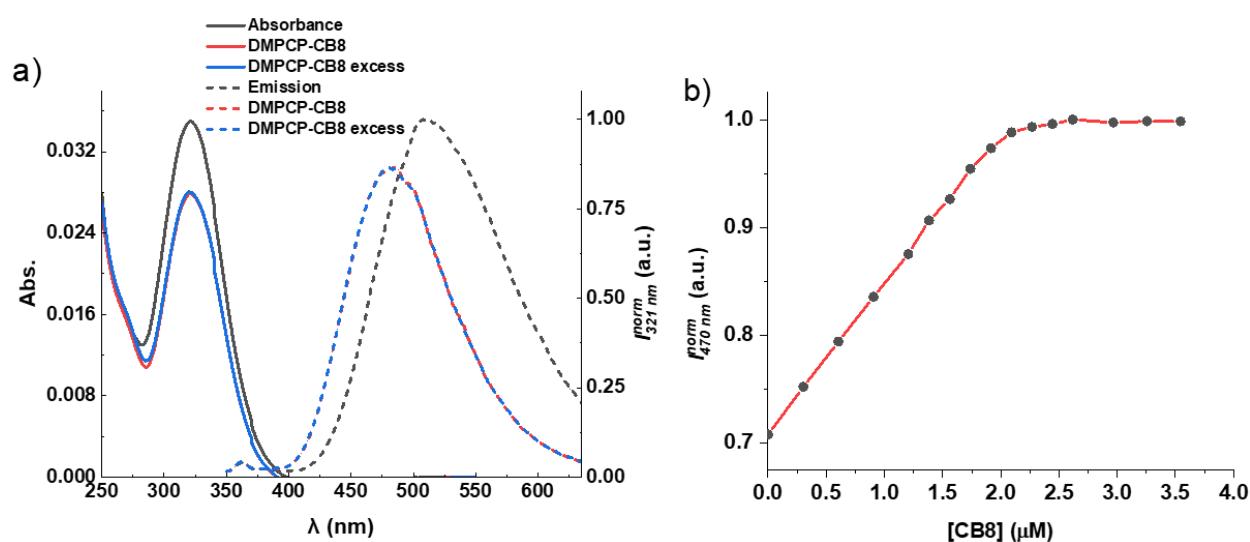


Figure 26. Spectrum of **DMPCP** with CB8 in water: (a) absorbance and fluorescence of pure **DMPCP** (2.08 μM) and addition of CB8 (2.15 μM and 4.11 μM). (b) Fluorescence titration of CB8 by **DMPCP** (2.08 μM). Results provided by Dr. Amrutha Prabodh.

The fluorescence titration curve clearly shows strong **MPCP**-CB8 binding, consistent with the NMR data. Because the four dyes bind very strongly to CB8, the IDA method calculates the binding constants. Whereas their binding to CB7 shows a difference, as also demonstrated by NMR, the binding state is shown in the next section, together with the determination of the binding constants.

3.1.3 Binding Constants K_a Determination

3.1.3.1 K_a Determination by NMR

It has been demonstrated that the combination with CB8 requires a competitive binding assay (CBA); Mem can be used as a competitor after experimentation.

To ensure the equilibrium was established, the prepared deuterated solutions were separately tested at regular intervals, especially for **DMVCP**, which takes four days due to the expansive structure. And to reduce the errors in the NMR spectra, different concentration ratios were tried several times. Take the example of **DMPCP**; in finding a significantly larger binding constant of **DMPCP** than memantine, 4.72 mM memantine solution was chosen to compete with 30.8 μM solution of **DMPCP** (over 100 times more than Mem) to obtain two similar proportions peaks (**Figure 27 a**).

$$K_{\text{rel}} = \frac{[\text{CB8} \supset \text{DMPCP}][\text{DMPCP}]_{\text{free}}}{[\text{CB8} \supset \text{Mem}][\text{Mem}]_{\text{free}}} \quad \text{Eq. 17}$$

$$[\text{CB8}]_{\text{Total}} = 30.8 \mu\text{M} = [\text{CB8} \supset \text{DMPCP}] + [\text{CB8} \supset \text{Mem}] \quad \text{Eq. 18}$$

$$[\text{Mem}]_{\text{Total}} = 4.72 \text{ mM} = [\text{Mem}]_{\text{free}} + [\text{CB8} \supset \text{Mem}] \quad \text{Eq. 19}$$

$$[\text{DMPCP}]_{\text{Total}} = 48.3 \mu\text{M} = [\text{DMPCP}]_{\text{free}} + [\text{CB8} \supset \text{DMPCP}] \quad \text{Eq. 20}$$

Equation 17 was used to determine K_{rel} for the interaction of **DMPCP** and Mem for CB8. For this purpose, A solution containing CB8 (30.8 μM), Mem (4.72 mM), and **DMPCP** (48.3 μM) was prepared and allowed it to reach equilibrium. Next, the relative concentration of **CB8** \supset **DMPCP** was determined and free **DMPCP** by integrating the appropriate resonances in the ^1H NMR spectrum. Using the concentration and the mass balance expression (**Equation 18**) allowed us to calculate $[\text{CB8} \supset \text{Mem}]$ (14.2 μM) and $[\text{CB8} \supset \text{DMPCP}]$ (16.6 μM). **Equation 19** is then used to calculate $[\text{Mem}]_{\text{free}}$ (4.71 mM) using the known value of $[\text{CB8} \supset \text{Mem}]$. Lastly, **Equation 20** is used to calculate $[\text{DMPCP}]_{\text{free}}$ (31.7 μM) using the known value of $[\text{CB8} \supset \text{DMPCP}]$.

Substitution of the values of $[\text{CB8} \supset \text{DMPCP}]$, $[\text{DMPCP}]_{\text{free}}$, $[\text{CB8} \supset \text{Mem}]$, and $[\text{Mem}]_{\text{free}}$ into **Equation 17** gave $K_{\text{rel}} = 173.60$. These determinations were done from independently prepared stock solutions, and the average values were used in the calculations of K_a and the error analysis shown below.

$$K_{\text{CB8} \supset \text{DMPCP}} = (K_{\text{CB8} \supset \text{P1}})(K_{\text{rel}}) \quad \text{Eq. 21}$$

$$K_{\text{CB8} \supset \text{DMPCP}} = 8.63 \times 10^{14} \text{ M}^{-1} \quad \text{Eq. 22}$$

$$\left(\frac{\sigma K_{\text{CB8} \supset \text{DMPCP}}}{K_{\text{CB8} \supset \text{DMPCP}}}\right)^2 = \left(\frac{\sigma K_{\text{CB8} \supset \text{Mem}}}{K_{\text{CB8} \supset \text{Mem}}}\right)^2 + \left(\frac{\sigma K_{\text{rel}}}{K_{\text{rel}}}\right)^2 \quad \text{Eq. 23}$$

$$\frac{\sigma K_{\text{CB8} \supset \text{DMPCP}}}{K_{\text{CB8} \supset \text{DMPCP}}} = 0.1418 \text{ (14.18\%)} \quad \text{Eq. 24}$$

$$\sigma K_{\text{CB8} \supset \text{DMPCP}} = (0.1418) \times (8.63 \times 10^{14} \text{ M}^{-1}) = 1.22 \times 10^{14} \text{ M}^{-1} \quad \text{Eq. 25}$$

$$K_{\text{CB8} \supset \text{DMPCP}} = (8.63 \pm 1.22) \times 10^{14} \text{ M}^{-1} \quad \text{Eq. 26}$$

Substitution of $K_{\text{CB8} \supset \text{Mem}} = (4.97 \pm 0.5) \times 10^{12} \text{ M}^{-1}$ and K_{rel} into **Equation 21** gave $K_{\text{CB8} \supset \text{DMPCP}} = 8.63 \times 10^{14} \text{ M}^{-1}$ (**Equation 22**). The uncertainty in $K_{\text{CB8} \supset \text{Mem}}$ can be determined using **Equation 23**. Substituting $\sigma(K_{\text{CB8} \supset 3})/K_{\text{CB8} \supset 3} = 0.1006$ and $\sigma(K_{\text{rel}})/K_{\text{rel}} = 0.10$ [Note that we are using the even more conservative 10%

error in this analysis] gives the percent error in $K_{\text{CB8}\rightarrow\text{DMPCP}}$ (Equation 24). Substituting Equation 22 into Equation 25 gives $\sigma(K_{\text{CB8}\rightarrow\text{DMPCP}})$ which can be combined with Equation 22 to give a final value for $K_{\text{CB8}\rightarrow\text{DMPCP}}$ (Equation 26).

As the binding of **DMPCP** and CB7 is relatively specific, the previous ^1H NMRs at different concentrations have shown no clear evidence that **DMPCP** can bind to CB7. Further experiments, therefore, demonstrated that after adding a large amount of CB7, a splitting of the single proton peak at CB7 was obtained and the signal peak influenced by **DMPCP** appeared (Figure 27 b). After integration and calculations based on the respective concentrations, the results showed that K_a was beyond the normal binding range and was deemed to be unbound.

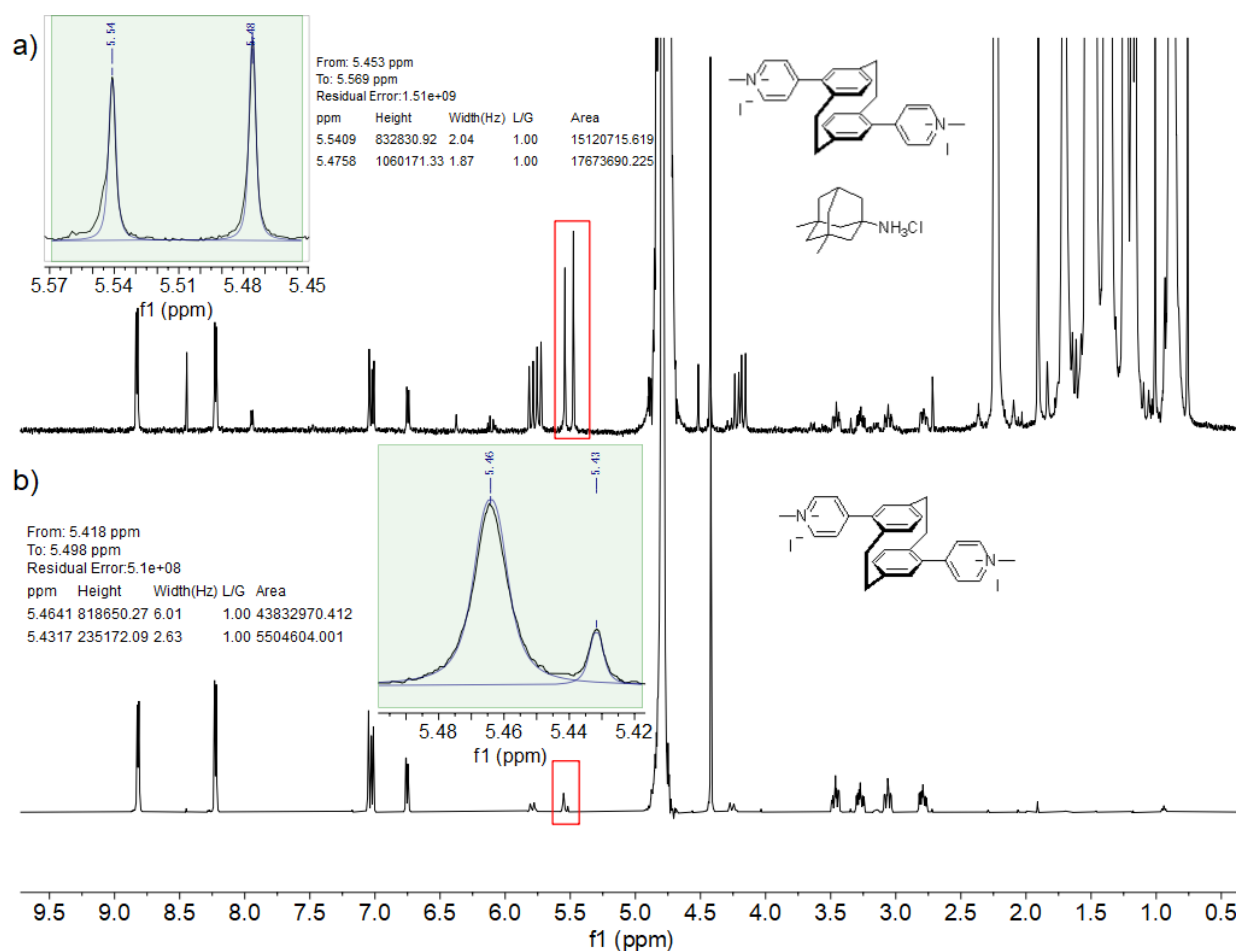


Figure 27. (a) The ^1H NMR spectra (500 MHz, D_2O , r.t.) were used in the CBA determination of K_{rel} for **CB8** \rightarrow **DMPCP** and **CB8** \rightarrow Mem. $[\text{CB8}]_{\text{Total}} = 30.8 \mu\text{M}$, $[\text{Mem}]_{\text{Total}} = 4.72 \text{ mM}$, $[\text{DMPCP}]_{\text{Total}} = 48.3 \mu\text{M}$, $K_{\text{rel}} = 173.60$. (b) The ^1H NMR spectra (400 MHz, D_2O , RT) were used in the DBA determination of K_a for **CB7** and **DMPCP**. $[\text{CB7}]_{\text{Total}} = 79.5 \mu\text{M}$, $[\text{DMPCP}]_{\text{Total}} = 581 \mu\text{M}$.

For the binding constants of **PCP** to **CB8**, CBA calculations were also performed with known values of **MPCP** as another competitor to be a reference; all detailed results are given in 5.2. Binding to **CB7**, as they all have low or no binding constants, were determined directly by fluorescence (FL) titration and given in the next section.

3.1.3.2 K_a Determination by FL

Meanwhile, spectroscopic methods were applied to determine their binding constants to confirm the results' accuracy further. The titration of $\text{CB8} \Rightarrow \text{berberine chloride}_2$ (BC_2) with PCP guests was carried out in water and phosphate buffer saline (PBS) as a basic test of whether an IDA can be set up for the quantification of K_a for PCP dyes. As for **MPCP** and **MVCP**, IDA could be used yet, but for **DMPCP** and **DMVCP** with higher K_a , the curve slope of IDA is no longer enough to measure it accurately; details see 5.2.

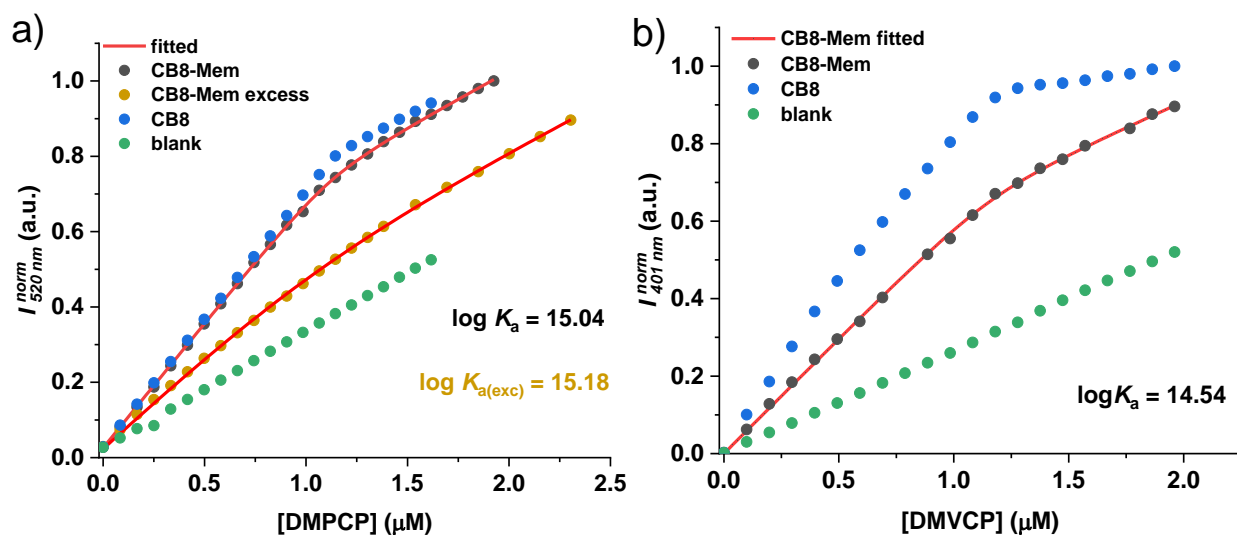


Figure 28. (a) Spectrum of **DMPCP** fluorescence titration by memantine (2.52 μM and excess 49.92 μM) with **CB8** (1.13 μM) in water. $K_a = 1.09 \times 10^{15}$, excess $K_{a(\text{exc})} = 1.50 \times 10^{15}$. (b) Spectrum of **DMVCP** fluorescence titration by memantine (1.18 μM) with **CB8** (1.45 μM) in water, $K_a = (3.49 \pm 0.83) \times 10^{14}$. Results provided by Dr. Amrutha Prabodh.

Then memantine as a guest in IDA was used for the **CB8** \Rightarrow **DMPCP** and **CB8** \Rightarrow **DMVCP** system, but it required a long waiting time due to slow kinetics not reproducible and efficient. Subsequently turned to guest displacement assay (GDA), where the dye was used to displace memantine bound with **CB8**. Compared with IDA, where memantine is used to displace dye, GDA, as a reverse titration method, avoids the drawbacks of IDA, despite that it still spent 24 hours of waiting time to ensure completion of kinetics. There was a clear change in fluorescence intensity when added **DMPCP** gradually during the titration, and the curve presented helpful for the linear fitting of K_a (**Figure 28**). These experiments were performed in the frame of our ongoing cooperation and Dr. Amrutha Prabodh provided the results.

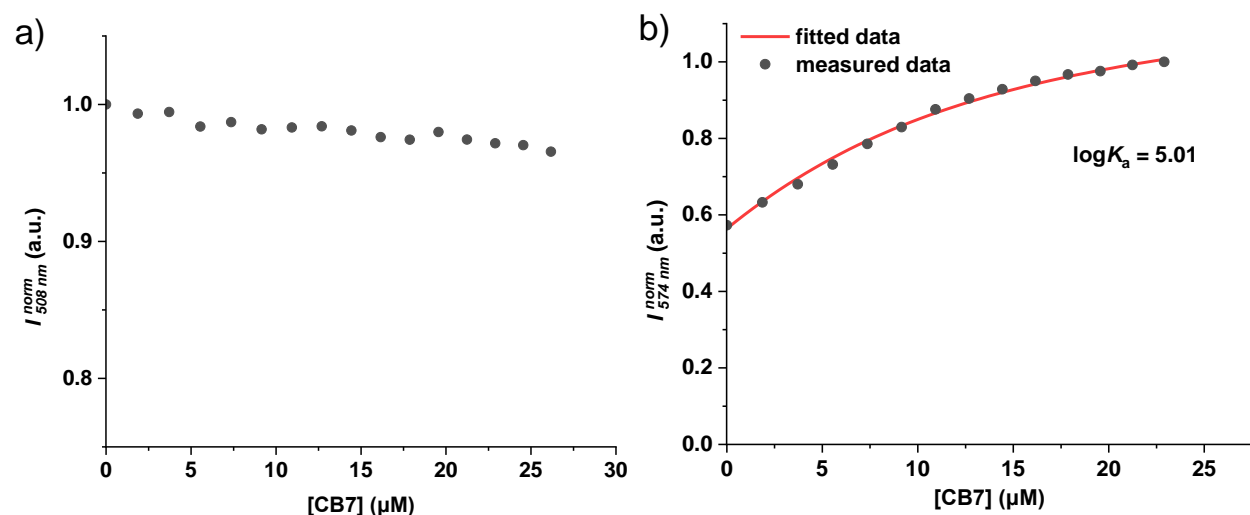


Figure 29. (a) Spectrum of **DMPCP** fluorescence titration by CB7 (375.21 μM) in water, $K_a < 4$, cannot get a fitting. (b) Spectrum of **DMVCP** fluorescence titration by (375.21 μM) in water, $K_a = 1.03 \times 10^5$

A further brief survey was carried out on PCP and CB7. Based on the previous study, **MPCP** has been proved to be able to enter the cavity of CB7, but only pyridine moiety. Then a curious phenomenon emerged on **DMPCP**; whatever NMR or fluorescence spectroscopy, the evidence was obtained that it can not bind with CB7. ^1H NMR of **DMPCP** (0.06 mM) at three times the concentration of CB7 shows that only a small moiety binding with CB; for the detection of fluorescence at the spectral concentration (8 μM), there are essentially no variations. This is probably because there are two positive charges on both sides of **3**, while CB7 can only hover around the edges of the two sides. Compared to **DMPCP**, there are relatively larger K_a of **MVCP** and **DMVCP** with longer “arms” (**Figure 29**).

3.1.3.3 Results

At this point, all the affinity constants results were completed and shown in **Table 2**. In the end a satisfactory result was exciting, *i.e.*, highly coincident spectroscopic K_a values with which in NMR, without doubt, a guest **DMPCP** with whopping K_a up to 10^{15} is rare, **DMVCP** also up to 10^{14} . They are single molecule guests with powerful capabilities of $\log K_a$ reaching 15, which is an important addition to the important host CB8. At the same time, their binding to CB7 is very weak, which makes PCP a more powerful candidate as a sensor thanks to their high selectivity.

From the experimental procedures and results, we can see that the different structures have effects on their binding process. The longer alkenyl pyridine allows longer dynamic binding time; simultaneously, the positive charges closer to the PCP core lead to better interaction with the CB8 portal. As a result, **DMPCP** binds better than **DMVCP**, likewise, **MPCP** better than **MVCP**. On the other hand, two charges give more opportunity for the PCP to approach the CB8 cavity, making them more tightly bound than one charge.

Table 2. Binding constants (K_a , M^{-1}) determined for the interaction between CB hosts and PCP Guests

PCP guest	CB based system	Medium ^[a]	Binding constants K_a	Detection method
MPCP (38)	CB8 \supset BC	water	$(2.33 \pm 0.20) \times 10^{13}$	FL, IDA
	CB8 \supset BC	PBS	$(5.00 \pm 1.10) \times 10^{11}$	FL, IDA
	CB8 \supset Mem	water	$(3.29 \pm 0.95) \times 10^{13}$	FL, GDA
	CB8 \supset Mem	D ₂ O	$(6.90 \pm 0.98) \times 10^{13}$	NMR, CBA
	CB7	water	$< 10^4$	FL, DBA
MVCP (50)	CB8 \supset BC	water	$(9.42 \pm 0.30) \times 10^{12}$	FL, IDA
	CB8 \supset BC	PBS	$(1.68 \pm 0.20) \times 10^{11}$	FL, IDA
	CB8 \supset MPCP	D ₂ O	$(6.20 \pm 0.82) \times 10^{12}$	NMR, CBA
	CB8 \supset Mem	D ₂ O	$(9.70 \pm 1.29) \times 10^{12}$	NMR, CBA
	CB7	water	$(4.66 \pm 0.51) \times 10^4$	FL, DBA
DMPCP (51)	CB8 \supset BC	water	$> 10^{14}$	FL, IDA
	CB8 \supset BC	PBS	$> 10^{13}$	FL, IDA
	CB8 \supset Mem	water	$(1.14 \pm 0.50) \times 10^{15}$	FL, GDA
	CB8 \supset MPCP	D ₂ O	$(2.81 \pm 0.37) \times 10^{14}$	NMR, CBA
	CB8 \supset Mem	D ₂ O	$(8.63 \pm 1.22) \times 10^{14}$	NMR, CBA
	CB7	water	$< 10^4$	FL, DBA
DMVCP (52)	CB8 \supset BC	water	$> 10^{14}$	FL, IDA
	CB8 \supset BC	PBS	$> 10^{13}$	FL, IDA
	CB8 \supset Mem	water	$(3.49 \pm 0.83) \times 10^{14}$	FL, GDA
	CB8 \supset MPCP	D ₂ O	$(6.73 \pm 0.88) \times 10^{13}$	NMR, CBA
	CB8 \supset Mem	D ₂ O	$(3.45 \pm 0.48) \times 10^{14}$	NMR, CBA
	CB7	water	$(1.03 \pm 0.02) \times 10^5$	FL, DBA

[a] water pH 7.0; PBS, phosphate buffer saline, pH 7.4

3.1.4 ITC Measurements and Discussion.

In a typical experiment, an aqueous solution of desalted CB8 was loaded into the cell and titrated with approximately 10x higher concentrated guest solutions prepared from the same deionized water source. **Figure 30** displays representative ITC graphs for the complex formation of four PCP guests with CB8. The binding enthalpy (ΔH) was accurately available from direct titration experiments. The binding constant K_a can be calculated from the slope of the fitted curve (**Figure 14**), but since these constants were out of the normal range of calculation and led to large errors, the binding free energies (ΔG) were calculated based on the K_a data measured by fluorescence. Binding entropic contribution ($-T\Delta S$) was obtained from a relationship $-T\Delta S = \Delta G - \Delta H$ (**Equation 16**) gave all the final data.^[123] Their free energies and enthalpies are quite large, exceeding 17 kcal/mol, and even if the free energy of **DMPCP** exceeds 20 kcal/mol,

enthalpy of **DMVCP** too. Entropy contributions show a pattern, with only **DMPCP** being negative and having longer arms of **DMVCP** showing positive entropy values. This result also confirms that the entropy factor contributes significantly to the overall free energy but is not the main factor. This coincided with the article published by Biedermann; namely, neither London dispersion interactions, nor electronic energies or entropic factors are decisive, selectivity-controlling factors for CB_n complexes.^[124]

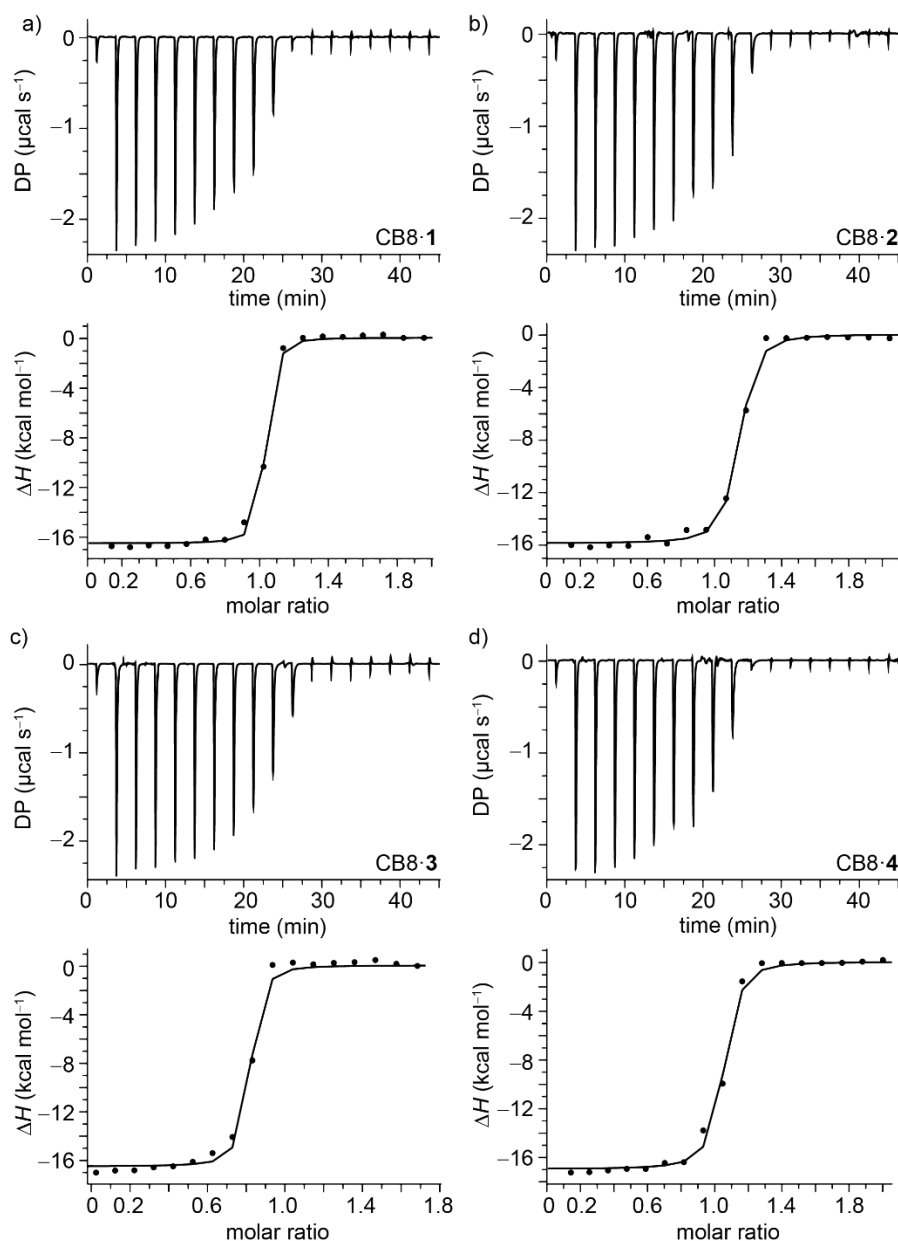


Figure 30. ITC isotherms (dilution heat corrected) for the titration of CB8 ($c = 55 \mu\text{M}$), (a) **MPCP** ($0 - 97.2 \mu\text{M}$), (b) **MVCP** ($0 - 102 \mu\text{M}$), (c) **DMPCP** ($0 - 88.3 \mu\text{M}$), (d) **DMVCP** ($0 - 99.5 \mu\text{M}$) at 25°C . Dr. Laura Marie Grimm performed experiments in the frame of our ongoing research cooperation.

In the following a comprehensive comparison of the binding affinity of CB7 and CB8 for PCPs was made; the data quoted contain guests that only combine the single molecule guest for CB7 and CB8, ignoring double guests or assistant binding guests. An overview of some of the strongest reported binders for CB7 and CB8, mostly positively charged demantoids and ferrocenes and some dyes, are shown in **Figure 32**.^[125]

It can be concluded that for CB7, there are many strong bindings, while for CB8, PCP is the strongest by far. In addition, PCPs have a distinct selectivity for CB8 relative to CB7. For CB8, the number of positive charges and distance from the PCP core are crucial factors in the K_a . In comparison, the longer small moiety is the key for the “arm” bind CB7, but for **DMPCP** and **MPCP** with short “arms” it seems not. The K_a of **DMPCP** was much lower than **MPCP**, although neither had an obvious binding phenomenon. The likely reason is that a symmetrical dipole prevents it from choosing one side to enter the small cavity of CB7 moreover the core of PCP is not short enough to allow both arms to close to the edge of CB7 at the same time. Conversely, in the diamantine scaffold in Isaacs guest design, the two $-NMe_3$ moieties are not symmetrical, so they can optimally engage with both portal regions of CB7 simultaneously.^[126] The same phenomenon is that **DMVCP** with two flexible and bendable “arms” shows greater affinity to CB7 among the PCPs.

Table 3 Summary of the binding parameters for the complexation PCPs guests with declined CB8 in deionized water, 25 °C, determined by ITC. The data was averaged from at least three dilution-heat-corrected experiments.

Host-guest complex	$\log K_a^{[a]}$	$\Delta G_{\text{exp}}^{[b]}$ (kcal mol ⁻¹)	$\Delta H_{\text{exp}}^{[c]}$ (kcal mol ⁻¹)	$-T\Delta S_{\text{exp}}^{[d]}$ (kcal mol ⁻¹)
CB8 \rightarrow MPCP	13.37	-18.3	-17.0	-1.3
CB8 \rightarrow MVCP	12.97	-17.7	-18.2	0.5
CB8 \rightarrow DMPCP	15.06	-20.6	-17.0	-3.6
CB8 \rightarrow DMVCP	14.54	-19.9	-20.6	0.7

[a] binding constants K_a values are obtained by fluorescence titration which is highly coincident with NMR. [b] Calculated from the K_a . [c] Binding constants could not be reliably obtained by direct ITC titrations. But the corresponding ΔH values could be measured accurately. [d] Calculated from the K_a (and derived ΔG) value and the ΔH value given in this table.

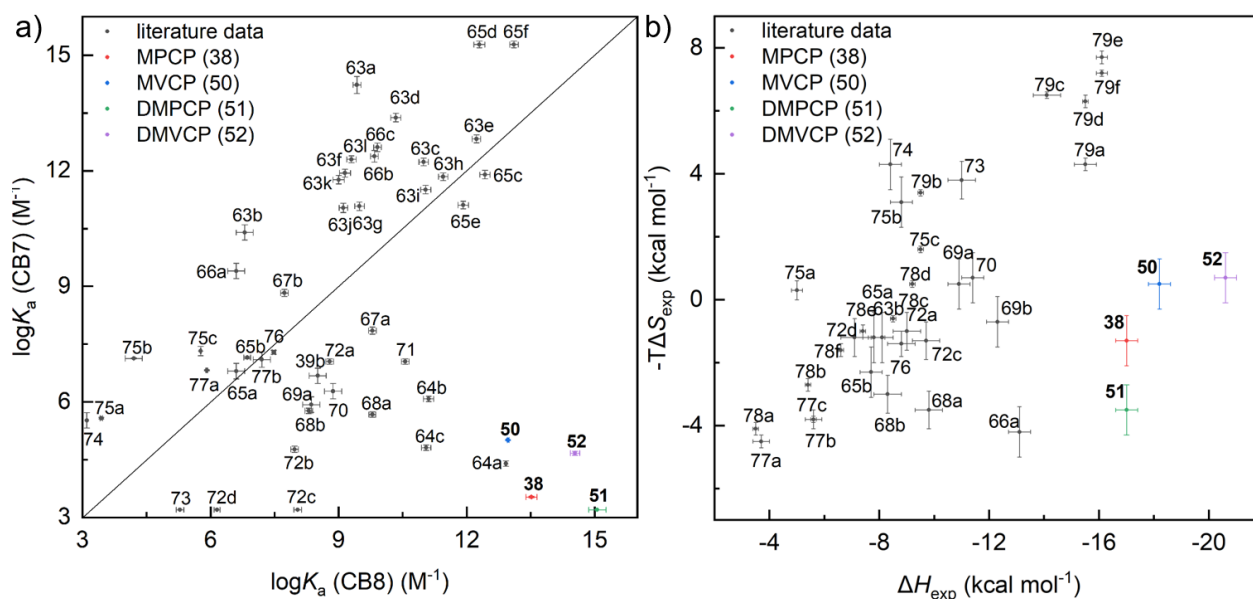


Figure 31. (a) Comparison of binding affinities of CB7 and CB8 for several adamantanes and ferrocene derivatives determined *etc.* that have been published in other papers, the details see **5.6 Figure 32** and

Table 8. [Note: Due to the lower $K_a < 4$ of **DMPCP** and **MPCP**, they are at the bottom of the plot, but does not represent the exact value of the corresponding]. (b) Correlation plot between entropic ($-T\Delta S$) and enthalpic (ΔH) contribution for CB8 literature (grey), and this study (color) affinity binders at $25 \pm 2^\circ\text{C}$ in solution (detailed information about the data origin/data sets is given in **5.6 Figure 32** and **Table 9**).

A literature survey for CB8 complexes for experimental ΔG , ΔH , and $T\Delta S$ binding contributions was analyzed known was analyzed for a more in-depth and intuitive comparison of the affinity scale. The resulting thermodynamic correlation graph included as many binders as possible reported as measured thermodynamic parameters for CB8, as shown in **Figure 31 b**. All CB8 complexes reported in the literature are exothermic but lower than -13 kcal mol^{-1} . Generally speaking, weak binders ($K_a < 10^6\text{ M}^{-1}$) do not reach enthalpic contributions higher than $\Delta H -10\text{ kcal mol}^{-1}$. Strikingly, the guest of maximum ΔH contribution is **DMVCP** up to -22 kcal mol^{-1} ; even the two lowest **MPCP** and **DMPCP** have exceeded all the guests reported in the literature.

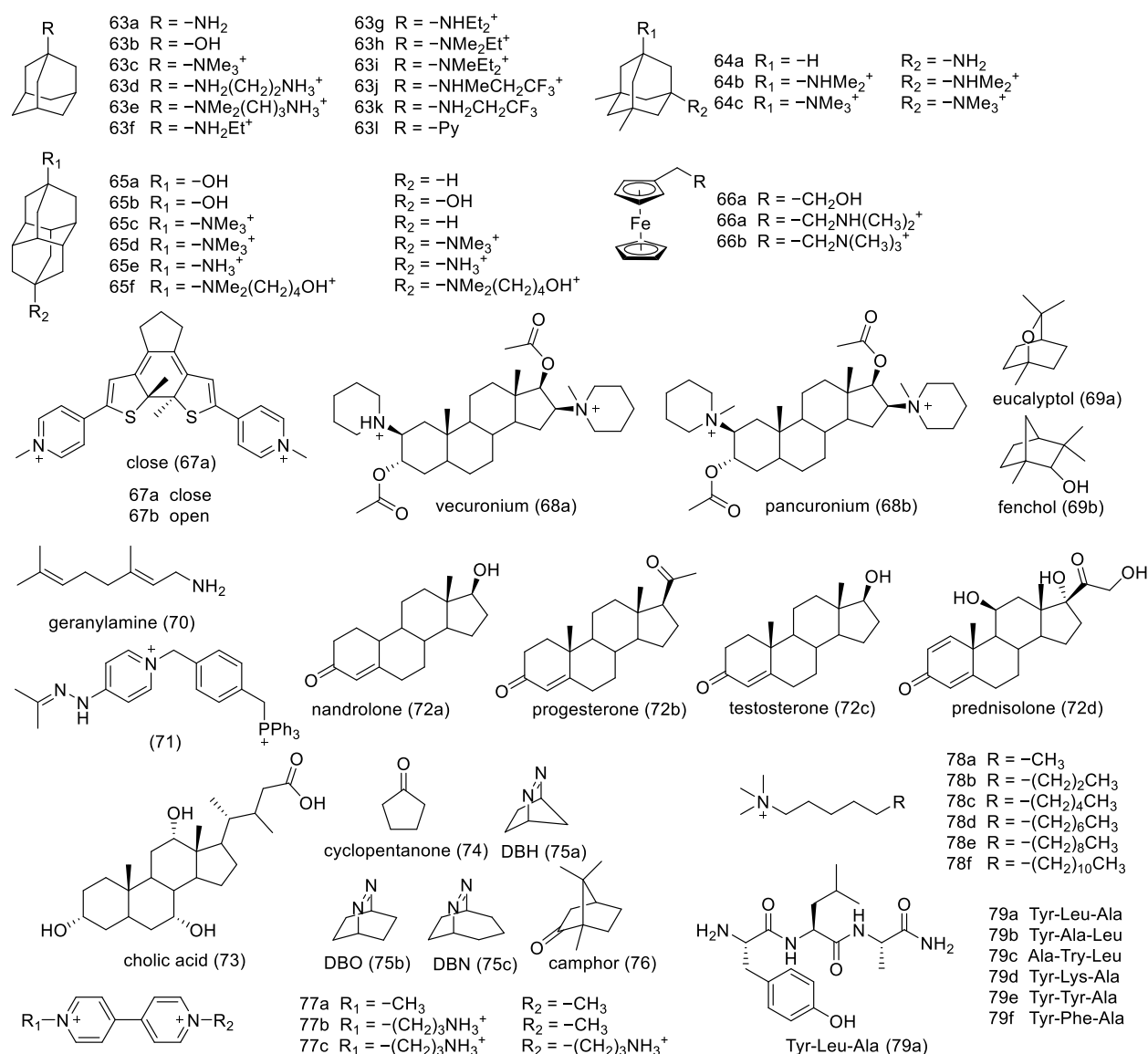


Figure 32. Compounds in literatures, correspond to **Figure 31**, **Table 8** and **Table 9**.

The entropic contributions, $-T\Delta S$, for CB8 complex formation span a narrower range from unfavorable -5 to favorable 8 kcal mol^{-1} , where most examples fall within -5 to 5 kcal mol^{-1} . For PCPs, the largest binding affinities for CB8, exhibit also at a low average level. It is clear that structures **79a-f** are a series of protein molecules with specific sequences and their entropy values are at levels greater than 4 kcal mol^{-1} . In contrast, their binding to CB8 is only average, so there is no direct influence of the entropy value on the binding power for different structural systems. Therefore, the effect of the structure itself on the enthalpy of entropy is variable, and it is challenging to summarise the laws that apply to a class of structures.

3.1.5 Chiral Application of (S_p)-MVCP (50)

For the majority of the compounds synthesized, three of them are chiral, except for **MVCP** which was done as mentioned in **3.1.1**, chiral isolation of **MPCP** has been reported and **DMVCP** was not subjected to chiral analysis. Not only for the complexity of the chiral separation but also because the binding constants are not affected by chirality when studying their properties for binding to the host, only chiral applications are analyzed in this chapter.

Detecting chiral transformations in (bio)chemical systems provides a useful experience for designing drugs and functional materials.^[127] Electron circular dichroism (ECD) spectroscopy, which measures the difference in absorption of circularly polarized light has been widely used to characterize chiral light-absorbing molecules.^[128] Considering that most (bio)chemical compounds of interest lack a strong chromophores group, little ECD signal is produced in the near UV or visible wavelength range, or even not at all. Chromogenic probes and chemical sensing can overcome this challenge.^[129] While **MPCP** has been reported to work as a dye for sensor, it also has certain limitations.^[34] Because **MPCP** becomes generated in HS the signal lies in the same region as the background signal of human blood serum (HS), making it unusable for detection in HS. Therefore **MVCP**, which consists of a vinyl group linking the pyridyl group and PCP, has a larger conjugated structure and has been tested with an absorption band in 350 nm to 450 nm , with an increased red shift of the absorption band compared to **MPCP** by 46 nm .

As expected, (S_p)-**MVCP** shows ECD and fluorescence detected circular dichroism (FD CD) signals without CB8. In addition to CB8, a slight red shift of the ECD and FD CD signals was observed, accompanied by a strong increase in fluorescence intensity and a ΔF signal upon binding to CB8 (**Figure 33**). This red shift uptake of the **CB8** \rightarrow (S_p)-**MVCP** complex may facilitate sensing in serum compared to the **CB8** \rightarrow (S_p)-**MPCP**. Alzheimer's drug memantine detection in serum was evaluated with the help of ΔF and ECD signals. The addition of $20 \mu\text{M}$ **CB8** \rightarrow (S_p)-**MVCP** to HS samples resulted in changes in the ECD and ΔF spectra of HS (the ECD and ΔF signals became positive in the 380 nm to 440 nm region). These signals appear slightly different from the HS background ECD and ΔF signals. When monitored at 407 nm , the gradual addition of the drug memantine to the complex (15 min equilibration time between each addition) decreased in the ECD and ΔF signals of the complex. Thus, ECD and ΔF can be followed by dye

displacement from the CB8 cavity with less interference from the HS background than in the case of **MPCP** as the indicator dye.

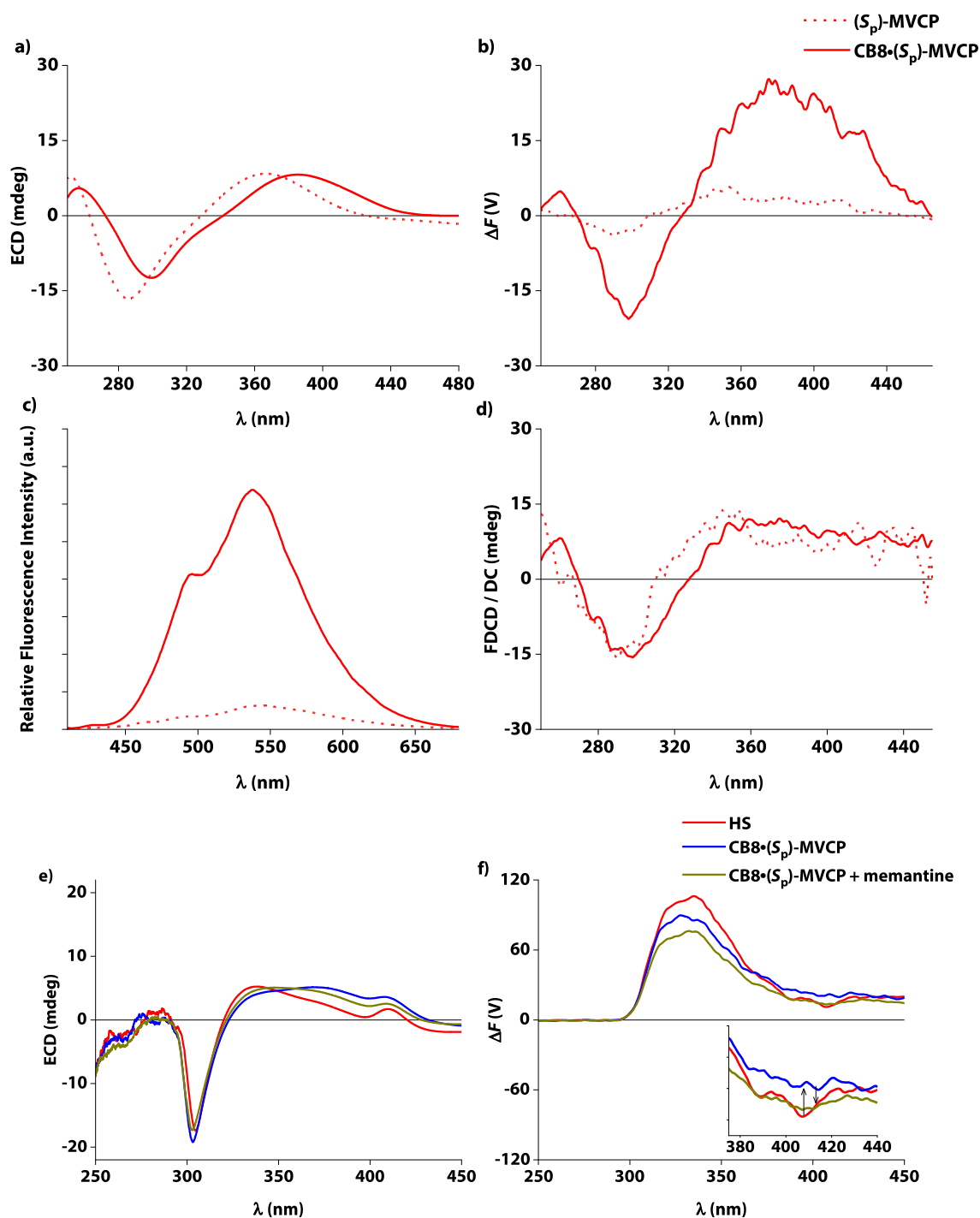


Figure 33. (a) ECD and (b) ΔF spectra of (S_p) -MVCP (45 μ M) in the absence and presence of CB8 (45 μ M) in DI-Water. Parameters used: HT = 800 V, BW = 4 nm, Acc = 20, LP-Filter = 480 nm, T = 25°C. (c) Enhancement in the fluorescence intensity of (S_p) -MVCP (45 μ M) upon addition of CB8 (45 μ M) in DI-Water, λ_{exc} = 400 nm. (d) FDCD spectra of (S_p) -MVCP (45 μ M) in the absence and presence of CB8 (45 μ M). (e) ECD and (f) ΔF spectra of $CB8 \cdot (S_p)$ -MVCP (20 μ M) in HS before and after the addition of memantine (20 μ M). The red line represents the ECD and ΔF background arising from HS alone. Parameters used: HT = 800 V, BW = 4 nm, Acc = 20, LP-Filter = 480 nm, T = 25°C. Results provided by

Dr. Amrutha Prabodh.

3.1.6 Conclusion

In summary, the interaction of four PCPs as a guest was studied with CB8 and CB7 using standard characterization methods of ^1H NMR spectroscopy, fluorescence spectroscopy, and ITC. By studying PCP derivatives binding with CB8, the monomeric structure shows the highest binding affinity to CB8 as a host, in addition to better selectivity for the small cavity of CB7.

Despite some successes in the computational determination of binding affinities of CB_n -guest complexes with simple guests,^[130] there are still many challenges. There are also various factors influencing the affinity for CB7 and CB8, direct host-guest binding interactions, London dispersion interactions^[131] and electronic energies, also including the entropic factors measured, and the energetic molecules in the solvent that are important drivers of guest binding.^[132]

Compared to previous structures from the literature, in conjunction with the current entropy-enthalpy law of PCP, the found structures bind CB8 more perfectly than expected. As PCP has more modification sites, better structures can be modified to be ultralight binders,^[119a, 133] while providing more possible applications in supramolecular sensing.

3.2 Exploration of Affinity New Cyclophanyl-derived Extended and Functionalized Chromophores

In our preliminary explorations, the [2.2]paracyclophane has been certificated a great affinity guest to CB8 macrocyclic host, encouraging an expansion of the range of applications. We elaborated to enhance/modulate sensing properties via host-guest supramolecular binding affinity of CB8 toward guests based on a series of new PCP derivatives including (MPCP, MVCP, pseudo-*para* DMPCP, pseudo-*meta* DMVCP). Three sensing strategies direct-binding assays (DBA), indicator displacement assays (IDA) and guest displacement assays (GDA), aided by the computational analysis were performed that exhibit high sensitivity, fast response time and technical simplicity to achieve optical signal transduction.

3.2.1 Exploration of Affinity on Extended [2.2]Paracyclophane Derivatives

3.2.1.1 Molecules Design and Synthesis.

Two structures of four charges were designed with different substitution to explore the effect of positive charges on the strength of the PCPs binding to CB8. Using carefully chosen reaction parameters and transformation steps of regioselective substitution on PCP followed by transition metal catalyzed Suzuki-Miyaura or Heck cross-coupling reactions afford desired PCPs were bearing pyridine and vinylpyridine moieties at peripheries. Representative are provided in **Figure 34**. The tetrasubstituted QMVCP was also targeted at different substitution positions of pyridine to investigate the effect of different positions of the methyl charge on the binding of PCPs.

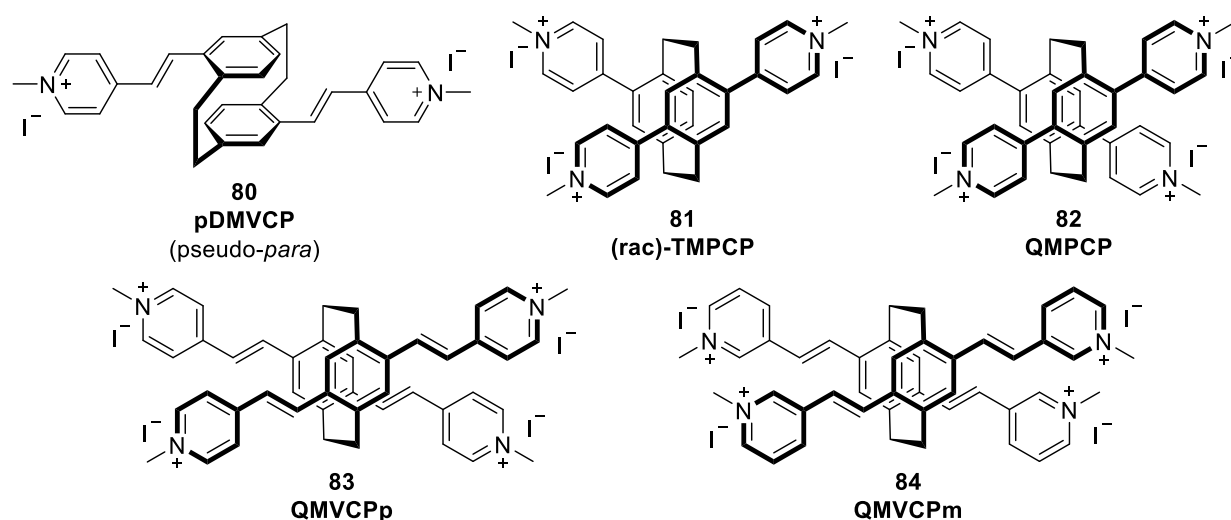
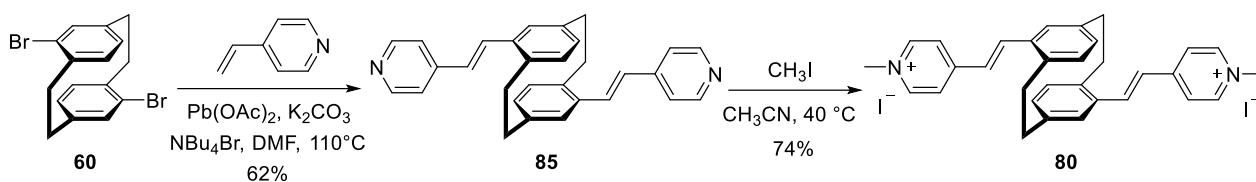


Figure 34. Chemical structures of pDMVCP (80), TMPCP (81), QMPCP (82), and QMVCPp (Hereafter this section will be referred to as QMVCPm) (84).

pDMVCP is a complement to the disubstituted DMVCP group, again using the same synthetic route as mDMVCP, except that the starting material is changed to 4,16-dibromo[2.2]paracyclophane (**Scheme 14**).

The molecular structure of product **85** was confirmed by X-ray analysis in addition to standard characterization methods (**Figure 35**).



Scheme 14. Synthesis route for 4,16-di(*N*-methyl-4'-pyridinium-(*E*)-vinyl)[2.2]paracyclophane iodide (**pDMPCP 80**).

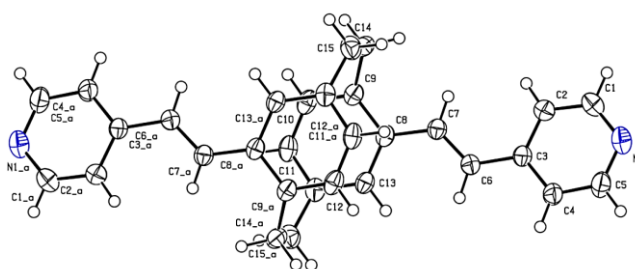
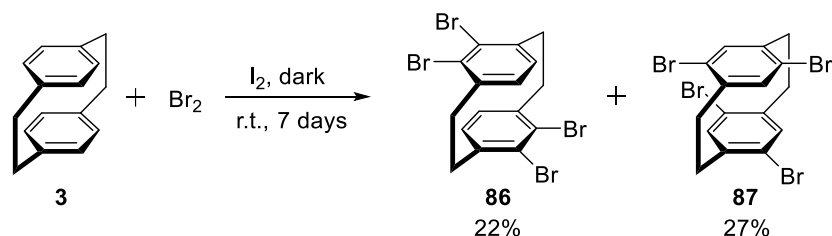


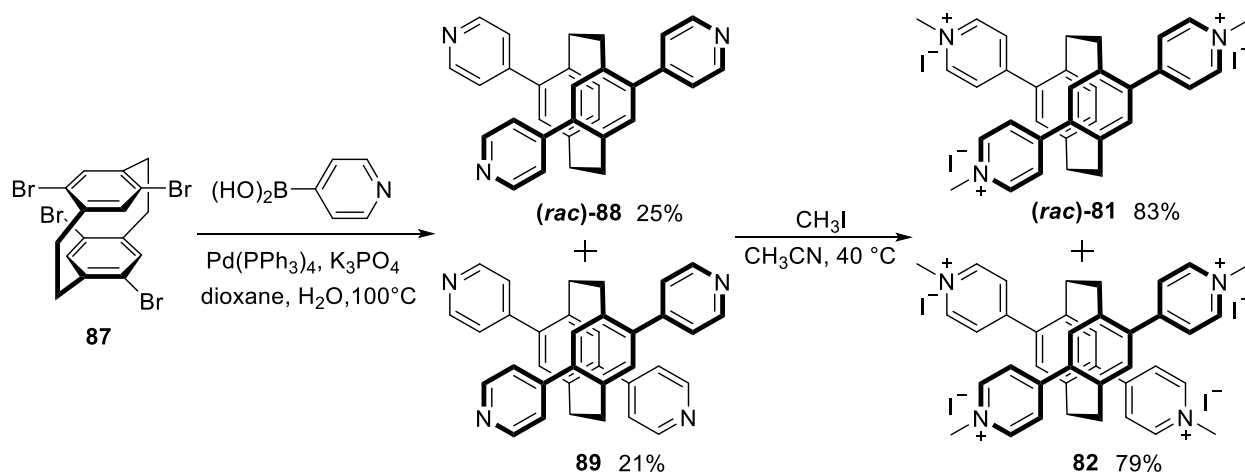
Figure 35 Single crystal X-rays structure of **85** drawn at 50% probability level. Dr. Salma Begum raised the crystal, and Dr. Olaf Fuhr provided the result.

The synthesis of tetrabromo-substituted PCP has been performed following the earlier reported procedure (**Scheme 15**).^[134] The final two products 4,5,12,13-tetrabromo[2.2]paracyclophane (**86**) and 4,7,12,15-tetrabromo[2.2]paracyclophane (**87**), were obtained, respectively, catalyzed by iodine bromination without solvent over seven days.



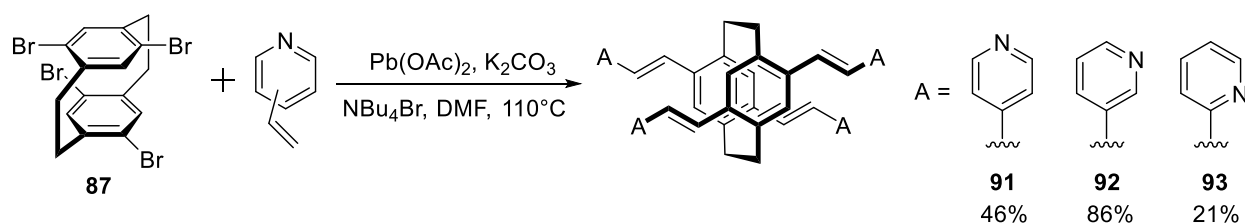
Scheme 15. Synthesis of tetrasubstituted PCP by bromine, 4,5,12,13-tetrabromo[2.2]paracyclophane (**86**) and 4,7,12,15-tetrabromo[2.2]paracyclophane (**87**).^[134]

The next reactions were the Suzuki coupling and Heck reaction employing brominated PCP. 4,7,12,15-tetrabromo[2.2]paracyclophane was used as the starting material for the Suzuki coupling reaction and unexpectedly the tri-substitute (**88**) without bromine was isolated from all the products. The final products were obtained in close to 1:1 yields of trisubstituted and tetrasubstituted PCPs. The tri-substitute PCPs are racemic. The final step was the methylation with iodomethane to give two afford the final products (**81** and **82**) (**Scheme 16**).



Scheme 16. Synthesis route for target PCPs by Suzuki coupling reaction, 4,7,12-tri(*N*-methyl-4'-pyridinium)[2.2]paracyclophane iodide (**TMPCP**, **81**) and 4,7,12,15-tetra(*N*-methyl-4'-pyridinium)[2.2]paracyclophane iodide (**QMPCP**, **82**).

4,7,12,15-Tetrabromo[2.2]paracyclophane was used for the Heck reactions, employing vinyl pyridine in three substituted positions. The different positions of the substituents resulted in various yields under the same reacted conditions, with the highest yielding 86% for the *meta*-substitution (**Scheme 17**). This reason can be explained by the properties of pyridine moiety, which has a lower electron cloud density in the pyridine system than the benzene ring, and is particularly pronounced at position 2 or 4 of the carbon atom. When an electrophilic substitution reaction occurs, it often takes place at position 3, which is the most electron-rich carbon atom in the ring. Thus, the alkenyl terminus of the 3-vinylpyridine was the richest in electrons compared to the other two, which were most readily formed in a complex with a palladium catalyst, so the highest yield was achieved. The physical properties of the three products are slightly dissimilar and will be demonstrated in the next chapter **3.3**. The *para*-substituted PCP structure (**91**) was confirmed by X-ray analysis (**Figure 36**). The crystal was formed by hydrogen bonds linked methanol molecules; once the solution dried out, the crystals would collapse.



Scheme 17. Synthesis of tetrasubstituted PCPs by Heck reaction, 4,7,12,15-tetra(4'-pyridyl-(*E*)-vinyl)[2.2]paracyclophane (**91**), 4,7,12,15-tetra(3'-pyridyl-(*E*)-vinyl)[2.2]paracyclophane (**92**), and 4,7,12,15-tetra(2'-pyridyl-(*E*)-vinyl)[2.2]paracyclophane (**93**).

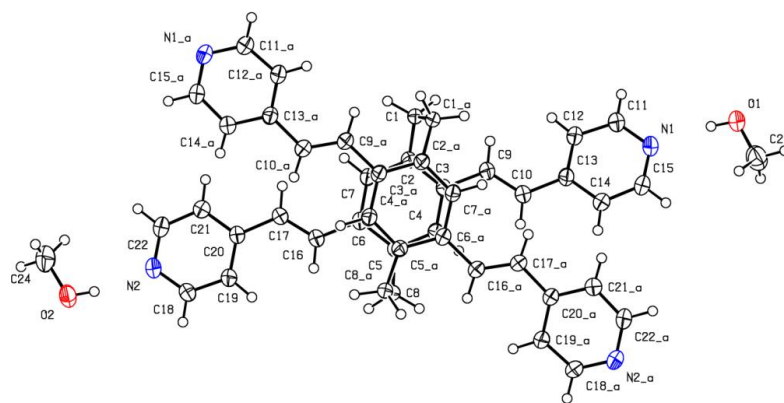
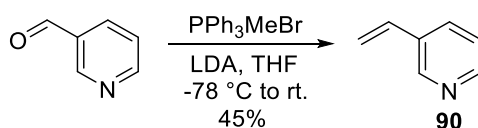


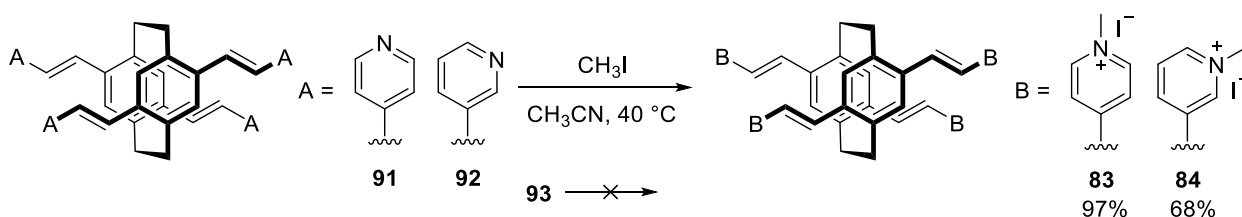
Figure 36. Single crystal X-rays molecular structure of **91** drawn at 50% probability level. Dr. Olaf Fuhr provided the result.

One of the ingredients 3-vinylpyridine (**90**) was formed by Wittig reaction reactions involving LDA under $-78\text{ }^{\circ}\text{C}$.^[135] The product is toxic and bad-smelling, so the next reaction was carried out quickly following purification.



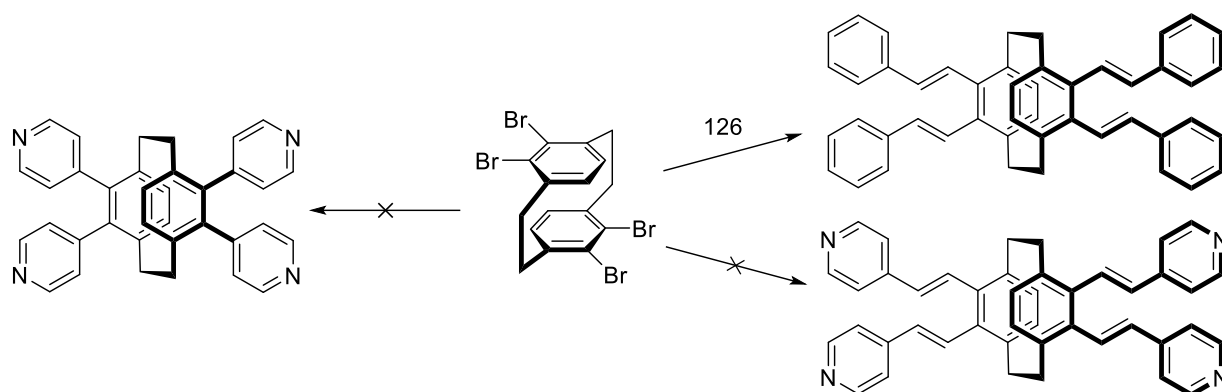
Scheme 18. Synthesis of 3-vinylpyridine (**90**)

For the final step, the methylation of iodomethane, in particular the reaction of the *ortho* structure **93**, was not successful, even when the temperature was raised to $70\text{ }^{\circ}\text{C}$. This is most likely because the four long “arms” created a considerable spatial and energy barrier that prevented the approach of iodomethane.



Scheme 19. Synthesis of target PCPs, 4,7,12,15-tetra(*N*-methyl-4'-pyridinium-(*E*)-vinyl)[2.2]paracyclophane iodide (**QMVCPP**, **83**), and 4,7,12,15-tetra(*N*-methyl-3'-pyridinium-(*E*)-vinyl)[2.2]paracyclophane iodide (**QMVCPM**, **84**).

The synthesis of PCP pyridyl derivatives with 4,5,12,13-tetrabromo[2.2]paracyclophane (**86**) as the starting material was unsuccessful via Suzuki coupling or Heck reactions. In contrast, Armin Meijere has reported the success of the Heck reaction with styrene.^[134] There are no more similar reports cyclization and re-reduction by other methods have been carried out more often.^[136] The lack of success may be a spatial barrier for Suzuki coupling, but for Heck reaction, it is most likely to be insufficiently active pyridine; the experiment with a more lively 3-vinylpyridine will be continued.



Scheme 20. Synthesis of 4,5,12,13-substituted PCP pyridyl derivatives.

3.2.1.2 Basic Affinity Analysis.

The feasibility analysis of binding affinity with CB8 was studied next.

The disubstituted **pDMVCP** was shown to be similar **DMVCP** on the NMR; the result was given in **5.3**.

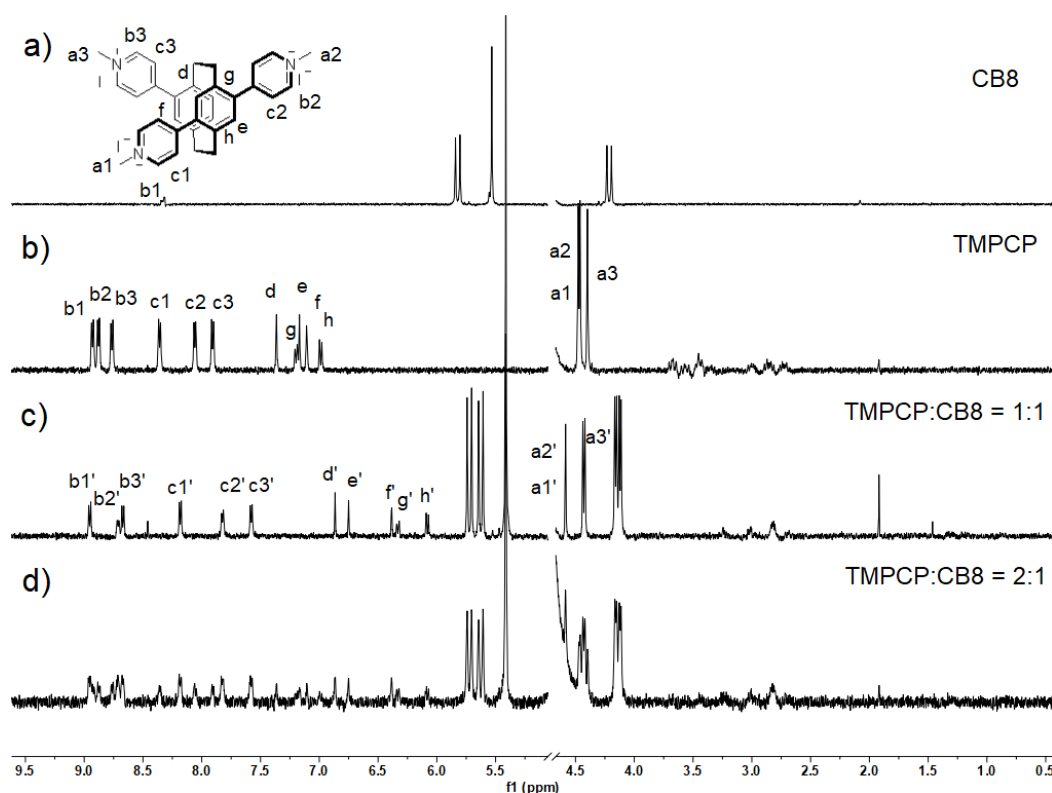


Figure 37. ^1H NMR spectra recorded (400 MHz, D_2O , r.t.) for (a) CB8 (50 μM) (b) **TMPCP** (200 μM), (c) a mixture of CB8 (100 μM) and **TMPCP** (100 μM), (d) a mixture of CB8 (50 μM) and **TMPCP** (100 μM). Primed (') resonances arise from the **CB8** \supset **TMPCP** complex.

The trisubstituted molecule is a novel structure, as the pyridyl is directly connected to the PCP core, the resulting rigidity of the overall structure is hard to predict, and it can be combined with CB8. However, the results (**Figure 37**) showed that the protons H^d to H^h on the PCP core was shifted to the upfield and entered

the CB8 cavity, and that the bridge alkane protons did the same. On the other hand, the protons on the three pyridyls, showed varying degrees of displacement into the upfield, indicating that they were also in the cavity, with only H^{b1} not moving significantly. Meanwhile, the protons on the edge of CB8 were observed to undergo cleavage due to asymmetric polarization of the PCP structure. It is therefore assumed that the whole structure is tilted into the cavity, but the exact state needs to be analyzed in conjunction with X-Ray crystallography.

In contrast, the tetrasubstituted molecule with a larger spatial configuration is symmetrical structures. The result shown (**Figure 38**) by NMR remain surprising that the protons H^d on PCP core shifted to upfield 0.55 ppm. The protons on the bridge appeared to be half shifted to the upfield and half shifted to the downfield. However, the protons on pyridyls had only a shift of 0.1 ppm, and protons on CB8 exhibited only displacement and no cleavage. It can be assumed that the symmetrical structure remains parallel to the CB8 level in the cavity.

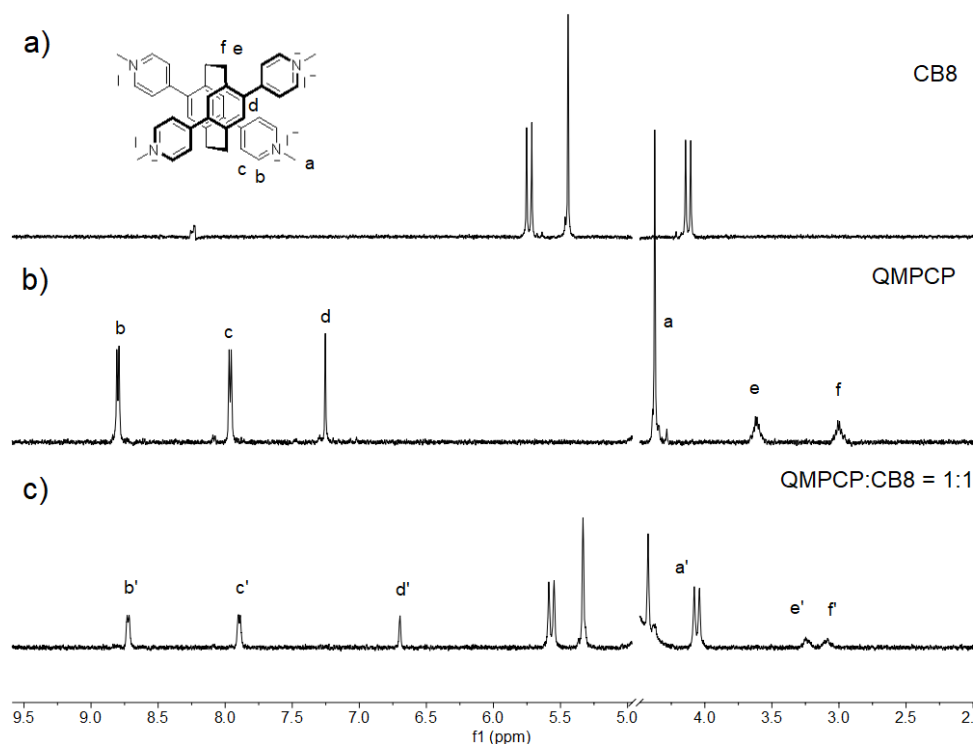


Figure 38. ¹H NMR spectra recorded (400 MHz, D₂O, r.t.) for (a) CB8 (50 μM) (b) **QMPCP** (200 μM), (c) a mixture of CB8 (100 μM) and **QMPCP** (100 μM). Primed (') resonances arise from the **CB8**⇌**QMPCP** complex.

Next is the tetrasubstituted **QMVCPP** with longer “arms”. Like other PCP derivatives with long “arms”, they are relatively slow to bind. Similar results are shown (**Figure 39**). The protons H^d to H^h on the PCP core all move to the upfield due to entering the cavity.

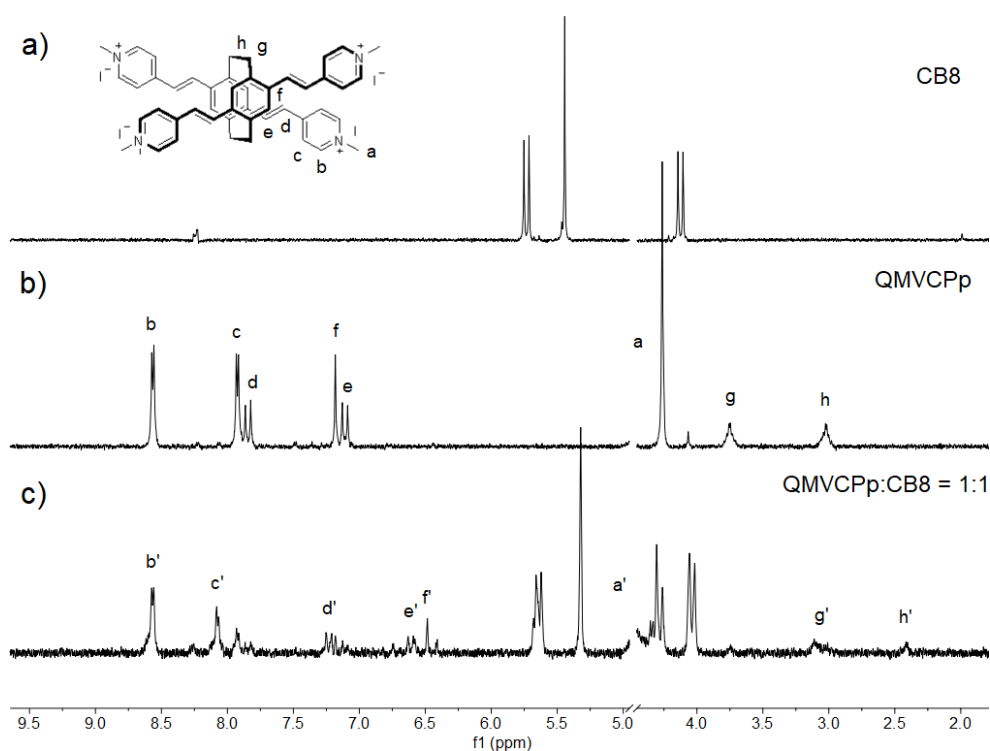


Figure 39. ^1H NMR spectra recorded (400 MHz, D_2O , r.t.) for (a) CB8 (50 μM) (b) QMVCPp (200 μM), (c) a mixture of CB8 (100 μM) and QMVCPp (100 μM). Primed (') resonances arise from the $\text{CB8} \rightarrow \text{QMVCPp}$ complex.

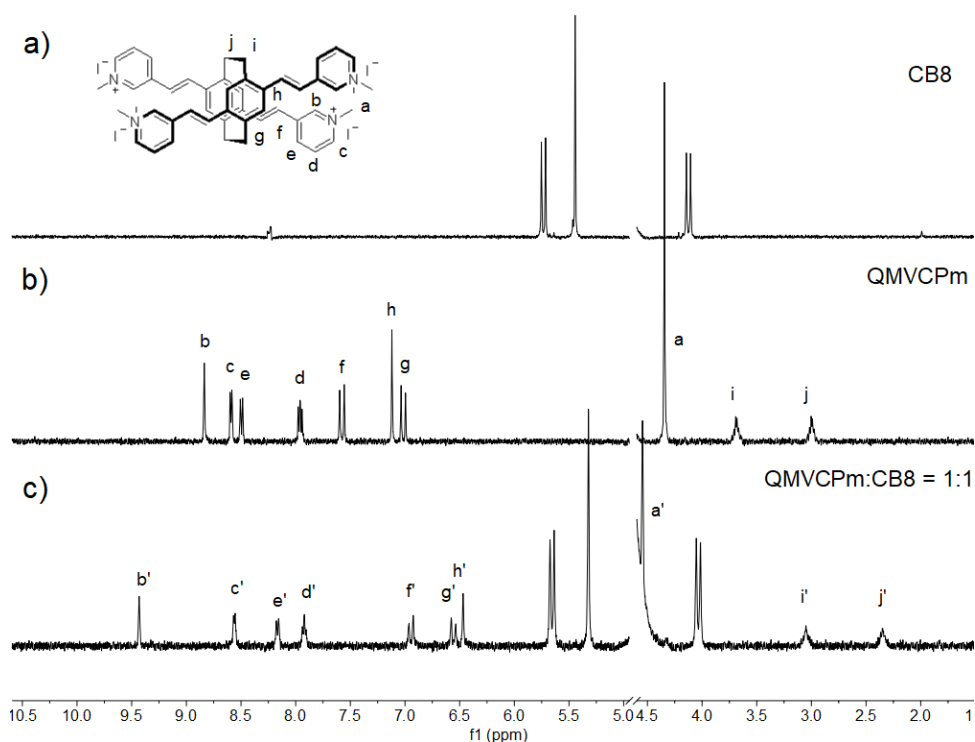


Figure 40. ^1H NMR spectra recorded (400 MHz, D_2O , r.t.) for (a) CB8 (0.05 mM) (b) QMVCPm (200 μM), (c) a mixture of CB8 (100 μM) and QMVCPm (100 μM). Primed (') resonances arise from the $\text{CB8} \rightarrow \text{QMVCPm}$ complex.

Combined with the results of **QMVCpM** (Figure 40), the difference lay in the pyridyls located in the end group. The NMR of **QMVCpM** showed no significant displacement of proton H^c, while H^b showed a visible shift towards the downfield at about 0.6 ppm. It can be concluded that the pyridine plane was not shifted when the N atom was in *para*, while in *meta* the asymmetrical pyridine was pulled towards the position near O atom of CB8 by the positive charge. It is like the four arms each locking outwards to the edge of the CB8.

3.2.1.3 Binding Constants K_a Determination.

NMR results demonstrated that the five PCP derivatives, although bulky, can still bind to CB8. Further their binding constants K_a were determined using the previous method with Mem as a competitor. The NMR was performed on the first, third and fourth days, during which the tubes were accompanied by physical shaking. A phenomenon was found that the PCP with the long “arms” took longer to reach equilibrium, **pDMVCP** took two days and two **QMVCp** took at least four days. The other two reached equilibrium faster and had a clearer NMR result. Table 4 shows the final calculations and the ¹H NMR data were detailed in 5.3.

Table 4. Binding constants (K_a , M⁻¹) determined for the interaction between CB8 host and PCP Guests

PCP guests	CB based system	Medium	Binding constants K_a	Detection method
pDMVCP (80)	CB8 \supset Mem	D ₂ O	$(6.31 \pm 0.89) \times 10^{13}$	NMR, CBA
TMPCP (81)	CB8 \supset Mem	D ₂ O	$(1.36 \pm 0.19) \times 10^{13}$	NMR, CBA
QMPCP (82)	CB8 \supset Mem	D ₂ O	$(4.22 \pm 0.60) \times 10^{13}$	NMR, CBA
QMVCpP (83)	CB8 \supset Mem	D ₂ O	$(4.93 \pm 0.70) \times 10^{14}$	NMR, CBA
QMVCpM (84)	CB8 \supset Mem	D ₂ O	$(4.32 \pm 0.61) \times 10^{14}$	NMR, CBA

The two rigid structured derivatives **TMPCP** and **QMPCP** have a minimum binding force but up to 10¹³. The two tetrasubstituted derivatives **QMVCpP** and **QMVCpM** with attached “arms” had a similar binding force up to 10¹⁴. Although their terminal groups were charged pyridines with different substitution directions, there was no significant effect on the binding force.

3.2.1.4 Discussion and Conclusion.

Combined with the data in the previous section, the results were summarized and shown in Figure 41. The general result was that, as the group with the vinyl “arms”, **pDMVCP** bound less strongly than the equally disubstituted **DMVCP**, and both derivatives of the tetrasubstitution bound with similar strength to **DMVCP**. The conclusion can be drawn that the orientation of the “arms” affected the bonding force, but four did not result in a higher strength, and the direction of the charge had no significant effect. The linear **pDMVCP**

and the monosubstituted **MVCP** have similar bonding forces, and the presence of two “arms” that are not in the same axial direction contributes to an order of magnitude better bonding of the PCP.

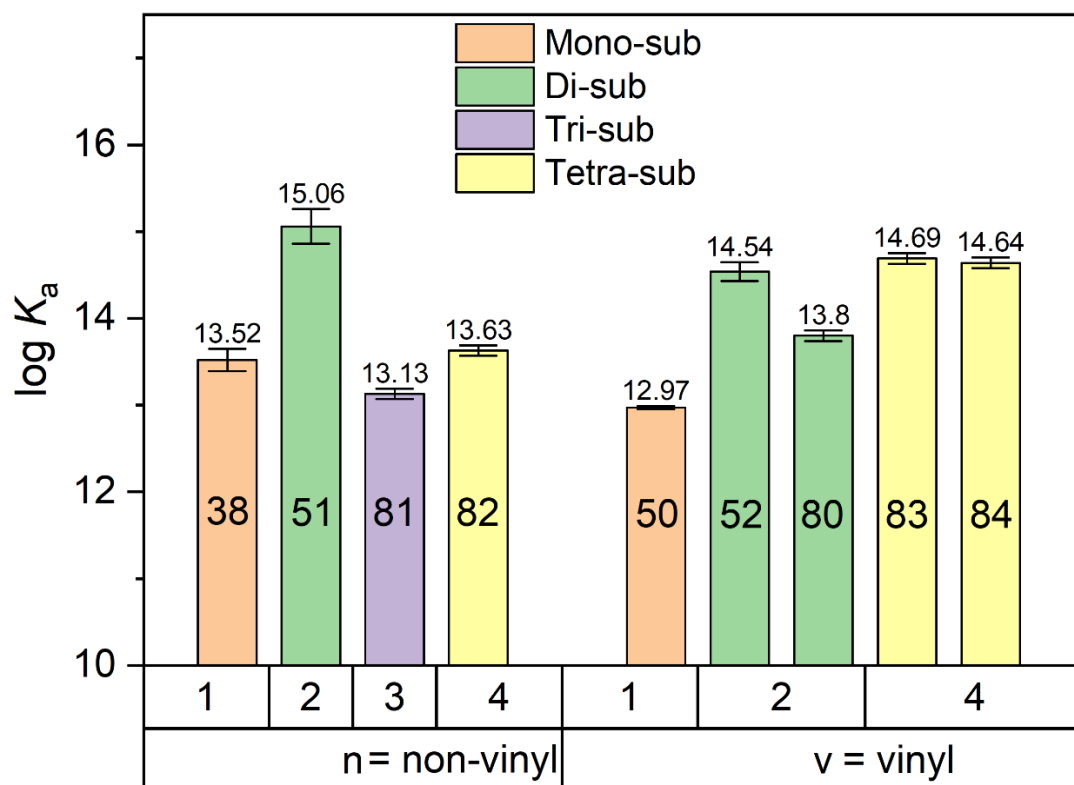


Figure 41. Binding constants (K_a , M^{-1}) comparison between acquired PCP guests with BC8.

Overall, there is no direct relationship between the binding constants and the number of substituents, which means that they are also not directly related to the number of charges. From the present results, odd substitutions, *i.e.*, asymmetric structures, achieve smaller binding constants, while symmetric structures can obtain stronger binding forces when the PCP core is symmetrically distributed in the CB8 cavity. The results of several measurements have shown that a symmetrical structure **DMPCP (51)** without long “arms” can fill the CB8 cavity more adequately. It can be further speculated that the combination of PCP and CB is influenced by numerous factors, with the role of high-energy water remaining an important influence.

3.2.2 Exploration of other [2.2]Paracyclophane Derivatives

The **MVCP** was shown to have potential as a probe and two additional compounds were designed simultaneously. **AMVCP** was aimed to add electron donors to the opposite side of **MVCP**, further increasing the fluorescence redshift of the dye and thus avoiding signal overlap with human body fluids in sensing.

3.2.2.1 Molecular Design and Synthesis.

pAMPCP (95) was originally designed to explore the effect of dimethylamine on the spectrum when in different positions on either one or both benzene rings of the PCP, hence dimethylamine in the pseudo-*para* position. **AMVCP** then substitutes dimethylamine in the *para* position, like **MVCP**, it has also been synthesized in enantiopure form.

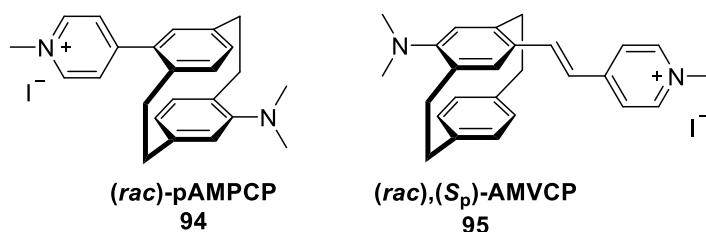
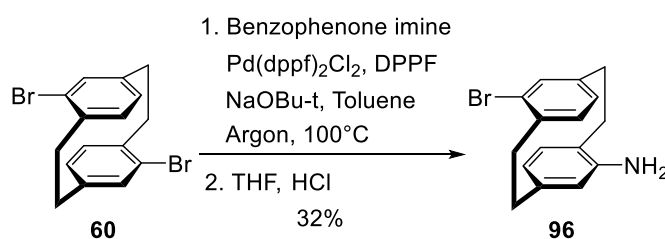


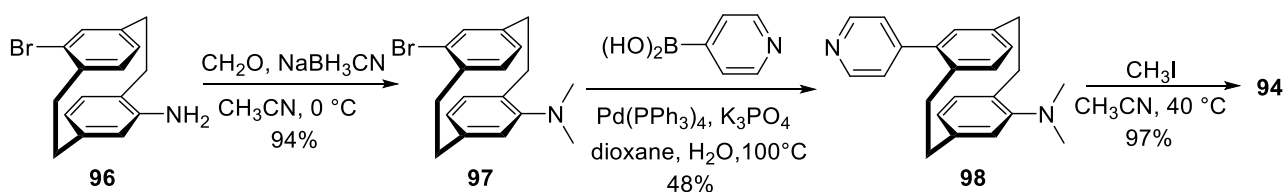
Figure 42. Chemical structures of **pAMPCP (94)**, and **AMVCP (95)**.

First for **pAMPCP**, 4,16-dibromo[2.2]paracyclophane was used as the starting material, where one of the bromine atoms was replaced with an amino group. This method has been reported with yields up to 50% on the mg scale, and 32% at several hundred milligram or gram.^[137] There are other accesses to get substituted amino[2.2]paracyclophane; one is direct amination of bromo[2.2]paracyclophane with sodium azide, but fails to give pseudo derivatives. There are also straightforward longer steps starting with the carboxylic acid and in several steps to cyanate then hydrolyzed,^[138] or through oxidative rearrangement of the oxime.^[122b]



Scheme 21. Synthesis of 4-bromo-16-amino[2.2]paracyclophane (**96**)

Then 4-bromo-16-amino[2.2]paracyclophane was used as precursor for methylation first, then Suzuki coupling reaction and finally *N*-methylation. The methylation of primary amines can also be carried out by iodomethane and under mild and controlled conditions. The Suzuki reaction here yields up to 48%, much higher than for the normal PCP.



Scheme 22. Synthesis route for **pAMPCP (94)**.

The molecular structure of the **pAMPCP (94)** was confirmed by X-ray analysis (**Figure 43**).

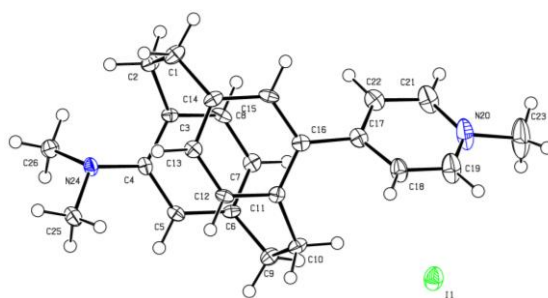
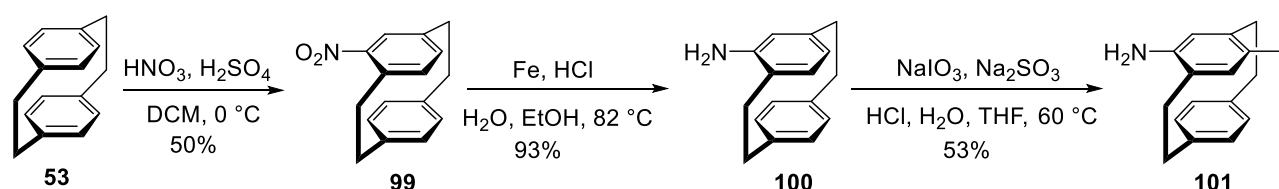


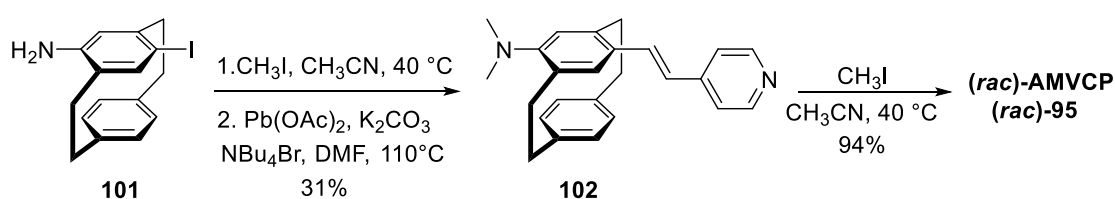
Figure 43. Single crystal X-ray molecular structure of **94** drawn at 50% probability level. Dr. Martin Nieger provided the result.

The *para*-structure **AMVCP** required a reduction from nitro to amino starting with **PCP**, followed by an iodination reaction to give 4-iodo-7-amino[2.2]paracyclophane (**101**), which has been reported previously.^[122c] Here, the iodination reaction followed the principle of benzene localization and activation mechanism.

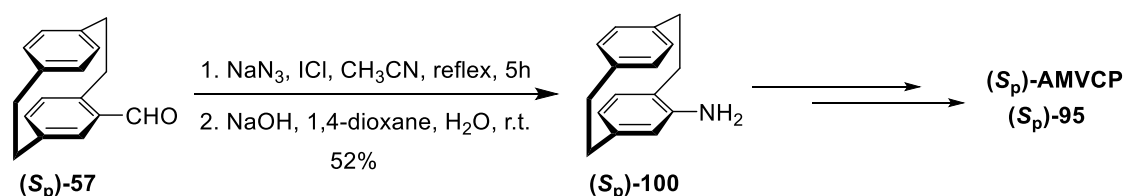


Scheme 23. Synthesis route for 4-iodo-7-amino[2.2]paracyclophane (**101**)

Here the amine methylation was followed by iodination but failed, so the iodination was followed by the methylation. (*rac*)-**AMVCP** was eventually obtained after the iodine Heck reaction followed by *N*-methylation.



Scheme 24. Synthesis route for (*rac*)-**AMVCP (95)**.



Scheme 25. Synthesis of (*S_p*)-4-amino[2.2]paracyclophane ((*S_p*)-**100**) and ((*S_p*)-**95**)

(*S_p*)-**AMVCP** was synthesized using the enantiomer pure (*S_p*)-4-formyl[2.2]paracyclophane (**57**) as the starting material, which was subjected to a radical azidation to give the enantiomer pure (*S_p*)-4-

amino[2.2]paracyclophane (**100**). Because the subsequent series of reactions did not involve racemization and therefore the *ee* value did not change, following the (*S_p*)-4-formyl[2.2]paracyclophane (**57**).

3.2.2.2 Affinity Analysis of pAMPCP (**95**).

pAMPCP had an extra electron donating dimethylamine group in the pseudo-*para* position compared to MPCP, resulting that electrons can be transferred in a limited way through space to the benzene ring where the pyridine was located. Its critical analysis with CB8 was shown next (**Figure 44**). It exhibited a similar state to MPCP, with the PCP core in the cavity and only a small displacement of protons outside the pyridine, with the methyl in the shielded region. The *N*-dimethyl protons immediately adjacent to the PCP core shifted towards the downfield, indicating a deshielded effect. In particular what looks like a structure of the same size as MPCP affected the hydrogen of CB8, causing the splitting of the inward proton.

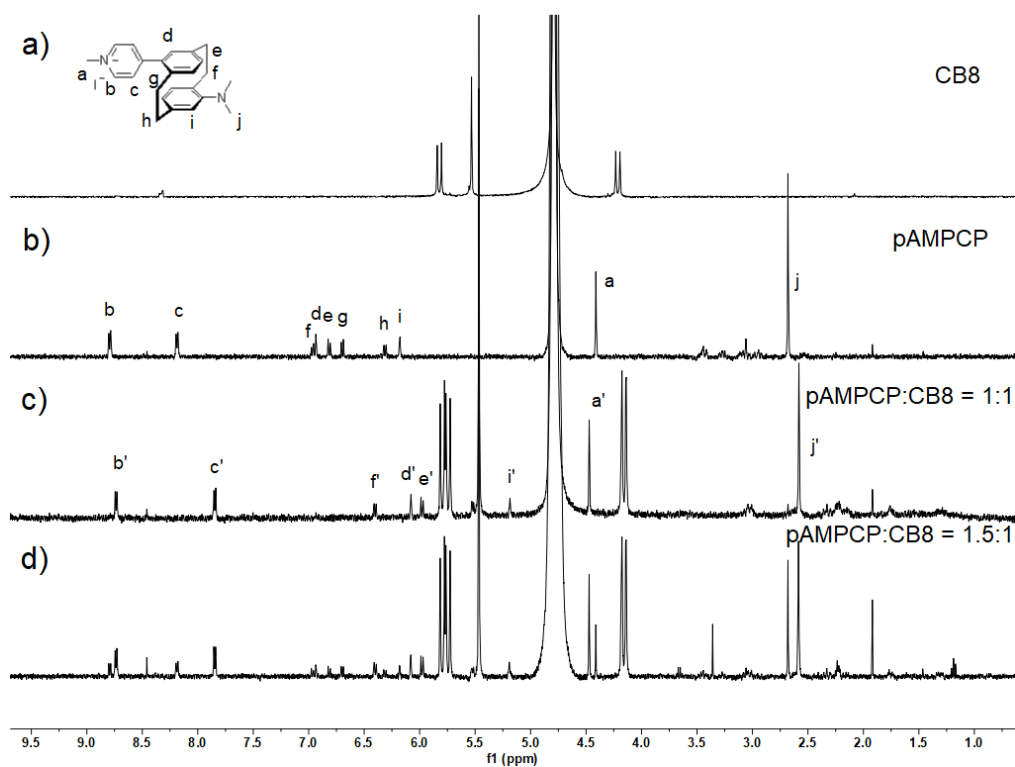


Figure 44. ^1H NMR spectra recorded (400 MHz, D_2O , r.t.) for (a) CB8 (50 μM), (b) pAMPCP (100 μM), (c) a mixture of CB8 (50 μM) and pAMPCP (50 μM), (d) a mixture of CB8 (50 μM) and pAMPCP (75 μM). Primed (') resonances arise from the **CB8** \rightleftharpoons **pAMPCP** complex.

The calculation of its binding constant with CB8 continued (**5.3, Figure 94**), resulting in a similar value to Mem: $K_{\text{rel}} = 1.64$, $K_{\text{a}} = (8.14 \pm 2.31) \times 10^{13}$. This result is consistent with the MPCP result, where the pseudo-*para*-substituted dimethylamine slightly increased the binding value and did not substantially change it. Isaacs reported that the measurements on adamantane were all based on ammonium salts.^[102] Theoretically the lone pair of electrons of the amino group could provide the conditions for forming

hydrogen bonds for the water molecules in the cavity, but the result showed that for PCP, the common amine groups had little effect on the whole structure.

The spectroscopic analysis was performed (**Figure 45**). Firstly, the results showed the affinity characteristics of **pAMPCP** 1:1 combination with CB8. The absorption spectrum was only slightly enhanced before and after binding. At the same time it showed almost no fluorescence when not bound and a significant fluorescence enhancement after binding. The excitation spectrum also appears to change significantly before and after binding. Its absorption spectrum showed two peaks, more than **MPCP** around 230 nm, which resulted from dimethylamine. After excitation experiments at different wavelengths, the peaks at 320 nm in the curve were used as the excitation wavelength.

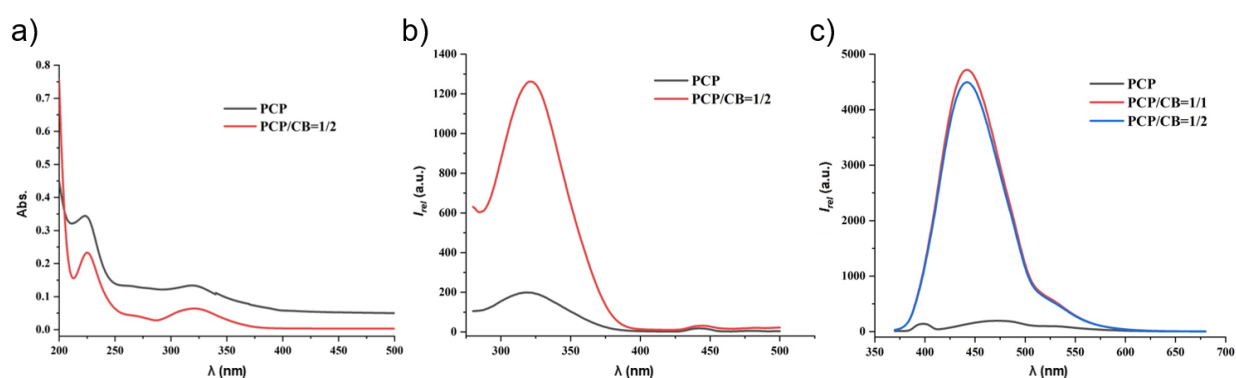


Figure 45. (a) UV-Vis absorption spectra of **pAMPCP** (10 μM) and CB8 (20 μM) are in water. (b) Excitation spectrum ($\lambda_{\text{ex}} = 320 \text{ nm}$) of 10 μM **pAMPCP** and CB8 (20 μM) in water. (c) Fluorescence emission spectrum ($\lambda_{\text{ex}} = 320 \text{ nm}$) of 10 μM **pAMPCP** and CB8 (10 μM and 20 μM) in water.

Table 5 gives the maximum wavelength changes in absorption and emission of **pAMPCP** and **MPCP** before and after binding. The absorption and emission spectra of **pAMPCP** showed a blue shift, resulting from the different dimethylamine group over **MPCP**. However, the blue shift in the emission spectrum was more pronounced, about 100 nm, than that of **MPCP**, with the result significantly reduced Stokes shift.

Table 5. Photophysical characters data of **pAMPCP** and **MPCP** before and after binding with CB8

PCP Dyes	Absorbance maximum		Emission maximum		Enhancement factor
	wavelength (nm)		wavelength (nm)		
	Before binding	After binding	Before binding	After binding	
MPCP	333	341	563	545	4.25
pAMPCP	320	323	475	445	≈ 20

Despite the fluorescence enhancement ratio as high as 20 before and after binding CB8, its emission spectral region like most general dyes, would cover the background of human body fluid and was therefore not suitable for use as a sensor candidate. Ultimately, used as a comparative exploration of the PCP, **pAMPCP** also showed certain characteristics that might be used in other areas in subsequent studies.

3.2.2.3 Affinity Analysis of AMVCP (95).

The structure of **AMVCP** is more optimized than **MVCP**; the addition of dimethylamine gave it a maximum wavelength redshift in emission theoretically. It was therefore synthesized with one of the pure enantiomers, the affinity of which with CB8 was analyzed by NMR as follows (**Figure 46**). The NMR comparison showed that the PCP core was inside the CB8 cavity, but there was no significant change in the NMR after increasing its concentration. Also, the free CB8 characteristic peaks were still present; the peak completely disappeared after adding an equal amount of memantine. It indicated that **AMVCP** had absolutely no competitive ability compared to memantine.

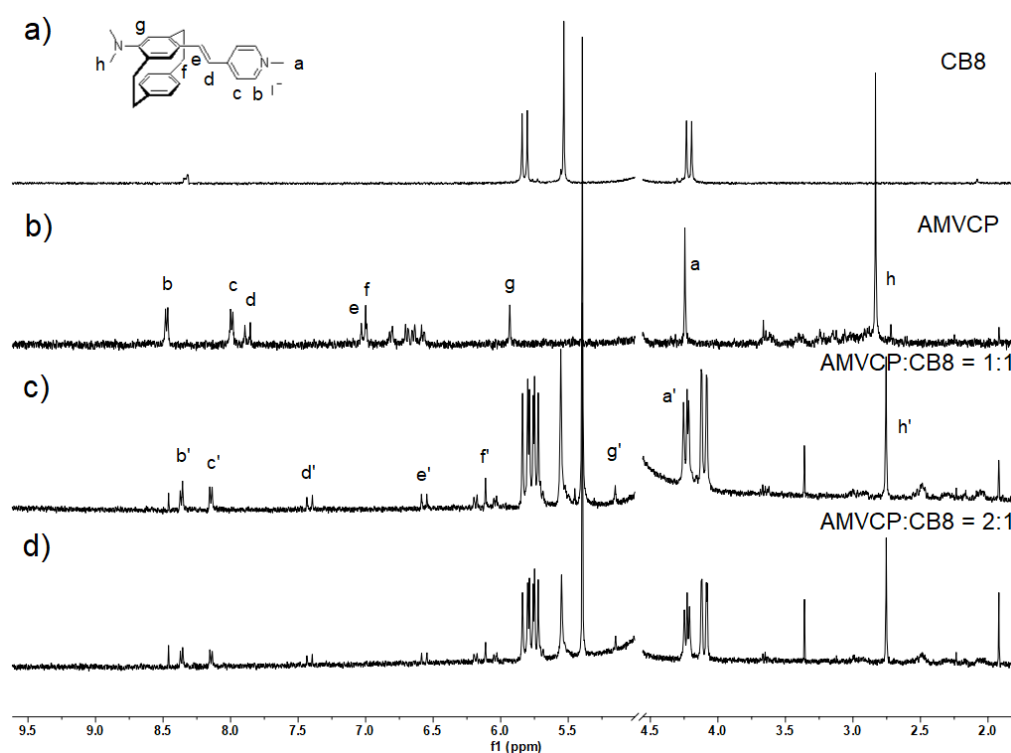


Figure 46. ^1H NMR spectra recorded (400 MHz, D_2O , r.t.) for (a) CB8 (50 μM) (b) **AMVCP** (50 μM), (c) a mixture of CB8 (50 μM) and **AMVCP** (50 μM), (d) a mixture of CB8 (50 μM) and **AMVCP** (100 μM). Primed (') resonances arise from the **CB8**⊃**AMVCP** complex.

The other results of its spectrum are shown below (**Figure 47**). Some results were in better agreement with the theory, with a red shift in its absorption and emission wavelengths. Similarly, dimethylamine increased to a characteristic peak in the absorption spectrum, which was tested at 550 nm as the excitation wavelength. Compared with **MVCP**, the absorption wavelength was redshifted by 165 nm and the emission wavelength by 32 nm.

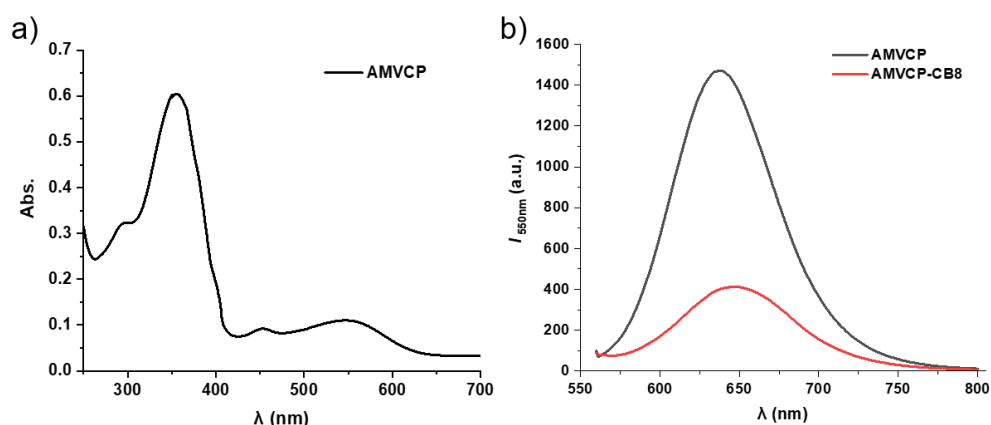
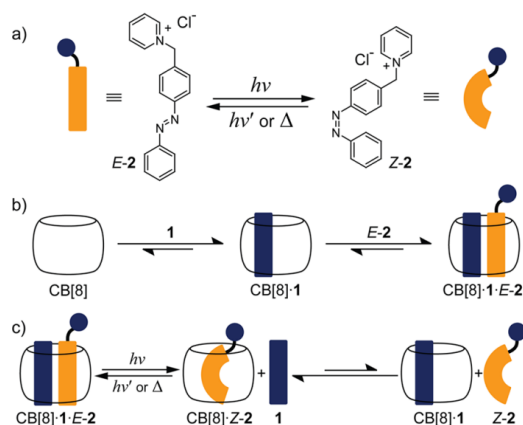


Figure 47. (a) UV-Vis absorption spectra of **AMVCP** (45 μM) in water. (b) Fluorescence emission spectrum ($\lambda_{\text{ex}} = 550 \text{ nm}$) of **AMVCP** (45 μM) and **CB8** (45 μM) in water.

But unexpectedly the fluorescence appears somewhat weakened after the addition of **CB8**, the exact opposite of the result of **MVCP**. In summary, **AMVCP** had some properties as a red dye, but did not meet expectations in combination with **CB** and competition with other analytes.

3.2.3 Exploration of Affinity on Azo-functionalized [2.2]Paracyclophane Derivatives

Azobenzene is a photo-switchable compound consisting of two benzene rings joined by a diaryl diazene $\text{N}=\text{N}$ double bond, a trigger already used in many materials.^[139] Azobenzene is able to bind **CB7** and **CB8**.^[140]



Scheme 26. (a) Isomerization of **2**; (b) Stepwise Formation of **CB[8]·1·E-2**; (c) Isomerization of **2** in the Presence of **CB[8]** and **1** and Equilibrium after UV Irradiation of **CB[8]·1·E-2**. Copyright © 2013 American Chemical Society.

It can come out of the **CB7** cavity by isomerization when binding **CB7**, as the **CB7** cavity is not large enough to accommodate the *cis*-azobenzene structure. When bound to **CB8**, it generally enters the **CB8** cavity synergistically with another small molecule, such as violet, and when the azobenzene isomerizes, it remains in the cavity alone, pushing out the violet molecule.^[141] Thus, the azobenzene-modified **PCP**

becomes the target molecule, because PCP will be in the center of the cavity when it binds to CB8, and it will be interesting to see which will continue to bind to CB8 if the azobenzene is isomerized.

3.2.3.1 Molecular Design and Synthesis.

The following two target diaryl diazene functionalized PCP molecules were designed (**Figure 48**). [2.2]Paracyclophane was substituted on one side by *N*-methylpyridine to ensure that it could bind to CB8, and on the other side, the pseudo *para* position was modified to azobenzene, *i.e.*, **AzoMPCP (104)**. The other is a structure **AzoFMPCP (105)** in which the benzene ring is substituted by two fluorine atoms, designed to raise the energy barrier for isomerization of the azo structure with a stronger electron-withdrawing group. **AzoPCP (106)** was used as a reference structure.

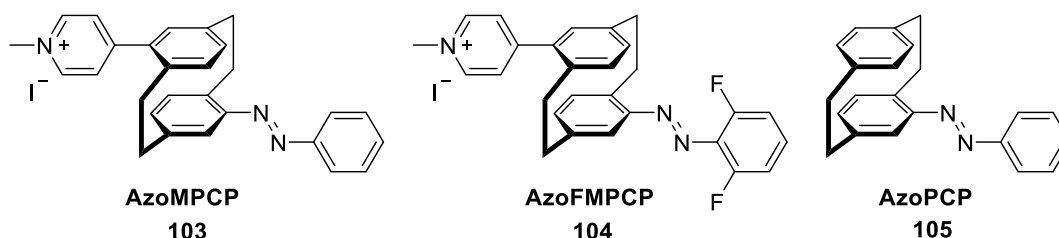
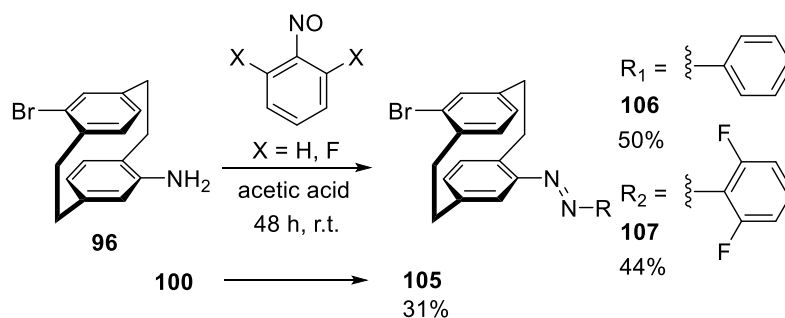
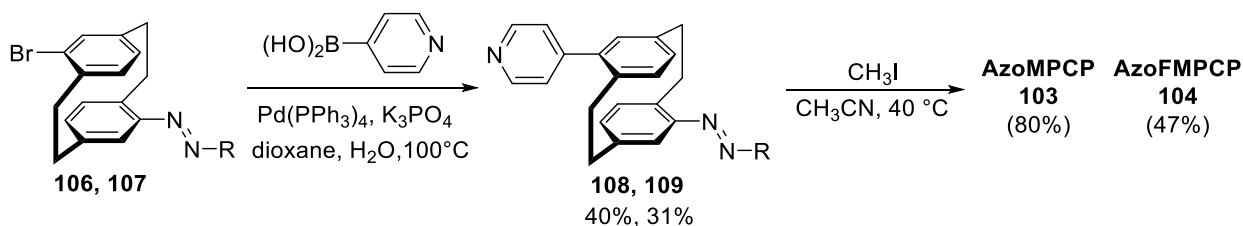


Figure 48. Chemical structures of **AzoMVCP (103)**, **AzoFMVCP (104)** and **AzoPCP (105)**,

4-Bromo-16-amino[2.2]paracyclophane (**96**) and 4-amino[2.2]paracyclophane (**100**) were used as precursors, respectively, followed by a diazotization to give an azobenzene derivative.



Scheme 27. Synthesis of 4-(*E*)-azophenyl-16-bromo[2.2]paracyclophane (**106**) and 4-(*E*)-azo-2',6'-difluorophenyl-16-bromo[2.2]paracyclophane (**107**), and 4-(*E*)-azophenyl[2.2]paracyclophane (**105**).



Scheme 28. Synthesis route for **AzoMPCP (103)** and **AzoFMPCP (104)**.

The final azo derivatives were coupled with a Suzuki reaction and a methylation to give the target compounds. In Suzuki coupling reactions, compound with fluorine atoms substitution have a lower yield. The molecular structure of **AzoMPCP (103)** was confirmed by single crystal X-ray analysis (**Figure 49**).

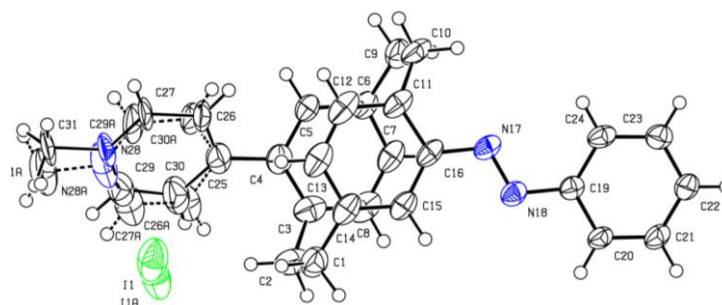


Figure 49. Single crystal X-ray molecular structure of **103** drawn at 50% probability level. Dr. Martin Nieger provided the result.

3.2.3.2 Affinity Analysis.

Firstly, **AzoMPCP** was spectroscopically characterized and in the absorption spectrum detected two absorption bands of the chromophore, the absorption $p-\pi^*$ transition at 223 nm and the $\pi-\pi^*$ transition at 328 nm in **5.3** (**Figure 96**). It was irradiated at 365 nm for half an hour, but then the NMR showed no significant change, indicating that the structural transformation was rapid and could not be maintained for enough time to be detected.

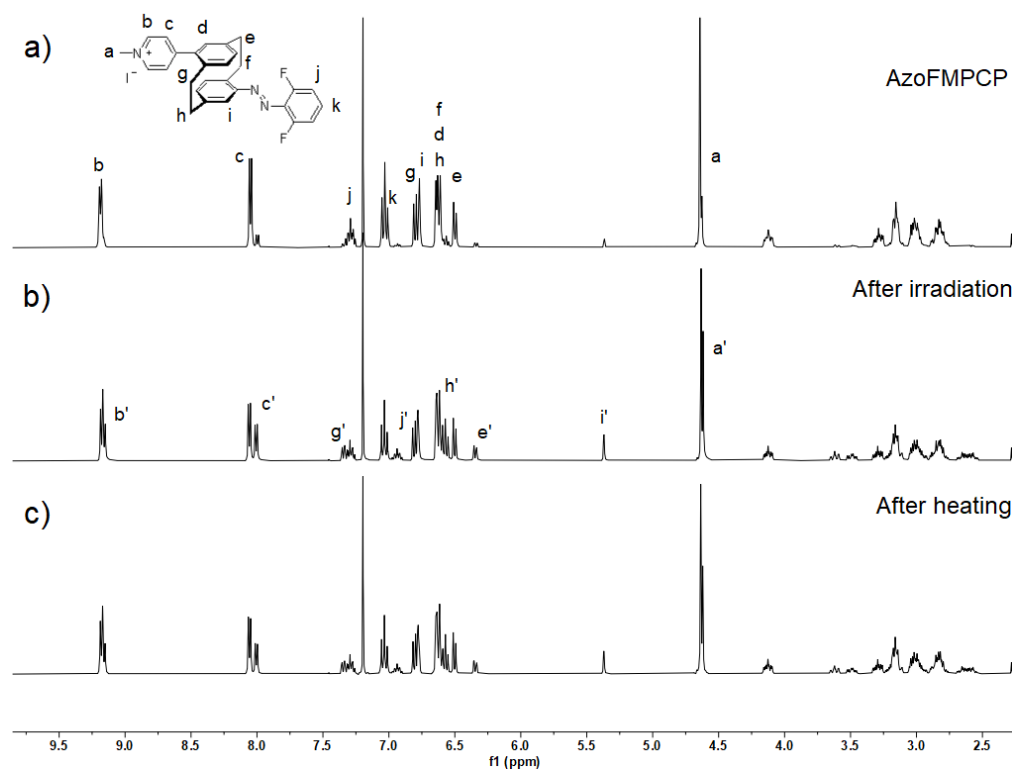


Figure 50. ^1H NMR spectra (400 MHz, CDCl_3 , r.t.) comparison of **AzoFMPCP**, (a) before irradiation, (b) after irradiation (at 365 nm for an hour), (c) after heating (at 80 °C for an hour). Primed (') was from isomerization.

Next **AzoFMPCP** was irradiated at 365 nm for an hour. ^1H NMR of **AzoFMPCP** showed some isomerization from *E* to *Z* after irradiation, the ratio of *E/Z* from 9/1 to 10/7 according to the integration of peaks of H^c (**Figure 50**). A shift of the peaks H^g H^i H^e H^i in the aromatic region was also observed, even for the protons on the bridge of PCP, and the methyl group on the pyridine. This result proved that the structure could be stable for a certain time. The NMR tube was then heated at 80 °C for an hour, resulting in a drop in the ratio of *E/Z* from 10/7 to 2/1. This result demonstrated that the structure of **AzoFMPCP** can be transformed to achieve isomerization, even if it requires more energy.

The 2D ^1H - ^1H COSY spectra of **AzoFMPCP** are shown in 5.3 (**Figure 97**). It successfully performed a structural transformation, so the combination with CB8 was the next step in our study.

Figure 51 (a) and (b) where the spectrum of **AzoFMPCP** alone and with excess CB8 in D_2O , respectively. Surprisingly the proportion of isomerization in water appeared to be different compared to that of deuterated chloroform. As seen in (b), almost all of the pyridine protons were bound to CB8, including all of the $\text{H}^{b''}$ to $\text{H}^{i''}$ on the PCP core (the protons of the bridge not marked).

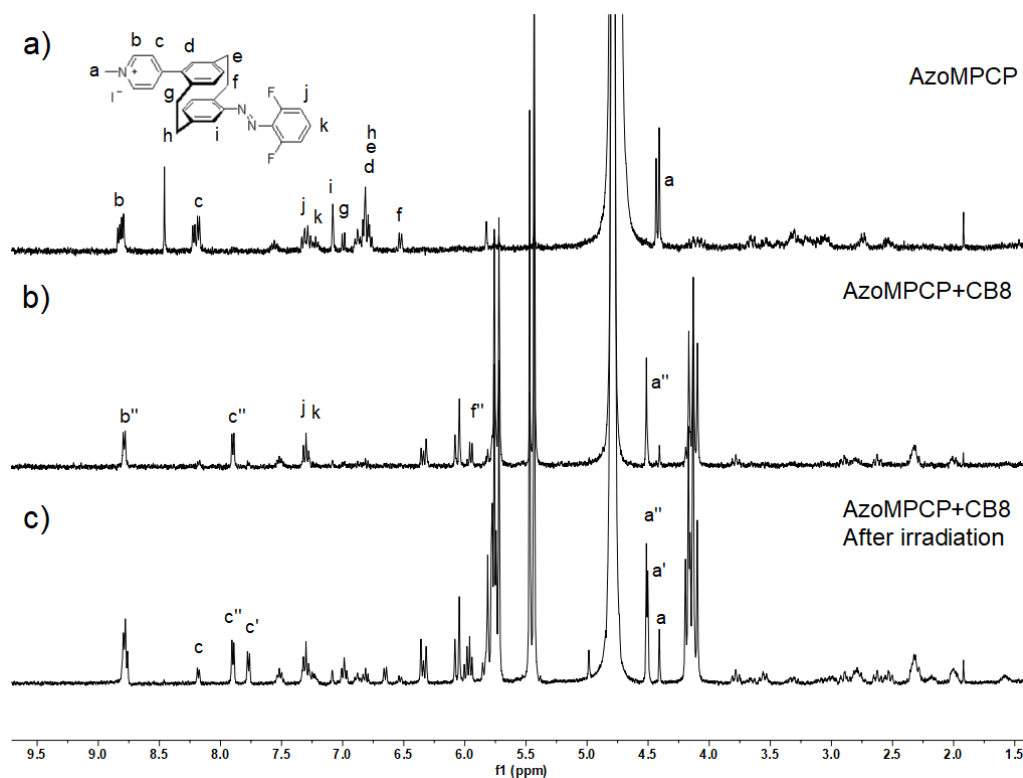


Figure 51. ^1H NMR spectra recorded (400 MHz, D_2O , r.t.) for (a) **AzoFMPCP**, (b) a mixture of CB8 and **AzoFMPCP**, (c) a mixture of CB8 and **AzoFMPCP** after irradiation (at 365 nm for an hour). Primed (') was from isomerization, and primed (') resonances arise from the **CB8** \rightleftharpoons **AzoFMPCP** complex.

When radiated again, the result was as shown in (c). The proton H^c on the pyridine appeared again in the bound state after isomerization. The variation, however, was that a small amount of unbound PCP signal was present, while the majority remained in the bound state, and of these, nearly 40% (H^c) were structurally

altered. The methyl group on the pyridine also appeared in three states; in contrast, the protons (H^j and H^k) on the benzene ring at the end of the azobenzene did not change significantly.

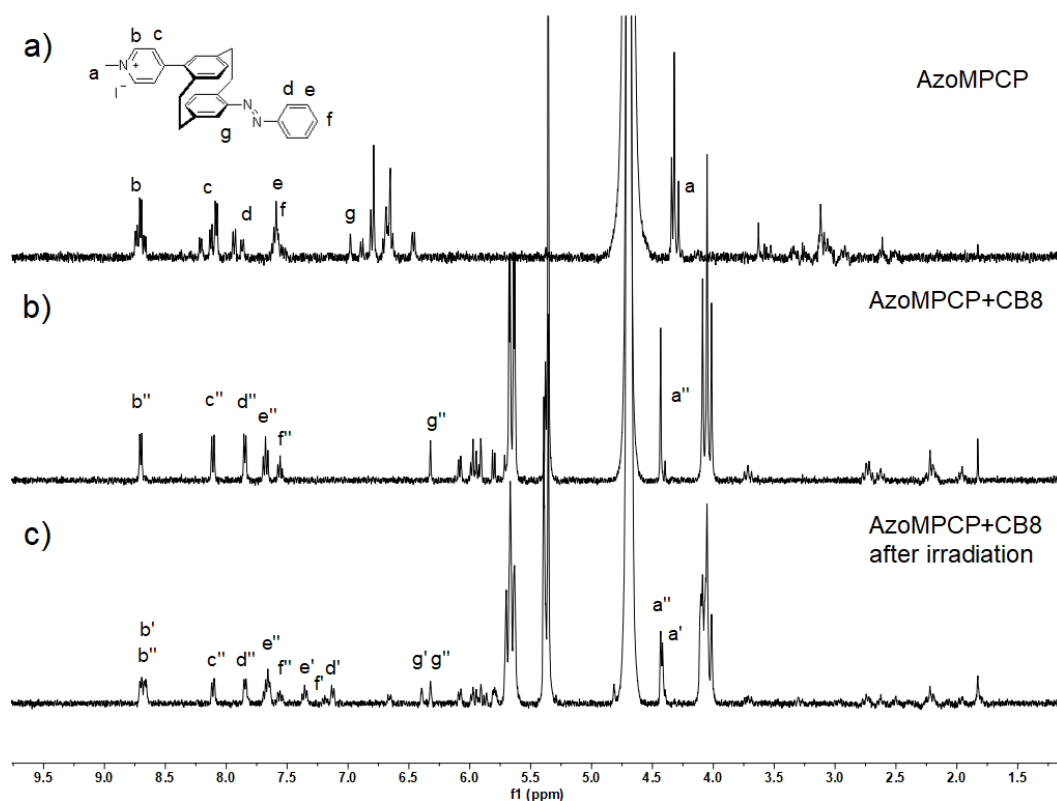


Figure 52. ^1H NMR spectra recorded (400 MHz, D_2O , r.t.) for (a) **AzoMPCP**, (b) a mixture of CB8 and **AzoMPCP**, (c) a mixture of CB8 and **AzoMPCP** after irradiation (at 365 nm for an hour). Primed (') was from isomerization, and primed (') resonances arise from the **CB8** \rightleftharpoons **AzoMPCP** complex.

In previous literature reports, only the *E*-configuration of azobenzene was tested on a binding constant with CB8, which was about 10^4 .^[77a, 98a] Combined with previous studies on PCP, it can be concluded that the binding capacity of azobenzene was not at the same level as PCP and that it cannot replace the PCP core in the CB8 cavity. To obtain a non-accidental result, therefore a binding CB8 experiment was also performed on **AzoMPCP** (**Figure 52**). By comparison, it can be concluded that the binding state of this type of molecule and CB8 was true with the PCP core in the cavity, while the pyridine and azo groups were on either edge (**Figure 53**).

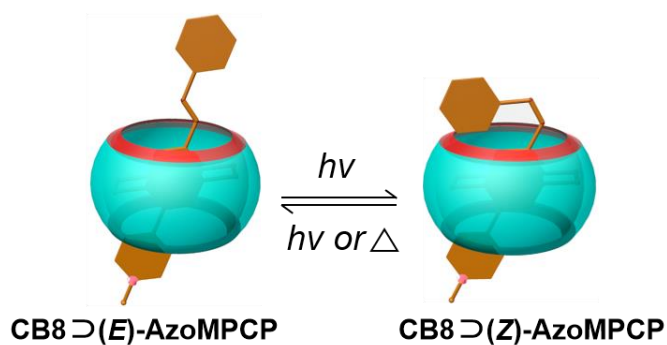


Figure 53. Schematic diagram of azophenyl PCP in combination with CB8

However, a unique phenomenon was the change in the isomeric ratio upon binding **AzoFMPCP** and CB8. For one, the result of (a) show that the originally *E*-configuration dominant conformation showed an increase in the isomeric *Z*-ratio in deuterated water, which was applied equally to both. After it was combined with CB8, the entire number of molecules were converted to *E*-conformation. It's an amazing phenomenon that CB8 can optimize conformation to a single class. Similarly, when the mixture **CB8**⇌**AzoMPCP** continued to be irradiated, the isomer came out again among the product, but unlike before, the conformation can be stable for a certain time in CB8. This could provide an alternative to the azobenzene-based photocontrol trigger that could be modified by the addition of PCP and control the azobenzene conformation with CB8 desired, even for the most common azo-benzenes.

3.2.4 Conclusion

This section describes the synthesis of various derivatives by modifying PCP and investigates their binding state to CB8. Two types of multisubstituted PCP were first synthesized via Heck reaction and Suzuki coupling, and then their binding constants to CB8 were calculated, leading to the conclusion that the disubstituted **DMPCP** remained by far the most strongly bound guest. It was also shown that the binding force was independent of the charge number and was related to the specific orientations of the substitution patterns structure of the PCPs, a relationship that needs to be further studied for in-depth understanding and shall be analyzed by X-ray of the crystals.

Two other dimethylamine-modified PCP were synthesized and proved by spectroscopic and NMR analyses to be unable to be used as simple candidates for chemosensing and their role needs to be studied subsequently.

Finally, PCP bearing azobenzene as a side-group component was synthesized, with different structures but exhibiting similar properties when combined with CB8. It was demonstrated by NMR that after binding to CB8, the PCP core remained in the cavity as a strong binding group, even if the radiation changed the conformation. This led to the conclusion that azobenzene does not bind with CB8 as well as PCP but also demonstrated that CB8 could purify the azobenzene isomer.

3.3 Supramolecular Skeleton and Cage based on [2.2]Paracyclophane

Supramolecular skeletons and cages were widely studied for their beauty and potential applications, and in this chapter PCP derivatives were used as a skeletal basis for research. The derivatives modified by vinyl pyridine, disubstituted and tetrasubstituted were carried out for their covalent and non-covalent incorporation into supramolecular cages. The pyridine terminus N provided a good electron donating effect and the double bond was able to provide a longer “arms” for the pyridine to assemble.

3.3.1 Molecules design and Synthesis.

Two crossed disubstituted and tetrasubstituted structures were chosen for the PCP-skeleton, while the corresponding ligands were chosen for some simpler structures. These ligands will be attempted in two groups, one for covalent bonding similar to Stoddart’s “blue box” and the other with metal-ligand bonds.

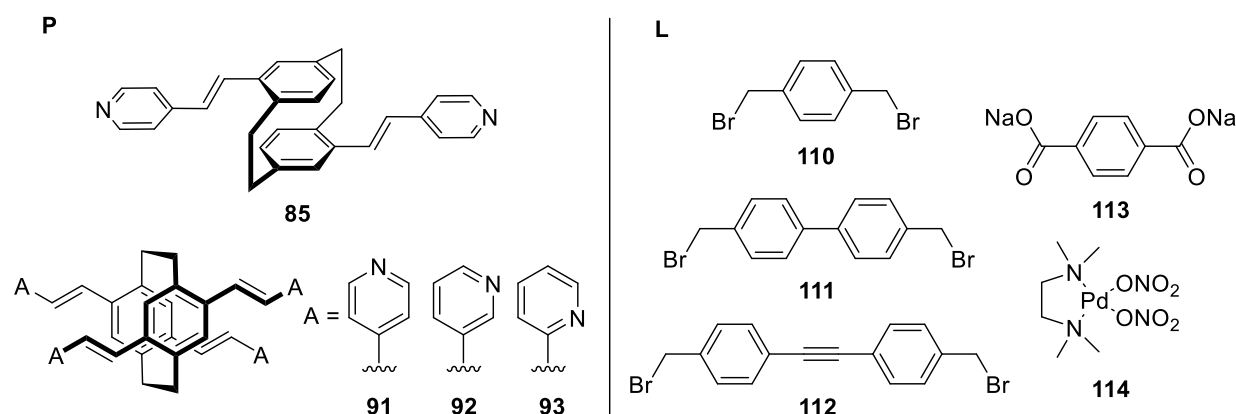
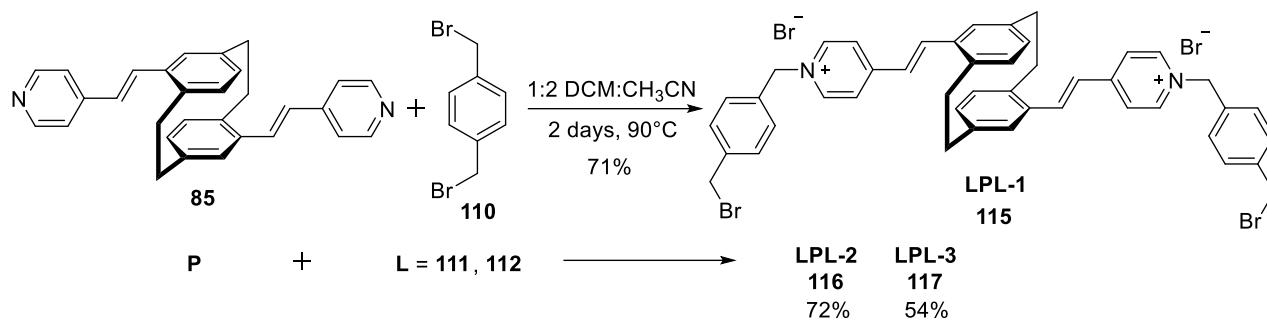


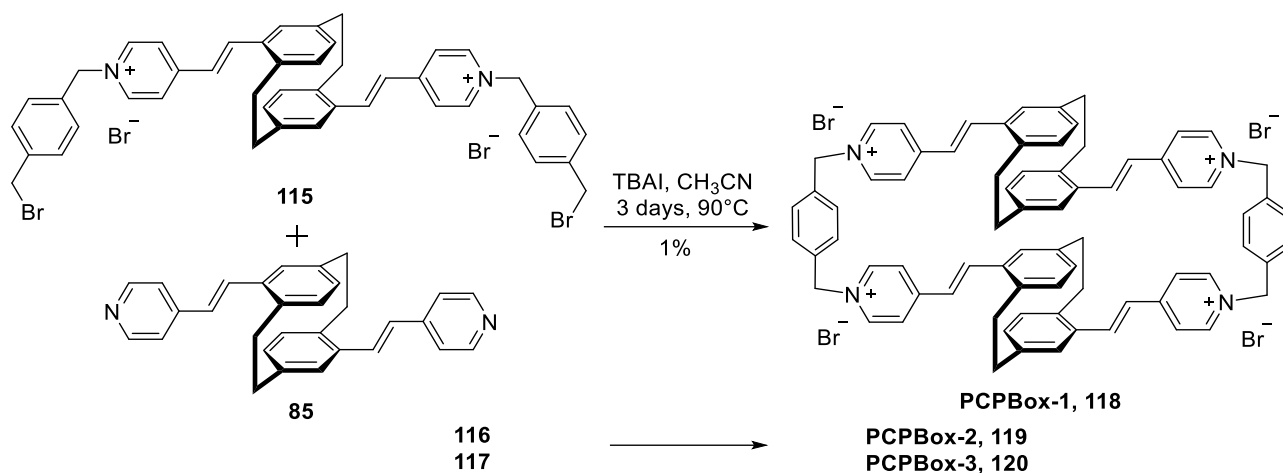
Figure 54. Molecular structures of the two components (**P** = PCP section and **L** = linker)

The two structures **pDMVCP (85)** and 1,4-bis(bromomethyl)benzene (**110**) were first synthesized using the “blue box” method to obtain a half-frame **LPL-1 (115)** first. The resulting structure cannot be purified by column chromatography because the two charges already made the structure very polarized. Because of the complexity of the structure, the relatively pure product was obtained by several washes. In the next step, the reaction solution’s dilute concentration (0.5 mM) was carried out for a long time (3 days) because the target molecule needed cyclization. A mixture in batches was purified by C18 reverse HPLC on a linear gradient from 5% to 95% acetonitrile with 0.1% aqueous TFA in deionized water with 0.1% aqueous TFA and with a flow rate of 10 mL/min at 25 °C to yield light yellow solid.



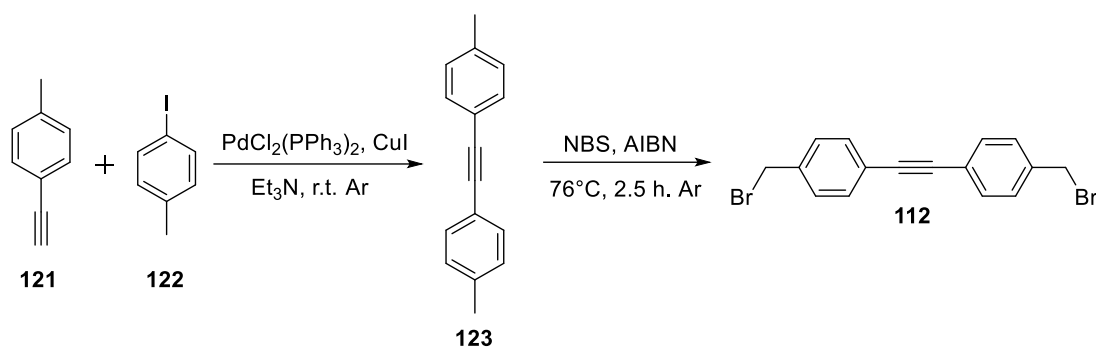
Scheme 29. Synthesis of **LPL-1, 2 and 3**.

The yield of this product is very low, due to its very low solubility in either water-soluble or non-water-soluble solvents. Anion exchange was attempted in the synthesis of **LPL-1**, exchanging water-soluble ions Br⁻ for PF₆⁻. But no better yields were obtained, and the final product **PCPBox-1** was ion exchanged for PF₆⁻ and had no better solubility when performing HPLC.



Scheme 30. Synthesis of **PCPBOX-1 (118), 2 and 3**

In addition to 1,4-bis(bromomethyl)benzene (**110**), other linkers 4,4'-bis(bromomethyl)-biphenyl (**111**) and 4,4'-bis(bromomethyl)tolan (**112**) were attempted for **pDMVCP**. Where 4,4'-bis(bromomethyl)tolan (**112**) was obtained by a classical two steps reaction, starting with 1-ethynyl-4-methylbenzene (**121**) and 1-iodo-4-methylbenzene (**122**) as the starting materials to give **123** via Sonogashira coupling, followed by a Wohl-Ziegler bromination.



Scheme 31. Synthesis route for linker 4,4'-bis(bromomethyl)tolan (**112**).

The two target products **PCPBox-2** and **PCPBox-3** were detected in the reactants through the MS, but in the final step it was found that they could not be separated through the reverse PHLC and that more impurities were preventing the separation. After MS analysis, the yield of **PCPBox-3** was extremely low and only product traces were detected (**Figure 98**, **Figure 99**).

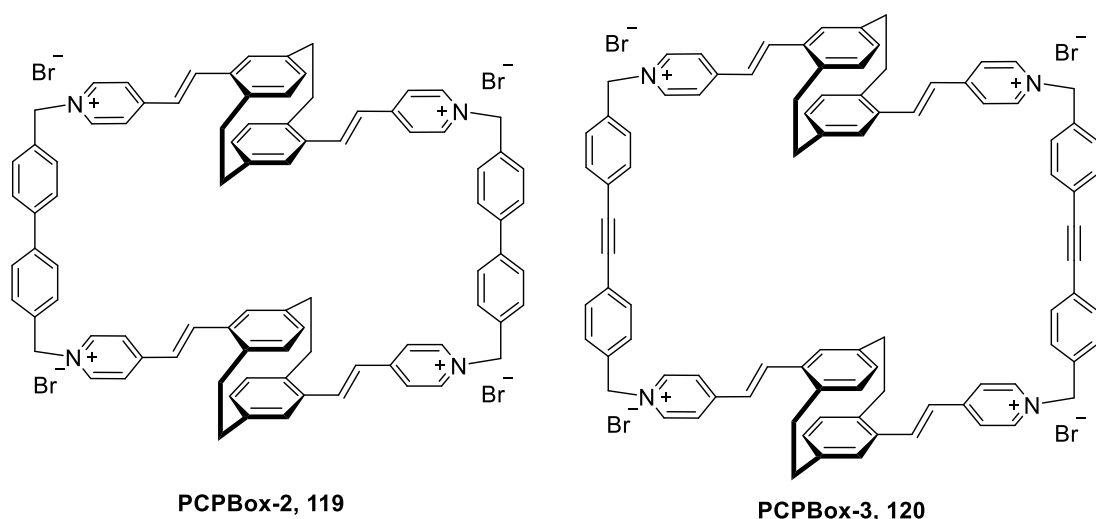
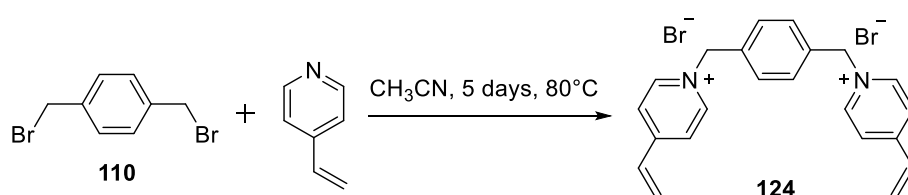


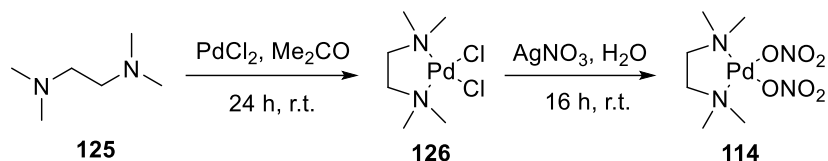
Figure 55. Molecular structures of **PCPBox-2** and **PCPBox-3**.

In a further attempt to use covalent bonding for the tetrasubstituted **QMVCPP** (**91**), the result was that no product connecting the four linkers was obtained, as the proximity of the four “arms” was accompanied by a large spatial resistance. The other way was to get the peripheral macrocycle **124** before reacting with the dibrominated PCP in Heck reaction. However, no conclusive results were obtained again. Compared to the previous method, the final Heck reaction was more difficult.



Scheme 32. Synthesis of 1,1'-(1,4-phenylenebis(methylene))bis(4-vinylpyridin-1-ium) bromine (**124**).

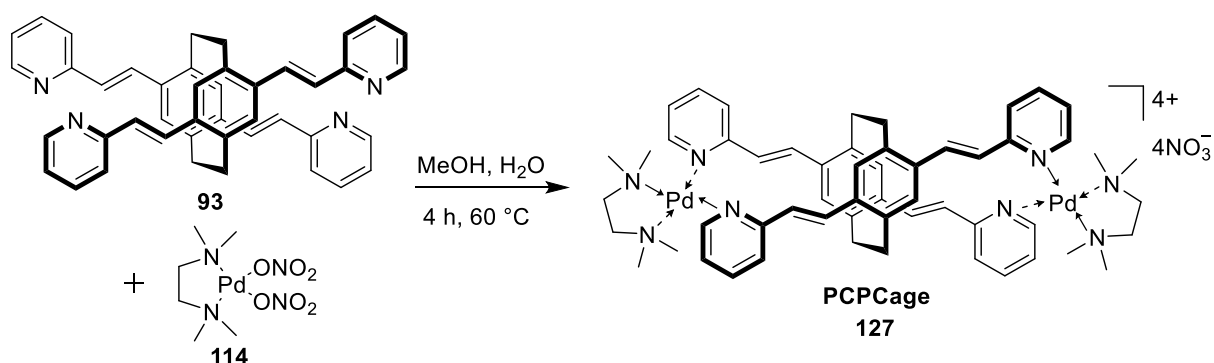
For the synthesis of coordination-driven assemblies, another option was subsequently tried. First the required ligands of palladium **126** and **114** were synthesized. These two palladium ligands were commonly used as molecular cages linkers and both were on substitution reactions at room temperature depending on the ease of complexation of the different ligands to palladium.



Scheme 33. Synthesis route for 4,4'-bis(bromomethyl)tolan (**114**).

The attempt was made on the disubstituted **pDMVCP** (**25**), and an additional sodium terephthalate (**113**) was added as another linker for assembly, but no cage-like product was obtained.

The three tetrasubstituted ligands **91**, **92**, and **93** were assembled and complexed with two palladium ligands **126** and **114**. After screening, the **QMVCPo** (**93**) and linker (**114**) were shown to yield products capable of 1:2 ratio reactions measured by ESI MS (**Figure 100**). This structure required further unambiguous confirmation from X-ray data and will therefore need to be investigated.



Scheme 34. Synthesis of **PCPCage** (**127**)

3.3.2 Characteristic Analysis.

The physical properties of the **PCPBox-1** were next studied and the results showed that absorption at 380 nm, the fluorescence emission was in the maximum region of 550 nm, and a half-peak width was approximately 200 nm (**Figure 101 a**). The structure had two interlocking spaces because of the PCP pseudo-*para* substitution, so it should have the same ability as the “bule box” to combine other guests as the host macrocycle.

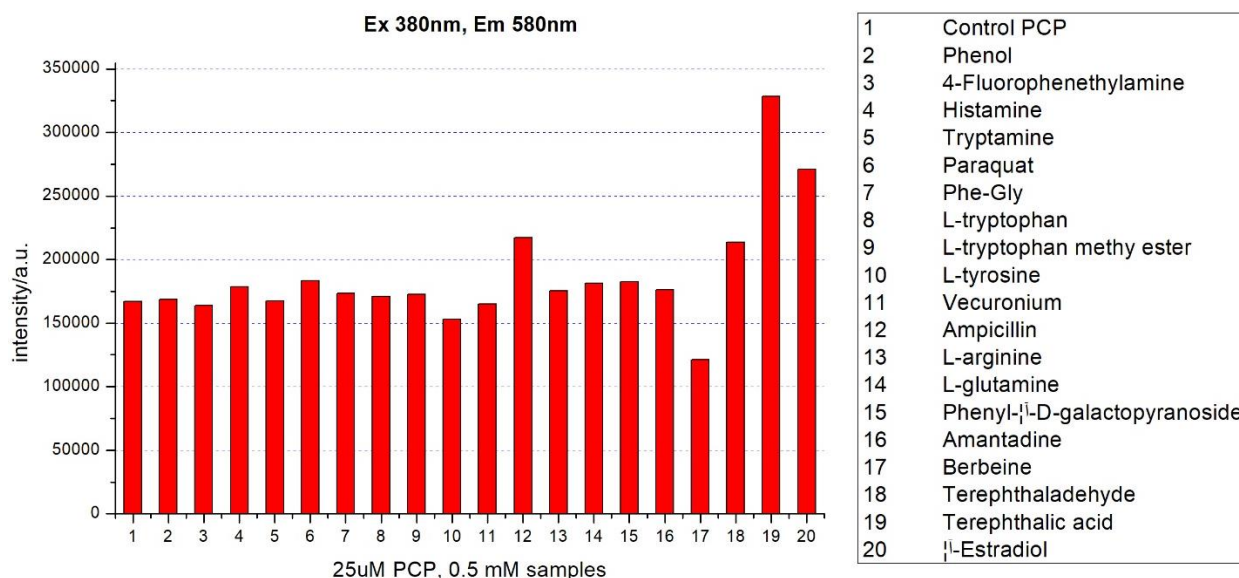


Figure 56. Fluorescence change in **PCPBox-1** solution (25 μ M) with adding samples (500 μ M).

The **PCPBox-1** was configured into a solution with a concentration of 25 μ M and divided into 20 groups, with the first group being a pure **PCPBox-1** solution as a control. The fluorescence intensity was measured in a well plate reader as a blank group, and then groups 2-19 were tested again for changes in fluorescence intensity by adding 19 different 0.5 mM small molecule solutions. The results were shown that the addition of several analytes resulted in a significant change in fluorescence (**Figure 56**), which were ampicillin, berberine, terephthalaldehyde, terephthalic acid, and β -estradiol, respectively. To verify this, several more analytes with significant changes were then taken and repeated in a 4.5% ethanol solution with consistent results and enhanced fluorescence of ampicillin (**Figure 101 b**). The results were as expected, and all these analytes had in common the presence of a benzene ring in the structure and the presence of a strongly planned atom such as oxygen in the substituent. In contrast to the charged paraquat, which carried the same positive charge to **PCPBox-1**, there is no significant binding.

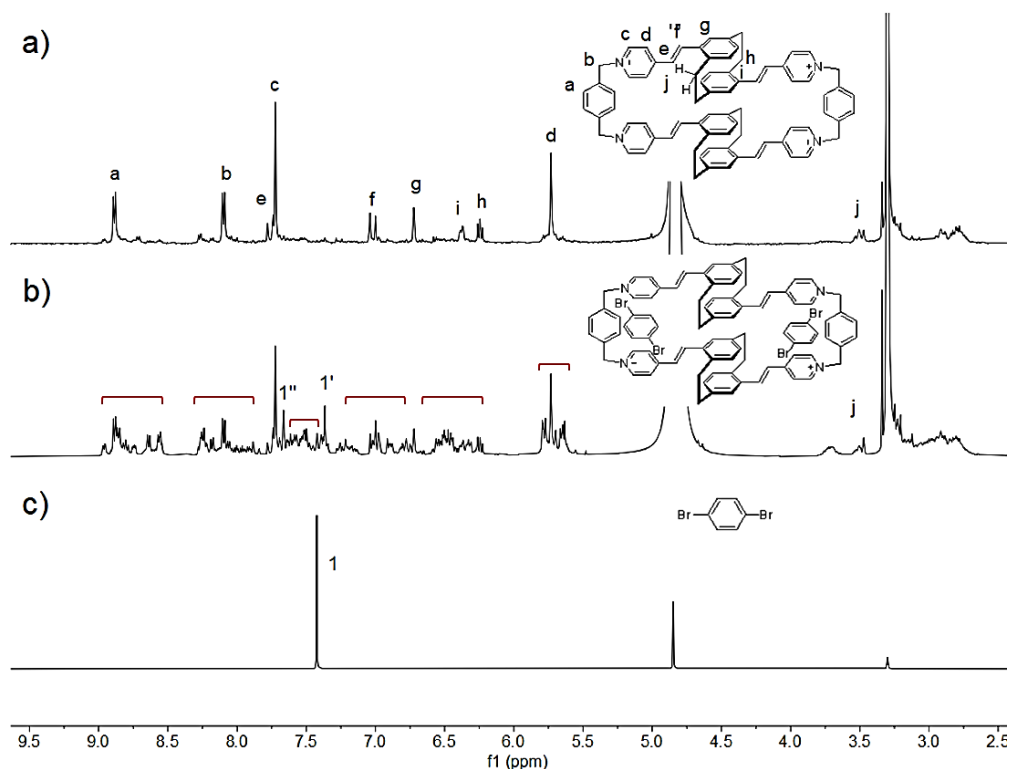


Figure 57. ^1H NMR spectra were recorded (400 MHz, D_2O , r.t.) for (a) **PCPBox-1**, (b) a mixture of guest and **PCPBox-1**, and (c) 1,4-dibromobenzene as a guest. Primed (',') resonances arise from **PCPBox-1**⊃guest complex.

In addition, NMR binding analysis was also done with the simple guest 1,4-dibromobenzene (**Figure 57**). The results showed that the proton peak above 1,4-dibromobenzene split into two parts, shifting towards up and down fields, respectively, while the box of the peaks showed irregular splitting of large divisions.

In summary, the **PCPBox-1** was tentatively shown to act as the host macrocycle for small molecule encapsulation, and we have been struggling for well-defined crystals. Structural assignments need complete and careful pieces of evidence in analysis. X-ray crystallography techniques can surely help in the exact assignment of the molecular-box cavity and structural orientation, and collecting other metrical data regarding the host-guest complexation considerably enhances our understanding when single crystal analysis is possible.

The position of N in pyridine can often influence the properties of the whole compound, for example in MOF^[142] and solar cells.^[143] The three tetrakispyridinyl substituted PCP synthesized earlier were observed in different colors in methanol solution (**Figure 58**). The 4-position of N in **QMVCPP** was in the deepest color, while **QMVCPPm** was the lightest.

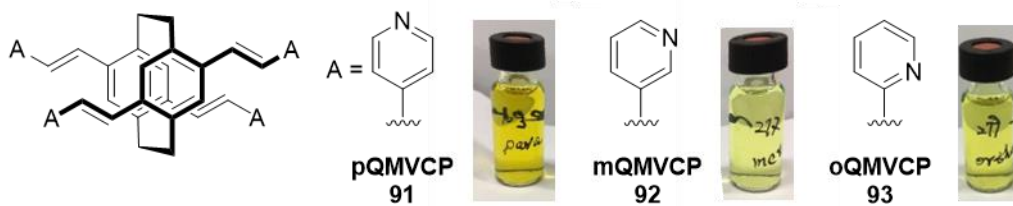


Figure 58. The methanol solution of **QMVCPP** (91), **QMVCPPm** (92), and **QMVCPPo** (93) at the same concentration.

They were spectroscopically characterized (**Figure 59**). Their common feature is the simultaneous display of three absorption peaks each at around 270 nm, 340 nm and 400 nm. **QMVCPP** exhibited a different absorption curve from the other two, showing no maximum absorption peak at 400 nm, instead appearing at 340 nm. The maximum excitation wavelength of 488 nm was obtained by simultaneous excitation with different wavelengths, and therefore the emission spectrum was used. The same **QMVCPP** in the emission spectrum showed a different emission peak from the other two, with the highest peak around 450 nm, thus also explaining the deeper color of its solution. And in terms of the solids, it showed an orange-red color, whereas the other two are a lighter orange.

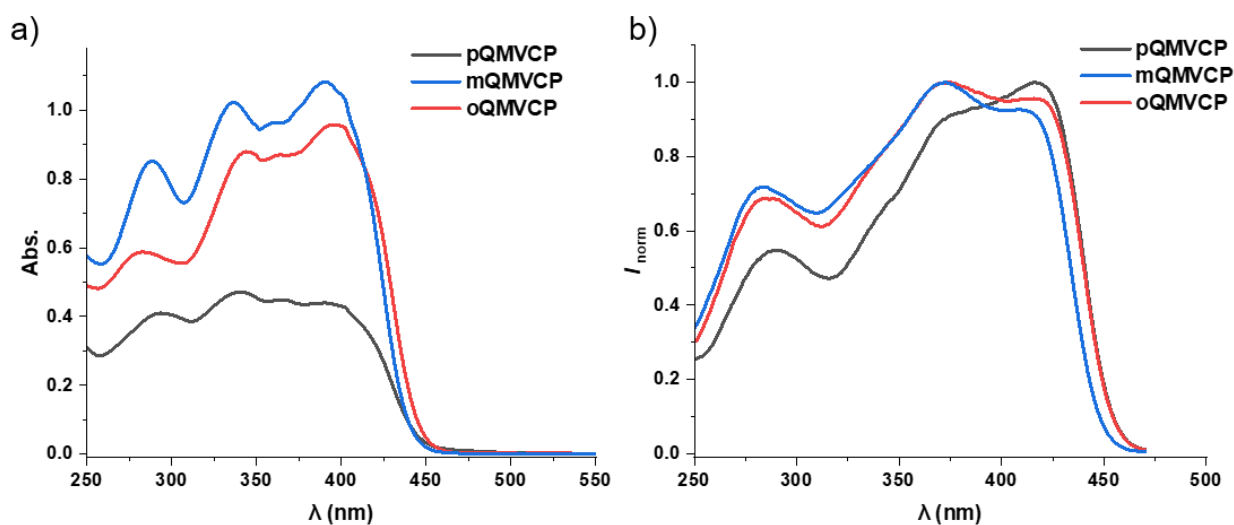


Figure 59. (a) UV-Vis absorption spectra of **QMVCPP** (24 μM), **QMVCPPm** (30 μM), and **QMVCPPo** (60 μM) in water. (b) Fluorescence emission spectrum ($\lambda_{\text{ex}} = 480 \text{ nm}$) **QMVCPP** (24 μM), and **QMVCPPm** (30 μM), and **QMVCPPo** (60 μM) in water. Dr. Changming Hu provided the results.

Combined with the results above, also thanks to the different N-positions **pQMVCPP** get the opportunity to form the cage directly, the other two need to add more linkers to try.

3.3.3 Other PCP compounds

Other PCP derivatives that have been synthesized are given here (**Figure 60**), which were used to construct various supramolecular assemblies. As part of this program, the synthetic potential of the newly prepared

chiral/chiral precursors is to be examined in the construction fundamentally important coordination and non-coordination molecular assemblies. Our laboratories' comprehensive research efforts are underway to achieve these important goals.

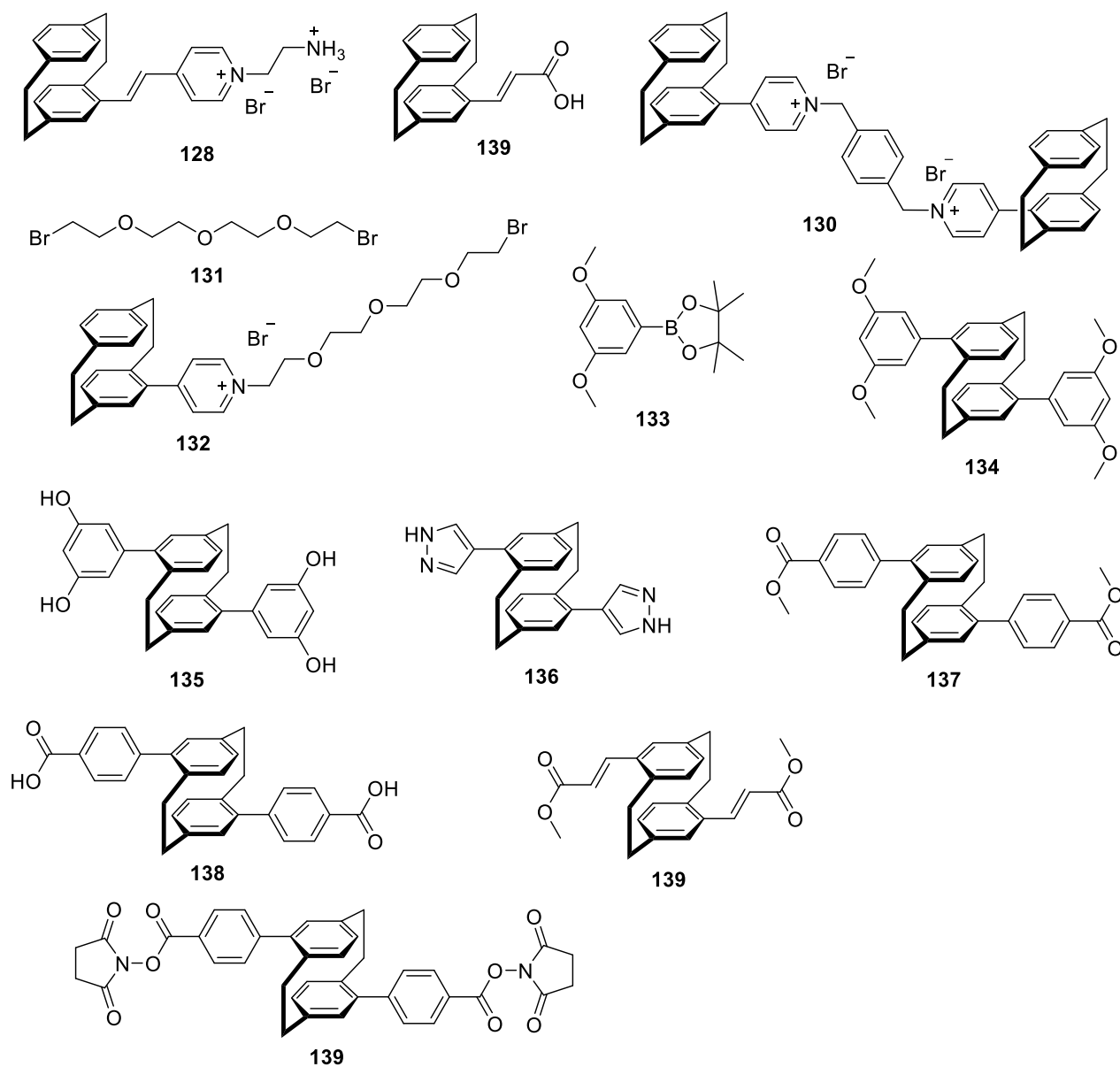


Figure 60. Other molecular structures synthesized basis on PCP.

4 Summary and Outlook

In this thesis, a series of [2.2]paracyclophane derivatives were designed and synthesized and have been used to investigate their affinity in the field of host-guest chemistry and supramolecular self-assembly. This study fabricated cucurbit[*n*]uril-based supramolecular assemblies with π -stacked cyclophanyl-derived pseudo *ortho*-, *meta*-, and *para*-substituted indicator dyes. The chromophore conjugation, their relative orientation, and substitution patterns of cyclophanyl scaffolds showed critical effects on modulating/enhancing sensing properties of the CB*n* host-guest supramolecular system. PCP molecular building blocks were used to construct various covalent/noncovalent assemblies with tailored properties and functions.

4.1 Exploration of Affinity on Foundational [2.2]Paracyclophane Derivatives

In the first section, three PCP derivatives were designed and synthesized based on **MPCP**, and their CB8 affinity analysis was carried out. Detailed spectroscopy demonstrated that they bound tightly to CB8 in a 1:1 model, but so weakly to CB7 that both **MPCP** and **DMPCP** were defined as unable to bind.

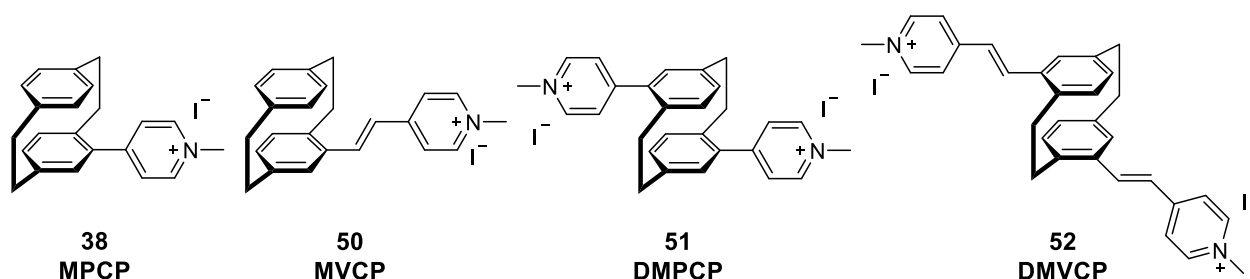


Figure 61. Chemical structures of **MPCP** (38), **MVCP** (50), **DMPCP** (51), and **DMVPCP** (52).

Next, they were systematically investigated by NMR and spectroscopy to calculate their binding constants to CB8 via a competition experiment by playing with Mem as a competitor (**Figure 62**). It was concluded that **DMPCP** was the strongest single-molecule guest for CB8 that had not been found to date. Moreover, these synthesized PCP derivatives have binding strengths at very high levels, which were not previously reported in the literatures. After comparison with literatures data, including CB7, the PCP-based guests can be considered a new type of potential candidates that is more selective for CB7 and CB8 in chemical sensing.

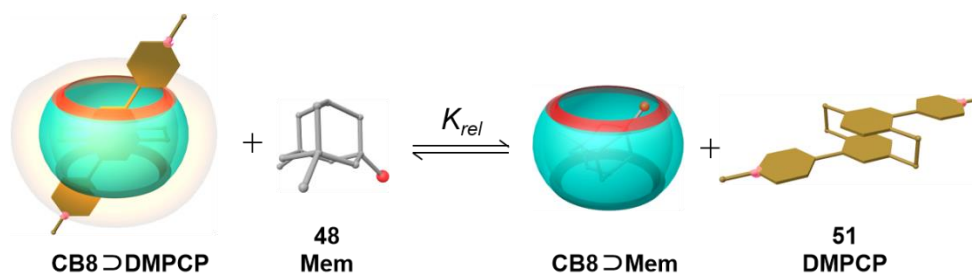


Figure 62. Schematic diagram of competitive displacement assay, replacing **DMPCP** with Mem in CB8

Finally, a calorimetric analysis of ITC was carried out, and the entropic and enthalpy values in favor of the combination of PCP and CB8 were obtained.

4.2 Exploration of Affinity on Extended and Functionalized [2.2]Paracyclophane Derivatives

In this section, diverse PCP derivatives, trisubstituted and tetrasubstituted PCPs, were first designed and synthesized. They were then studied for their ability to bind to CB8 while ignoring the larger branched structures. Therefore, their binding constants to CB8 were calculated via NMR with Mem as the competitor. The results were compared with those of the previous CB8 and it was concluded that **DMPCP** remains the strongest guest among them that binds to CB8. It was concluded that the number of positive charges of the PCP derivatives was not related to the binding strength, but to the backbone substitution pattern of the PCP structure itself.

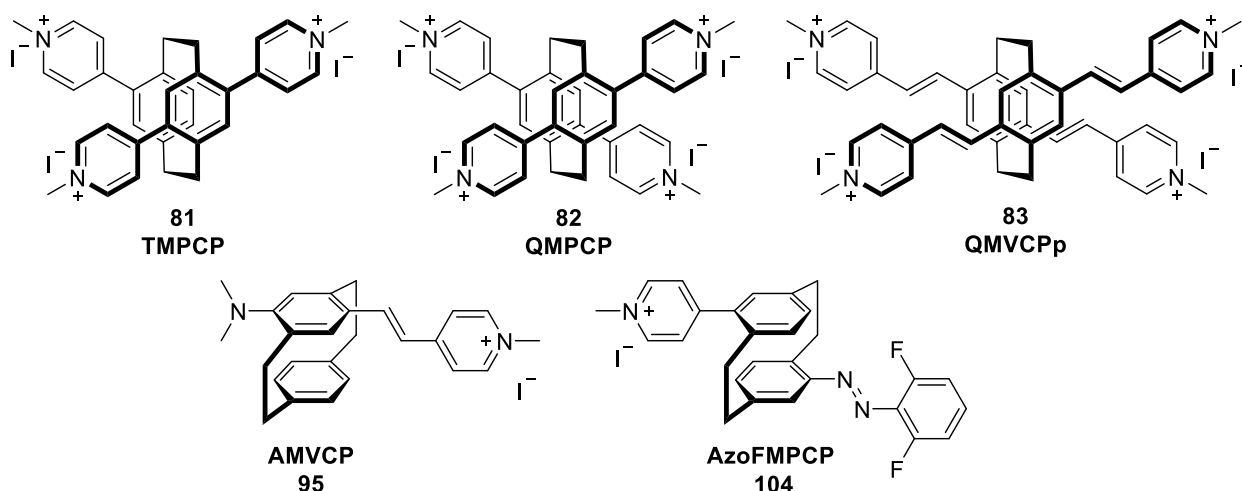


Figure 63. Chemical structures of **TMPCP (81)**, **QMPCP (82)**, **QMVCP (83)**, **AMVCP (95)** and **AzoFMVCP (104)**.

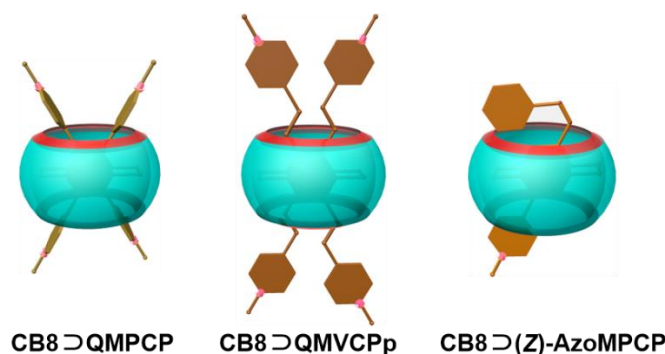


Figure 64. Schematic diagram of **QMPCP (82)**, **QMVCP (83)**, and **AzoFMVCP (104)** combined with CB8.

In addition, two other PCP derivatives have been synthesized and analyzed. One was a dimethylamine-modified PCP, which NMR and spectroscopy resolved. The final results proved that they did not qualify as a chemosensing candidate; the problem is either the emission wavelength region or the ability to bind CB8.

Azophenyl-modified PCP was synthesized and demonstrated its ability to bind to CB8. It was found by UV radiation that one of the structures performed isomeric transformation under normal conditions and can be stable. NMR then concluded that the structures were always able to keep the PCP core within the cavity when bound to CB8.

4.3 Supramolecular Skeleton and Cage based on [2.2]Paracyclophane

The feasibility of the functionalized PCP scaffold for supramolecular self-assembly was explored in combination with some linkers using the intermediates from the synthesis of the PCP guests. In this case, the covalent bond formed by the disubstituted **pDMVCP** via pyridinium was synthesized into the **PCPBox-1**, which showed that it could be used as a host to encapsulate small molecules in the cavities formed as “bule box”.

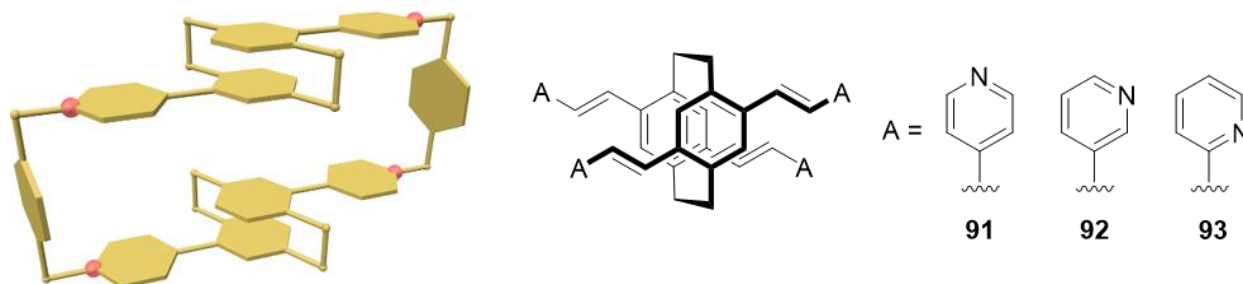


Figure 65. Schematic diagram of **PCPBOX-1 (118)** and molecular structures for tetrasubstituted PCP.

Lastly, the feasibility of tetrasubstitution for supramolecular self-assembly was explored, and other types of PCP structures were tried and synthesized.

In conclusion, the [2.2]paracyclophane, as a rigid structure and at the same time with an overall sphere-like electronic distribution, is good at acting as a guest for bonding with CB8. But also because of the specificity of its structure, it is more challenging to modify it properly. This also provides a broader scope for it to be applied in supramolecular topology and applications and more potential in supramolecular self-assembly.

5 Experimental Section

5.1 General Remarks

Parts of the general information are standardized descriptions and were adapted from previous group members.^[144]

Nomenclature of [2.2]Paracyclophane

The complicated IUPAC nomenclature for cyclophanes is rarely used. Instead, Vögtle *et al.* developed a specific and straight-forward nomenclature, based on a core-substituent ranking (**Figure 3**).^[145]

The core structure is named according to the length of the aliphatic bridges in brackets (e.g. [n.m]) and the benzene substitution patterns (*ortho*, *meta*, or *para*). [2.2]Paracyclophane belongs to the D_{2h} symmetry, broken by the first substituent, resulting in two planar chiral enantiomers. The arene bearing the substituent is set to a chirality plane, and the first atom of the cyclophane structure outside the plane and closest to the chirality center is defined as the “*pilot atom*”. If both arenes are substituted, the substituent with higher priority according to the CAHN-INGOLD-PRELOG (CIP) nomenclature is preferred.^[146] The stereo descriptor is determined by the sense of rotation viewed from the pilot atom. An unambiguous numeration is needed to describe the positions of the substituents correctly. The numbering of the arenes follows the sense of rotation determined by CIP. To indicate the stereochemistry of the planar chirality, a subscripted *p* is added. Unfortunately, the numbering of the second arene is inconsistent in the literature. In this thesis, the rotating direction of the numbering of the second ring is set in a way that is viewed from the center of the molecule, the sense of rotation consistent. Therefore, another description based on the benzene substitution patterns is preferred for disubstituted [2.2]paracyclophanes. Substitution on the other ring is commonly named pseudo-(*ortho*, *meta*, *para*, or *geminal*).

Materials and Methods

The starting materials, solvents, and reagents were purchased from abcr, Acros, Alfa Aesar, Apollo Scientific, Carbolution, ChemPUR, Fluka, Fluorochem, Merck, Riedel-de Haën, Sigma Aldrich, Strem, TCI, or Thermo Fisher Scientific and used without further purification unless stated otherwise.

Solvents of technical quality were purified by distillation or with the solvent purification system MB SPS5 (acetonitrile, dichloromethane, diethyl ether, tetrahydrofuran, toluene) from MBraun. Solvents of *p.a.* quality were purchased from Acros, Fisher Scientific, Sigma Aldrich, Roth, or Riedel-de Haën and were used without further purification. Diphenyl ether and α,α,α -trifluoro toluene were distilled over calcium hydride. *n*-Pentane was distilled over sodium and benzophenone. Other solvents were obtained from commercial suppliers: anhydrous benzene (Sigma Aldrich, <0.005% water), anhydrous *N,N*-dimethylformamide (Sigma Aldrich, <0.005% water), anhydrous 1,4-dioxane (Sigma Aldrich, <0.005% water), anhydrous dimethyl sulfoxide (Sigma Aldrich, <0.005% water), anhydrous ethanol (Sigma Aldrich,

<0.005% water), anhydrous methanol (Sigma Aldrich, <0.005% water), anhydrous isopropanol (Sigma Aldrich, <0.005% water).

Oxygen-free solvents were obtained by the freeze-pump-thaw (three cycles) technique.

Air- and moisture-sensitive reactions were carried out under argon atmosphere in oven-dried glassware using standard Schlenk techniques.

A MBraun LABmaster with argon atmosphere was used for reaction set-ups in the Glovebox. All materials used were dried for at least 24 h at 100 °C before bringing them into the glovebox.

flat-bottom crimp neck vials from ChromaGlobe with aluminum crimp cap were used for certain reactions.

Liquids were added with a stainless-steel cannula and solids were added in a powdered shape.

Reactions at low temperatures were cooled using flat dewars produced by ISOTHERM (Karlsruhe) with water/ice or isopropanol/anhydrous ice mixtures.

Solvents were evaporated under reduced pressure at 45 °C using a rotary evaporator. For solvent mixtures, each solvent was measured volumetrically.

Flash column chromatography was performed using Merck silica 60 (0.040 × 0.063 mm, 230–400 mesh ASTM) and quartz sand (glowed and purified with hydrochloric acid).

The Rayonet reactor Model RPR-100 with (16) 14W light bulbs (254 nm) was used for the irradiation with UV light.

Reaction Monitoring

All reactions were monitored by thin-layer chromatography (TLC) using silica-coated aluminum plates (Merck, silica 60, F254). UV active compounds were detected with a UV-lamp at 254 nm and 366 nm excitation. Vanillin, basic potassium permanganate, ninhydrin, or Seebach solution was used as TLC-stain when required.

GC-MS (gas chromatography-mass spectrometry) measurements were performed on an Agilent Technologies model 6890N (electron impact ionization), equipped with an Agilent 19091S-433 column (5% phenyl methyl siloxane, 30 m, 0.25 µm) and a 5975B VL MSD detector with a turbopump. Helium was used as a carrier gas.

Nuclear Magnetic Resonance Spectroscopy (NMR)

NMR spectra were recorded on a Bruker Avance 400 NMR instrument at 400 MHz for ¹H NMR, 101 MHz for ¹³C NMR, or a Bruker Avance 500 NMR instrument at 500 MHz for ¹H NMR, 126 MHz for ¹³C NMR.

The NMR spectra were recorded at room temperature in deuterated solvents acquired from Eurisotop, Sigma Aldrich, or Deutero. The chemical shift δ is displayed in parts per million [ppm] and the references used were the ^1H and ^{13}C peaks of the solvents themselves:

d_1 -chloroform (CDCl_3): 7.26 ppm for ^1H and 77.16 ppm for ^{13}C

d_6 -dimethyl sulfoxide ($\text{DMSO-}d_6$): 2.50 ppm for ^1H and 39.52 ppm for ^{13}C

d_4 -methanol (CD_3OD): 3.31 ppm for ^1H and 49.00 ppm for ^{13}C

d_3 -acetonitrile (CD_3CN): 1.94 ppm for ^1H and 118.26 ppm for ^{13}C

For the characterization of centrosymmetric signals, the median point was chosen for multiplets in the signal range. The following abbreviations were used to describe the proton splitting pattern: d = doublet, t = triplet, m = multiplet, dd = doublet of a doublet, ddd = doublet of doublet of a doublet, dddd = doublet of doublet of doublet of a doublet, dt = doublet of a triplet. Absolute values of the coupling constants “ J ” are given in Hertz [Hz] in absolute value and decreasing order. Signals of the ^{13}C spectrum were assigned by distortionless enhancement by polarization transfer (DEPT) spectra DEPT90 and DEPT135 or phase-edited heteronuclear single quantum coherence (HSQC). They were specified in the following way: + = primary or tertiary carbon atoms (positive phase), – = secondary carbon atoms (negative phase), and C_q = quaternary carbon atoms (no signal).

Infrared Spectroscopy (IR)

The infrared spectra were recorded with a Bruker, Alpha P instrument. All samples were measured by attenuated total reflection (ATR). The positions of the absorption bands are given in wavenumbers $\tilde{\nu}$ in cm^{-1} and were measured in the range from 3600 cm^{-1} to 500 cm^{-1} .

Characterization of the absorption bands was done in dependence on the absorption strength with the following abbreviations: vs (very strong, 0–9%), s (strong, 10–39%), m (medium, 40–69%), w (weak, 70–89%), vw (very weak, 90–100%).

Mass Spectrometry (MS)

Electron ionization (EI) and fast atom bombardment (FAB) experiments were conducted using a Finnigan, MAT 90 (70 eV) instrument, with 3-nitrobenzyl alcohol (3-NBA) as matrix and reference for high resolution. For the interpretation of the spectra, molecular peaks $[\text{M}]^+$, peaks of protonated molecules $[\text{M}+\text{H}]^+$ and characteristic fragment peaks are indicated with their mass-to-charge ratio (m/z) and their intensity in percent, relative to the base peak (100%) is given. In the case of high-resolution measurements, the maximum tolerated error is ± 5 ppm.

APCI and ESI experiments were recorded on a Q-Exactive (Orbitrap) mass spectrometer (Thermo Fisher Scientific, San Jose, CA, USA) equipped with a HESI II probe to record high resolution. The tolerated error is ± 5 ppm of the molecular mass. The spectra were interpreted by molecular peaks $[\text{M}]^+$, peaks of

protonated molecules $[M+H]^+$ and characteristic fragment peaks and indicated with their mass-to-charge ratio (m/z).

High-Performance Liquid Chromatography (HPLC)

Analysis of the enantiomeric excess was conducted using an AGILENT HPLC 1100 series system with a G1322A degasser, a G1211A pump, a G1313A autosampler, a G1316A column oven, and a G1315B diode array system using a Daicel Chiralpak® AD-H (4.6 × 250 mm, 5 μm particle size), Daicel Chiralpak® OD-H (4.6 × 250 mm, 5 μm particle size), Daicel Chiralpak® OJ-H (4.6 × 250 mm, 5 μm particle size), or YMC CHIRAL ART Amylose-SA column (4.6 × 250 mm, 5 μm particle size) columns were used with HPLC-grade *n*-hexane/isopropanol as mobile phase, respectively.

Analytic HPLC was measured with the 1200 Series from AGILENT TECHNOLOGIES with a YMC C18-column JH08S04-2546WT with 250×4.8 mm and 4 μm (column material). Preparative HPLC separation was performed with a JASCO LC-NetII / ADC HPLC system equipped with two PU-2087 Plus pumps, a CO-2060 Plus thermostat, an MD-2010 Plus diode array detector and a CHF-122SC fraction collector from ADVANTEC or PURIFLASH® 4125 from INTERCHIM, equipped with InterSoft V5.1.08 software and a UV diode array detector. The stationary phase was in both systems a VDSpher column with C18-M-SE, 250×20 mm and 10 μm from VDSOPTILAB. For the elution, a linear gradient was used from 5% to 95% MeCN with 0.1% aqueous TFA in diH₂O with 0.1% aqueous TFA and a flow rate of 10 mL/min at 25 °C.

Absorption Spectroscopy

Absorbance spectra were measured at 25°C in Milli-Q water or PBS buffer on a JASCO V-730 double-beam UV-Vis spectrophotometer. PMMA cuvettes with a light path of 10 mm and dimensions of 10 × 10 mm from Brand with a spectroscopic cut-off at 220 nm were utilized for UV-Vis absorption experiments. The samples were equilibrated using a water thermostatic cell holder STR-812, while the cuvettes were equipped with a stirrer allowing rapid mixing.

Fluorescence Spectroscopy

Steady-state emission spectra and time-resolved emission profiles were recorded on a JASCO FP- 8300 fluorescence spectrometer equipped with a 450 W Xenon arc lamp, double-grating excitation, and emission monochromators. Emission spectra were corrected for source intensity (lamp and grating) and the emission spectral response (detector and grating) by standard correction curves. All titration and kinetic experiments were carried out at 25 °C using a water thermostatic cell holder STR-812, while the cuvettes were equipped with a stirrer allowing rapid mixing. PMMA cuvettes with a light path of 10 mm and dimensions of 10 × 10 mm from Brand with a spectroscopic cut-off at 220 nm were utilized for fluorescence-based titration experiments.

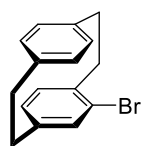
96-well Plate Reader

Salt-adaptive analytes distinction assay was performed in a CLARIOstar Plus fluorescence plate reader (BMG Labtech). The total volume of solution before titration was 200 μL in each microplate well. All

titration and kinetic experiments were carried out at 25°C with a temperature control system. For detection settings, the excitation was in the wavelength range from 450 nm to 490 nm, and emission was collected from 530 nm to 570 nm with a dichroic mirror at 511.2 nm. The pump speed of the injector was selected as 430 $\mu\text{L/s}$ for the titration steps. Shaking of the microplate was carried out at 300 rpm for 60 seconds before each cycle.

5.2 Exploration of Affinity on Functional [2.2]Paracyclophane Derivatives

(*rac*)-4-Bromo[2.2]paracyclophane (54)



To iron powder (27.0 mg, 482 μmol , 2.00 mol%) were added 5 mL of a solution of bromine (1.25 mL, 3.91 g, 24.5 mmol, 1.02 equiv.) in dichloromethane (30 mL). After stirring for 1 hour at room temperature, the reaction mixture was diluted with dichloromethane (40 mL) and [2.2]paracyclophane (5.00 g, 24.0 mmol, 1.00 equiv.) was added. The reaction mixture was stirred for 30 minutes followed by the dropwise addition of the remaining bromine solution over 5 hours. The reaction mixture was stirred overnight at room temperature and a saturated aqueous solution of $\text{Na}_2\text{S}_2\text{O}_3$ was added. After discoloration of the reaction mixture, the aqueous phase was extracted with dichloromethane (3×100 mL) and the combined organic phases were dried over Na_2SO_4 . The solvent was removed under reduced pressure to obtain the colorless solid (6.14 g, 21.4 mmol, 89%).

$R_f = 0.43$ (cyclohexane)

^1H NMR (400 MHz, CDCl_3 , ppm) $\delta = 7.09$ (dd, $J = 7.8, 2.0$ Hz, 1H, H_{Ar}), 6.52–6.46 (m, 1H, H_{Ar}), 6.45–6.36 (m, 5H, H_{Ar}), 3.39 (ddd, $J = 13.4, 10.1, 2.2$ Hz, 1H, H_{PC}), 3.13 (ddd, $J = 13.0, 10.1, 6.0$ Hz, 1H, H_{PC}), 3.08–2.94 (m, 4H, H_{PC}), 2.89–2.81 (m, 1H, H_{PC}), 2.75 (ddd, $J = 13.4, 10.4, 6.0$ Hz, 1H, H_{PC}).

^{13}C NMR (100 MHz, CDCl_3 , ppm) $\delta = 141.6$ (C_q , C_{Ar}), 139.3 (C_q , C_{Ar}), 139.1 (C_q , C_{Ar}), 137.3 (+, CH, C_{Ar}), 135.1 (+, CH, C_{Ar}), 133.3 (+, CH, C_{Ar}), 133.0 (C_q , C_{Ar}), 132.9 (+, CH, C_{Ar}), 132.3 (+, CH, C_{Ar}), 131.5 (+, CH, C_{Ar}), 128.7 (+, CH, C_{Ar}), 127.0 (C_q , C_{Ar}), 35.9 (–, CH_2), 35.5 (–, CH_2), 34.8 (–, CH_2), 33.5 (–, CH_2).

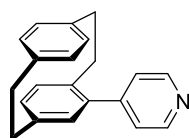
MS (EI, 70 eV, 20 $^\circ\text{C}$, %) $m/z = 287/289$ (100/97) $[\text{M}+\text{H}]^+$, 364 (28) $[\text{M}+\text{H}]^+$, 156 (24) $[\text{C}_{11}\text{H}_{10}\text{N}]^+$, 286 (23) $[\text{M}-\text{C}_5\text{H}_2\text{N}]^+$.

HRMS-EI (m/z): $[\text{M} + \text{H}]^+$, calc. for $\text{C}_{16}\text{H}_{16}^{81}\text{Br}$, 287.0430; found: 287.0427

IR (ATR, $\tilde{\nu}$) = 2924 (s), 2849 (m), 1585 (w), 1475 (m), 1390 (m), 1034 (s), 897 (s), 839 (vs), 806 (m), 793 (s), 718 (s), 708 (vs), 691 (m), 667 (s), 640 (vs), 577 (m), 513 (vs), 473 (s) cm^{-1} .

The analytical data match those reported in the literature.^[122a]

(*rac*)-4-(4'-Pyridyl) [2.2]paracyclophane (55)



A vessel was charged with (*rac*)-4-bromo[2.2]paracyclophane (1.28 g, 3.00 mmol, 1.00 equiv.), pyridine-4-boronic acid (1.08 g, 6.00 mmol, 2.00 equiv.), palladium-tetrakis(triphenylphosphine) (208 mg, 180 μmol , 0.04 equiv.), potassium phosphate (1.59 g, 7.50 mmol, 1.60 equiv.) under argon atmosphere. Then dioxane (16 mL) and water (8 mL) were added, and the mixture was heated under reflux for 16 h. The reaction mixture was then cooled down to room temperature, extracted with ether (3×20 mL), and the extracts were dried by MgSO_4

and evaporated under reduced pressure. The crude solid was purified by column chromatography on silica gel by cyclohexane/ethyl acetate 2:1 to obtain the title compound (304 mg, 1.1 mmol, 24%) as a white solid.

$R_f = 0.43$ (cyclohexane/ethyl acetate 2:1)

$^1\text{H NMR}$ (400 MHz, CDCl_3 , ppm) $\delta = 8.70$ (d, $J = 5.6$ Hz, 2H, H_{Py}), 7.42 (dd, $J = 4.6, 1.4$ Hz, 2H, H_{Py}), 6.64 (dd, $J = 8.0, 3.5$ Hz, 2H, H_{Ar}), 6.59 (dd, $J = 7.8, 5.0$ Hz, 3H, H_{Ar}), 6.54 (d, $J = 2.0$ Hz, 2H, H_{Ar}), 3.40 (ddd, $J = 12.6, 10.1, 2.9$ Hz, 1H, H_{PC}), 3.20–3.11 (m, 2H, H_{PC}), 3.09–2.88 (m, 3H, PC-H), 2.66 (ddd, $J = 13.1, 10.1, 4.5$ Hz, 1H, H_{PC}).

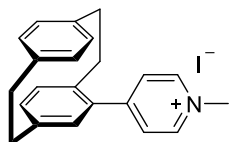
$^{13}\text{C NMR}$ (101 MHz, CDCl_3 , ppm) $\delta = 149.7$ (+, CH, 2C, C_{Py}), 148.9 (C_{q} , C_{Py}), 140.2 (C_{q} , C_{Ar}), 139.6 (C_{q} , C_{Ar}), 139.5 (C_{q} , C_{Ar}), 139.1 (C_{q} , C_{Ar}), 137.3 (C_{q} , C_{Ar}), 136.2 (+, CH, C_{Ar}), 133.6 (+, CH, C_{Ar}), 133.3 (+, CH, C_{Ar}), 139.7 (+, CH, C_{Ar}), 132.0 (+, CH, C_{Ar}), 132.0 (+, CH, C_{Ar}), 129.7 (+, CH, C_{Ar}), 124.6 (+, CH, 2C, C_{Py}), 35.5 (–, CH_2), 35.2 (–, CH_2), 34.9 (–, CH_2), 33.9 (–, CH_2).

MS (ESI, 70 eV, 20 °C, %) $m/z = 286/287$ (100/22) $[\text{M}+\text{H}]^+$.

HRMS-ESI (m/z): $[\text{M}+\text{H}]^+$, calc. for $\text{C}_{21}\text{H}_{20}\text{N}$, 286.1590; found: 286.1588.

IR (ATR, $\tilde{\nu}$) = 3023 (w), 2953 (w), 2927 (s), 2897 (w), 2854 (m), 1594 (vs), 1541 (w), 1496 (w), 1475 (w), 1439 (w), 1409 (s), 1400 (s), 1213 (w), 1092 (w), 992 (w), 898 (m), 850 (s), 824 (vs), 793 (s), 734 (m), 717 (vs), 667 (w), 647 (vs), 622 (vs), 594 (s), 558 (s), 516 (vs), 483 (vs), 436 (m), 424 (m), 378 (w) cm^{-1} .

(rac)-4-(N-methyl-4'-pyridinium)[2.2]paracyclophane iodide (MPCP, 38)



A solution of a mixture of (*rac*)-4-(4'-pyridyl)[2.2]paracyclophane (148 mg, 519 μmol , 1.00 equiv.) and methyl iodide (3.21 mmol, 200 μmL) in acetonitrile (12 mL) was stirred at 40 °C for 12 h protected from light. After the solution was

cooled to room temperature, the solvent was removed under reduced pressure to give a crude product, which was washed with water (20 mL), and dried in air to yield (172 mg, 402 μmol , 78%) a light-yellow solid.

$^1\text{H NMR}$ (400 MHz, CDCl_3 , ppm) $\delta = 9.22$ (d, $J = 6.5$ Hz, 2H, H_{Py}), 8.08–8.01 (m, 2H, H_{Py}), 6.72–6.68 (m, 3H, H_{Ar}), 6.66–6.56 (m, 3H, H_{Ar}), 6.44 (dd, $J = 7.9, 2.0$ Hz, 1H, H_{Ar}), 4.70 (s, 3H, CH_3), 3.34 (ddd, $J = 13.7, 10.1, 3.6$ Hz, 1H, H_{PC}), 3.25–3.05 (m, 5H, H_{PC}), 3.01–2.90 (m, 1H, H_{PC}), 2.79 (ddd, $J = 14.1, 10.0, 5.1$ Hz, 1H, H_{PC}).

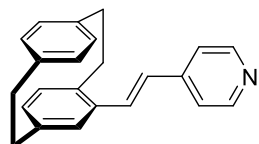
$^{13}\text{C NMR}$ (100 MHz, CDCl_3 , ppm) $\delta = 145.1$ (+, CH, 2C, C_{Py}), 141.4 (C_{q} , C_{Py}), 139.8 (C_{q} , C_{Ar}), 139.1 (C_{q} , C_{Ar}), 137.1 (+, CH, 2C, C_{Ar}), 136.4 (C_{q} , 2C, C_{Ar}), 133.7 (+, CH, C_{Ar}), 132.8 (C_{q} , C_{Ar}), 132.8 (+, CH, C_{Ar}), 132.5 (+, CH, C_{Ar}), 131.9 (+, CH, C_{Ar}), 129.8 (C_{q} , C_{Ar}), 127.9 (+, CH, 2C, C_{Py}), 48.7 (+, CH_3), 35.3 (–, CH_2), 35.3 (–, CH_2), 34.0 (–, CH_2), 29.7 (–, CH_2).

MS (ESI, 70 eV, 20 °C, %) $m/z = 300/301$ (100/23) $[\text{M}]^+$,

HRMS-ESI (m/z): $[M-I]^+$, calc. for $C_{22}H_{22}N$, 300.1747; found: 300.1744.

IR (ATR, $\tilde{\nu}$) = 3504 (m), 3489 (m), 3465 (m), 3441 (m), 2924 (m), 1638 (vs), 1561 (m), 1514 (s), 1500 (m), 1460 (m), 1220 (m), 1197 (s), 849 (vs), 805 (s), 720 (vs), 646 (vs), 554 (m), 514 (vs), 484 (vs), 462 (s), 448 (vs), 438 (vs), 428 (vs), 412 (vs), 402 (vs), 387 (vs), 378 (vs) cm^{-1} .

(rac)-4-(4'-Pyridyl-(E)-vinyl)[2.2]paracyclophane (56)



A vessel was charged with (*rac*)-4-bromo[2.2]paracyclophane (1.44 g, 5.00 mmol, 1.00 equiv.), 4-vinylpyridine (1.05 g, 10.0 mmol, 2.00 equiv.), palladium acetate (56 mg, 250 μ mol, 0.05 equiv.), tetrapropylammonium bromide (1.33 g, 5.00 mmol, 1.00 equiv.), potassium carbonate (1.73 mg, 12.5 mmol, 2.50 equiv.), and DMF (25 mL) under argon. The reaction mixture was heated at 110 $^{\circ}C$ for 24 h. Then the reaction was cooled to room temperature, diluted with CH_2Cl_2 , and washed with brine. The organic layer was dried with Na_2SO_4 and concentrated. The residual liquid (containing a small DMF) was precipitated with hexane and collected by filtration. The crude solid was purified by column chromatography on silica gel by cyclohexane/ethyl acetate 2:1 to obtain the title compound (820 mg, 2.60 mmol, 53%) as an orange solid.

R_f = 0.45 (dichloromethane/methanol 20:1)

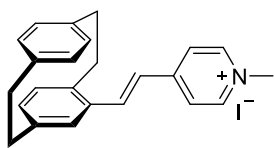
1H NMR (400 MHz, $CDCl_3$, ppm) δ = 8.64–8.58 (m, 2H, H_{Py}), 7.43–7.36 (m, 3H, H_{Py} , $CH=CH$), 6.80 (d, J = 16.1 Hz, 1H, H_{Ar}), 6.70 (d, J = 1.8 Hz, 1H, H_{Ar}), 6.62 (dd, J = 7.9, 1.8 Hz, 1H, H_{Ar}), 6.57–6.53 (m, 3H, H_{Ar}), 6.50 (d, J = 7.8 Hz, 1H, H_{Ar}), 6.43 (dd, J = 7.9, 1.8 Hz, 1H, H_{Ar}), 3.64–3.53 (m, 1H, H_{PC}), 3.25–3.10 (m, 3H, H_{PC}), 3.10–2.86 (m, 4H, H_{PC}).

^{13}C NMR (100 MHz, $CDCl_3$, ppm) δ = 150.3 (+, CH, 2C, C_{Py}), 145.1 (C_q , C, C_{Py}), 140.2 (C_q , C, C_{Ar}), 139.4 (C_q , C, C_{Ar}), 139.1 (C_q , C, C_{Ar}), 136.3 (C_q , C, C_{Ar}), 135.2 (+, CH, C_{Ar}), 133.1 (+, CH, C_{Ar}), 133.1 (+, CH, C_{Ar}), 133.0 (+, CH, 2C, C_{Ar}), 131.8 (+, CH, C_{Ar}), 131.1 (+, $CH=CH$), 130.5 (+, CH, C_{Ar}), 130.1 (+, CH, C_{Ar}), 126.3 (+, $CH=CH$), 120.9 (+, CH, 2C, C_{Py}), 35.5 (–, CH_2), 35.2 (–, CH_2), 35.1 (–, CH_2), 33.9 (–, CH_2).

MS (EI, 70 eV, 20 $^{\circ}C$, %) m/z = 312/313 (100/32) $[M+H]^+$.

HRMS-EI (m/z): $[M+H]^+$, calc. for $C_{23}H_{21}N$, 312.1747; found: 312.1742.

IR (ATR, $\tilde{\nu}$) = 2927 (m), 2856 (w), 1591 (vs), 1409 (s), 1214 (w), 1082 (w), 958 (vs), 948 (s), 936 (m), 895 (m), 875 (s), 857 (m), 846 (s), 796 (vs), 775 (m), 737 (w), 718 (vs), 653 (s), 633 (s), 584 (s), 554 (s), 544 (s), 520 (vs), 513 (vs), 482 (s), 467 (s), 455 (s), 431 (m), 411 (w), 394 (w), 384 (m) cm^{-1} .

(rac)-4-(N-Methyl-4'-pyridinium-(E)-vinyl)[2.2]paracyclophane iodide (MVCP, 50)

A solution of a mixture of (*rac*)-4-(4'-pyridyl-(*E*)-vinyl)[2.2]paracyclophane iodide (105 mg, 500 μmol , 1.00 equiv.) and methyl iodide (3.21 mmol, 200 μmL) in acetonitrile (10 mL) was stirred at 40 °C for 16 h protected from light. After the solution was cooled to room temperature, removed solvent under reduced pressure to give a residue, washed with water (20 mL), and dried in air to yield (121 mg, 267 μmol , 79%) a brown yellow solid.

$R_f = 0.5$ (dichloromethane/methane 5:1)

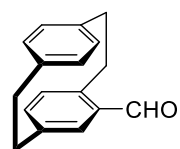
^1H NMR (400 MHz, DMSO- d_6 , ppm) $\delta = 8.87$ (d, $J = 6.5$ Hz, 2H, H_{Py}), 8.38 (d, $J = 6.6$ Hz, 2H, H_{Py}), 7.96 (d, $J = 16.1$ Hz, 1H, CH=CH), 7.30 (d, $J = 16.1$ Hz, 1H, CH=CH), 6.96 (d, $J = 1.7$ Hz, 1H, H_{Ar}), 6.63 (dd, $J = 7.8, 1.7$ Hz, 1H, H_{Ar}), 6.59–6.52 (m, 3H, H_{Ar}), 6.45 (q, $J = 1.1$ Hz, 2H, H_{Ar}), 4.28 (s, 3H, CH_3), 3.84–3.72 (m, 1H, H_{PC}), 3.13–3.07 (m, 3H, H_{PC}), 3.04–2.97 (m, 3H, H_{PC}), 2.93–2.88 (m, 1H, H_{PC}).

^{13}C NMR (101 MHz, DMSO- d_6 , ppm) $\delta = 153.3$ (C_q , C_{Ar}), 145.4 (+, 2C, CH, C_{Py}), 141.5 (C_q , C_{Ar}), 140.7 (C_q , C_{Ar}), 139.6 (C_q , C_{Ar}), 139.4 (C_q , C_{Ar}), 138.9 (+, CH=CH), 135.8 (C_q , C_{Ar}), 135.7 (+, CH, C_{Ar}), 135.0 (+, CH, C_{Ar}), 133.6 (+, CH, C_{Ar}), 133.5 (+, CH, C_{Ar}), 132.1 (+, CH, C_{Ar}), 131.3 (+, CH, C_{Ar}), 130.7 (+, CH, C_{Ar}), 124.1 (+, 2C, CH, C_{Py}), 123.9 (+, CH=CH), 47.3 (+, CH_3), 35.3 (–, CH_2), 35.2 (–, CH_2), 35.0 (–, CH_2), 33.6 (–, CH_2).

MS (EI, m/z , 70 eV, 70 °C): 326.3 (100) $[\text{M}]^+$, 326 (100), 327 (25).

HRMS–EI (m/z): $[\text{M}-\text{I}]^+$ calc. for $\text{C}_{24}\text{H}_{24}\text{N}$, 326.1903; found: 326.1909.

IR (ATR, $\tilde{\nu}$) = 3009 (m), 2922 (m), 2850 (m), 1639 (s), 1612 (vs), 1587 (s), 1564 (m), 1514 (s), 1500 (m), 1480 (m), 1468 (m), 1449 (m), 1319 (m), 1183 (vs), 1154 (s), 1143 (s), 1118 (s), 1101 (s), 1082 (s), 1050 (m), 963 (s), 936 (m), 885 (m), 868 (s), 819 (vs), 798 (s), 728 (m), 717 (s), 642 (s), 615 (m), 582 (m), 520 (s), 506 (vs), 489 (s), 470 (m), 465 (m), 453 (m), 446 (m), 428 (m), 419 (m), 401 (m), 384 (m) cm^{-1} .

(rac)-4-Formyl[2.2]paracyclophane (57)

[2.2]paracyclophane (12.0 g, 57.6 mmol, 1.00 equiv.) was dissolved in CH_2Cl_2 (300 mL) under argon and cooled to 0 °C. Titanium(IV) tetrachloride (12.6 mL, 115 mmol, 1.05 equiv.) and dichloromethoxymethane (5.50 mL, 60.5 mmol, 2.00 equiv.) were added subsequently. The mixture was stirred at 0 °C to room temperature for 6 h, poured into ice water (200 mL), and stirred for another 1 h. The two phases were separated, and the aqueous phase was extracted with CH_2Cl_2 (100 mL). The combined organic phases were dried over MgSO_4 and concentrated under reduced pressure. The crude product was purified by column chromatography on silica (cyclohexane/ethyl acetate 20:1) followed by recrystallization in 200 mL hot cyclohexane to give (*rac*)-4-formyl[2.2]paracyclophane (12.8 g, 54.1 mmol, 94%) as a white solid.

$R_f = 0.42$ (cyclohexane/ethyl acetate 10:1)

^1H NMR (400 MHz, CDCl_3) $\delta = 9.95$ (s, 1H, O=CH), 7.02 (d, $J = 2.0$ Hz, 1H, H_{Ar}), 6.73 (dd, $J = 7.8, 2.0$ Hz, 1H, H_{Ar}), 6.59 (d, $J = 7.8$ Hz, 1H, H_{Ar}), 6.56 (d, $J = 1.9$ Hz, 1H, H_{Ar}), 6.50 (dd, $J = 7.8, 1.8$ Hz, 2H, H_{Ar}), 6.43 (dd, $J = 7.9, 1.9$ Hz, 1H, H_{Ar}), 6.38 (dd, $J = 7.9, 1.9$ Hz, 1H, H_{Ar}), 4.11 (ddd, $J = 13.1, 9.9, 1.8$ Hz, 1H, H_{PC}), 3.28–3.15 (m, 3H, H_{PC}), 3.13–3.02 (m, 3H, H_{PC}), 2.95 (ddd, $J = 13.1, 10.2, 6.7$ Hz, 1H, H_{PC}).

^{13}C NMR (101 MHz, CDCl_3) $\delta = 192.1$ (+, CH, C=O), 143.4 (C_q , C_{Ar}), 140.8 (C_q , C_{Ar}), 139.6 (C_q , C_{Ar}), 139.6 (C_q , C_{Ar}), 138.2 (+, CH, C_{Ar}), 136.7 (C_q , C_{Ar}), 136.5 (+, CH, C_{Ar}), 136.2 (+, CH, C_{Ar}), 133.4 (+, CH, C_{Ar}), 133.0 (+, CH, C_{Ar}), 132.5 (+, CH, C_{Ar}), 132.3 (+, CH, C_{Ar}), 35.4 (–, CH_2), 35.3 (–, CH_2), 35.1 (–, CH_2), 33.7 (–, CH_2).

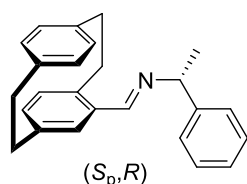
MS (70 eV, EI), m/z (%): 236 (76) $[\text{M}]^+$, 104 (100) $[\text{C}_8\text{H}_8]^+$.

HRMS–EI (m/z): $[\text{M}]^+$ calc. for $\text{C}_{17}\text{H}_{16}\text{O}$ 236.1201; found: 236.1201.

IR (ATR $\tilde{\nu}$) = 2924 (w), 2850 (w), 1677 (m), 1588 (w), 1554 (w), 1497 (w), 1436 (w), 1409 (w), 1282 (w), 1226 (w), 1180 (w), 1115 (w), 906 (w), 874 (w), 795 (w), 772 (w), 658 (w), 635 (m), 623 (m), 516 (m) cm^{-1} .

The analytical data and spectral properties are consistent with literature.^[120]

(S_p,R)-[*N*-1-(phenylethyl)]-4-[2.2]paracyclophanyl methanimine (**58**)



A solution of racemic 4-formyl[2.2]paracyclophane (23.5 g, 99.0 mmol, 1.00 equiv.) and *R*(+)-phenylethylamine (12.1 g, 100 mmol, 1.00 equiv.) in 300 mL of toluene was refluxed under magnetic stirring. The reaction course was followed by ^1H NMR because the product proved unstable under either SiO_2 , or thin layer chromatography (TLC). After 5 h the reaction was completed, the solvent was evaporated in vacuo and the crude product was crystallized from 250 mL of *n*-hexane, affording a white solid. After filtration, the solid was recrystallized from 150 mL of *n*-hexane. The residue was recrystallized twice out of hot hexane to obtain (S_p,R)-[*N*-1-(phenylethyl)]-4-[2.2]paracyclophanyl methanimine (13.2 g, 38.9 mmol, 39%) as light yellow solid determined by ^1H NMR spectroscopy.

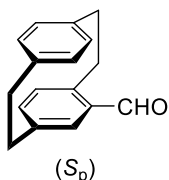
^1H NMR (400 MHz, CDCl_3) $\delta = 8.37$ (s, 1H, N=CH), 7.56–7.49 (m, 2H, 2H, H_{Ar}), 7.40 (dd, $J = 8.5, 6.9$ Hz, 2H, H_{Ar}), 7.31–7.27 (m, 1H, H_{Ar}), 7.00 (d, $J = 2.0$ Hz, 1H, H_{Ar}), 6.58 (dd, $J = 7.8, 2.0$ Hz, 1H, H_{Ar}), 6.53–6.46 (m, 3H, H_{Ar}), 6.38 (dt, $J = 7.9, 1.1$ Hz, 1H, H_{Ar}), 6.29 (dt, $J = 7.7, 1.1$ Hz, 1H, H_{Ar}), 4.57 (q, $J = 6.6$ Hz, 1H, N-CHPhCH₃), 3.98–3.83 (m, 1H, H_{PC}), 3.23–2.98 (m, 6H, H_{PC}), 2.93–2.80 (m, 2H, H_{PC}), 1.66 (d, $J = 6.6$ Hz, 3H, CH₃).

^{13}C NMR (101 MHz, CDCl_3) $\delta = 158.6$ (+, CH, C=N), 145.7 (C_q , C_{Ar}), 140.5 (C_q , C_{Ar}), 140.1 (C_q , C_{Ar}), 139.4 (C_q , C_{Ar}), 139.4 (C_q , C_{Ar}), 136.1 (C_q , C_{Ar}), 135.3 (+, CH, C_{Ar}), 134.3 (+, CH, C_{Ar}), 133.6 (+, CH, C_{Ar}), 133.2 (+, CH, C_{Ar}), 132.9 (+, CH, C_{Ar}), 132.0 (+, CH, C_{Ar}), 131.1 (+, CH, C_{Ar}), 128.5 (+, CH, 2C, C_{Ar}),

126.8 (+, CH, C_{Ar}), 126.6 (+, CH, 2C, C_{Ar}), 70.4 (+, CH, N-CHPhCH₃), 35.4 (-, CH₂), 35.1 (-, CH₂), 34.99 (-, CH₂), 33.9 (-, CH₂), 25.0 (+, CH₃).

The analytical data and spectral properties are consistent with the literature.^[120]

(*S_p*)-4-Formyl[2.2]paracyclophane (**57**)



The intermediate (*S_p*,*R*)-[*N*-1-(Phenylethyl)]-4-[2.2]paracyclophanyl methanimine was hydrolyzed by column chromatography on silica using dichloromethane as eluent to get (*S_p*)-4-formyl[2.2]paracyclophane as a white solid with 98% *ee* (**Figure 66**).

The analytical data was identical to that of the racemate.

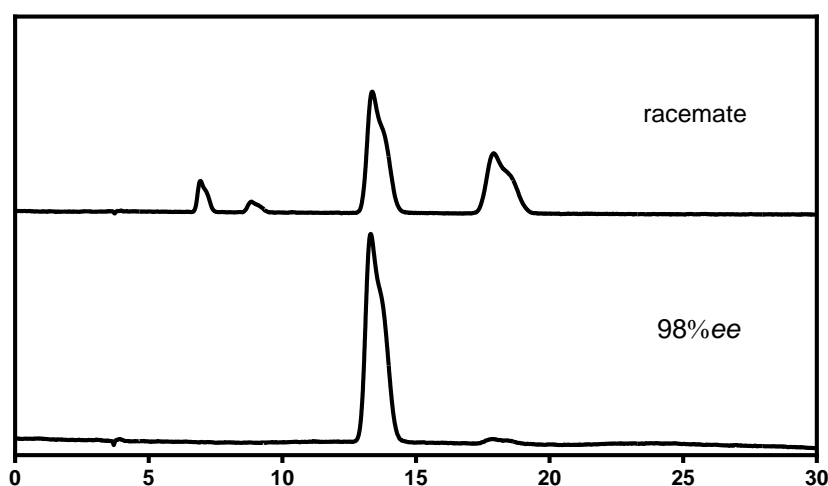
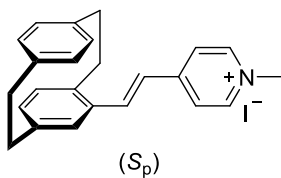


Figure 66. Analytical HPLC run of 4-formyl[2.2]paracyclophane on a chiral OD-H column using 1% isopropanol in *n*-hexane with a flow rate of 1 mL/min. Detection was performed at 330 nm. The % *ee* values were measured via integration of enantiomeric peak.

(*S_p*)-4-(*N*-Methyl-4'-pyridinium-(*E*)-vinyl)[2.2]paracyclophane iodide ((*S_p*)-MVCP, **50**)

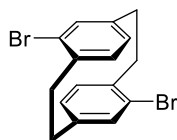


1,4-Dimethylpyridinium iodide (438 mg, 0.55 mmol, 1.1 equiv.), followed by (*S_p*)-4-formyl[2.2]paracyclophane (400 mg, 0.5 mmol, 1.0 equiv.), methanol (10 mL) and 3 drops of piperidine. The reaction stirred and heated at 65 °C for 2 h. The reaction mixture was allowed to reach room temperature at which point

most compounds precipitated. Acetic acid was added to those reactions involving aldehydes with hydroxyl groups. In some cases, adding ethyl acetate was necessary to induce precipitation. The crude product was purified by column chromatography on silica (dichloromethane/ methane 5:1) to give (*S_p*)-4-(*N*-methyl-4'-pyridinium-(*E*)-vinyl)[2.2]paracyclophane iodide ((*S_p*)-MVCP) (168 mg, 0.37 mmol, 22%) as brown yellow solids.

The analytical data was identical to that of the racemate.

4,16-Dibromo[2.2]paracyclophane (59)



To iron powder (60.0 mg, 1.00 mmol, 4.80 equiv.) were added 10 mL of a solution of 2.60 mL bromine (8.10 g, 50.0 mmol, 2.10 equiv.) in 40 mL dichloromethane. After stirring for 1 h, the reaction mixture was diluted with 40 mL dichloromethane and [2.2]paracyclophane (5.00 g, 24.0 mmol, 1.00 equiv.) was added. The mixture was stirred for further 30 min, followed by dropwise addition of the residual bromine solution over 5 h. The reaction mixture was stirred for 72 h. A saturated aqueous solution of Na₂SO₃ was added to the reaction mixture, which was stirred for 1 h. The organic phase was filtrated and the residual solid was dried. The product was recrystallized from methanol to obtain 4,16-dibromo[2.2]paracyclophane (3.21 g, 8.77 mmol, 37%) as a colorless solid.

R_f = 0.43 (cyclohexane)

¹H NMR (400 MHz, CDCl₃, ppm) δ = 7.14 (dd, *J* = 7.8, 1.9 Hz, 2H, H_{Ar}), 6.51 (d, *J* = 1.8 Hz, 2H, H_{Ar}), 6.44 (d, *J* = 7.8 Hz, 2H, H_{Ar}), 3.50 (ddd, *J* = 13.0, 10.4, 2.3 Hz, 2H, H_{PC}), 3.16 (ddd, *J* = 12.6, 10.3, 4.9 Hz, 2H, H_{PC}), 2.95 (ddd, *J* = 12.8, 10.6, 2.3 Hz, 2H, H_{PC}), 2.85 (ddd, *J* = 13.2, 10.7, 4.9 Hz, 2H, H_{PC}).

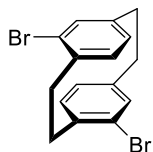
¹³C NMR (100 MHz, CDCl₃, ppm) δ = 141.2 (C_q, 2C, C_{Ar}), 138.6 (C_q, 2C, C_{Ar}), 137.3 (+, CH, 2C, C_{Ar}), 134.1 (+, CH, 2C, C_{Ar}), 128.3 (+, CH, 2C, C_{Ar}), 126.8 (C_q, 2C, C_{Ar}-Br), 35.4 (-, 2C, CH₂), 32.9 (-, 2C, CH₂).

MS (EI, 70 eV, 20 °C, %) *m/z* = 368/366/364 (24/46/24) [M]⁺, 184/182 (92/100) [M-C₈H₇Br]⁺, 104/103 (97/32) [C₈H₇]⁺.

HRMS-EI (*m/z*): [M]⁺, calc. for C₁₆H₁₄⁷⁹Br⁸¹Br, 365.9442; found: 365.9294.

IR (ATR, $\tilde{\nu}$) = 2934 (s), 2850 (m), 1584 (m), 1536 (m), 1473 (m), 1449 (m), 1432 (w), 1390 (vs), 1234 (w), 1186 (s), 1157 (m), 1105 (m), 1030 (vs), 899 (vs), 887 (s), 856 (vs), 830 (vs), 771 (w), 705 (vs), 698 (vs), 669 (vs), 649 (vs), 584 (m), 523 (vs), 465 (vs), 439 (m), 394 (s) cm⁻¹.

The analytical data match those reported in the literature.^[147]

(rac)-4,15-Dibromo[2.2]paracyclophane (60)

To a solution of [2.2]paracyclophane (5.00 g, 24.0 mmol, 1.00 equiv.) in CCl_4 (90 mL) was added bromine (7.40 mL, 23.0 g, 144 mmol, 6.00 equiv.) at room temperature, and the mixture was heated at 60 °C for 3 h. The progress of the reaction was monitored by TLC (silica gel, cyclohexane/ CH_2Cl_2 , 10/1). A precipitate was formed. The mixture was cooled in an ice bath, and aqueous sodium bisulfite solution was added (decolorization). The formed crystals were removed by filtration and washed with water three times, followed by EtOH. After air-drying, this residue pseudo-para-dibromo[2.2]paracyclophane (**59**) was isolated as a colorless solid.

The filtrate was carefully washed with CH_2Cl_2 , the organic layers were combined, washed with water and sat. NaCl solution, and finally dried with MgSO_4 . After complete solvent removal the residue was dissolved in CH_2Cl_2 and the solution was cooled to 0 °C. The crystals formed were shown to be a 1:1-mixture of **59** and **60**. Recrystallization from CH_2Cl_2 and cooling of the solution to 0 °C allowed the separation of the pseudo-para isomer **59** to yield 29%. To the combined filtrates an aqueous solution of EtOH 50 mL was added and after standing at room temperature for 16 h pure pseudo-ortho-dibromo[2.2]paracyclophane (**60**) could be removed by filtration to yield 17% combined.

^1H NMR (400 MHz, CDCl_3 , ppm) δ = 7.14 (dd, J = 7.8, 1.7 Hz, 2H, H_{Ar}), 6.51 (d, J = 1.5 Hz, 2H, H_{Ar}), 6.44 (d, J = 7.8 Hz, 2H, H_{Ar}), 3.50 (ddd, J = 13.0, 10.4, 2.2 Hz, 2H, H_{PC}), 3.16 (ddd, J = 12.7, 10.4, 4.9 Hz, 2H, H_{PC}), 2.94 (ddd, J = 9.9, 8.5, 3.3 Hz, 2H, H_{PC}), 2.85 (ddd, J = 13.2, 10.8, 4.9 Hz, 2H, H_{PC}).

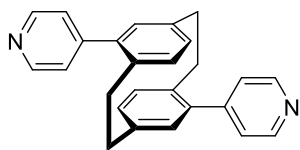
^{13}C NMR (101 MHz, CDCl_3 , ppm) δ = 141.2 (C_q , 2C, C_{Ar}), 138.6 (C_q , 2C, C_{Ar}), 137.3 (+, CH, 2C, C_{Ar}), 134.1 (+, CH, 2C, C_{Ar}), 128.3 (+, CH, 2C, C_{Ar}), 126.8 (C_q , 2C, $\text{C}_{\text{Ar}}-\text{Br}$), 35.4 (–, 2C, CH_2), 32.9 (–, 2C, CH_2).

MS (ESI, 70 eV, 20 °C, %) m/z = 365/367/369 (50/100/47) $[\text{M}+\text{H}]^+$, 366 (35) $[\text{M}]^+$, 377/379/381 (92/100) $[\text{M}+\text{CH}_2]^+$.

HRMS-ESI (m/z): $[\text{M}]^+$, calc. for $\text{C}_{16}\text{H}_{14}^{79}\text{Br}^{81}\text{Br}$, 365.9442; found: 365.9438.

IR (ATR, $\tilde{\nu}$) = 2934 (s), 2850 (w), 1584 (m), 1536 (m), 1475 (m), 1449 (m), 1432 (w), 1390 (vs), 1186 (m), 1030 (vs), 899 (vs), 887 (s), 856 (vs), 830 (vs), 705 (vs), 700 (vs), 669 (vs), 649 (vs), 523 (s), 465 (vs), 394 (m), 380 (w) cm^{-1} .

The analytical data is consistent with the literature.^[121]

4,16-Di(4'-pyridyl)[2.2]paracyclophane (61)

A vessel was charged with 4, 16-dibromo[2.2]paracyclophane (545 mg, 1.49 mmol, 1.00 equiv.), pyridine-4-boronic acid (458 mg, 3.73 mmol, 2.50 equiv.), palladium-tetrakis(triphenylphosphine) (103 mg, 89 μ mol, 0.06 equiv.), potassium phosphate (637 mg, 4.47 mmol, 2.00 equiv.), 1,4-dioxane (12 mL) and water (6 mL) under argon atmosphere. The mixture was heated at 100 °C for 16 h. Then the reaction mixture was cooled down to room temperature, extracted with ether (3 \times 20 mL), and the extracts were dried (MgSO_4) and evaporated under reduced pressure. The residue was purified by column chromatography to give 4,16-di(4'-pyridyl)[2.2]paracyclophane as a white solid (213 mg, 588 μ mol, 39%).

R_f = 0.25 (dichloromethane /ethyl acetate 1:3)

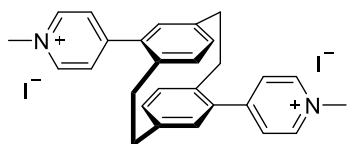
^1H NMR (400 MHz, CDCl_3 , ppm) δ = 8.66 (d, J = 6.1 Hz, 4H, H_{Py}), 7.37 (d, J = 6.0 Hz, 4H, H_{Py}), 6.62 (dd, J = 4.9, 2.9 Hz, 4H, H_{Ar}), 6.53 (dd, J = 7.9, 1.9 Hz, 2H, H_{Ar}), 3.37 (ddd, J = 13.9, 10.0, 4.1 Hz, 2H, H_{PC}), 3.02 (ddd, J = 14.0, 10.2, 4.7 Hz, 2H, H_{PC}), 2.85 (ddd, J = 14.1, 10.2, 4.1 Hz, 2H, H_{PC}), 2.73 (ddd, J = 13.3, 10.0, 4.7 Hz, 2H, H_{PC}).

^{13}C NMR (100 MHz, CDCl_3 , ppm) δ = 150.2 (+, CH, 4C, C_{Py}), 148.4 (C_q , 2C, C_{Py}), 140.2 (C_q , 2C, C_{Ar}), 139.6 (C_q , 2C, C_{Ar}), 137.2 (C_q , 2C, C_{Ar}), 135.1 (+, CH, 2C, C_{Ar}), 132.3 (+, CH, 2C, C_{Ar}), 130.4 (+, CH, 2C, C_{Ar}), 124.5 (+, CH, 4C, C_{Py}), 34.7 (–, 2C, CH_2), 33.6 (–, 2C, CH_2).

MS (ESI, 70 eV, 20 °C, %) m/z = 363 (100) $[\text{M}+\text{H}]^+$, 364 (28) $[\text{M}+\text{H}]^+$, 156 (24) $[\text{C}_{11}\text{H}_{10}\text{N}]^+$, 286 (23) $[\text{M}-\text{C}_5\text{H}_2\text{N}]^+$.

HRMS-ESI (m/z): $[\text{M}+\text{H}]^+$, calc. for $\text{C}_{26}\text{H}_{23}\text{N}_2$, 363.1856; found: 363.1850.

IR (ATR, $\tilde{\nu}$) = 2948 (w), 2929 (m), 2895 (w), 2853 (w), 1591 (vs), 1538 (m), 1475 (m), 1453 (w), 1436 (m), 1415 (m), 1400 (s), 1322 (w), 1213 (m), 1181 (m), 1118 (m), 1103 (m), 1065 (m), 990 (m), 914 (m), 873 (w), 822 (vs), 751 (m), 734 (s), 721 (vs), 707 (s), 694 (s), 667 (s), 653 (vs), 620 (vs), 608 (m), 571 (vs), 558 (s), 538 (vs), 518 (s), 483 (vs), 438 (m), 422 (s), 392 (m), 381 (m) cm^{-1} .

4,16-Di(*N*-methyl-4'-pyridinium)[2.2]paracyclophane iodide (pseudo-*para*-DMPCP, 51)

A solution of a mixture of 4,16-di-(4'-pyridyl)[2.2]paracyclophane (74 mg, 110 μ mol, 1.00 equiv.) and methyl iodide (3.21 mmol, 200 μ L) in acetonitrile (5 mL) was stirred at 40 °C for 16 h protected from light. After the solution was cooled to room temperature, removed solvent under reduced pressure to give a residue, washed with DCM (20 mL), and dried in air to yield (125 mg, 193 μ mol, 95%) a light-yellow solid.

^1H NMR (400 MHz, DMSO-d_6 , ppm) δ = 9.05 (d, J = 6.4 Hz, 4H, H_{Py}), 8.32 (d, J = 6.9 Hz, 4H, H_{Py}), 7.10 (d, J = 7.9 Hz, 2H, H_{Ar}), 7.05 (d, J = 1.8 Hz, 2H, H_{Ar}), 6.58 (dd, J = 7.8, 1.8 Hz, 2H, H_{Ar}), 4.40 (s, 6H, CH_3),

3.36 (td, $J = 9.7, 4.8$ Hz, 2H, H_{PC}), 3.23 (ddd, $J = 14.0, 9.9, 4.9$ Hz, 2H, H_{PC}), 2.99 (ddd, $J = 13.6, 9.9, 4.0$ Hz, 2H, H_{PC}), 2.71 (ddd, $J = 13.7, 10.2, 5.0$ Hz, 2H, H_{PC}).

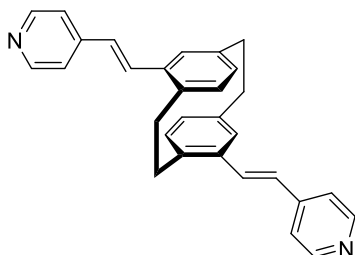
^{13}C NMR (101 MHz, DMSO- d_6 , ppm) $\delta = 155.4$ (+, CH, 4C, C_{Py}), 145.9 (C_q , 2C, C_{Py}), 140.8 (C_q , 2C, C_{Ar}), 139.0 (C_q , 2C, C_{Ar}), 136.9 (C_q , 2C, C_{Ar}), 136.0 (+, CH, 2C, C_{Ar}), 133.1 (+, CH, 2C, C_{Ar}), 132.7 (+, CH, 2C, C_{Ar}), 127.8 (+, CH, 4C, C_{Py}), 47.6 (+, 2C, CH_3), 34.5 (-, 2C, CH_2), 33.5 (-, 2C, CH_2).

MS (ESI, 70 eV, 20 °C, %) $m/z = 196/197$ (100/97) $[\text{M}]^{2+}$.

HRMS-ESI (m/z): $[\text{M}]^{2+}$, calc. for $\text{C}_{28}\text{H}_{28}\text{N}_2$, 196.1121; found: 196.1121.

IR (ATR, $\tilde{\nu}$) = 1636 (m), 1215 (m), 1188 (s), 1067 (vs), 972 (w), 847 (s), 805 (w), 557 (m), 484 (vs), 456 (vs), 442 (vs), 388 (s) cm^{-1}

(rac)-4,15-Di(4'-pyridyl-(E)-vinyl)[2.2]paracyclophane (62)



A vessel was charged with 4,15-dibromo[2.2]paracyclophane (732 mg, 2.00 mmol, 1.00 equiv.), 4-vinylpyridine (842 mg, 8.00 mmol, 4.00 equiv.), palladium acetate (22.0 mg, 99.0 μmol , 0.05 equiv.), tetrapropylammonium bromide (1.33 mg, 5.00 mmol, 2.50 equiv.), potassium acetate (1.38 mg, 10.0 mmol, 5.0 equiv.), and DMF (25 mL) under argon, and heated at 110 °C for 48 hours. Then the reaction was

cooled to room temperature, diluted with CH_2Cl_2 (3×25 mL), and washed with brine. The organic layer was dried with Na_2SO_4 and concentrated. The residual liquid was purified by silica gel column chromatography to give 4,15-di((E)-4'-pyridinylvinyl)[2.2]paracyclophane as a light orange solid (531 mg, 1.28 mmol, 45%).

$R_f = 0.35$ (dichloromethane /methanol 20:1)

^1H NMR (400 MHz, CDCl_3 , ppm) $\delta = 8.65\text{--}8.61$ (m, 4H, H_{Py}), 7.42 (d, $J = 6.2$ Hz, 4H, H_{Py}), 7.38 (d, $J = 16.2$ Hz, 2H, CH=CH), 6.86 (d, $J = 16.2$ Hz, 2H, CH=CH), 6.80 (d, $J = 1.9$ Hz, 2H, H_{Ar}), 6.66 (d, $J = 7.8$ Hz, 2H, H_{Ar}), 6.47 (dd, $J = 7.9, 1.9$ Hz, 2H, H_{Ar}), 3.66–3.52 (m, 2H, H_{PC}), 3.25–3.12 (m, 2H, H_{PC}), 3.09–2.96 (m, 2H, H_{PC}), 2.92–2.81 (m, 2H, H_{PC}).

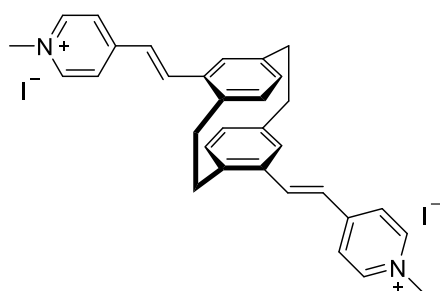
^{13}C NMR (100 MHz, CDCl_3 , ppm) $\delta = 150.3$ (+, CH, 4C, C_{Py}), 145.0 (C_q , 2C, C_{Ar}), 140.1 (C_q , 2C, C_{Ar}), 138.7 (C_q , 2C, C_{Ar}), 136.8 (C_q , 2C, C_{Py}), 132.0 (+, CH, 2C, C_{Ar}), 131.6 (+, CH, 2C, C_{Ar}), 130.7 (+, 2C, CH=CH), 130.1 (+, CH, 2C, C_{Ar}), 126.5 (+, 2C, CH=CH), 120.9 (+, CH, 4C, C_{Py}), 35.0 (-, 2C, CH_2), 33.6 (-, 2C, CH_2).

MS (EI, 70 eV, 20 °C, %) $m/z = 415/416$ (100/32) $[\text{M}+\text{H}]^+$, 193 (75) $[\text{C}_{30}\text{H}_{27}\text{N}_2]^+$

HRMS-EI (m/z): $[\text{M}+\text{H}]^+$, calc. for $\text{C}_{28}\text{H}_{28}\text{N}_2$, 415.2169; found: 415.2166.

IR (ATR, $\tilde{\nu}$) = 3021 (w), 2934 (w), 2922 (w), 1591 (vs), 1545 (w), 1487 (w), 1482 (w), 1472 (w), 1405 (m), 1215 (w), 1198 (w), 990 (w), 958 (vs), 912 (w), 891 (w), 871 (m), 850 (m), 805 (vs), 799 (vs), 737 (w), 720 (s), 687 (w), 650 (w), 632 (m), 603 (w), 558 (w), 547 (s), 531 (vs), 507 (vs), 484 (m), 469 (w), 458 (w), 441 (w), 424 (w), 404 (w), 378 (w) cm^{-1} .

(rac)-4,15-Di(*N*-Methyl-4'-pyridinium-(*E*)-vinyl)[2.2]paracyclophane iodide (pseudo-*meta*-DMVCP, 52)



A solution of a mixture of 4,15-di(4'-pyridyl-(*E*)-vinyl)[2.2]paracyclophane (84.0 mg, 232 μmol , 1.00 equiv.) and methyl iodide (3.21 mmol, 200 μL) in acetonitrile (10 mL) was stirred at 40 $^{\circ}\text{C}$ for 8 h protected from light. After the solution was cooled to room temperature, removed solvent under reduced pressure to give a residue, washed with water (20 mL), and dried in air to yield an orange solid (98.2 mg, 140 μmol , 69%).

^1H NMR (400 MHz, DMSO-d_6 , ppm) δ = 8.89 (d, J = 6.5 Hz, 4H, H_{Py}), 8.40 (d, J = 6.5 Hz, 4H, H_{Py}), 7.98 (d, J = 16.1 Hz, 2H, $\text{CH}=\text{CH}$), 7.36 (d, J = 16.0 Hz, 2H, $\text{CH}=\text{CH}$), 7.08 (d, J = 1.7 Hz, 2H, H_{Ar}), 6.65–6.52 (m, 4H, H_{Ar}), 4.30 (s, 6H, CH_3), 3.86–3.77 (m, 2H, H_{PC}), 3.24–3.12 (m, 2H, H_{PC}), 3.10–2.98 (m, 2H, H_{PC}), 2.94–2.81 (m, 2H, H_{PC}).

^{13}C NMR (101 MHz, DMSO-d_6 , ppm) δ = 153.2 (C_q , 2C, C_{Py}), 145.4 (+, CH, 4C, C_{Py}), 141.2 (C_q , 2C, C_{Ar}), 140.6 (C_q , 2C, C_{Ar}), 138.4 (+, 2C, $\text{CH}=\text{CH}$), 136.3 (C_q , 2C, C_{Ar}), 134.1 (+, CH, 2C, C_{Ar}), 132.5 (+, CH, 2C, C_{Ar}), 131.1 (+, CH, 2C, C_{Ar}), 124.2 (+, CH, 4C, C_{Py}), 124.2 (+, 2C, $\text{CH}=\text{CH}$), 47.4 (+, 2C, CH_3), 34.8 (–, 2C, CH_2), 33.7 (–, 2C, CH_2).

MS (ESI, 70 eV, 20 $^{\circ}\text{C}$, %) m/z = 222 (100) $[\text{M}]^{2+}$.

HRMS-ESI (m/z): $[\text{M}-2\text{I}]^{2+}$, calc. for $\text{C}_{32}\text{H}_{32}\text{N}_2$, 222.1277; found: 222.1277.

IR (ATR, $\tilde{\nu}$) = 3019 (m), 3013 (m), 2924 (w), 1638 (s), 1608 (vs), 1587 (s), 1561 (m), 1516 (s), 1483 (w), 1466 (m), 1441 (w), 1323 (w), 1187 (vs), 975 (w), 962 (m), 887 (w), 877 (m), 824 (s), 730 (w), 708 (w), 517 (vs), 497 (w), 486 (w), 466 (w) cm^{-1} .

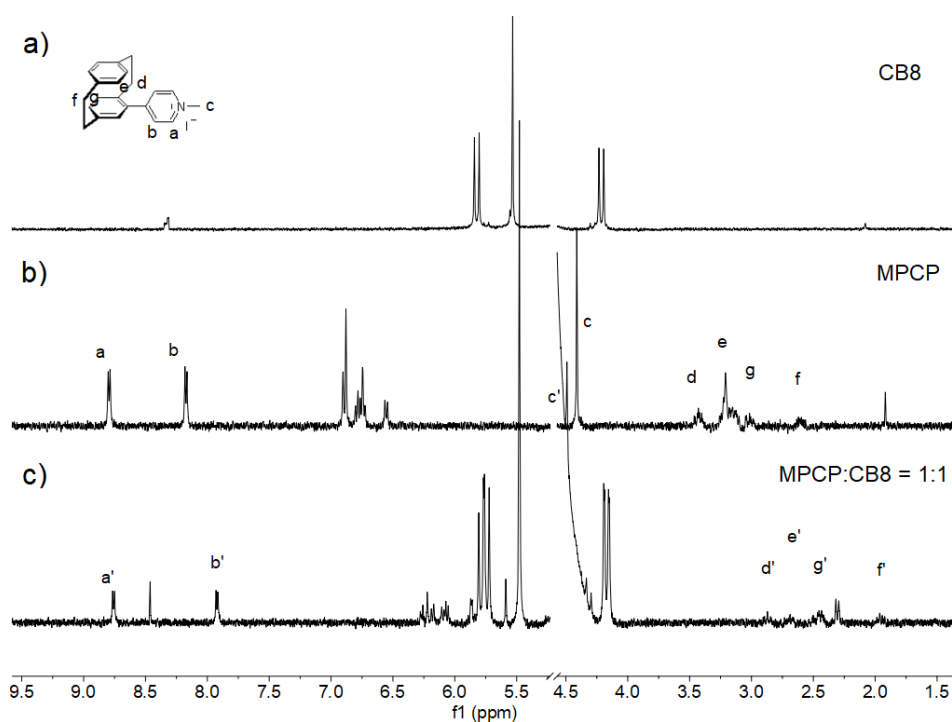
CB8 \supset MPCP (63)

Figure 67. ^1H NMR spectra was recorded (400 MHz, D_2O , r.t.) for (a) CB8 (50 μM), (b) MPCP (200 μM), (c) a mixture of CB (100 μM) and MPCP (100 μM) = 1:1. Primed (') resonances arise from the **CB8 \supset MPCP** complex.

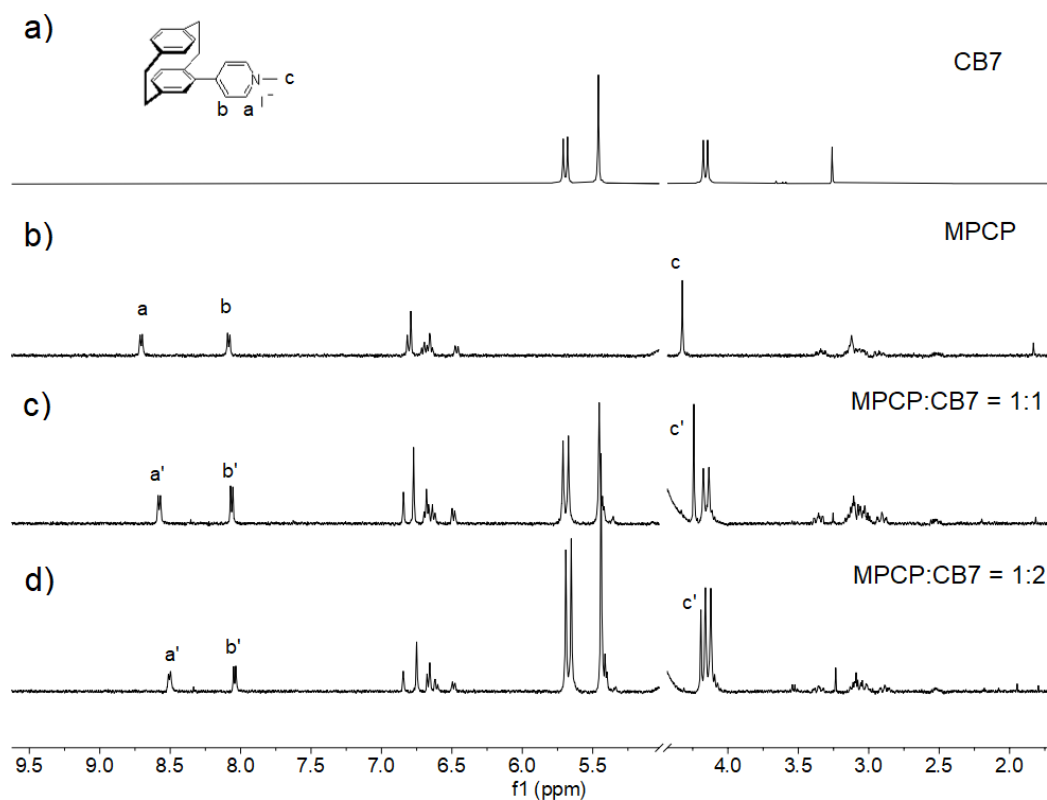


Figure 68. ^1H NMR spectra was recorded (400 MHz, D_2O , r.t.) for (a) CB7 (200 μM), (b) MPCP (100 μM): CB7 (100 μM) = 1:1, (c) a mixture of MPCP (67 μM) and CB7 (133 μM) = 1:2. Primed (') resonances arise from the **CB7 \supset MPCP** complex.

HRMS-ESI (m/z): [M]⁺, calc. for C₇₀H₇₀N₃₃O₁₆, 1628.5673/ 1629.5707/ 1630.5740 (100/76/28); found: 1628.5697/ 1629.5732/ 1630.5757 (72/60/27).

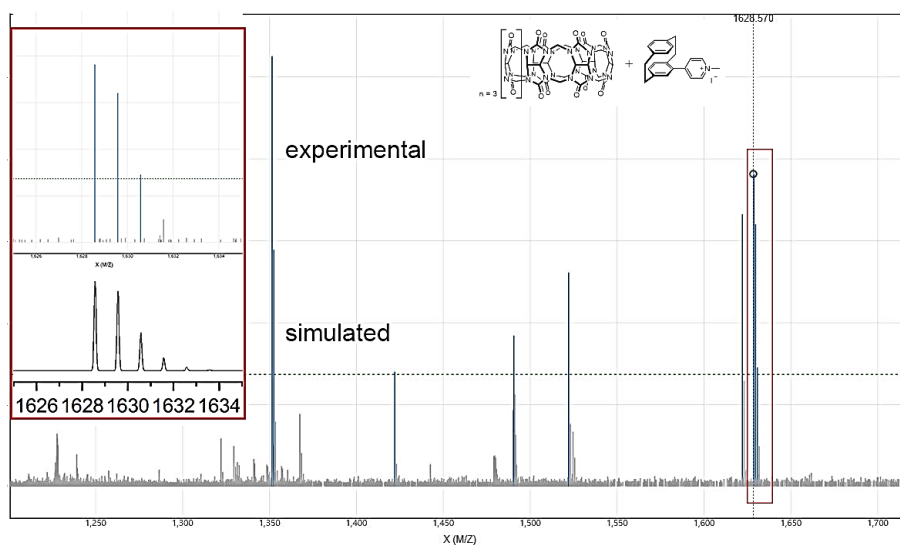


Figure 69. ESI mass spectra of **CB8⊃MPCP**.

CB8⊃MVCP (64)

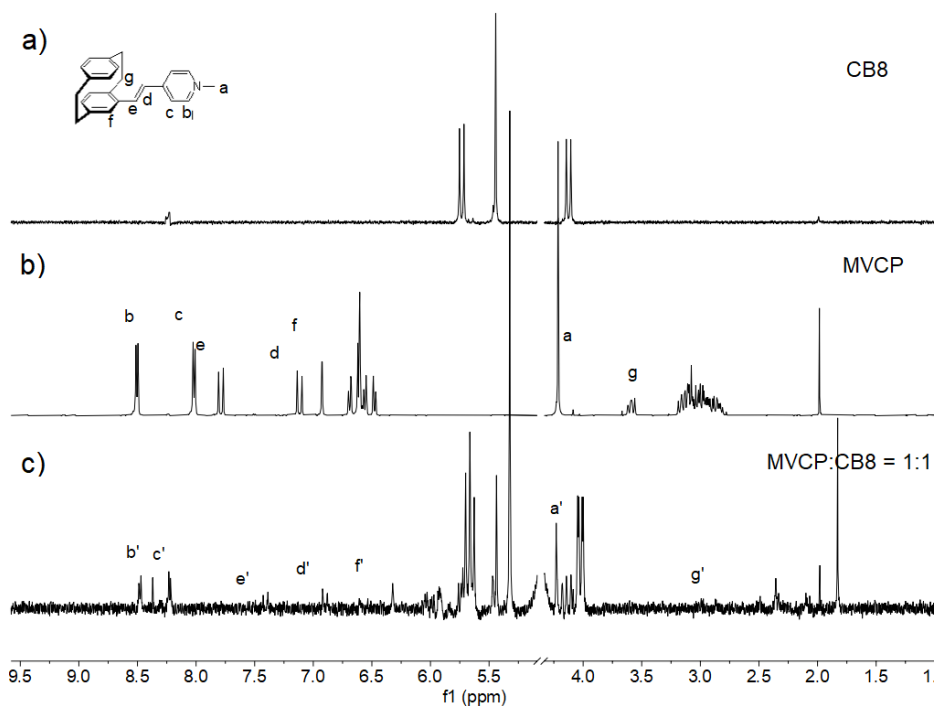


Figure 70. ¹H NMR spectra was recorded (400 MHz, D₂O, r.t.) for (a) **CB8** (50 μM), (b) **MVCP** (200 μM), (c) a mixture of **CB8** (125 μM) and **MVCP** (125 μM) 1:1, (d) a mixture of **CB8** (125 μM) and **MVCP** (250 μM) = 2:1. Primed (') resonances arise from the **CB8⊃MVCP** complex.

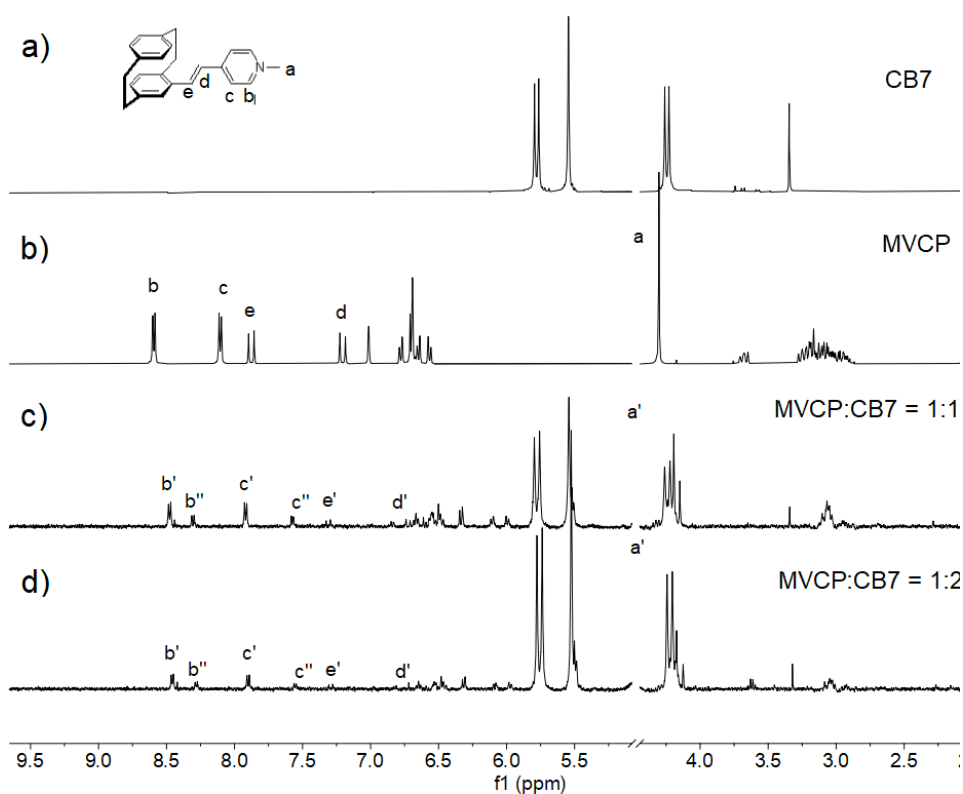


Figure 71. ^1H NMR spectra was recorded (400 MHz, D_2O , r.t.) for (a) **CB7** (200 μM), (b) **MVCP** (200 μM), (c) a mixture of **MVCP** (100 μM) and **CB7** (100 μM) = 1:1, (d) a mixture of **MVCP** (67 μM) and **CB7** (133 μM) = 1:2. Primed ('and') resonances arise from the **CB7** \supset **MVCP** complex.

HRMS-ESI (m/z): $[\text{M}]^+$, calc. for $\text{C}_{72}\text{H}_{72}\text{N}_{33}\text{O}_{16}$, 1654.5830/ 1655.5863/ 1656.5897 (100/78/30); found: 1654.5869/ 1655.5895 / 1656.5896 (51/41/12).

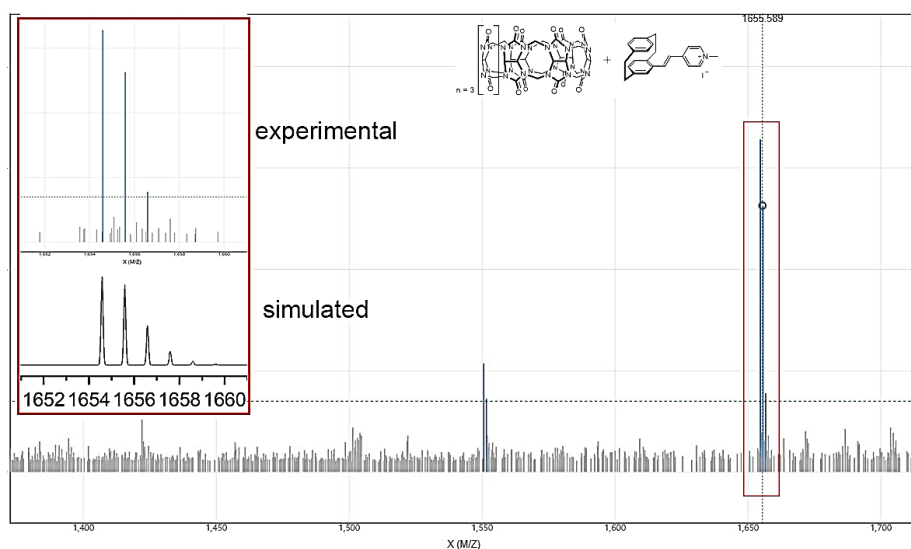


Figure 72. ESI mass spectra of **CB8** \supset **MVCP**.

CB8 \Rightarrow DMVCP (66)

HRMS-ESI (m/z): [M]²⁺, calc. for C₈₀H₈₀N₃₄O₁₆, 886.3241/ 886.8257/ 887.3274 (100/87/37); found: 886.3256/ 886.8269/ 887.3283 (32/33/14).

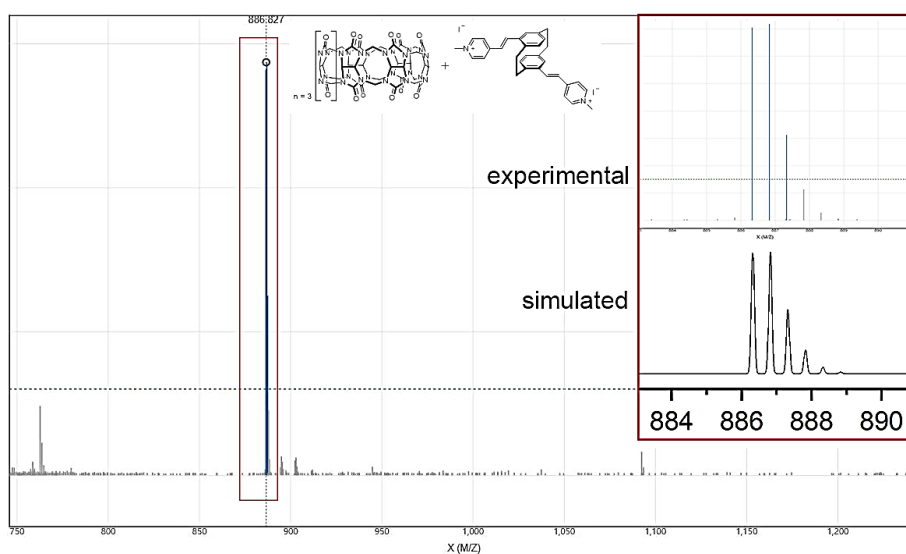


Figure 73. ESI mass spectra of **CB8 \Rightarrow DMVCP**

Photophysical characterization for PCP compounds

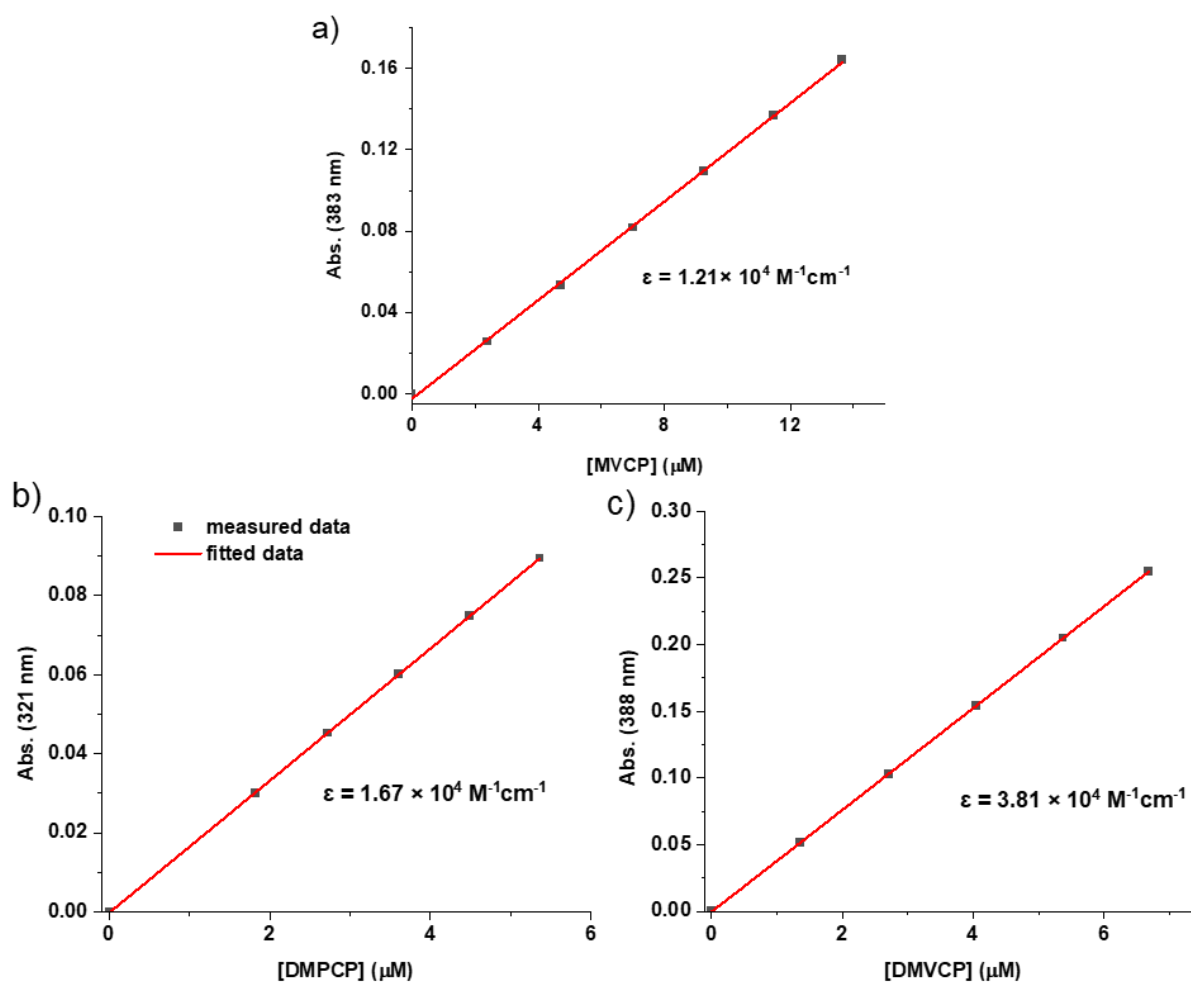


Figure 74. Absorption spectrum of ϵ titration in water: (a) **MVCP** at 383 nm, $\epsilon = 1.21 \times 10^4 \text{ M}^{-1} \text{ cm}^{-1}$. (b) **DMPCP** at 321 nm, $\epsilon = 1.67 \times 10^4 \text{ M}^{-1} \text{ cm}^{-1}$. (c) **DMVCP** at 388 nm, $\epsilon = 3.81 \times 10^4 \text{ M}^{-1} \text{ cm}^{-1}$. Dr. Amrutha Prabodh provided the results.

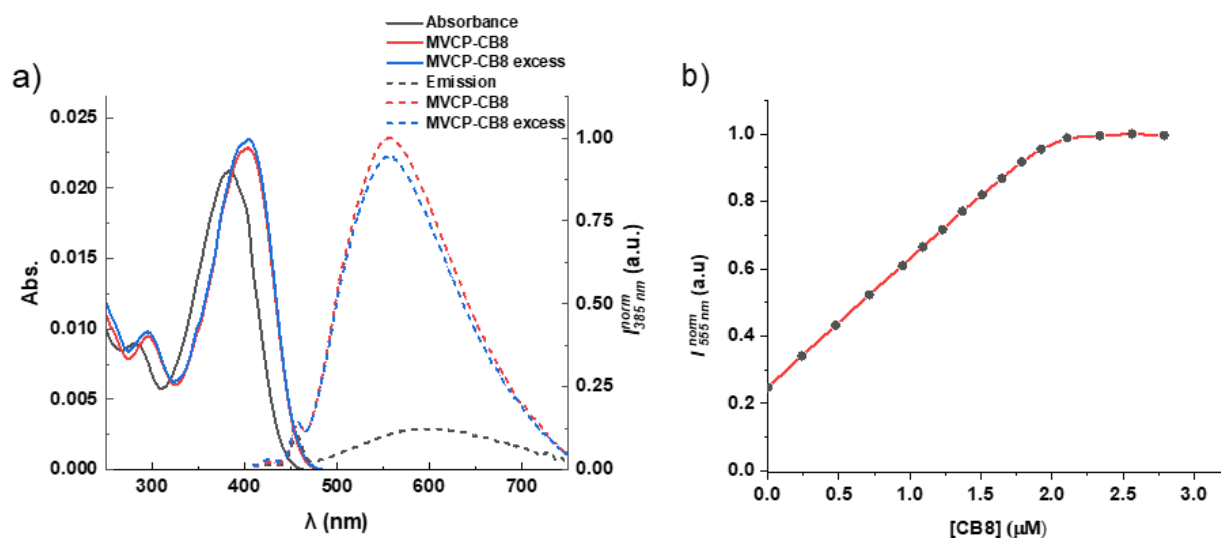


Figure 75. Spectrum of **MVCP** with CB8 in water: (a) absorbance and fluorescence of pure **MVCP** (2.05 μM) and addition of CB8 (2.16 μM and 4.13 μM). (b) fluorescence titration of CB8 by **MVCP** (2.06 μM). Dr. Amrutha Prabodh provided the results.

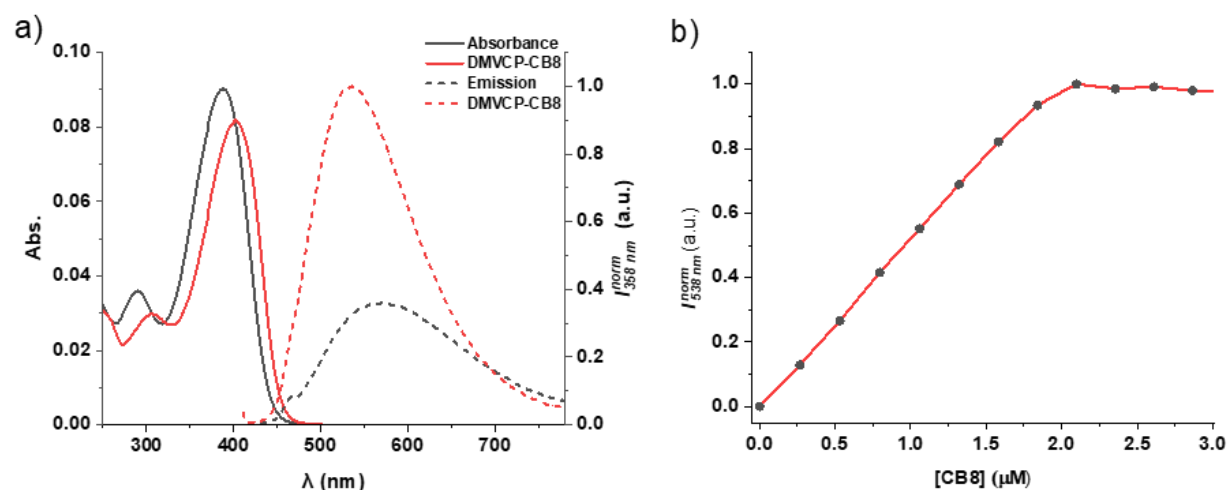


Figure 76. Spectrum of **DMVCP** with CB8 in water: (a) absorbance and fluorescence of pure **DMVCP** (2.08 μM) and addition of CB8 (2.16 μM). (b) Fluorescence titration of CB8 by **DMVCP** (2.08 μM). Dr. Amrutha Prabodh provided the results.

CB8 \supset MPCP

Selected ^1H NMR spectra from the K_a and K_{rel} measurements

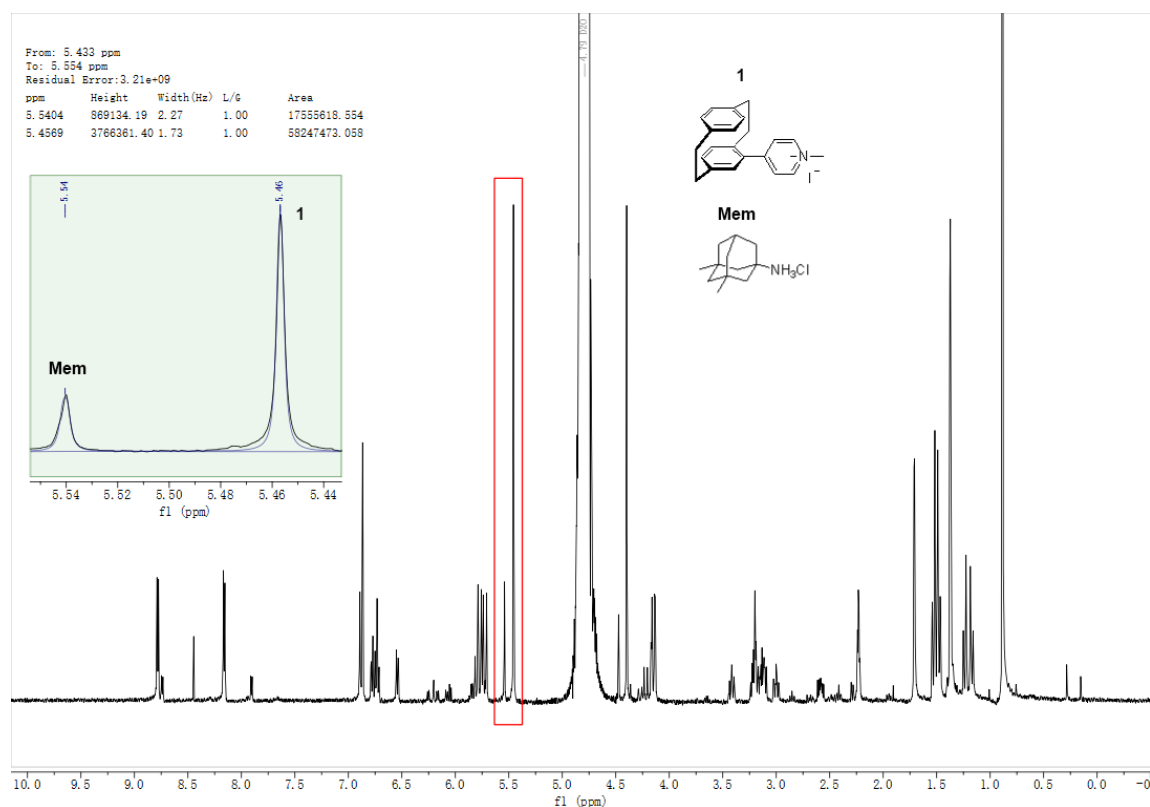


Figure 77. One of the ^1H NMR spectra (500 MHz, D_2O , r.t.) was used to determine K_{rel} for **CB8** \supset **MPCP** and **CB8** \supset **Mem**. $[\text{CB8}]_{\text{Total}} = 54.0 \mu\text{M}$, $[\text{Mem}]_{\text{Total}} = 152 \mu\text{M}$, $[\text{MPCP}]_{\text{Total}} = 74.9 \mu\text{M}$, $K_{rel} = 13.88$.

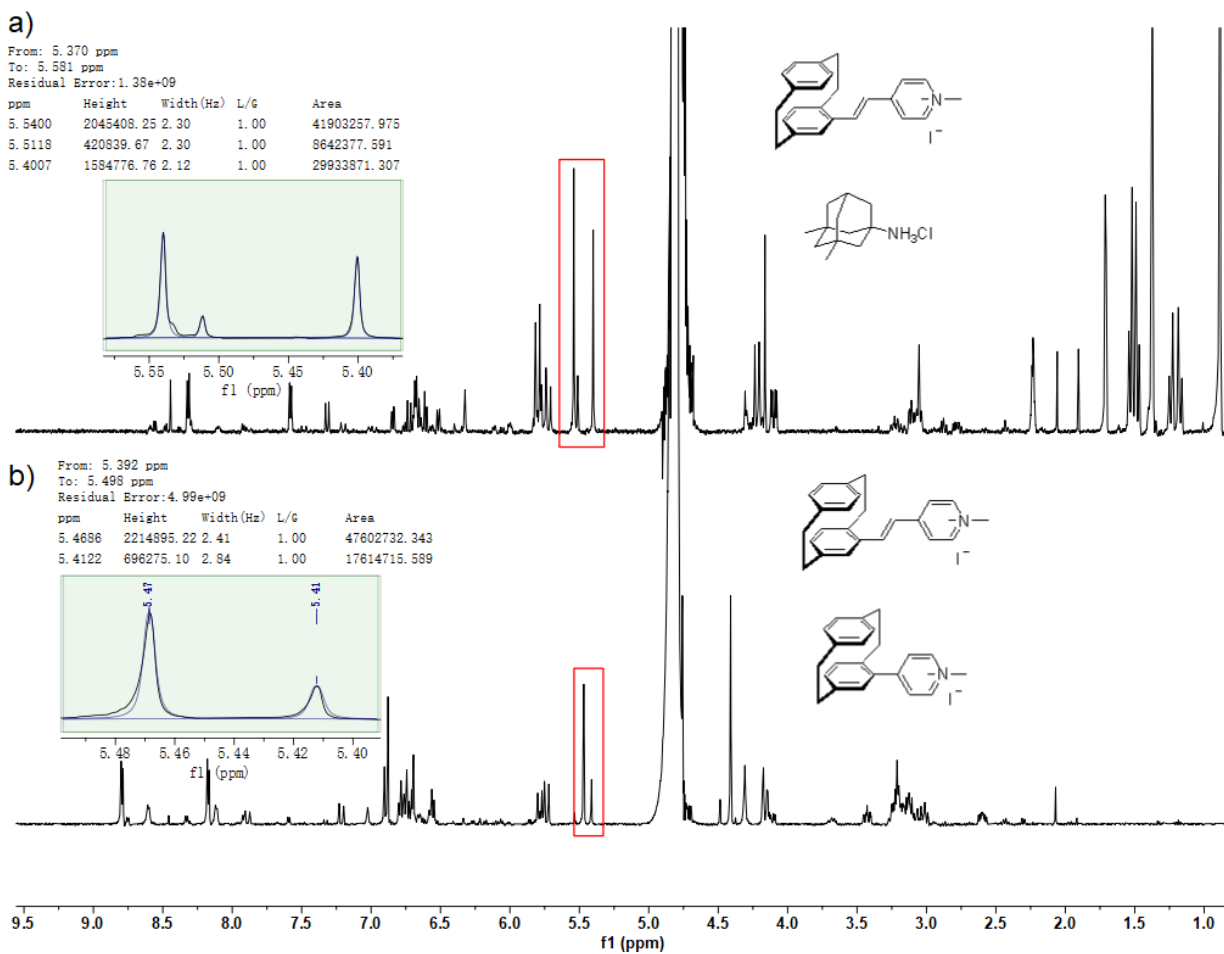
CB8 \rightarrow MVCP

Figure 78. (a) One of the ^1H NMR spectra (500 MHz, D_2O , r.t.) was used to determine K_{rel} for CB8 \rightarrow MVCP and CB8 \rightarrow Mem. $[\text{CB8}]_{\text{Total}} = 54.0 \mu\text{M}$, $[\text{Mem}]_{\text{Total}} = 152 \mu\text{M}$, $[\text{MVCP}]_{\text{Total}} = 69.5 \mu\text{M}$, $K_{\text{rel}} = 1.83$. (b) One of the ^1H NMR spectra (500 MHz, D_2O , RT) used to determine K_{rel} for CB8 \rightarrow MPCP and CB8 \rightarrow MVCP. $[\text{CB8}]_{\text{Total}} = 46.9 \mu\text{M}$, $[\text{MPCP}]_{\text{Total}} = 74.9 \mu\text{M}$, $[\text{MVCP}]_{\text{Total}} = 69.5 \mu\text{M}$, $K_{\text{rel}} = 0.27$.

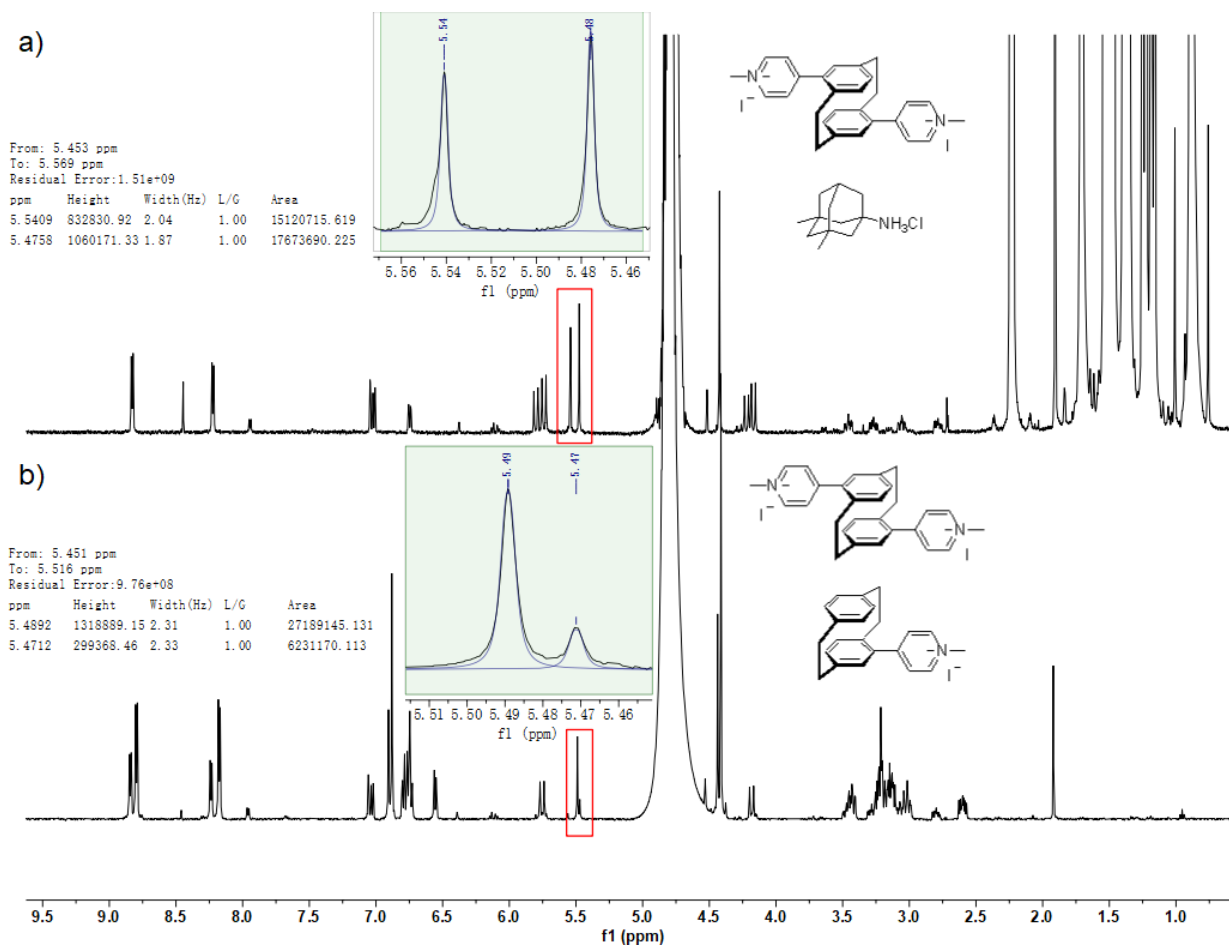
CB8DMPCP


Figure 79. (a) One of the ^1H NMR spectra (500 MHz, D_2O , r.t.) was used to determine K_{rel} for **CB8**DMPCP and **CB8**Mem. $[\text{CB8}]_{\text{Total}} = 30.8 \mu\text{M}$, $[\text{Mem}]_{\text{Total}} = 4.72 \text{ mM}$, $[\text{DMPCP}]_{\text{Total}} = 48.3 \mu\text{M}$, $K_{\text{rel}} = 173.60$. (b) One of the ^1H NMR spectra (500 MHz, D_2O , RT) used to determine K_{rel} for **CB8**MPCP and **CB8**DMPCP. $[\text{CB8}]_{\text{Total}} = 32.6 \mu\text{M}$, $[\text{MPCP}]_{\text{Total}} = 156 \mu\text{M}$, $[\text{DMPCP}]_{\text{Total}} = 80.6 \mu\text{M}$, $K_{\text{rel}} = 12.04$.

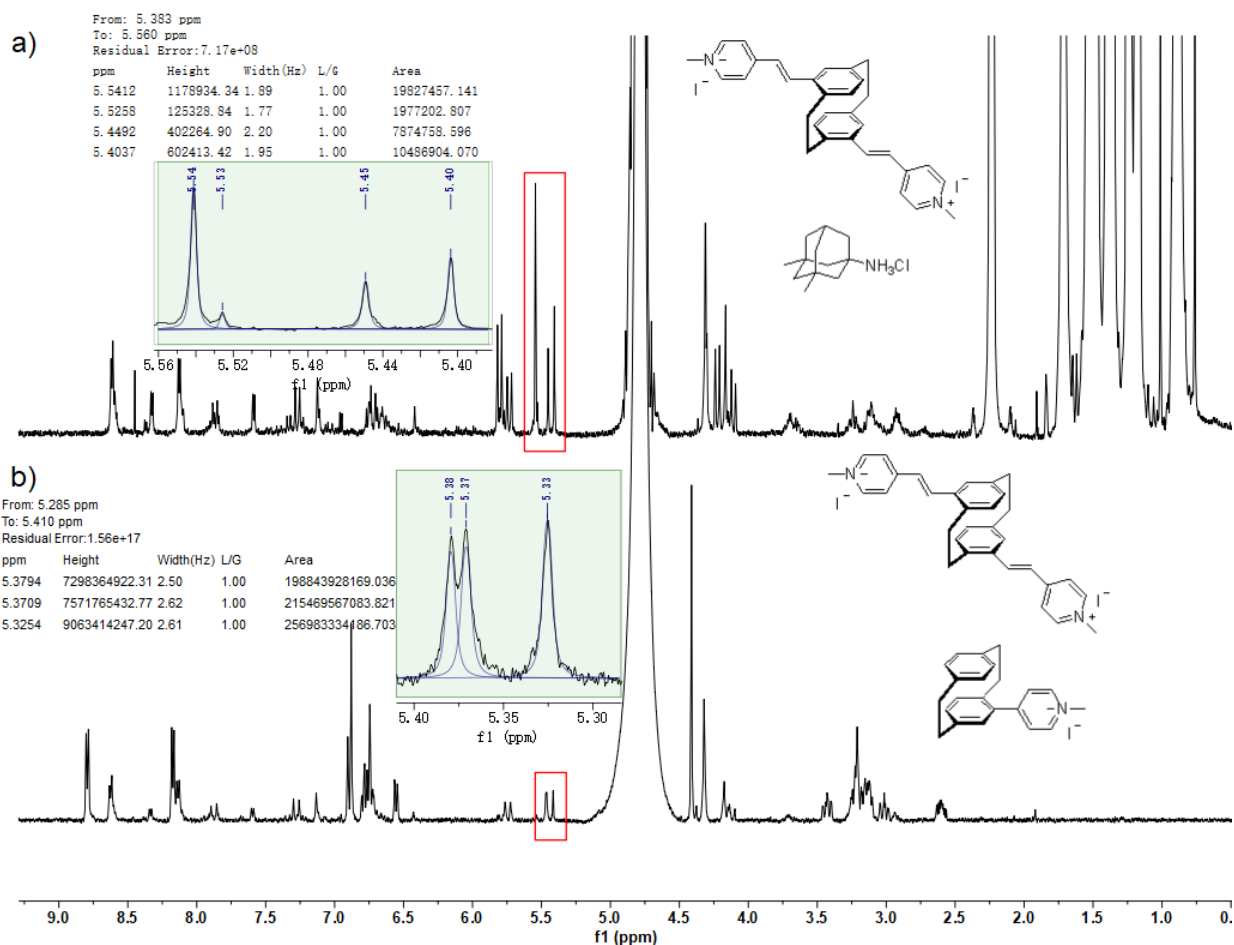
CB8 \rightarrow DMVCP

Figure 80. (a) One of the ^1H NMR spectra (500 MHz, D_2O , r.t.) was used to determine K_{rel} for **CB8** \rightarrow **DMVCP** and **CB8** \rightarrow **Mem**. $[\text{CB8}]_{\text{Total}} = 30.8 \mu\text{M}$, $[\text{Mem}]_{\text{Total}} = 4.72 \mu\text{M}$, $[\text{DMVCP}]_{\text{Total}} = 46.8 \mu\text{M}$, $K_{\text{rel}} = 69.33$. (b) One of the ^1H NMR spectra (500 MHz, D_2O , RT) used to determine K_{rel} for **CB8** \rightarrow **MPCP** and **CB8** \rightarrow **DMVCP**. $[\text{CB8}]_{\text{Total}} = 32.6 \mu\text{M}$, $[\text{MPCP}]_{\text{Total}} = 156 \mu\text{M}$, $[\text{DMVCP}]_{\text{Total}} = 93.0 \mu\text{M}$, $K_{\text{rel}} = 2.89$.

IDA for PCP and CB8 in PBS

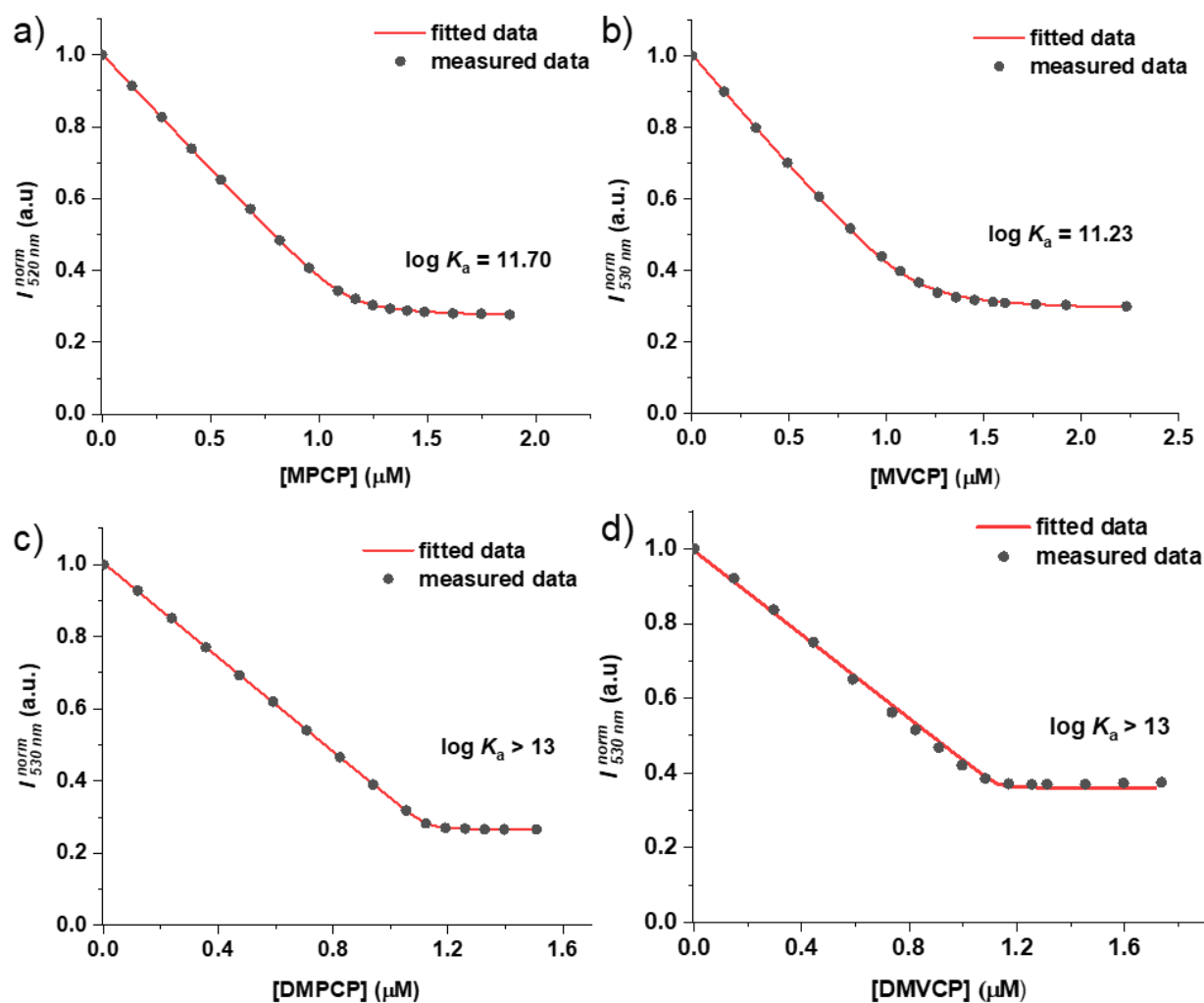


Figure 81. (a) Spectrum of **MPCP** fluorescence titration by BC (122 μM) with CB8 (1.13 μM) in PBS, $K_a = 5.00 \times 10^{11}$. (b) Spectrum of **MVCP** fluorescence titration by BC (122 μM) with CB8 (1.13 μM) in PBS, $K_a = 1.68 \times 10^{11}$. (c) Spectrum of **DMPCP** fluorescence titration by BC (122 μM) with CB8 (1.13 μM) in PBS, $K_a \geq 2.11 \times 10^{13}$. (d) Spectrum of **DMVCP** fluorescence titration by BC (122 μM) with CB8 (1.13 μM) in PBS, $K_a \geq 1.56 \times 10^{13}$. Dr. Amrutha Prabodh provided the results.

IDA for PCP and CB8 by BC in water

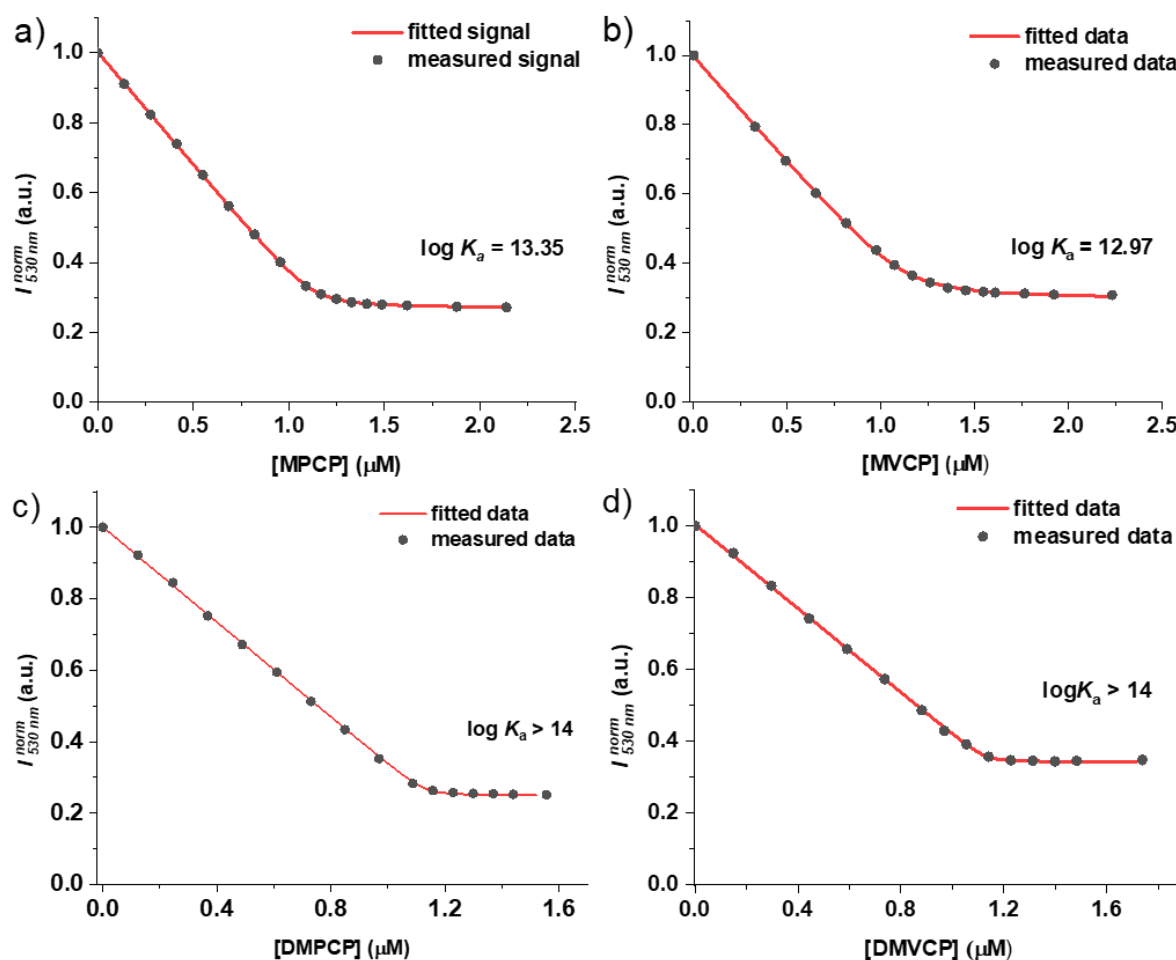


Figure 82. (a) Spectrum of MPCP fluorescence titration by BC (122 μM) with CB8 (1.13 μM) in water, $K_a = 2.33 \times 10^{13}$. (b) Spectrum of MPCP fluorescence titration by BC (122 μM) with CB8 (1.13 μM) in water, $K_a = 9.42 \times 10^{12}$. (c) Spectrum of DMPCP fluorescence titration by BC (122 μM) with CB8 (1.13 μM) in water, $K_a > 14$. (d) Spectrum of DMVCP fluorescence titration by BC (122 μM) with CB8 (1.13 μM) in water, $K_a > 14$. Dr. Amrutha Prabodh provided the results.

DBA for MVCP and CB7 in water

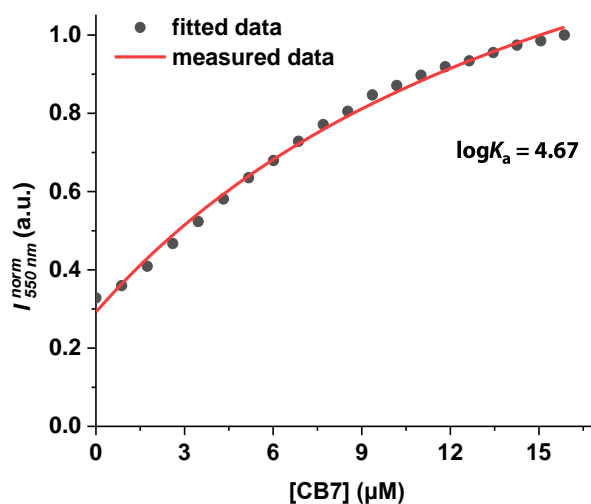
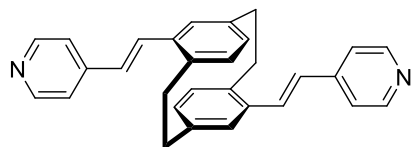


Figure 83. Spectrum of MVCP fluorescence titration by CB7 (349.77 μM) in water, $K_a = 4.66 \times 10^4$.

5.3 Exploration of Affinity on Extended and Functionalized [2.2]Paracyclophane Derivatives

4,16-Di(4'-pyridyl-(*E*)-vinyl)[2.2]paracyclophane (85)



A vessel was charged with 4,16-dibromo[2.2]paracyclophane (5.49 g, 15.0 mmol, 1.00 equiv), 4-vinylpyridine (7.89 g, 75.0 mmol, 5.00 equiv.), palladium acetate (168 mg, 750 μ mol, 0.05 equiv.), tetrapropylammonium bromide (7.99 g, 30.0 mmol, 2.00 equiv.), potassium carbonate (6.22 g, 30.0 mmol, 3.00 equiv.), and DMF (75 mL) under argon. The reaction mixture was heated at 110 °C for 18 hours. Then the reaction was cooled to room temperature, diluted with dichloromethane, and washed with brine. The organic layer was dried with Na₂SO₄ and concentrated and purified by flash column chromatography on silica gel using dichloromethane/methanol 20:1, obtaining the title compound (3.86 mg, 9.31 mmol, 62%) as an orange solid.

R_f = 0.4 (dichloromethane/methanol 20:1)

¹H NMR (400 MHz, CDCl₃, ppm) δ = 8.67–8.58 (m, 4H, H_{Py}), 7.46–7.36 (m, 6H, H_{Py} , CH=CH), 6.81 (d, J = 16.2 Hz, 2H, CH=CH), 6.74 (d, J = 1.9 Hz, 2H, H_{Ar}), 6.64 (dd, J = 7.8, 1.9 Hz, 2H, H_{Ar}), 6.44 (d, J = 7.8 Hz, 2H, H_{Ar}), 3.67–3.55 (m, 2H, H_{PC}), 3.22–3.11 (m, 2H, H_{PC}), 3.08–2.93 (m, 4H, H_{PC}).

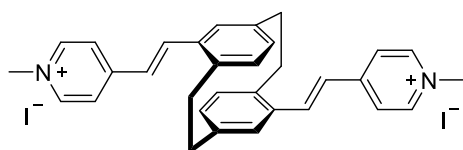
¹³C NMR (100 MHz, CDCl₃, ppm) δ = 150.3 (+, CH, 4C, C_{Py}), 145.0 (C_q , 2C, C_{Py}), 139.6 (C_q , 2C, C_{Ar}), 138.9 (C_q , 2C, C_{Ar}), 136.4 (C_q , 2C, C_{Ar}), 133.8 (+, 2C, C_{Ar}), 131.1 (+, 2C, CH=CH), 130.6 (+, 2C, C_{Ar}), 130.5 (+, 2C, C_{Ar}), 126.7 (+, 2C, CH=CH), 120.9 (+, CH, 4C, C_{Py}), 34.6 (–, 2C, CH₂), 33.3 (–, 2C, CH₂).

MS (EI, 70 eV, 20 °C, %) m/z = 415/416 (100/32) [M+H]⁺, 154 (87) 137 (56), 136 (67).

HRMS-EI (m/z): [M+H]⁺, calc. for C₃₀H₂₆N₂, 415.2169; found: 415.2383.

IR (ATR, $\tilde{\nu}$) = 3016 (w), 2928 (w), 1588 (vs), 1548 (m), 1490 (w), 1477 (w), 1438 (w), 1411 (s), 1341 (w), 1329 (w), 1306 (w), 1241 (w), 1220 (w), 1197 (w), 1142 (w), 989 (m), 972 (vs), 942 (w), 894 (w), 875 (s), 857 (s), 803 (vs), 783 (m), 741 (m), 721 (m), 656 (m), 628 (m), 565 (s), 534 (vs), 518 (vs), 480 (m), 470 (m) cm⁻¹.

4,16-Di(*N*-methyl-4'-pyridinium-(*E*)-vinyl)[2.2]paracyclophane iodide (pDMPCP, 80)



4,16-Di-((*E*)-4'-pyridylvinyl)[2.2]paracyclophane (100 mg, 240 μ mol, 1.00 equiv.) dissolved in acetonitrile 5 mL, then methyl iodide (200 μ L) was added. The mixture was stirred at 40 °C for 16 h, excluded of the light. The solvent was removed under reduced pressure to give a residue and then washed with dichloromethane and methanol to obtain

4,16-di(*N*-methyl-4'-pyridinium-(*E*)-vinyl)[2.2]paracyclophane iodide (125 mg, 179 μmol , 74%) as a yellow solid.

^1H NMR (400 MHz, DMSO- d_6 , ppm) δ = 8.88 (d, J = 6.4 Hz, 4H, H_{Py}), 8.39 (d, J = 6.4 Hz, 4H, H_{Py}), 8.01 (d, J = 16.1 Hz, 2H, CH=CH), 7.31 (d, J = 15.9 Hz, 2H, CH=CH), 7.02 (s, 2H, H_{Ar}), 6.63–6.51 (m, 4H, H_{Ar}), 4.29 (s, 6H, CH_3), 3.81 (td, J = 11.5, 10.9, 6.1 Hz, 2H, H_{PC}), 3.23–2.87 (m, 6H, H_{PC}).

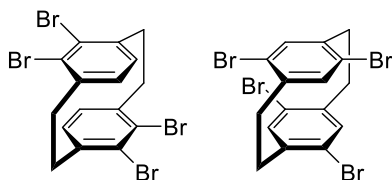
^{13}C NMR (100 MHz, DMSO- d_6 , ppm) δ = 153.2 (C_q , 2C, C_{Py}), 145.4 (+, 4C, C_{Py}), 141.3 (C_q , 2C, C_{Ar}), 140.3 (C_q , 2C, C_{Ar}), 138.8 (+, 2C, CH=CH), 136.1 (C_q , 2C, C_{Ar}), 134.3 (+, 2C, C_{Ar}), 132.7 (+, 2C, C_{Ar}), 131.5 (+, 2C, C_{Ar}), 124.4 (+, 2C, CH=CH), 124.2 (+, 4C, C_{Py}), 47.4 (+, 2C, CH_3), 34.6 (–, 2C, CH_2), 33.0 (–, 2C, CH_2).

MS (ESI, 70 eV, 20 $^\circ\text{C}$, %) m/z = 222/223/223 (100/32/5) $[\text{M}]^{2+}$.

HRMS-ESI (m/z): $[\text{M}-2\text{I}]^{2+}$, calc. for $\text{C}_{32}\text{H}_{32}\text{N}_2$, 222.1277/222.6294; found: 222.1273/222.6289.

IR (ATR, $\tilde{\nu}$) = 3020 (w), 2935 (w), 1638 (vs), 1615 (vs), 1587 (w), 1561 (w), 1517 (s), 1482 (w), 1466 (m), 1442 (w), 1326 (m), 1211 (w), 1183 (vs), 972 (s), 962 (vs), 874 (vs), 854 (w), 822 (vs), 657 (m), 552 (w), 521 (vs), 506 (vs) cm^{-1} .

4,5,12,13- And 4,7,12,15-tetrabromo[2.2]paracyclophane (86, 87)



[2.2]Paracyclophane (5.00 g, 24.0 mmol, 1.00 equiv.) was slowly added in a 250 g flask to a mixture of bromine (46.5 mg, 15.0 mL, 291 mmol, 12.1 equiv.) and iodine (75.0 mg, 296 μmol , 0.012 equiv.). The solution was kept in the dark (vigorous evolution of hydrogen

bromide!) and stirred for 7 d at room temperature in a flask wrapped with aluminum foil to exclude light. The reaction mixture was then decomposed by adding 300 ml of 20% aqueous sodium hydroxide. The precipitate is collected by filtration, washed with hot ethanol (3×50 mL), and dried in vacuo, as a mixture in equal amounts. The product mixture was extracted with dichloromethane (4×80 mL) to separate the isomers, yielding a residue of almost pure 4,5,12,13-tetrabromo[2.2]paracyclophane. A pure sample of 4,7,12,15-tetrabromo[2.2]paracyclophane was obtained by chromatography of 1 g of the mixture over 100 g of silica gel to yield a colorless solid (3.45 g, 6.59 mmol, 27%). And 4,5,12,13-tetrabromo[2.2]paracyclophane was combined to yield the final branch colorless solid (2.79 g, 5.33 mmol, 22%).

4,5,12,13-Tetrabromo[2.2]paracyclophane

R_f = 0.55 (cyclohexane)

^1H NMR (400 MHz, CDCl_3 , ppm) δ = 6.99 (s, 4H, H_{Ar}), 3.42–3.29 (m, 4H, H_{PC}), 3.16–3.04 (m, 4H, H_{PC}).

^{13}C NMR (100 MHz, CDCl_3 , ppm) δ = 140.7 (C_q , 4C, C_{Ar}), 129.3 (C_q , 4C, C_{Ar}), 128.7 (+, 4C, C_{Ar}), 34.6 (–, 4C, CH_2).

MS (EI, 70 eV, 20 °C, %) m/z = 526/524/522 (19/28/19) $[\text{M}+\text{H}]^+$, 264/262/260/ (47/100/48) $[\text{C}_8\text{H}_6\text{Br}_2]^+$.

HRMS-EI (m/z): $[\text{M}+\text{H}]^+$, calc. for $\text{C}_{16}\text{H}_{12}^{79}\text{Br}_2^{81}\text{Br}_2$, 523.7632; found: 523.7731.

IR (ATR, $\tilde{\nu}$) = 3456 (s), 3445 (s), 3414 (s), 3405 (s), 2934 (s), 1436 (vs), 1373 (vs), 1062 (vs), 837 (vs), 771 (s), 764 (s), 735 (vs), 707 (vs), 673 (vs), 523 (vs), 477 (s), 465 (s), 436 (s), 424 (s), 414 (s), 405 (s), 395 (s), 384 (s) cm^{-1} .

4,7,12,15-Tetrabromo[2.2]paracyclophane

R_f = 0.5 (cyclohexane)

^1H NMR (400 MHz, CDCl_3 , ppm) δ = 7.20 (s, 4H, H_{Ar}), 3.30–3.17 (m, 4H, H_{PC}), 3.14–2.92 (m, 4H, H_{PC}).

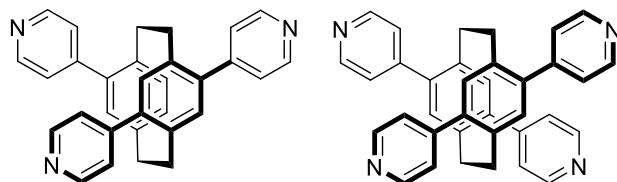
^{13}C NMR (100 MHz, CDCl_3 , ppm) δ = 140.3 (C_q , 4C, C_{Ar}), 134.4 (+, 4C, C_{Ar}), 125.3 (C_q , 4C, C_{Ar}), 32.7 (–, 4C, CH_2).

MS (EI, 70 eV, 20 °C, %) m/z = 526/524/522 (19/28/19) $[\text{M}+\text{H}]^+$, 264/262/260/ (48/100/49) $[\text{C}_8\text{H}_6\text{Br}_2]^+$.

HRMS-EI (m/z): $[\text{M}+\text{H}]^+$, calc. for $\text{C}_{16}\text{H}_{12}^{79}\text{Br}_2^{81}\text{Br}_2$, 523.7632; found: 523.7731.

IR (ATR, $\tilde{\nu}$) = 3456 (s), 3445 (s), 3414 (s), 3405 (s), 2934 (s), 1436 (vs), 1373 (vs), 1062 (vs), 914 (s), 837 (vs), 771 (s), 764 (s), 735 (vs), 707 (vs), 673 (vs), 523 (vs), 477 (s), 465 (s), 436 (s), 424 (s), 414 (s), 405 (s), 395 (s), 384 (s) cm^{-1} .

4,7,12-Tri(4'-pyridinyl)[2.2]paracyclophane (88), 4,7,12,15-tetra(4'-pyridinyl)[2.2]paracyclophane (89)



A vessel was charged with 4,7,12,15-tetrabromo[2.2]paracyclophane (500 mg, 954 μmol , 1.00 equiv.), pyridine-4-boronic acid (939 mg, 7.64 mmol, 8.00 equiv.), palladium-tetrakis(triphenylphosphine) (70.0 mg, 6.00 μmol , 0.06 equiv.), potassium phosphate (1.06 g, 50.0 μmol , 5.23 equiv.), dioxane (16 mL) and water (8 mL) under argon atmosphere. The mixture was heated under reflux for 16 h. The reaction mixture was then cooled to room temperature, and extracted with DCM (3×50 mL), the extracts were dried with MgSO_4 and evaporated under reduced pressure. The crude solid was purified by flash column chromatography on silica gel using dichloromethane /methanol 20:1, then obtain the compounds 4,7,12-tri(4'-pyridinyl)[2.2]paracyclophane (105 mg, 239 μmol , 25%) and 4,7,12,15-tetra(4'-pyridinyl)[2.2]paracyclophane (102 mg, 197 μmol , 21%) respectively as colorless solid.

4,7,12-Tri(4'-pyridinyl)[2.2]paracyclophane

$R_f = 0.24$ (dichloromethane /methanol 20:1)

$^1\text{H NMR}$ (400 MHz, CDCl_3 , ppm) $\delta = 8.81\text{--}8.75$ (m, 2H, H_{Py}), $8.72\text{--}8.67$ (m, 2H, H_{Py}), $8.63\text{--}8.56$ (m, 2H, H_{Py}), $7.55\text{--}7.49$ (m, 2H, H_{Py}), $7.34\text{--}7.29$ (m, 2H, H_{Py}), $7.18\text{--}7.11$ (m, 2H, H_{Py}), $6.88\text{--}6.80$ (m, 2H, H_{Ar}), 6.77 (dd, $J = 8.1, 6.6$ Hz, 3H, H_{Ar}), 3.62 (ddd, $J = 13.6, 10.1, 1.7$ Hz, 1H, H_{PC}), $3.55\text{--}3.45$ (m, 1H, H_{PC}), $3.36\text{--}3.25$ (m, 2H, H_{PC}), 3.08 (ddd, $J = 13.7, 10.5, 6.4$ Hz, 1H, H_{PC}), $2.99\text{--}2.92$ (m, 1H, H_{PC}), $2.72\text{--}2.53$ (m, 2H, H_{PC}).

$^{13}\text{C NMR}$ (100 MHz, CDCl_3 , ppm) $\delta = 150.3$ (+, 2C, C_{Py}), 150.2 (+, 2C, C_{Py}), 150.0 (+, 2C, C_{Py}), 148.2 (C_{q} , C_{Py}), 147.7 (C_{q} , C_{Py}), 147.5 (C_{q} , C_{Py}), 140.2 (C_{q} , C_{Ar}), 139.8 (C_{q} , C_{Ar}), 138.4 (C_{q} , C_{Ar}), 138.1 (C_{q} , C_{Ar}), 138.0 (C_{q} , C_{Ar}), 137.8 (C_{q} , C_{Ar}), 137.4 (C_{q} , C_{Ar}), 135.0 (+, CH, C_{Ar}), 133.1 (C_{q} , C_{Ar}), 132.5 (C_{q} , C_{Ar}), 132.5 (C_{q} , C_{Ar}), 129.7 (C_{q} , C_{Ar}), 124.1 (+, 2C, CH, C_{Py}), 123.6 (+, 2C, CH, C_{Py}), 123.5 (+, 2C, CH, C_{Py}), 34.5 (-, CH_2), 33.8 (-, CH_2), 33.3 (-, CH_2), 33.2 (-, CH_2).

MS (70 eV, ESI), m/z (%): 440/441 (100/44) $[\text{M}+\text{H}]^+$.

HRMS-EI (m/z) calc. for $\text{C}_{31}\text{H}_{25}\text{N}_3$, 440.2122; found: 440.2114.

IR (ATR, $\tilde{\nu}$) = 3020 (w), 2958 (w), 2936 (w), 2917 (w), 2871 (w), 2863 (w), 1591 (vs), 1541 (s), 1475 (m), 1456 (w), 1441 (w), 1409 (s), 1401 (m), 1380 (w), 1215 (w), 1181 (w), 1065 (w), 992 (m), 882 (m), 827 (vs), 820 (vs), 803 (s), 756 (m), 728 (m), 720 (m), 710 (s), 688 (m), 680 (s), 669 (m), 653 (w), 639 (s), 623 (s), 591 (w), 571 (m), 562 (m), 548 (s), 524 (m), 511 (w), 496 (vs), 476 (vs), 450 (s), 436 (m), 426 (m), 418 (m), 411 (m), 398 (w), 388 (w), 378 (m) cm^{-1} .

4,7,12,15-Tetra(4'-pyridinyl)[2.2]paracyclophane

$R_f = 0.2$ (dichloromethane /methanol 20:1)

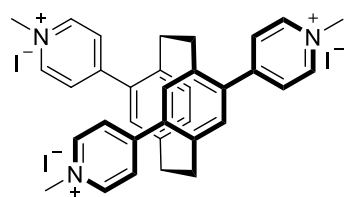
$^1\text{H NMR}$ (400 MHz, CDCl_3 , ppm) $\delta = 8.73\text{--}8.61$ (m, 8H, H_{Py}), $7.28\text{--}7.26$ (m, 8H, H_{Py}), 6.88 (s, 4H, H_{Ar}), $3.67\text{--}3.51$ (m, 4H, H_{PC}), $2.97\text{--}2.81$ (m, 4H, H_{PC}).

$^{13}\text{C NMR}$ (100 MHz, CDCl_3 , ppm) $\delta = 150.4$ (+, 8C, C_{Py}), 147.4 (q, 4C, C_{Py}), 138.8 (q, 4C, C_{Ar}), 137.8 (q, 4C, C_{Ar}), 132.59 (+, 4C, C_{Ar}), 123.38 (+, 8C, C_{Py}), 33.29 (-, 4C, CH_2).

MS (70 eV, ESI), m/z (%): 517/518 (100/39) $[\text{M}+\text{H}]^+$.

HRMS-EI (m/z) calc. for $\text{C}_{36}\text{H}_{29}\text{N}_4$, 517.2387; found: 517.2390.

IR (ATR, $\tilde{\nu}$) = 1589 (vs), 1543 (m), 1411 (s), 826 (vs), 812 (vs), 727 (m), 718 (m), 693 (vs), 671 (s), 541 (s), 528 (s), 484 (vs), 469 (s), 458 (s), 419 (m) cm^{-1} .

4,7,12-Tri(*N*-methyl-4'-pyridinium)[2.2]paracyclophane iodide (TMPCP, 81)

4,7,12-Tri(4'-pyridinyl)[2.2]paracyclophane (40.0 mg, 91.0 μmol , 1.00 equiv) dissolved in acetonitrile 5 mL, then methyl iodide (129 mg, 0.50 mL, 10.0 equiv.) was added. The mixture was stirred at 40 °C for 16 h, excluding the light. The solvent was removed under reduced pressure to give a residue and then recrystallized from methanol to obtain 4,7,12-tri(*N*-methyl-4'-pyridinium)[2.2]paracyclophane iodide (65.2 mg, 75.1 μmol , 83%) as a yellow solid.

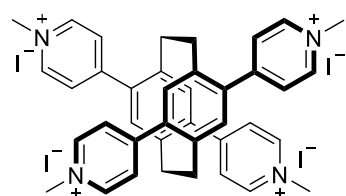
^1H NMR (400 MHz, DMSO- d_6 , ppm) δ = 9.13 (d, J = 6.4 Hz, 2H, H_{Py}), 9.09 (d, J = 6.5 Hz, 2H, H_{Py}), 8.99 (d, J = 6.5 Hz, 2H, H_{Py}), 8.48 (d, J = 6.3 Hz, 2H, H_{Py}), 8.13 (d, J = 6.5 Hz, 2H, H_{Py}), 7.99 (d, J = 6.4 Hz, 2H, H_{Py}), 7.50 (s, 1H, H_{Ar}), 7.26 (dd, J = 7.8, 1.8 Hz, 1H, H_{Ar}), 7.24 (s, 1H, H_{Ar}), 7.14 (d, J = 1.8 Hz, 1H, H_{Ar}), 6.79 (d, J = 7.9 Hz, 1H, H_{Ar}), 4.45 (s, 3H, CH_3), 4.44 (s, 3H, CH_3), 4.39 (s, 3H, CH_3), 3.59 (dd, J = 13.1, 9.8 Hz, 1H, H_{PC}), 3.45–3.33 (m, 4H, H_{PC}), 3.06–2.86 (m, 2H, H_{PC}), 2.73–2.85 (m, 1H, H_{PC}).

^{13}C NMR (100 MHz, DMSO- d_6 , ppm) δ = 153.8 (C_q , C_{Py}), 153.6 (C_q , C_{Py}), 153.1 (C_q , C_{Py}), 146.3 (+, 2C, CH, C_{Py}), 146.2 (+, 2C, CH, C_{Py}), 146.0 (+, 2C, CH, C_{Py}), 140.8 (C_q , C_{Ar}), 140.6 (C_q , C_{Ar}), 130.0 (C_q , C_{Ar}), 139.5 (C_q , C_{Ar}), 139.4 (C_q , C_{Ar}), 136.7 (C_q , C_{Ar}), 136.1 (+, CH, C_{Ar}), 135.7 (+, CH, C_{Ar}), 135.3 (C_q , C_{Ar}), 133.9 (+, CH, C_{Ar}), 133.8 (+, CH, C_{Ar}), 130.1 (+, CH, C_{Ar}), 127.8 (+, 2C, CH, C_{Py}), 127.1 (+, 2C, CH, C_{Py}), 126.8 (+, 2C, CH, C_{Py}), 47.9 (+, CH_3), 47.8 (+, CH_3), 47.6 (+, CH_3), 33.9 (–, CH_2), 33.6 (–, CH_2), 33.5 (–, CH_2), 33.1 (–, CH_2).

MS (ESI, 70 eV, 20 °C, %) m/z = 306 (100) $[\text{M}+\text{I}]^{2+}$, 378 (20) $[\text{M}+2\text{I}]^+$.

HRMS-ESI (m/z): $[\text{M}+\text{I}]^{2+}$, calc. for $\text{C}_{34}\text{H}_{34}\text{IN}_3$, 305.5893/306.0910; found: 305.5892/306.0908. $[\text{M}+2\text{I}]^+$, calc. for $\text{C}_{34}\text{H}_{34}\text{I}_2\text{N}_3$, 738.0837/739.0871; found: 738.0836/739.0870.

IR (ATR, $\tilde{\nu}$) = 3398 (s), 3378 (s), 3374 (s), 3367 (s), 3359 (s), 3347 (m), 3339 (m), 1635 (vs), 1561 (m), 1514 (s), 1458 (s), 1193 (s), 836 (vs), 816 (s), 727 (s), 623 (m), 599 (s), 581 (s), 569 (s), 547 (vs), 524 (vs), 494 (vs), 466 (vs), 449 (vs), 441 (vs), 424 (vs), 415 (vs), 405 (vs), 395 (vs), 388 (vs), 382 (vs) cm^{-1} .

4,7,12,15-Tetra(*N*-methyl-4'-pyridinium)[2.2]paracyclophane iodide (QMPCP, 82)

4,7,12,15-Tetra-(4'-pyridine)[2.2]paracyclophane (15.0 mg, 29 μmol , 1.00 equiv.) dissolved in acetonitrile 5 mL, then methyl iodide (100 μL) was added. The mixture was stirred at 40 °C for 12 h excluding the light. The solvent was removed under reduced pressure to give a residue and then recrystallized from methanol to obtain 4,7,12,15-tetra(*N*-methyl-4'-pyridinium)[2.2]paracyclophane iodide (25.1 mg, 23.1 μmol , 79%) as a yellow solid.

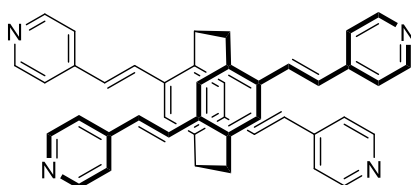
^1H NMR (400 MHz, DMSO- d_6 , ppm) δ = 9.09 (d, J = 6.3 Hz, 8H, H_{Py}), 8.19 (d, J = 6.2 Hz, 8H, H_{Py}), 7.52 (s, 4H, H_{Ar}), 4.45 (s, 12H, CH_3), 3.56–3.68 (m, 4H, H_{PC}), 3.27–3.19 (m, 4H, H_{PC}).

^{13}C NMR (100 MHz, DMSO- d_6 , ppm) δ = 152.1 (C_q , 4C, C_{Py}), 146.2 (+, 8C, C_{Py}), 140.5 (C_q , 4C, C_{Ar}), 137.4 (C_q , 4C, C_{Ar}), 133.5 (+, 4C, C_{Ar}), 127.0 (+, 8C, C_{Py}), 47.8 (+, 4C, CH_3), 33.3 (–, 4C, CH_2).

HRMS-ESI (m/z): $[\text{M}+2\text{I}]^{2+}$, calc. for $\text{C}_{48}\text{H}_{48}\text{N}_4\text{I}_2$, 467.0979/467.5996; found: 467.0977/467.5992 (100/54). $[\text{M}+\text{I}]^{3+}$, calc. for $\text{C}_{48}\text{H}_{48}\text{N}_4\text{I}_3$, 269.0969/269.4314; found: 269.0967/269.4311 (65/7). $[\text{M}]^{4+}$, calc. for $\text{C}_{48}\text{H}_{48}\text{N}_4$, 170.0964/170.3473; found: 170.0964/170.3472 (34/8).

IR (ATR, $\tilde{\nu}$) = 3444 (m), 3431 (m), 3415 (m), 3410 (m), 3401 (m), 3393 (m), 3381 (m), 3370 (m), 3343 (m), 3029 (m), 3010 (m), 1635 (vs), 1561 (m), 1519 (s), 1459 (m), 1436 (m), 1191 (s), 1044 (m), 830 (vs), 693 (m), 555 (m), 537 (s), 526 (s), 506 (m), 486 (s), 469 (vs), 446 (vs), 441 (vs), 419 (vs), 414 (vs), 405 (vs), 398 (vs), 388 (vs), 377 (vs) cm^{-1} .

4,7,12,15-Tetra(4'-pyridyl)-(E)-vinyl[2.2]paracyclophane (91)



A vessel was charged with 4,7,12,15-tetrabromo[2.2]paracyclophane (1.00 g, 1.91 mmol, 1.00 equiv.), 4-vinylpyridine (3.01 mg, 28.6 mmol, 3.05 mL, 15.0 equiv.), palladium acetate (21.0 mg, 93.5 μmol , 0.05 equiv.), tetrapropylammonium bromide (1.27 g, 4.78 mmol,

2.50 equiv.), potassium carbonate (1.32 g, 9.55 mmol, 5.00 equiv.), and DMF (12 mL) under argon. The reaction mixture was heated at 110 $^{\circ}\text{C}$ for 18 hours. Then the reaction was cooled to room temperature, diluted with CH_2Cl_2 , and washed with brine. The organic layer was dried with MgSO_4 and concentrated, and purified by flash column chromatography on silica gel using dichloromethane/methanol 20:1, obtaining the title compound (549 mg, 885 μmol , 46%) as an orange solid.

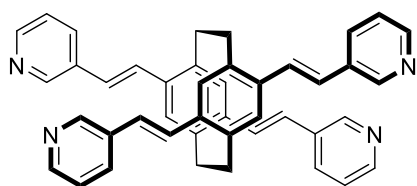
R_f = 0.3 (dichloromethane/methanol 20:1)

^1H NMR (400 MHz, CDCl_3 , ppm) δ = 8.67–8.61 (m, 8H, H_{Py}), 7.41 (d, J = 16.2 Hz, 4H, $\text{CH}=\text{CH}$), 7.36–7.27 (m, 8H, H_{Py}), 7.00 (s, 4H, H_{Ar}), 6.81 (d, J = 16.1 Hz, 4H, $\text{CH}=\text{CH}$), 3.72–3.60 (m, 4H, H_{PC}), 3.01–2.88 (m, 4H, H_{PC}).

^{13}C NMR (100 MHz, CDCl_3 , ppm) δ = 150.5 (+, CH, 8C, C_{Py}), 144.4 (C_q , 4C, C_{Py}), 138.6 (C_q , 4C, C_{Ar}), 136.6 (C_q , 4C, C_{Ar}), 129.1 (+, 4C, $\text{CH}=\text{CH}$), 129.0 (+, 4C, C_{Ar}), 126.7 (+, 4C, $\text{CH}=\text{CH}$), 120.8 (+, CH, 8C, C_{Py}), 33.1 (–, 2C, CH_2), 1.0 (–, 2C, CH_2).

HRMS-ESI (m/z): $[\text{M}+\text{H}]^+$, calc. for $\text{C}_{44}\text{H}_{36}\text{N}_4$, 621.3013/622.3047; found: 621.3010/622.3043 (45/100).

IR (ATR, $\tilde{\nu}$) = 3377 (w), 3369 (w), 3356 (w), 3349 (w), 3340 (w), 3332 (w), 3325 (w), 3315 (w), 3299 (w), 3288 (w), 3284 (w), 3269 (w), 3258 (w), 3245 (w), 3216 (w), 3033 (w), 2934 (w), 1589 (vs), 1547 (m), 1459 (w), 1412 (m), 1324 (w), 1217 (w), 965 (s), 833 (m), 799 (s), 592 (m), 524 (s), 514 (m), 497 (w) cm^{-1} .

4,7,12,15-Tetra(3'-pyridyl-(E)-vinyl)[2.2]paracyclophane (92)

A vessel was charged with 4,7,12,15-tetrabromo[2.2]paracyclophane (200 mg, 382 μmol , 1.00 equiv.), 3-vinylpyridine (241 mg, 2.29 mmol, 6.00 equiv.), palladium acetate (4.30 mg, 19.2 μmol , 0.05 equiv.), tetrapropylammonium bromide (254 mg, 955 μmol , 2.5 equiv.), potassium carbonate (264 mg, 1.91 mmol, 5.00 equiv.), and DMF (8 mL) under argon. The reaction mixture was heated at 110 °C for 16 hours. Then the reaction was cooled to room temperature, diluted with CH_2Cl_2 , and washed with brine. The organic layer was dried with MgSO_4 and concentrated, and purified by flash column chromatography on silica gel using dichloromethane/methanol 20:1, obtaining the title compound (203 mg, 327 μmol , 86%) as an orange solid.

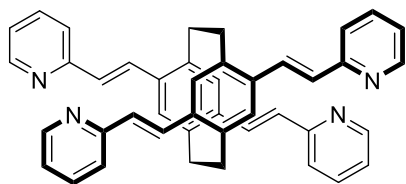
$R_f = 0.4$ (dichloromethane/methanol 20:1)

$^1\text{H NMR}$ (400 MHz, CDCl_3 , ppm) $\delta = 8.71$ (d, $J = 2.3$ Hz, 4H, H_{Py}), 8.55 (dd, $J = 4.8, 1.6$ Hz, 4H, H_{Py}), 7.75 (dt, $J = 7.9, 2.0$ Hz, 4H, H_{Py}), 7.37–7.32 (m, 4H, H_{Py}), 7.28 (d, $J = 16.5$ Hz, 4H, CH=CH), 7.00 (s, 4H, H_{Ar}), 6.87 (d, $J = 16.2$ Hz, 4H, CH=CH), 3.63 (q, $J = 5.7$ Hz, 4H, H_{PC}), 2.98–2.87 (m, 4H, H_{PC}).

$^{13}\text{C NMR}$ (100 MHz, CDCl_3 , ppm) $\delta = 148.8$ (+, 4C, C_{Py}), 148.2 (+, 4C, C_{Py}), 138.2 (C_{q} , 4C, C_{Ar}), 136.7 (C_{q} , 4C, C_{Ar}), 133.1 (+, 4C, C_{Py}), 133.0 (C_{q} , 4C, C_{Ar}), 128.5 (+, 4C, C_{Ar}), 127.1 (+, 4C, CH=CH), 125.3 (+, 4C, CH=CH), 123.8 (+, 4C, C_{Py}), 33.1 (–, 4C, CH_2).

HRMS-ESI (m/z): $[\text{M}+\text{H}]^+$, calc. for $\text{C}_{44}\text{H}_{36}\text{N}_4$, 621.3013/622.3047; found: 621.3032/622.3001 (48/100).

IR (ATR, $\tilde{\nu}$) = 2931 (w), 1564 (w), 1485 (w), 1472 (w), 1460 (w), 1412 (m), 1323 (w), 1306 (w), 1238 (w), 1215 (w), 1183 (w), 1122 (w), 1099 (w), 1021 (m), 956 (vs), 904 (m), 873 (w), 858 (w), 846 (w), 826 (m), 790 (s), 758 (w), 700 (vs), 633 (m), 620 (m), 603 (m), 575 (w), 569 (w), 550 (w), 524 (w), 511 (w), 497 (m), 462 (w), 448 (w), 424 (w), 414 (w), 397 (m), 384 (w) cm^{-1} .

4,7,12,15-Tetra(2'-pyridyl-(E)-vinyl)[2.2]paracyclophane (93)

A vessel was charged with 4,7,12,15-tetrabromo[2.2]paracyclophane (500 mg, 961 μmol , 1.00 equiv.), 2-vinylpyridine (750 mg, 7.20 mmol, 7.50 μL), palladium acetate (11.0 mg, 49.0 μmol , 0.05 equiv.), tetrapropylammonium bromide (635 mg, 2.40 mmol, 2.50 equiv.), potassium carbonate (660 mg, 4.80 mmol, 5.00 equiv.), and DMF (12 mL) under argon. The reaction mixture was heated at 110 °C for 17 hours. Then the reaction was cooled to room temperature, diluted with CH_2Cl_2 , and washed with brine. The organic layer was dried with MgSO_4 and concentrated. The crude product was purified via flash column chromatography on silica gel using dichloromethane/methanol 20:1, obtaining the title compound (123 mg, 198 μmol , 21%) as an orange solid.

$R_f = 0.45$ (dichloromethane/methanol 20:1)

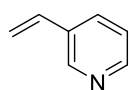
^1H NMR (400 MHz, CDCl_3 , ppm) δ = 8.68 (ddd, J = 4.8, 1.9, 0.9 Hz, 4H, H_{Py}), 7.82 (d, J = 15.8 Hz, 4H, CH=CH), 7.66 (td, J = 7.6, 1.8 Hz, 4H, H_{Py}), 7.22 (dt, J = 7.9, 1.1 Hz, 4H, H_{Py}), 7.18 (ddd, J = 7.5, 4.8, 1.1 Hz, 4H, H_{Py}), 7.09 (s, 4H, H_{Ar}), 6.99 (d, J = 15.8 Hz, 4H, CH=CH), 3.77–3.64 (m, 4H, H_{PC}), 3.03–2.90 (m, 4H, H_{PC}).

^{13}C NMR (100 MHz, CDCl_3 , ppm) δ = 155.9 (C_q , 4C, C_{Py}), 149.9 (+, 4C, C_{Py}), 139.0 (C_q , 4C, C_{Ar}), 136.9 (C_q , 4C, C_{Ar}), 136.5 (+, 4C, C_{Py}), 129.3 (+, 4C, CH=CH), 128.9 (+, 4C, C_{Ar}), 128.1 (+, 4C, CH=CH), 122.9 (+, 4C, C_{Py}), 122.0 (+, 4C, C_{Py}), 33.2 (–, 4C, CH_2).

HRMS-ESI (m/z): $[\text{M}+\text{H}]^+$, calc. for $\text{C}_{44}\text{H}_{36}\text{N}_4$, 621.3013/622.3047; found: 621.3032/622.3001 (48/100).

IR (ATR, $\tilde{\nu}$) = 2922 (m), 1581 (vs), 1558 (s), 1483 (w), 1466 (vs), 1426 (vs), 1299 (w), 1203 (m), 1147 (s), 1091 (w), 1048 (w), 990 (w), 963 (vs), 907 (m), 887 (m), 860 (m), 829 (m), 771 (vs), 739 (vs), 715 (s), 676 (w), 635 (w), 612 (s), 550 (w), 526 (m), 500 (m), 479 (m), 456 (m), 446 (m), 431 (w), 426 (w), 401 (vs), 390 (w) cm^{-1} .

3-Vinylpyridine (90)



To a solution of methyl triphenylphosphonium bromide (1.78 g, 5.00 mmol, 1.00 equiv.) in THF (25 mL) at -78 °C was added LDA (536 mg, 5.00 mmol, 1.00 equiv.). Then 3-pyridinecarboxaldehyde (537 mg, 570 μL , 10.0 mmol, 1.00 equiv.) was added dropwise, and the resulting mixture was allowed to warm up to room temperature for 2 h. The reaction was quenched with water (50 mL) and extracted with cyclohexane (2×50 mL). The combined organic extracts were dried over MgSO_4 , filtered, and concentrated in vacuo. The crude product was purified via flash column chromatography on silica gel using cyclohexane/ethyl acetate 4:3, obtaining the title compound (251 mg, 2.39 mmol, 45%) as colorless liquid as colorless liquid, but due to toxicity and stench, it will be used directly in next step in a small amount of solution.

R_f = 0.4 (cyclohexane/ethyl acetate 4:3)

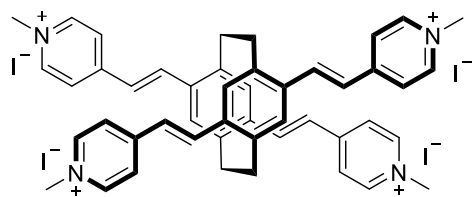
^1H NMR (400 MHz, CDCl_3 , ppm) δ = 8.59 (d, J = 2.3 Hz, 1H, H_{Py}), 8.46 (dd, J = 4.8, 1.7 Hz, 1H, H_{Py}), 7.69 (dt, J = 7.9, 2.0 Hz, 1H, H_{Py}), 7.26–7.18 (m, 1H, H_{Py}), 6.67 (dd, J = 17.7, 11.0 Hz, 1H, CH=CH), 5.80 (d, J = 17.7 Hz, 1H, CH=CH), 5.35 (d, J = 11.0 Hz, 1H, CH=CH).

^{13}C NMR (100 MHz, CDCl_3 , ppm) δ = 148.9 (+, CH, C_{Py}), 148.3 (+, CH, C_{Py}), 133.5 (+, CH=CH₂), 133.0 (C_q , C_{Py}), 132.6 (+, CH, C_{Py}), 123.4 (+, CH, C_{Py}), 116.2 (–, CH_2).

MS (EI, 70 eV, 20 °C, %) m/z = 105/104 (100/78) $[\text{M}]^+$.

HRMS-EI (m/z): $[\text{M}]^+$, calc. for $\text{C}_7\text{H}_7\text{N}$, 105.0578; found: 105.0781.

IR (ATR, $\tilde{\nu}$) = 1480 (m), 1473 (m), 1411 (m), 1400 (s), 1024 (s), 989 (vs), 914 (vs), 813 (vs), 713 (vs), 662 (m), 628 (s), 397 (s) cm^{-1} .

4,7,12,15-Tetra(*N*-Methyl-4'-pyridinium-(*E*)-vinyl)[2.2]paracyclophane iodide (QMVCPP, 83)

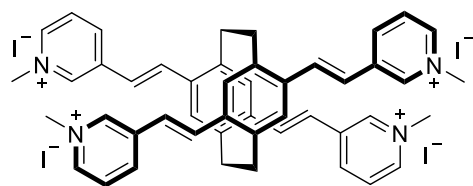
4,7,12,15-Tetra-(4'-pyridyl-(*E*)-vinyl)[2.2]paracyclophane (150 mg, 242 μmol , 1.00 equiv.) dissolved in acetonitrile 6 mL, then methyl iodide (150 μL) was added. The mixture was stirred at 40 °C for 14 h excluding the light. The solvent was removed under reduced pressure to give a residue and then recrystallized from methanol to obtain 4,7,12,15-tetra-(*N*-methyl-4'-pyridinium-(*E*)-vinyl)[2.2]paracyclophane iodide (280 mg, 236 μmol , 97%) as a red solid.

^1H NMR (400 MHz, DMSO- d_6 , ppm) δ = 8.89 (d, J = 6.5 Hz, 8H, H_{Py}), 8.21 (d, J = 6.5 Hz, 8H, H_{Py}), 7.99 (d, J = 16.1 Hz, 4H, CH=CH), 7.18 (d, J = 16.6 Hz, 4H, CH=CH), 7.16 (s, 4H, H_{Ar}), 4.34 (s, 12H, CH_3), 3.98–3.93 (m, 4H, H_{PC}), 3.03–2.98 (m, 4H, H_{PC}).

^{13}C NMR (100 MHz, DMSO- d_6 , ppm) δ = 152.6 (C_q , 4C, C_{Py}), 145.4 (+, 4C, C_{Py}), 141.4 (C_q , 4C, C_{Ar}), 137.5 (C_q , 4C, C_{Ar}), 136.5 (+, 4C, CH=CH), 131.0 (+, 4C, C_{Ar}), 125.1 (+, 4C, CH=CH), 124.5 (+, 4C, C_{Py}), 47.5 (+, 12C, CH_3), 33.1 (–, 4C, CH_2).

HRMS-ESI (m/z): $[\text{M}]^{4+}$, calc. for $\text{C}_{48}\text{H}_{48}\text{N}_4^{4+}$, 170.0964, found: 170.0965 (13); $[\text{M}+\text{I}]^{3+}$, calc. for $\text{C}_{48}\text{H}_{48}\text{N}_4\text{I}^{3+}$, 269.0969/269.4314, found: 269.0969/269.4313 (24/12); $[\text{M}+2\text{I}]^{2+}$, calc. for $\text{C}_{48}\text{H}_{48}\text{N}_4\text{I}_2^{2+}$, 467.0979/467.5996, found: 467.0981/467.5997 (81/40); $[\text{M}+3\text{I}]^+$, calc. for $\text{C}_{48}\text{H}_{48}\text{N}_4\text{I}_3^+$, 1061.1008, found: 1061.1010(4).

IR (ATR, $\tilde{\nu}$) = 3465 (m), 3439 (m), 3427 (m), 3391 (m), 1638 (s), 1604 (vs), 1562 (s), 1514 (s), 1466 (s), 1330 (m), 1320 (m), 1210 (m), 1190 (vs), 1169 (s), 975 (s), 965 (m), 880 (m), 837 (s), 561 (m), 543 (m), 516 (vs), 477 (m), 465 (m), 395 (m), 385 (s), 377 (s) cm^{-1} .

4,7,12,15-Tetra(*N*-methyl-3'-pyridinium-(*E*)-vinyl)[2.2]paracyclophane iodide (QMVCpm, 84)

4,7,12,15-Tetra-((*E*)-vinyl-3'-pyridyl)[2.2]paracyclophane (62.0 mg, 99.9 μmol , 1.00 equiv.) dissolved in acetonitrile 6 mL, then methyl iodide (2.00 μL) was added. The mixture was stirred at 40 °C for 14 h excluding the light. The solvent was removed under reduced pressure to give a residue and then recrystallized from methanol to obtain 4,7,12,15-tetra-(*N*-methyl-3'-pyridinium-(*E*)-vinyl)[2.2]paracyclophane iodide (81.1 mg, 68.1 μmol , 68%) as an orange solid.

^1H NMR (400 MHz, DMSO- d_6 , ppm) δ = 9.36 (s, 4H, H_{Py}), 8.88 (d, J = 6.0 Hz, 4H, H_{Py}), 8.61 (d, J = 8.2 Hz, 4H, H_{Py}), 8.14 (dd, J = 8.2, 5.9 Hz, 4H, H_{Py}), 7.73 (d, J = 16.2 Hz, 4H, CH=CH), 7.11 (d, J = 16.3 Hz, 8H, CH=CH), 7.11 (s, 4H, H_{Ar}), 4.42 (s, 12H, CH_3), 3.85 (q, J = 6.7 Hz, 4H, H_{PC}), 3.02 (h, J = 8.5 Hz, 4H, H_{PC}).

^{13}C NMR (100 MHz, DMSO- d_6 , ppm) δ = 143.7 (+, 4C, C_{Py}), 143.4 (+, 4C, C_{Py}), 141.9 (+, 4C, C_{Py}), 140.1 (C_{q} , 4C, C_{Py}), 137.7 (C_{q} , 4C, C_{Ar}), 137.1 (C_{q} , 4C, C_{Ar}), 131.7 (+, 4C, CH=CH), 129.9 (+, 4C, C_{Ar}), 127.9 (+, 4C, C_{Py}), 122.6 (+, 4C, CH=CH), 48.6 (+, 4C, CH_3), 33.0 (–, 4C, CH_2).

HRMS-ESI (m/z): $[\text{M}]^{4+}$, calc. for $\text{C}_{48}\text{H}_{48}\text{N}_4^+$, 170.0964/170.3473; found: 170.0964/170.3472 (34/8); $[\text{M}+\text{I}]^{3+}$, calc. for $\text{C}_{48}\text{H}_{48}\text{N}_4\text{I}^{3+}$, 269.0969/269.4314; found: 269.0967/269.4311 (65/7); $[\text{M}+2\text{I}]^{2+}$, calc. for $\text{C}_{48}\text{H}_{48}\text{N}_4\text{I}_2^{2+}$, 467.0979/467.5996; found: 467.0977/467.5992 (100/54).

IR (ATR, $\tilde{\nu}$) = 3463 (w), 3427 (m), 3414 (m), 3023 (w), 3014 (w), 1615 (s), 1579 (m), 1504 (s), 1466 (w), 1298 (m), 953 (vs), 799 (m), 721 (w), 667 (vs), 533 (m), 473 (s), 443 (m), 419 (s), 398 (s), 388 (m), 378 (m) cm^{-1} .

CB8 \supset pDMVCP

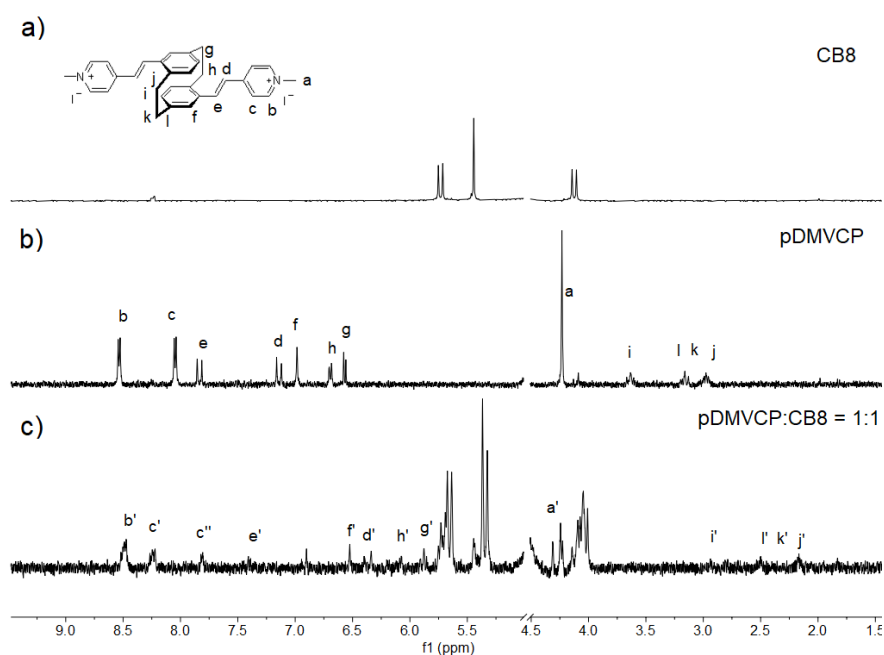


Figure 84. ^1H NMR spectra was recorded (400 MHz, D_2O , r.t.) for (a) CB8 (50 μM), (b) pDMVCP (200 μM), (c) a mixture of CB8 (100 μM) and pDMVCP (100 μM) 1:1. Primed (') resonances arise from the CB8 \supset pDMVCP complex.

HRMS-ESI (m/z): $[M]^{2+}$, calc. for $C_{80}H_{80}N_{34}O_{16}$, 886.3241/ 886.8257/ 887.3274 (100/87/37); found: 886.3187/ 886.8198 / 887.3210 (100/98/46).

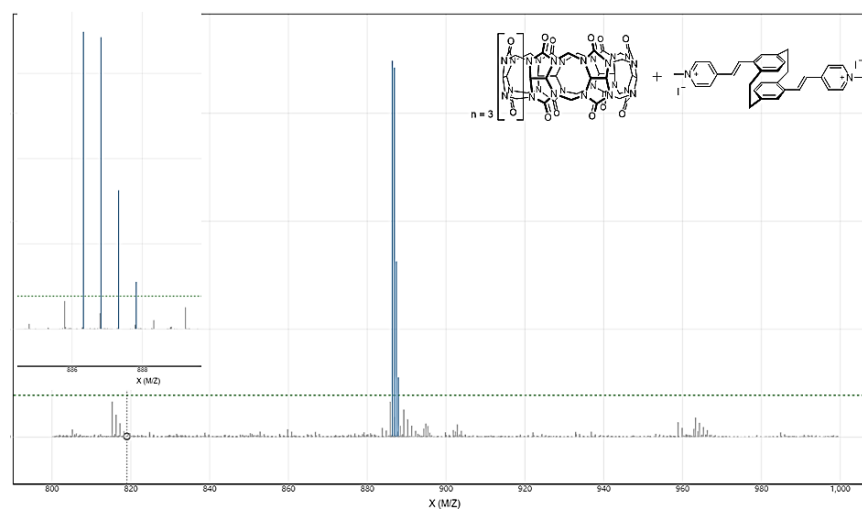


Figure 85. ESI mass spectra of **CB8-pDMVCP**.

CB8-TMPCP

HRMS-ESI (m/z): $[M]^{3+}$, calc. for $C_{82}H_{82}N_{35}O_{16}$, 604.2221/ 604.5565/ 604.8910/ 605.2254 (100/89/39/11); found: 604.2186/ 604.5523 / 604.8868/ 605.2207 (92/100/51/14). $[M+I]^{2+}$, calc. for $C_{82}H_{82}N_{35}IO_{16}$, 969.7856/ 970.2873, found 969.7796/ 970.2810 (20/22).

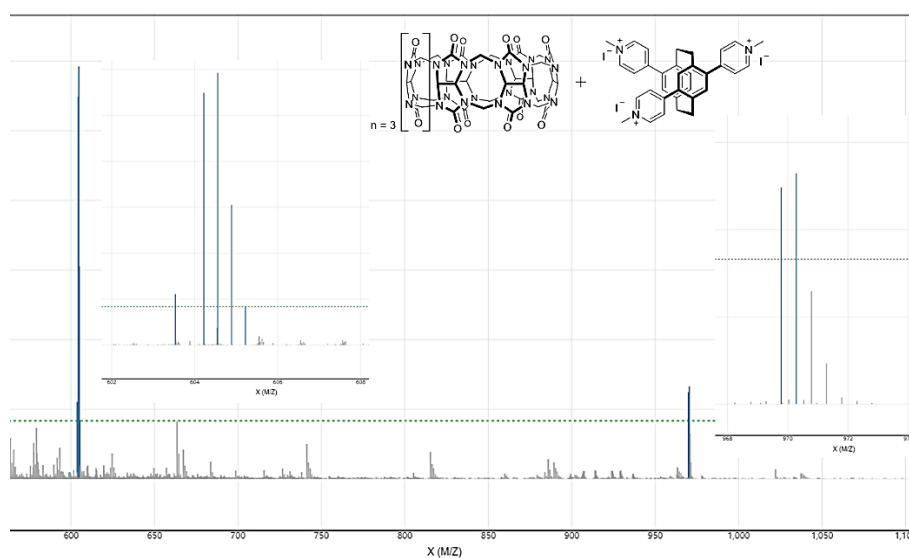


Figure 86. ESI mass spectra of **CB8-TMPCP**.

CB8 \supset QMPCP

HRMS-ESI (m/z): $[M]^{4+}$, calc. for $C_{88}H_{88}N_{36}O_{16}$, 476.1789/ 476.4298/ 476.6806 (100/95/45); found: 476.1757/ 476.4263 / 476.6770 (43/47/26).

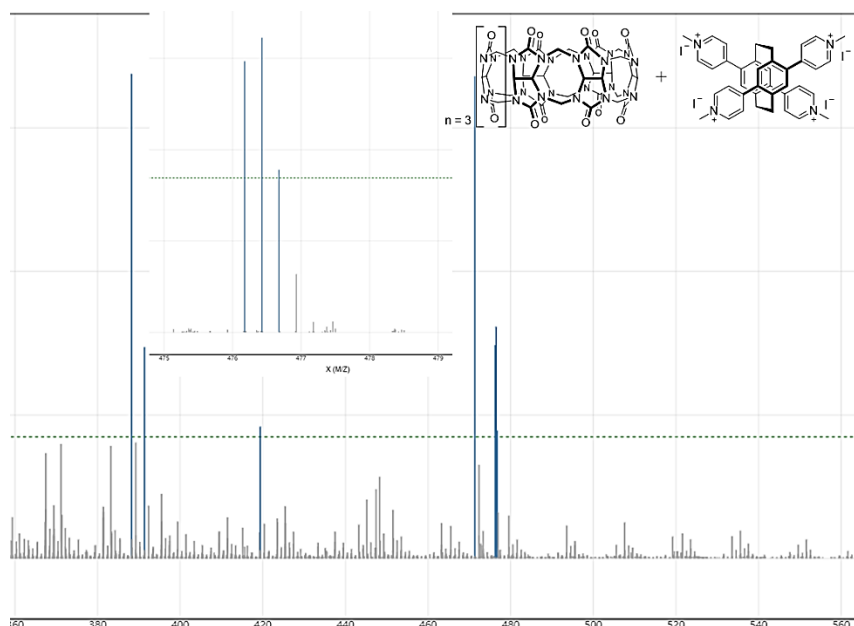


Figure 87. ESI mass spectra of CB8 \supset QMPCP.

CB8 \supset QMVCpm

HRMS-ESI (m/z): $[M]^{4+}$, calc. for $C_{96}H_{96}N_{36}O_{16}$, 502.4454/ 502.1946/ 502.6963 (100/96/51); found: 502.1915/ 502.4421 / 502.6928 (13/15/8).

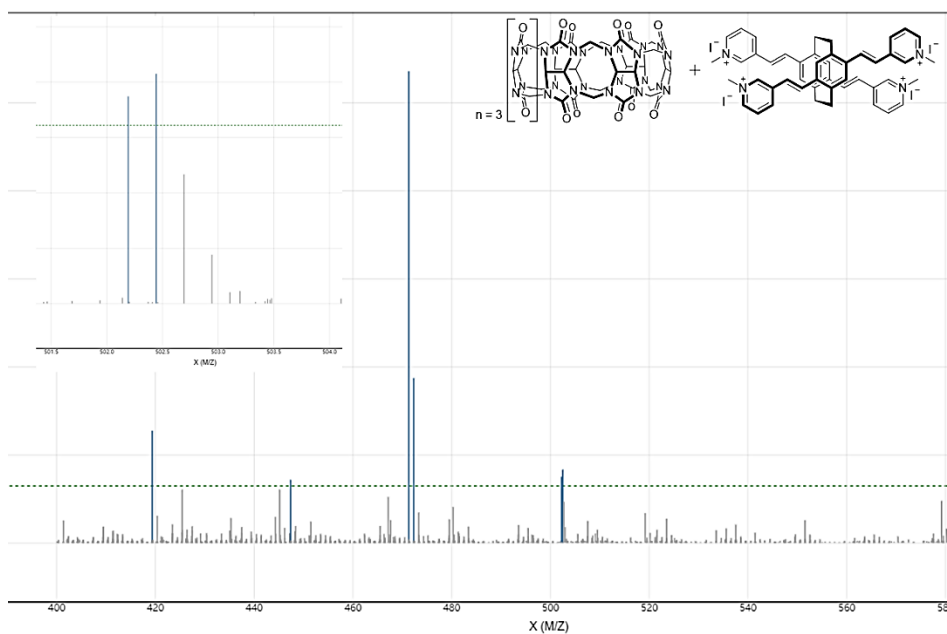


Figure 88. ESI mass spectra of CB8 \supset QMVCpm.

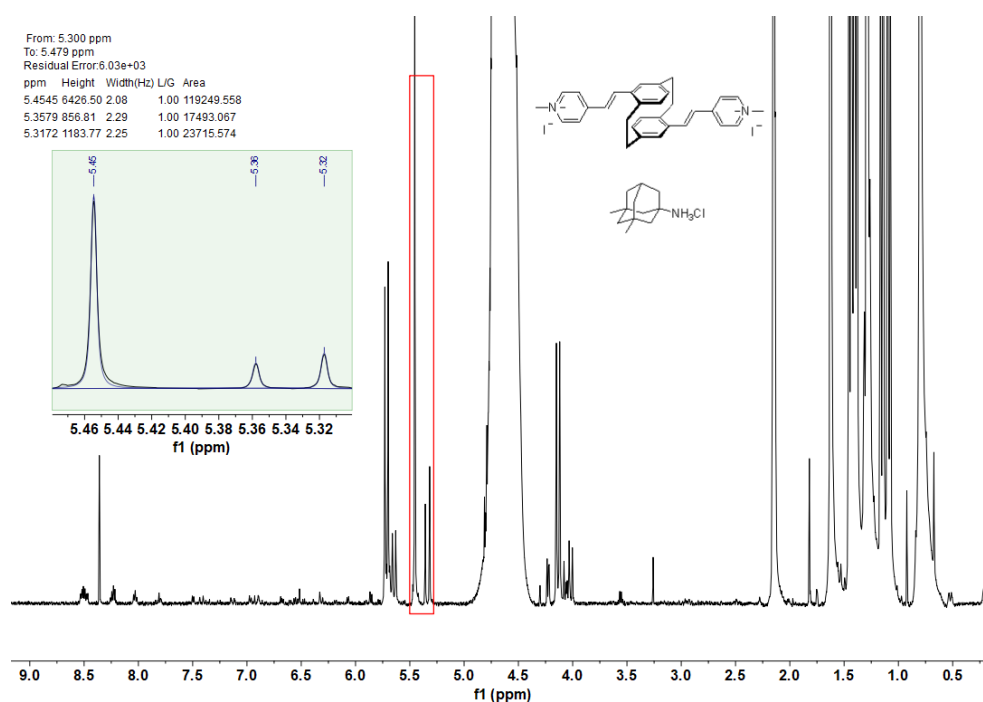


Figure 89. One of the ^1H NMR spectra (400 MHz, D_2O , r.t.) was used to determine K_{rel} for $\text{CB8} \rightleftharpoons \text{pDMPCP}$ and $\text{CB8} \rightleftharpoons \text{Mem}$. $[\text{CB8}]_{\text{Total}} = 60.0 \mu\text{M}$, $[\text{Mem}]_{\text{Total}} = 2.46 \text{ mM}$, $[\text{pDMPCP}]_{\text{Total}} = 810 \mu\text{M}$, $K_{\text{rel}} = 12.69$.

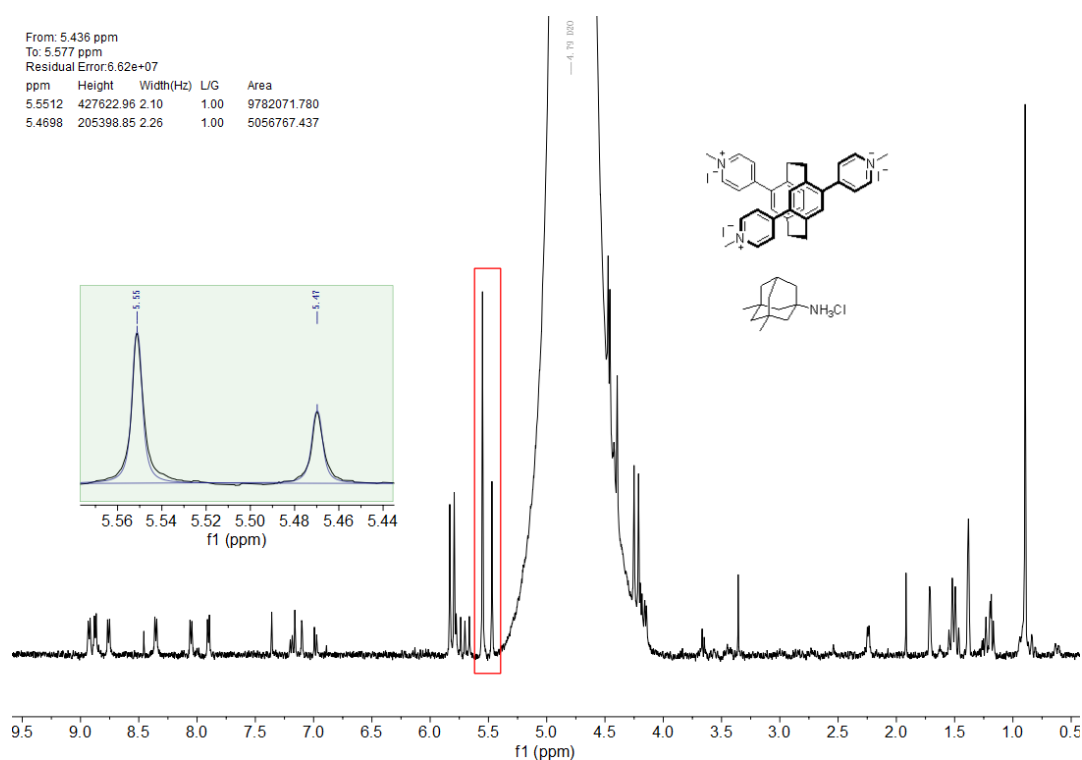


Figure 90. One of the ^1H NMR spectra (500 MHz, D_2O , r.t.) was used to determine K_{rel} for $\text{CB8} \rightleftharpoons \text{TMPCP}$ and $\text{CB8} \rightleftharpoons \text{Mem}$. $[\text{CB8}]_{\text{Total}} = 47.7 \mu\text{M}$, $[\text{Mem}]_{\text{Total}} = 179 \mu\text{M}$, $[\text{TMPCP}]_{\text{Total}} = 735 \mu\text{M}$, $K_{\text{rel}} = 2.74$.

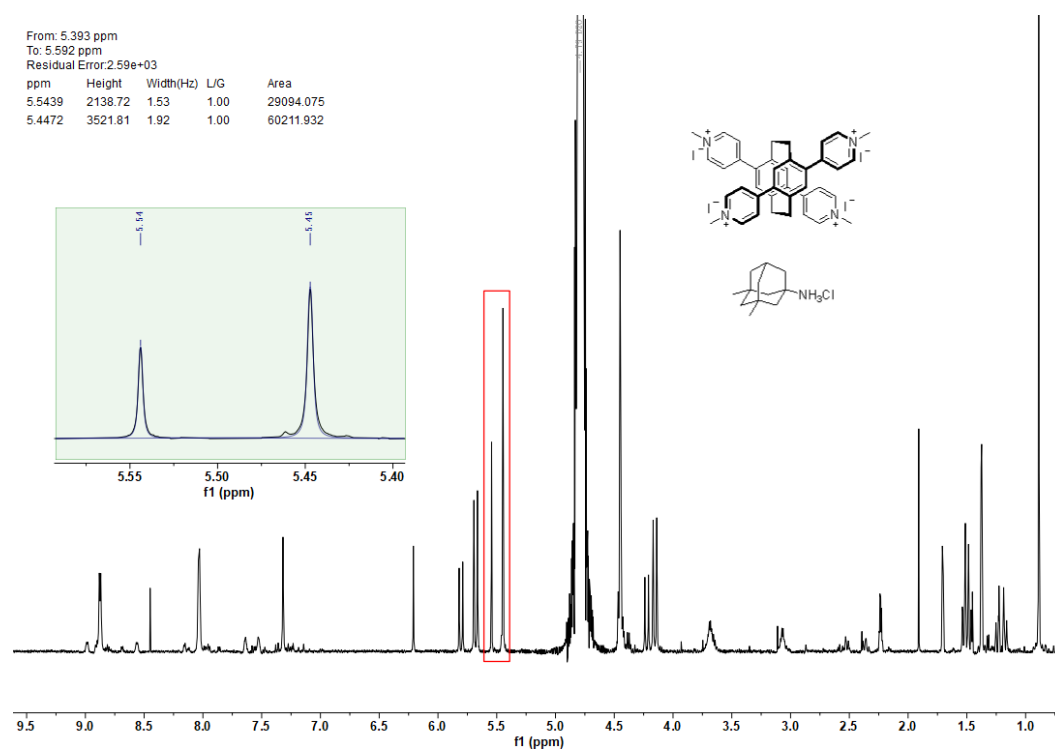


Figure 91. One of the ^1H NMR spectra (500 MHz, D_2O , r.t.) was used to determine K_{rel} for $\text{CB8} \rightleftharpoons \text{QMPCP}$ and $\text{CB8} \rightleftharpoons \text{Mem}$. $[\text{CB8}]_{\text{Total}} = 477 \mu\text{M}$, $[\text{Mem}]_{\text{Total}} = 179 \mu\text{M}$, $[\text{QMPCP}]_{\text{Total}} = 72.1 \mu\text{M}$, $K_{\text{rel}} = 8.50$.

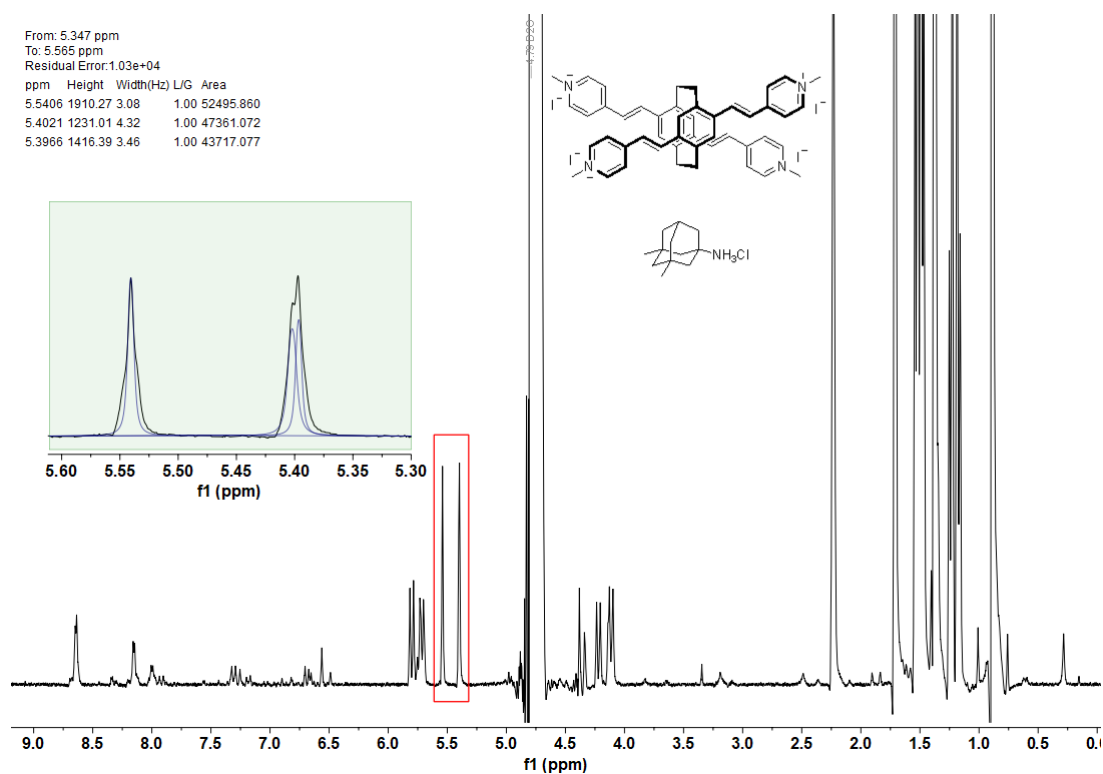


Figure 92. One of the ^1H NMR spectra (400 MHz, D_2O , r.t.) was used to determine K_{rel} for $\text{CB8} \rightleftharpoons \text{QMVCPP}$ and $\text{CB8} \rightleftharpoons \text{Mem}$. $[\text{CB8}]_{\text{Total}} = 60.0 \mu\text{M}$, $[\text{Mem}]_{\text{Total}} = 2.46 \text{ mM}$, $[\text{QMVCPP}]_{\text{Total}} = 80.8 \mu\text{M}$, $K_{\text{rel}} = 99.19$.

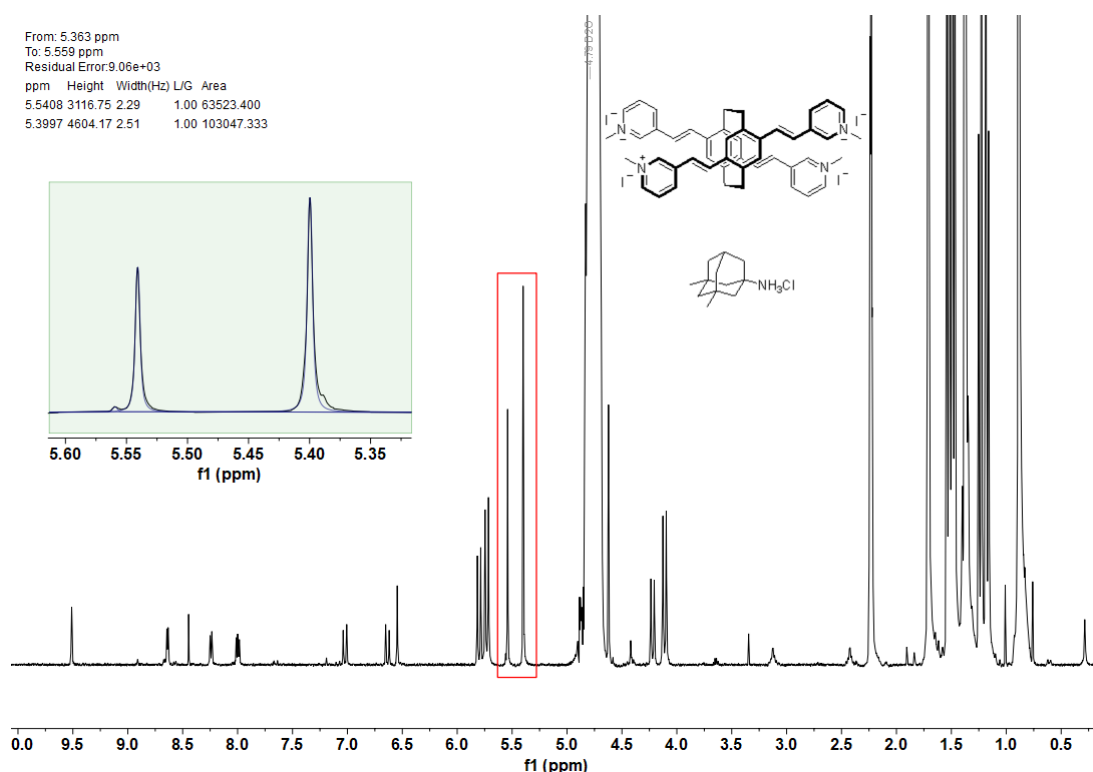
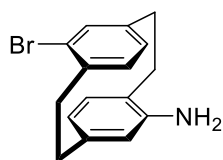


Figure 93. One of the ^1H NMR spectra (400 MHz, D_2O , r.t.) was used to determine K_{rel} for $\text{CB8} \supset \text{QMVCpM}$ and $\text{CB8} \supset \text{Mem}$. $[\text{CB8}]_{\text{Total}} = 60.0 \mu\text{M}$, $[\text{Mem}]_{\text{Total}} = 2.46 \text{ mM}$, $[\text{QMVCpM}]_{\text{Total}} = 82.5 \mu\text{M}$, $K_{\text{rel}} = 86.84$.

4-Bromo-16-amino[2.2]paracyclophane (96)



To a solution of 4,16-dibromo[2,2]paracyclophane (2.90 g, 7.92 mmol, 1.00 equiv.) in toluene (100 mL) was added benzophenone imine (1.51 g, 8.32 mmol, 1.05 equiv.), (1,1'-Bis(diphenylphosphino)ferrocene)palladium dichloride (323 mg, 396 μmol , 0.05 equiv.), DPPF (869 mg, 1.19 mmol, 0.15 equiv.), and sodium *t*-butoxide (2.28 g, 23.8 mmol, 3.00 equiv.). The mixture was stirred at 100 $^\circ\text{C}$ under argon for 16 hours. After the reaction mixture was cooled to room temperature, and diluted with CH_2Cl_2 (100 mL), acetic acid was added to the mixture until the stirred solution tested acidic (pH 6), washed with water ($3 \times 50 \text{ mL}$), and saturated aqueous NaCl solution ($3 \times 50 \text{ mL}$) and dried over magnesium sulfate. The solvent was removed under reduced pressure to give a residue. The intermediate product was directly used as crude for the following reaction.

A solution of crude product in THF (35.0 mL) was added to concentrated HCl (2.50 mL), and stirred at room temperature for 4 h. After the yellow mixture faded, the white precipitate formed was filtered, washed with ether ($3 \times 5.0 \text{ mL}$), and dried in vacuo. The remaining solid in ethanol (4.0 mL) was stirred, and saturated NaOH was added dropwise until the mixture tested basic (pH 9). The crude product was purified via flash column chromatography on silica gel using dichloromethane/methanol 20:1, obtaining the title compound (765 mg, 2.50 mmol, 32%) as a light brown solid.

$R_f = 0.3$ (cyclohexane/ dichloromethane 1:1)

^1H NMR (400 MHz, CDCl_3 , ppm) δ = 7.15 (dd, J = 7.7, 1.8 Hz, 1H, H_{Ar}), 6.66 (dd, J = 7.7, 1.8 Hz, 1H, H_{Ar}), 6.47 (d, J = 1.8 Hz, 1H, H_{Ar}), 6.36 (d, J = 7.7 Hz, 1H, H_{Ar}), 6.25 (d, J = 7.7 Hz, 1H, H_{Ar}), 5.42 (d, J = 2.0 Hz, 1H, H_{Ar}), 3.47 (ddd, J = 12.8, 10.4, 1.8 Hz, 1H, H_{PC}), 3.21–2.99 (m, 3H, H_{PC}), 2.98–2.74 (m, 3H, H_{PC}), 2.74–2.59 (m, 1H, H_{PC}).

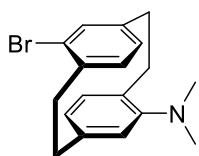
^{13}C NMR (100 MHz, CDCl_3 , ppm) δ = 144.7 (C_q , C_{Ar}), 140.9 (C_q , C_{Ar}), 140.4 (C_q , C_{Ar}), 138.4 (C_q , C_{Ar}), 137.4 (+, CH, C_{Ar}), 134.4 (+, CH, C_{Ar}), 133.5 (+, CH, C_{Ar}), 127.0 (+, CH, C_{Ar}), 126.2 (C_q , C_{Ar}), 124.1 (C_q , C_{Ar}), 121.9 (+, CH, C_{Ar}), 121.3 (+, CH, C_{Ar}), 35.3 (–, CH_2), 33.1 (–, CH_2), 32.4 (–, CH_2), 31.7 (–, CH_2).

MS (EI, 70 eV, 20 °C, %) m/z = 301/303 (17/17) $[\text{M}]^+$, 109 (100) $[\text{C}_8\text{H}_9\text{N}]^+$.

HRMS-EI (m/z): $[\text{M}]^+$, calc. for $\text{C}_{16}\text{H}_{75}^{79}\text{BrN}$, 301.0461; found: 301.1777.

IR (ATR, $\tilde{\nu}$) = 3437 (w), 3356 (w), 2951 (w), 2921 (m), 2891 (w), 2849 (m), 1611 (s), 1584 (m), 1562 (m), 1537 (w), 1497 (w), 1475 (w), 1449 (w), 1432 (m), 1422 (m), 1390 (m), 1276 (w), 1244 (w), 1204 (w), 1184 (w), 1030 (s), 929 (w), 895 (s), 885 (w), 870 (s), 853 (w), 823 (s), 796 (w), 769 (s), 720 (m), 705 (s), 660 (vs), 637 (m), 584 (m), 550 (m), 527 (s), 514 (s), 494 (vs), 469 (vs), 432 (s), 419 (m), 401 (s), 387 (s) cm^{-1} .

4-(*N,N*-Dimethylamino)-16-bromo[2.2]paracyclophane (97)



To 4-amino-16-bromo[2.2]paracyclophane (580 mg, 1.92 mmol, 1.00 equiv.) and of 37% aqueous formaldehyde (1.60 mL, 20.0 mmol) in 50 mL acetonitrile, cooled in an ice bath, was added sodium cyanoborohydride (362 mg, 5.76 mmol, 3.00 equiv.).

Glacial acetic acid (0.50 mL) was added over 10 min, the reaction mixture was warmed to room temperature and the reaction was stirred for 2 h. An additional 0.50 mL of glacial acetic acid was added, and stirring was continued for another 1 h. The reaction mixture was poured into 150 mL of diethyl ether and then washed with 1 M KOH solution (3×20 mL) and brine (20 mL). The ether solution was dried over magnesium sulfate and evaporating the solvent under reduced pressure. The crude material was of sufficient purity for the following steps and not further purified to obtain white solid (496 mg, 1.50 mmol, 78%).

R_f = 0.35 (cyclohexane/ethyl acetate 40:1)

^1H NMR (400 MHz, CDCl_3 , ppm) δ = 6.79 (dd, J = 7.7, 1.8 Hz, 1H, H_{Ar}), 6.73 (dd, J = 7.7, 1.8 Hz, 1H, H_{Ar}), 6.51 (d, J = 1.7 Hz, 1H, H_{Ar}), 6.36 (dd, J = 9.3, 7.7 Hz, 2H, H_{Ar}), 5.68 (d, J = 1.8 Hz, 1H, H_{Ar}), 3.52–3.40 (m, 2H, H_{PC}), 3.11 (ddt, J = 11.2, 9.4, 5.7 Hz, 2H, H_{PC}), 3.00–2.77 (m, 4H, H_{PC}), 2.72 (s, 6H, H_{PC}).

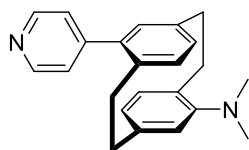
^{13}C NMR (100 MHz, CDCl_3 , ppm) δ = 151.9 (C_q , C_{Ar}), 141.9 (C_q , C_{Ar}), 140.0 (C_q , C_{Ar}), 138.2 (C_q , C_{Ar}), 137.0 (+, CH, C_{Ar}), 135.5 (+, CH, C_{Ar}), 133.3 (+, CH, C_{Ar}), 130.5 (C_q , C_{Ar}), 128.1 (+, CH, C_{Ar}), 126.3 (C_q , C_{Ar}), 123.3 (+, CH, C_{Ar}), 120.8 (+, CH, C_{Ar}), 43.7 (+, 2C, CH_3), 35.4 (–, CH_2), 34.6 (–, CH_2), 33.4 (–, CH_2), 33.1 (–, CH_2).

MS (EI, 70 eV, 20 °C, %) $m/z = 329/331$ (31/30) $[M]^+$, 104 (100) $[C_8H_9]^+$, 147 (100) $[M-C_8H_9Br]^+$.

HRMS-EI (m/z): $[M]^+$, calc. for $C_{18}H_{20}^{79}BrN$, 329.0779; found: 329.2198.

IR (ATR, $\tilde{\nu}$) = 2934 (m), 2919 (m), 1582 (s), 1492 (s), 1475 (s), 1449 (m), 1432 (m), 1411 (s), 1404 (s), 1391 (m), 1332 (m), 1305 (m), 1201 (m), 1184 (m), 1136 (s), 1122 (s), 1102 (s), 1092 (s), 1060 (s), 1030 (vs), 996 (s), 987 (s), 956 (m), 901 (vs), 854 (vs), 829 (s), 762 (m), 734 (m), 705 (vs), 667 (vs), 660 (vs), 616 (s), 557 (m), 540 (m), 533 (m), 523 (m), 493 (vs), 473 (vs), 438 (m), 431 (m), 401 (s), 390 (s) cm^{-1} .

4-Pyridyl-16-(*N,N*-dimethylamino)[2.2]paracyclophane (98)



A vessel was charged with 4-(*N,N*-dimethylamino)-16-bromo [2.2]paracyclophane (853 mg, 2.58 mmol, 1.00 equiv.), pyridine-4-boronic acid (495 mg, 3.10 mmol, 1.50 equiv.), palladium-tetrakis(triphenylphosphine) (215 mg, 190 μ mol, 0.07 equiv.), potassium phosphate (1.32 g, 6.20 mmol, 2.40 equiv.), dioxane (20 mL)

and water (8 mL) under argon. The mixture was heated under reflux for 16 h. Then the reaction mixture was then cooled to room temperature, extracted with ether (3 \times 50 mL). The extracts were dried by $MgSO_4$ and evaporated under reduced pressure. The crude solid was purified by flash column chromatography on silica gel using cyclohexane/ ethyl acetate 2:1 to yield the title compound (5.20 g, 20.5 mmol, 43%) as a yellow solid.

$R_f = 0.45$ (cyclohexane/ethyl acetate 1:1)

1H NMR (400 MHz, $CDCl_3$, ppm) $\delta = 8.64$ – 8.58 (m, 2H, H_{Py}), 7.38 – 7.32 (m, 2H, H_{Py}), 6.75 (dd, $J = 7.7$, 1.9 Hz, 1H, H_{Ar}), 6.51 (d, $J = 1.9$ Hz, 1H, H_{Ar}), 6.47 (d, $J = 7.7$ Hz, 1H, H_{Ar}), 6.39 (d, $J = 7.7$ Hz, 1H, H_{Ar}), 6.13 (dd, $J = 7.7$, 1.8 Hz, 1H, H_{Ar}), 5.71 (d, $J = 1.8$ Hz, 1H, H_{Ar}), 3.44 (ddd, $J = 12.8$, 9.3, 2.9 Hz, 1H, H_{PC}), 3.31 (ddd, $J = 13.6$, 10.1, 3.6 Hz, 1H, H_{PC}), 3.13 (ddd, $J = 13.0$, 9.4, 6.1 Hz, 1H, H_{PC}), 2.96–2.81 (m, 2H, H_{PC}), 2.81–2.67 (m, 2H, H_{PC}), 2.72 (s, 6H, H_{PC}), 2.52 (ddd, $J = 13.1$, 10.1, 4.8 Hz, 1H, H_{PC}).

^{13}C NMR (100 MHz, $CDCl_3$, ppm) $\delta = 151.9$ (C_q , C_{Py}), 149.6 (+, CH, 2C, C_{Py}), 149.2 (C_q , C_{Ar}), 140.6 (C_q , C_{Ar}), 140.5 (C_q , C_{Ar}), 139.2 (C_q , C_{Ar}), 136.5 (C_q , C_{Ar}), 135.1 (+, CH, C_{Ar}), 134.7 (+, CH, C_{Ar}), 132.0 (+, CH, C_{Ar}), 130.7 (C_q , C_{Ar}), 129.6 (+, CH, C_{Ar}), 124.7 (+, CH, 2C, C_{Py}), 123.4 (+, CH, C_{Ar}), 121.2 (+, CH, C_{Ar}), 43.8 (+, 2C, CH_3), 34.8 (–, CH_2), 34.6 (–, CH_2), 33.7 (–, CH_2), 33.5 (–, CH_2).

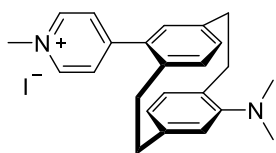
MS (ESI, 70 eV, 20 °C, %) $m/z = 329$ (100) $[M+H]^+$.

HRMS-ESI (m/z): $[M+H]^+$, calc. for $C_{23}H_{24}N_2$, 329.2013; found: 329.2009.

IR (ATR, $\tilde{\nu}$) = 2932 (s), 2927 (s), 2850 (m), 1592 (vs), 1560 (w), 1540 (m), 1490 (s), 1476 (m), 1452 (s), 1436 (m), 1409 (s), 1402 (vs), 1329 (m), 1302 (m), 1213 (w), 1193 (m), 1166 (w), 1156 (w), 1137 (m), 1116 (m), 1092 (m), 1067 (m), 1050 (m), 992 (vs), 956 (m), 908 (s), 891 (m), 863 (m), 827 (s), 790 (m), 761 (m), 732 (vs), 711 (s), 694 (m), 687 (m), 663 (s), 643 (m), 633 (s), 622 (s), 602 (m), 594 (m), 571 (s),

550 (m), 527 (m), 501 (s), 482 (s), 455 (m), 443 (m), 436 (m), 429 (m), 412 (m), 399 (m), 392 (m), 381 (m) cm^{-1} .

4-Pyridinium-16-(*N,N*-dimethylamino)-[2.2]paracyclophane iodide (pAMPCP, 94)



4-Pyridyl-16-(*N,N*-dimethylamino)[2.2]paracyclophane (144 mg, 440 μmol , 1.00 equiv.) dissolved in acetonitrile 6 mL, then methyl iodide (300 μL) was added. The mixture was stirred at 40 $^{\circ}\text{C}$ for 16 h, excluding of the light. The solvent was removed under reduced pressure to give a residue and then

recrystallized from methanol to obtain 16-(*N,N*-dimethylamino)-4-pyridinium[2.2]paracyclophane iodide (201 mg, 427 μmol , 97%) as an orange solid.

^1H NMR (400 MHz, DMSO- d_6 , ppm) δ = 9.02 (d, J = 6.4 Hz, 2H, H_{Py}), 8.30–8.21 (m, 2H, H_{Py}), 6.95–6.86 (m, 2H, H_{Ar}), 6.81 (d, J = 8.1 Hz, 1H, H_{Ar}), 6.68 (d, J = 7.6 Hz, 1H, H_{Ar}), 6.03 (dd, J = 7.6, 1.8 Hz, 1H, H_{Ar}), 5.80 (d, J = 1.8 Hz, 1H, H_{Ar}), 3.48–3.35 (m, 2H, H_{PC}), 4.41 (s, 3H, CH_3), 3.21–2.99 (m, 3H, H_{PC}), 2.99–2.78 (m, 2H, H_{PC}), 2.75 (s, 6H, CH_3), 2.51–2.40 (m, 1H, H_{PC}).

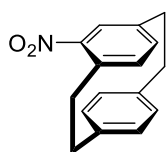
^{13}C NMR (100 MHz, DMSO- d_6 , ppm) δ = 155.4 (C_q , C_{Py}), 151.7 (C_q , C_{Ar}), 145.1 (+, CH, 2C, C_{Py}), 140.7 (C_q , C_{Ar}), 139.8 (C_q , C_{Ar}), 137.6 (C_q , C_{Ar}), 136.0 (+, CH, C_{Ar}), 135.3 (+, CH, C_{Ar}), 135.0 (+, CH, C_{Ar}), 132.4 (+, CH, C_{Ar}), 131.3 (+, CH, C_{Ar}), 130.1 (C_q , C_{Ar}), 127.4 (+, CH, 2C, C_{Py}), 122.7 (+, CH, C_{Ar}), 121.0 (+, CH, C_{Ar}), 47.2 (–, CH_3), 43.4 (–, 2C, CH_3), 34.2 (–, CH_2), 34.1 (–, CH_2), 33.0 (–, CH_2), 33.0 (–, CH_2).

MS (ESI, 70 eV, 20 $^{\circ}\text{C}$, %) m/z = 343/344 (100/26) $[\text{M}]^+$.

HRMS-ESI (m/z): $[\text{M}]^+$, calc. for $\text{C}_{24}\text{H}_{27}\text{N}_2$, 343.2169; found: 343.2165.

IR (ATR, $\tilde{\nu}$) = 3458 (w), 3446 (w), 3437 (w), 3425 (w), 3418 (w), 3408 (w), 3400 (w), 3388 (w), 2925 (w), 2895 (w), 2851 (w), 1639 (vs), 1585 (m), 1561 (w), 1516 (w), 1492 (m), 1458 (m), 1436 (w), 1408 (m), 1330 (w), 1289 (w), 1215 (m), 1194 (s), 1162 (m), 1137 (s), 1116 (s), 1092 (s), 1052 (s), 1043 (s), 993 (s), 958 (m), 904 (m), 890 (w), 854 (s), 843 (s), 809 (m), 765 (w), 741 (w), 724 (m), 683 (w), 669 (s), 626 (m), 601 (w), 586 (m), 552 (m), 541 (m), 516 (m), 486 (vs), 460 (vs), 439 (vs), 419 (vs), 408 (vs), 395 (vs), 382 (vs) cm^{-1} .

(*rac*)-4-Nitro[2.2]paracyclophane (99)



[2.2]Paracyclophane (4.00 g, 19.2 mmol, 1.00 equiv.) was dissolved in dichloromethane (380 mL) and cooled to 0 $^{\circ}\text{C}$. A mixture of sulfuric acid (95% aq. solution, 4.31 mL, 76.8 mmol, 4.00 equiv.) and nitric acid (70% aq. solution, 2.29 mL, 38.4 mmol, 2.00 equiv.) was slowly added. The mixture was warmed to room temperature. After 16 h, the reaction

mixture was decanted onto the ice, leaving any dark orange tar in the reaction vessel. The biphasic mixture was stirred for 15 min, and the layers were separated. The aqueous phase was extracted with

dichloromethane (3×100 mL). The combined organic layers were dried over sodium sulfate, and the solvent was removed under reduced pressure. The crude solid was purified by flash column chromatography on silica gel using dichloromethane /cyclohexane 1:1 to yield the title compound (5.20 g, 20.5 mmol, 43%) as a yellow solid.

$R_f = 0.45$ (cyclohexane/ethyl acetate 5:1)

$^1\text{H NMR}$ (400 MHz, CDCl_3 , ppm) $\delta = 7.22$ (d, $J = 1.9$ Hz, 1H, H_{Ar}), 6.79 (dd, $J = 7.8, 1.9$ Hz, 1H, H_{Ar}), 6.64–6.60 (m, 2H, H_{Ar}), 6.58–6.53 (m, 2H, H_{Ar}), 6.48 (dd, $J = 7.9, 1.8$ Hz, 1H, H_{Ar}), 4.03 (ddd, $J = 13.3, 9.3, 2.2$ Hz, 1H, H_{PC}), 3.24–3.13 (m, 4H, H_{PC}), 3.12–3.03 (m, 2H, H_{PC}), 2.90 (ddd, $J = 13.3, 9.9, 7.2$ Hz, 1H, H_{PC}).

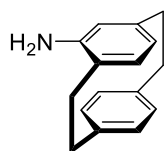
$^{13}\text{C NMR}$ (100 MHz, CDCl_3 , ppm) $\delta = 149.3$ (C_q, C_{Ar}), 142.1 (C_q, C_{Ar}), 139.8 (C_q, C_{Ar}), 139.3 (C_q, C_{Ar}), 137.8 (+, CH, C_{Ar}), 137.4 (+, CH, C_{Ar}), 136.5 (C_q, C_{Ar}), 133.2 (+, CH, C_{Ar}), 133.1 (+, CH, C_{Ar}), 132.4 (+, CH, C_{Ar}), 130.0 (+, CH, C_{Ar}), 129.6 (+, CH, C_{Ar}), 36.0 (–, CH_2), 35.0 (–, CH_2), 34.8 (–, CH_2), 34.5 (–, CH_2).

MS (EI, 70 eV, 20 °C, %) $m/z = 253$ (23) $[\text{M}]^+$, 104 (100) $[\text{C}_8\text{H}_9]^+$.

HRMS-EI (m/z): $[\text{M}]^+$, calc. for $\text{C}_{16}\text{H}_{15}\text{NO}_2$, 253.1103; found: 253.1128.

IR (ATR, $\tilde{\nu}$) = 2922 (w), 2853 (w), 1513 (vs), 1482 (s), 1451 (m), 1436 (m), 1411 (w), 1401 (w), 1333 (vs), 1300 (s), 1244 (w), 1201 (m), 1180 (m), 1132 (w), 1113 (w), 1095 (m), 1072 (w), 945 (w), 931 (w), 904 (s), 884 (w), 870 (vs), 843 (w), 805 (vs), 789 (s), 756 (m), 722 (m), 703 (s), 694 (s), 673 (s), 633 (vs), 582 (m), 562 (w), 540 (w), 507 (vs), 465 (w), 439 (w), 429 (w), 411 (w), 401 (w), 387 (w), 378 (m) cm^{-1} .

(*rac*)-4-Amino[2.2]paracyclophane (100)



A solution of EtOH (40 mL) and H_2O (40 mL) was suspended (*rac*)-4-nitro[2.2]paracyclophane (1.05 g, 4.15 mmol, 1.00 equiv.), and the mixture was stirred for 30 min. Iron powder (1.16 g, 20.7 mmol, 5.00 equiv.) was added, and the mixture was heated to reflux at 82 °C. Concentrated HCl (5 mL) was added carefully over 10 min, and the mixture was stirred at this temperature until no starting material was detected by TLC (2 h). The reaction mixture was allowed to cool to room temperature and poured onto ice/sat. aq. NaHCO_3 (60 mL). The mixture was extracted with ethyl acetate (3×35 mL) (filtration of the mixture did not improve the workup procedure). The combined organic phases were dried (Na_2SO_4) and filtered, and the solvent was removed under reduced pressure. The crude solid was purified by flash column chromatography on silica gel using cyclohexane/ethyl acetate 10:1 to yield the title compound (865 mg, 3.87 mmol, 93%) as a yellow solid.

$R_f = 0.45$ (cyclohexane/ethyl acetate 4:1)

$^1\text{H NMR}$ (400 MHz, CDCl_3 , ppm) $\delta = 7.20$ (dd, $J = 7.8, 2.0$ Hz, 1H, H_{Ar}), 6.61 (dd, $J = 7.8, 2.0$ Hz, 1H, H_{Ar}), 6.41 (dd, $J = 7.8, 1.9$ Hz, 2H, H_{Ar}), 6.29 (d, $J = 7.6$ Hz, 1H, H_{Ar}), 6.15 (dd, $J = 7.6, 1.8$ Hz, 1H, H_{Ar}),

5.40 (d, $J = 1.8$ Hz, 1H, H_{Ar}), 3.53–3.39 (m, 2H, NH_2), 3.20–2.92 (m, 6H, H_{PC}), 2.85 (ddd, $J = 12.5, 8.9, 6.3$ Hz, 1H, H_{PC}), 2.73–2.63 (m, 1H, H_{PC})

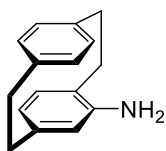
^{13}C NMR (100 MHz, $CDCl_3$, ppm) $\delta = 145.1$ (C_q, C_{Ar}), 141.2 (C_q, C_{Ar}), 139.1 (C_q, C_{Ar}), 139.1 (C_q, C_{Ar}), 135.4 (+, CH, C_{Ar}), 133.6 (+, CH, C_{Ar}), 132.6 (+, CH, C_{Ar}), 131.6 (+, CH, C_{Ar}), 126.9 (+, CH, C_{Ar}), 124.6 (C_q, C_{Ar}), 122.9 (+, CH, C_{Ar}), 122.4 (+, CH, C_{Ar}), 35.5 (–, CH_2), 35.1 (–, CH_2), 33.1 (–, CH_2), 32.4 (–, CH_2).

MS (EI, 70 eV, 20 °C, %) $m/z = 223/224$ (73/11) $[M]^+$, 119 (100) $[M-C_8H_9]^+$.

HRMS-EI (m/z): $[M]^+$, calc. for $C_{16}H_{17}N$, 223.1356; found: 223.2207

IR (ATR, $\tilde{\nu}$) = 2921 (s), 2891 (m), 2850 (m), 1612 (vs), 1592 (s), 1567 (m), 1497 (s), 1438 (m), 1424 (vs), 1285 (s), 892 (m), 864 (s), 795 (vs), 761 (m), 747 (m), 715 (vs), 688 (m), 659 (vs), 585 (vs), 557 (s), 541 (s), 530 (s), 510 (vs), 490 (vs), 456 (vs), 435 (vs), 418 (s), 407 (s), 397 (s), 388 (vs), 377 (vs) cm^{-1} .

(*S_P*)-4-Amino[2.2]paracyclophane (100)



In a vial, a suspension of sodium azide (3.30 g, 50.8 mmol, 3.00 equiv.) in 100 mL acetonitrile was added dropwise over 10 min iodo monochloride (5.50 g 33.9 mmol, 2.00 equiv.) at 0 °C. Then (*S_P*)-4-formyl[2.2]paracyclophane (4.00 g, 16.9 mmol, 1.00 equiv.) was added and the orange suspension was refluxed for 3 h, cooled down to

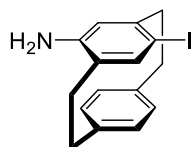
room temperature and 5 mL of an aqueous thiosulfate solution were added. The reaction mixture was extracted with dichloromethane (3×30 mL) and the combined organic phases were washed again with aqueous thiosulfate solution (three times) followed by brine and drying over Na_2SO_4 .

The solvents were removed under reduced pressure and the residue was dissolved in 25 mL 1,4-dioxane and 25 mL aqueous 2 N NaOH solution and stirred for 16 h at room temperature. Then 15 mL 6N hydrochloric acid was added, and the reaction mixture was stirred for another 30 min. Afterwards, 2 N aqueous NaOH solution was added until basic pH, and the reaction mixture was extracted with dichloromethane (3×10 mL). The combined organic phases were washed with brine, dried over Na_2SO_4 and the solvents were evaporated under reduced pressure. The crude solid was purified by flash column chromatography on silica gel using cyclohexane/ethyl acetate 7:1 to yield the title compound (1.98 g, 8.87 mmol, 52%) as a yellow solid.

The analytical data was identical to the racemate.

Because the reaction process is a radical azidation, the *ee* value did not change, following the (*S_P*)-4-formyl[2.2]paracyclophane (**57**).

(*rac*)-4-Iodo-7-amino[2.2]paracyclophane (101)



In a round bottom flask (*rac*)-4-amino[2.2]paracyclophane (476 mg, 2.13 mmol, 1.00 equiv.) was dissolved in tetrahydrofuran (10 mL), and water (10 mL) was added. Afterwards, NaIO₃ (422 mg, 2.13 mmol, 1.00 equiv.) and Na₂SO₃ (537 mg, 4.30 mmol, 2.00 equiv.) were added. Every 30 min, 1 M HCl (100 μL) was given to the reaction mixture, which was stirred for 4h at 60 °C. Then saturated aqueous Na₂S₂O₃ (20 mL) was added, the phases were separated, and the aqueous layer was extracted with diethyl ether (3 × 15 mL). The combined organic phases were dried with Na₂SO₄ and the solvent was removed under reduced pressure. The crude solid was purified by flash column chromatography on silica gel using dichloromethane to yield the title compound (391 mg, 1.12 mmol, 53% yield) as a light yellow solid.

R_f = 0.3 (dichloromethane)

¹H NMR (400 MHz, CDCl₃, ppm) δ = 7.24–7.14 (m, 2H, H_{Ar}), 6.57 (s, 1H, H_{Ar}), 6.42 (ddd, *J* = 13.8, 7.9, 2.0 Hz, 2H, H_{Ar}), 5.43 (s, 1H, H_{Ar}), 3.27 (d, *J* = 1.0 Hz, 2H, NH₂), 3.25–3.16 (m, 2H, H_{PC}), 3.16–2.95 (m, 4H, H_{PC}), 2.75–2.64 (m, 1H, H_{PC}), 2.56 (ddd, *J* = 13.3, 9.8, 7.0 Hz, 1H, H_{PC}).

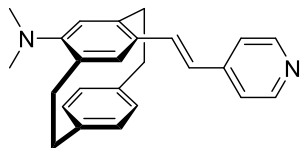
¹³C NMR (101 MHz, CDCl₃, ppm) δ = 145.29 (C_q, C_{Ar}), 144.27 (C_q, C_{Ar}), 143.60 (C_q, C_{Ar}), 138.69 (C_q, C_{Ar}), 138.6 (C_q, C_{Ar}), 132.9 (+, CH, C_{Ar}), 131.6 (+, CH, C_{Ar}), 123.0 (+, CH, C_{Ar}), 127.8 (+, CH, C_{Ar}), 126.5 (C_q, C_{Ar}), 123.1 (+, CH, C_{Ar}), 89.3 (C_q, C_{Ar}), 39.0 (–, CH₂), 33.2 (–, CH₂), 32.7 (–, CH₂), 32.0 (–, CH₂).

MS (ESI, 70 eV, 20 °C, %) *m/z* = 350/351 (100/17) [M+H]⁺.

HRMS-ESI (*m/z*): [M+H]⁺, calc. for C₁₆H₁₆IN, 350.0434; found: 350.0397.

IR (ATR, $\tilde{\nu}$) = 3461 (m), 3367 (vs), 2949 (w), 2922 (m), 2907 (m), 2885 (m), 2860 (w), 2839 (m), 1612 (s), 1594 (w), 1548 (m), 1476 (vs), 1432 (m), 1390 (vs), 1299 (m), 1264 (m), 1252 (m), 1244 (m), 1180 (w), 1163 (w), 1146 (w), 898 (vs), 870 (vs), 827 (w), 799 (vs), 713 (vs), 690 (m), 679 (s), 591 (vs), 557 (m), 533 (vs), 520 (vs), 462 (vs), 436 (s), 428 (s), 416 (vs), 392 (vs), 380 (vs) cm⁻¹.

(*rac*)-4-(4'-Pyridyl-(*E*)-vinyl)-7-(*N,N*-dimethylamino)[2.2]paracyclophane (102)



To a solution of acetonitrile (15 mL) was suspended added 4-iodo-7-amino[2.2]paracyclophane (200 mg, 570 μmol, 1.00 equiv.), potassium hydroxide (97.0 mg, 1.71 mmol, 3.00 equiv.) and the mixture was stirred at 80 °C for 16 h. The reaction mixture was diluted with 10 mL of water and extracted with DCM (3 × 15 mL), and the combined organic layer was dried over anhydrous Na₂SO₄, filtered and concentrated in vacuo. The crude product is allowed to be used directly next step.

A vessel was charged with the crude product (200 mg, 530 μmol, 1.00 equiv.), 4-vinylpyridine (140 mg, 1.33 mmol, 2.50 equiv.), palladium acetate (6.00 mg, 27.0 μmol, 0.05 equiv.), potassium carbonate (141 mg, 530 μmol, 1.00 equiv.), tetrapropylammonium bromide (184 mg, 1.33 mmol, 2.50 equiv.), and DMA (10 mL) under argon. The reaction mixture was heated at 100 °C for 2 days. Then the reaction was cooled

to room temperature, diluted with CH_2Cl_2 , and washed with brine. The organic layer was dried with Na_2SO_4 and concentrated. The organic layer was dried with MgSO_4 and concentrated. The crude product was purified via flash column chromatography on silica gel using cyclohexane/ethyl acetate 5:1, obtaining the title compound (62.0 mg, 170 μmol , 31%) as an orange solid.

$R_f = 0.25$ (cyclohexane/ethyl acetate 3:1)

^1H NMR (400 MHz, CDCl_3 , ppm) $\delta = 8.56$ (d, $J = 5.2$ Hz, 2H, H_{Py}), 7.44–7.34 (m, 3H, $\text{CH}=\text{CH}$, H_{Py}), 6.78–6.71 (m, 1H, H_{Ar}), 6.67 (s, 1H, H_{Ar}), 6.65 (d, $J = 15.9$ Hz, 1H, $\text{CH}=\text{CH}$), 6.60 (dd, $J = 7.9, 2.0$ Hz, 1H), 6.49 (dd, $J = 7.8, 1.9$ Hz, 1H), 6.44 (dd, $J = 7.8, 1.9$ Hz, 1H), 5.62 (s, 1H, H_{Ar}), 3.52 (ddd, $J = 13.5, 9.9, 1.6$ Hz, 1H, H_{PC}), 3.41 (ddd, $J = 13.7, 8.0, 2.4$ Hz, 1H, H_{PC}), 3.23–2.90 (m, 5H, H_{PC}), 2.81 (s, 6H, CH_3), 2.78–2.65 (m, 1H, H_{PC}).

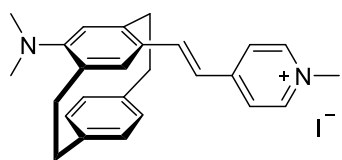
^{13}C NMR (100 MHz, CDCl_3 , ppm) $\delta = 152.2$ (C_q , C_{Py}), 150.1 (+, CH, 2C, C_{Py}), 145.8 (C_q , C_{Ar}), 140.4 (C_q , C_{Ar}), 139.7 (C_q , C_{Ar}), 138.3 (C_q , C_{Ar}), 134.5 (+, CH, C_{Ar}), 131.9 (+, CH, C_{Ar}), 131.0 (+, CH, C_{Ar}), 130.9 (+, CH, $\text{CH}=\text{CH}$), 130.8 (+, CH, C_{Ar}), 130.4 (C_q , C_{Ar}), 129.4 (+, CH, C_{Ar}), 129.1 (C_q , C_{Ar}), 122.8 (+, CH, $\text{CH}=\text{CH}$), 122.4 (+, CH, C_{Ar}), 120.5 (+, CH, 2C, C_{Py}), 43.0 (+, 2C, CH_3), 36.2 (–, CH_2), 35.0 (–, CH_2), 33.6 (–, CH_2), 33.5 (–, CH_2).

MS (ESI, 70 eV, 20 °C, %) $m/z = 354/355$ (100/29) $[\text{M}]^+$, 249/250 (59/48) $[\text{M}-\text{C}_8\text{H}_9]^+$.

HRMS-ESI (m/z): $[\text{M}]^+$, calc. for $\text{C}_{25}\text{H}_{26}\text{N}_2$, 354.2096; found: 354.3640.

IR (ATR, $\tilde{\nu}$) = 3469 (m), 3021 (m), 2997 (m), 2919 (s), 2905 (s), 2887 (s), 2876 (s), 2847 (s), 2789 (s), 1639 (s), 1565 (vs), 1509 (vs), 1500 (vs), 1469 (vs), 1449 (vs), 1432 (vs), 1421 (s), 1402 (s), 1356 (s), 1333 (s), 1313 (vs), 1298 (vs), 1264 (s), 1225 (s), 1218 (s), 1184 (vs), 1154 (vs), 1129 (vs), 1119 (vs), 1062 (vs), 1048 (vs), 992 (s), 972 (vs), 945 (s), 928 (s), 912 (s), 902 (s), 890 (vs), 866 (s), 826 (s), 807 (vs), 788 (vs), 764 (m), 720 (vs), 688 (m), 596 (s), 568 (s), 514 (vs), 500 (vs), 487 (vs), 435 (s), 424 (m) cm^{-1} .

(rac)-4-(N-Methyl-4'-pyridinium-(E)-vinyl)-7-(N,N-dimethylamino)[2.2]paracyclophane iodide (AMVCP, 95)



4-(4'-Pyridyl-(E)-vinyl)-7-(N,N-dimethylamino)[2.2]paracyclophane

(100 mg, 282 μmol , 1.00 equiv.) dissolved in acetonitrile 6 mL, then methyl iodide (200 μL) was added. The mixture was stirred at 40 °C for 16 h excluded of the light. The solvent was removed under reduced pressure to

give a residue and then recrystallized from methanol to obtain the title compound (128 mg, 257 μmol , 91%) as an orange solid.

^1H NMR (400 MHz, CDCl_3 , ppm) $\delta = 8.81$ (d, $J = 6.5$ Hz, 2H, H_{Py}), 7.89 (d, $J = 6.5$ Hz, 2H, H_{Py}), 7.74 (d, $J = 15.6$ Hz, 1H, $\text{CH}=\text{CH}$), 6.83 (s, 1H, H_{Ar}), 6.76–6.67 (m, 2H, $\text{CH}=\text{CH}$, H_{Ar}), 6.53 (d, $J = 7.8$ Hz, 1H, H_{Ar}), 6.45 (s, 2H, H_{Ar}), 5.57 (s, 1H, H_{Ar}), 4.44 (s, 3H, CH_3), 3.64–3.54 (m, 1H, H_{PC}), 3.37 (dd, $J = 13.9, 8.1$

Hz, 1H, H_{PC}), 3.27–3.12 (m, 2H, H_{PC}), 3.03–2.87 (m, 2H, H_{PC}), 2.91 (s, 6H, CH₃), 2.78 (ddd, $J = 14.0, 10.0, 6.6$ Hz, 2H, H_{PC}).

¹³C NMR (100 MHz, CDCl₃, ppm) $\delta = 154.4$ (C_q, C_{Py}), 154.3 (C_q, C_{Ar}), 144.3 (C_q, C_{Ar}), 143.9 (+, 2C, C_{Py}), 139.8 (+, CH, C_{Ar}), 139.4 (C_q, C_{Ar}), 138.1 (+, CH, C_{Ar}), 136.1 (+, CH, C_{Ar}), 131.7 (+, CH, C_{Ar}), 131.6 (C_q, C_{Ar}), 130.6 (+, CH, C_{Ar}), 129.4 (+, CH, C_{Ar}), 129.0 (C_q, C_{Ar}), 126.6 (C_q, C_{Ar}), 122.7 (+, 2C, C_{Py}), 122.0 (+, CH, C_{Ar}), 117.1 (+, CH, C_{Ar}), 47.7 (+, CH₃), 42.5 (+, 2C, CH₃), 37.2 (–, CH₂), 35.5 (–, CH₂), 33.6 (–, CH₂), 33.5 (–, CH₂).

MS (ESI, 70 eV, 20 °C, %) $m/z = 369/370$ (100/27) [M]⁺.

HRMS-ESI (m/z): [M]⁺, calc. for C₂₆H₂₉N₂, 369.2326; found: 369.2323.

IR (ATR, $\tilde{\nu}$) = 3432 (m), 3411 (m), 3403 (m), 2914 (m), 2844 (m), 1560 (vs), 1545 (vs), 1509 (vs), 1500 (vs), 1475 (vs), 1468 (vs), 1459 (vs), 1432 (vs), 1405 (s), 1357 (s), 1330 (s), 1296 (vs), 1265 (s), 1179 (vs), 1153 (vs), 1130 (vs), 1120 (vs), 1064 (vs), 1043 (vs), 993 (s), 955 (vs), 939 (vs), 905 (s), 887 (vs), 866 (vs), 809 (vs), 795 (vs), 720 (s), 711 (s), 687 (s), 667 (s), 637 (m), 630 (m), 598 (s), 569 (s), 554 (s), 540 (s), 513 (vs), 500 (vs), 486 (vs), 462 (vs), 453 (vs), 441 (vs), 432 (vs), 419 (vs), 402 (vs), 384 (vs) cm⁻¹.

CB8 \supset pAMPCP

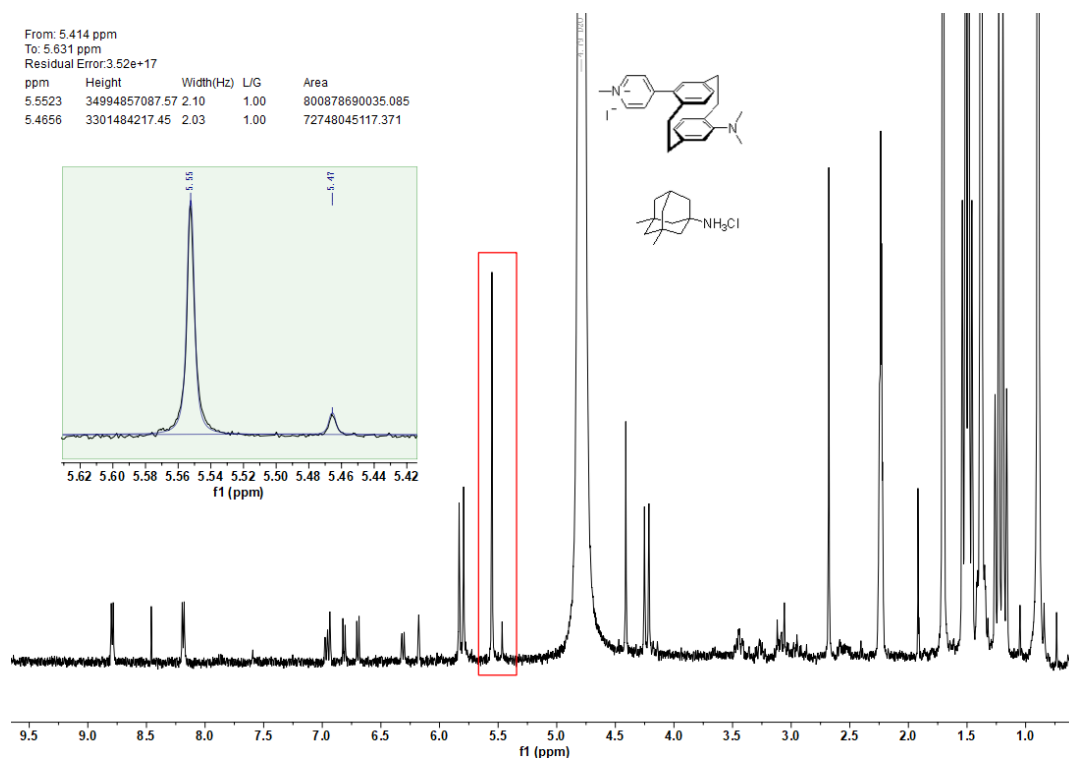


Figure 94. One of the ¹H NMR spectra (400 MHz, D₂O, r.t.) was used to determine K_{rel} for CB8 \supset pAMPCP and CB8 \supset Mem. [CB8]_{Total} = 52.5 μ M, [Mem]_{Total} = 1.49 mM, [pAMPCP]_{Total} = 85.0 μ M, $K_{rel} = 1.64$.

CB8⇌AMVCP

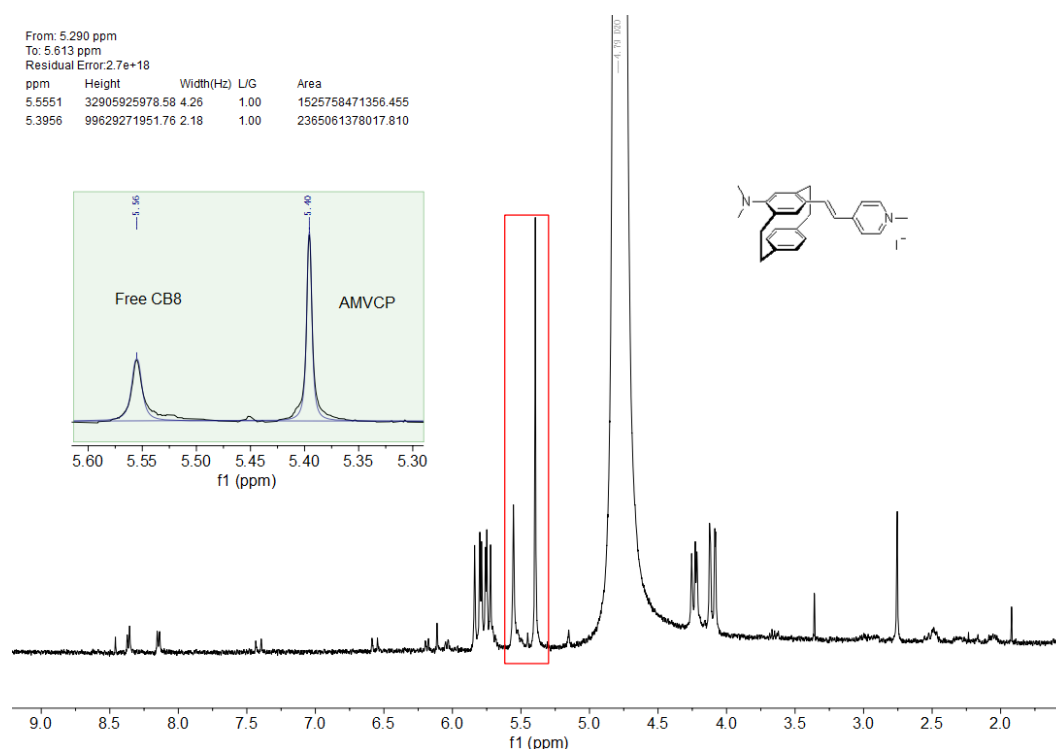
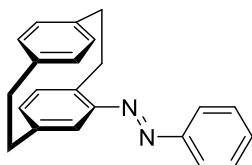


Figure 95. One of the ^1H NMR spectra (400 MHz, D_2O , r.t.) was used to determine K_a for $\text{CB8} \rightleftharpoons \text{AMVCP}$.
 $[\text{CB8}]_{\text{Total}} = 129 \mu\text{M}$, $[\text{AMVCP}]_{\text{Total}} = 142 \mu\text{M}$.

4-(*E*)-Azophenyl[2.2]paracyclophane (**105**)

To a solution of 4-amino[2,2]paracyclophane (223 mg, 1.00 mmol, 1.00 equiv.) in acetic acid (10 mL), nitrosobenzene (214 mg, 2.00 mmol, 2.00 equiv.) was added and the reaction mixture was stirred for 48 hours at 21 °C. The reaction mixture was extracted with dichloromethane, washed with water and brine, dried by MgSO_4 ,

filtered, and concentrated under reduced pressure. The crude product was purified via flash column chromatography on silica gel using cyclohexane/ethyl acetate 20:1, obtaining the title compound (98.0 mg, 314 μmol , 31%) as a yellow solid.

$R_f = 0.4$ (cyclohexane/ethyl acetate 20:1)

^1H NMR (400 MHz, CDCl_3 , ppm) $\delta = 7.93\text{--}7.85$ (m, 2H, H_{Ar}), 7.49 (dd, $J = 8.3, 6.7$ Hz, 2H, H_{Ar}), 7.46–7.38 (m, 1H, H_{Ar}), 6.64–6.47 (m, 5H, H_{Ar}), 6.29 (qd, $J = 7.8, 1.8$ Hz, 2H, H_{Ar}), 4.16 (ddd, $J = 12.8, 10.2, 2.5$ Hz, 1H, H_{PC}), 3.20 (ddd, $J = 12.9, 10.3, 2.4$ Hz, 1H, H_{PC}), 3.12–2.97 (m, 5H, H_{PC}), 2.89 (ddd, $J = 12.9, 10.3, 5.8$ Hz, 1H, H_{PC}).

^{13}C NMR (100 MHz, CDCl_3 , ppm) $\delta = 153.3$ (C_q , C_{Ar}), 150.7 (C_q , C_{Ar}), 141.3 (C_q , C_{Ar}), 141.1 (C_q , C_{Ar}), 140.2 (C_q , C_{Ar}), 139.2 (C_q , C_{Ar}), 135.7 (+, CH, C_{Ar}), 135.2 (+, CH, C_{Ar}), 133.3 (+, CH, C_{Ar}), 133.0 (+, CH,

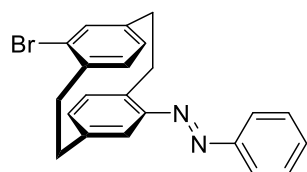
C_{Ar}), 132.0 (+, CH, C_{Ar}), 131.3 (+, CH, C_{Ar}), 130.6 (+, CH, C_{Ar}), 129.2 (+, 2C, CH, C_{Ar}), 122.8 (+, 2C, CH, C_{Ar}), 121.5 (+, CH, C_{Ar}), 35.9 (-, CH_2), 35.3 (-, CH_2), 34.9 (-, CH_2), 32.6 (-, CH_2).

MS (EI, 70 eV, 20 °C, %) $m/z = 313/314$ (100/22) $[M+H]^+$.

HRMS-EI (m/z): $[M+H]^+$, calc. for $C_{22}H_{20}N_2$, 313.1700; found: 313.1696.

IR (ATR, $\tilde{\nu}$) = 2928 (m), 2918 (w), 2850 (w), 1442 (w), 905 (m), 897 (w), 861 (m), 796 (m), 762 (vs), 720 (vs), 686 (vs), 663 (m), 646 (vs), 594 (s), 540 (w), 527 (m), 507 (vs) cm^{-1} .

4-(*E*)-Azophenyl-16-bromo[2.2]paracyclophane (106)



To a solution of 4-amino-16-bromo[2.2]paracyclophane (405 mg, 1.34 mmol, 1.00 equiv.) in acetic acid (20 mL) nitrosobenzene (287 mg, 2.68 mmol, 2.00 equiv.) was added and the reaction mixture was stirred for 48 hours at room temperature. The reaction mixture was extracted with dichloromethane,

washed with water and brine, dried by $MgSO_4$, filtered, and concentrated under reduced pressure. The crude product was purified via flash column chromatography on silica gel using cyclohexane/ethyl acetate 20:1, obtaining the title compound (263 mg, 672 μ mol, 50%) as a yellow solid.

$R_f = 0.4$ (cyclohexane/ethyl acetate 20:1)

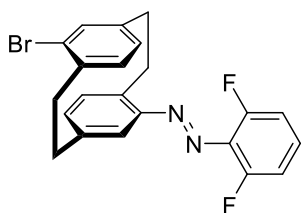
1H NMR (400 MHz, $CDCl_3$, ppm) $\delta = 8.00$ – 7.92 (m, 2H, H_{Ar}), 7.60 – 7.53 (m, 2H, H_{Ar}), 7.53 – 7.47 (m, 1H, H_{Ar}), 7.30 (dd, $J = 7.9, 2.0$ Hz, 1H, H_{Ar}), 6.67 (d, $J = 2.0$ Hz, 1H, H_{Ar}), 6.64 – 6.58 (m, 2H, H_{Ar}), 6.39 (dd, $J = 7.8, 1.8$ Hz, 1H, H_{Ar}), 6.29 (d, $J = 7.8$ Hz, 1H, H_{Ar}), 4.26 (ddd, $J = 13.1, 7.6, 5.8$ Hz, 1H, H_{PC}), 3.52 (ddd, $J = 13.1, 10.2, 2.6$ Hz, 1H, H_{PC}), 3.26 – 3.05 (m, 4H, H_{PC}), 3.02 – 2.93 (m, 1H, H_{PC}), 2.86 (ddd, $J = 13.3, 10.7, 5.5$ Hz, 1H, H_{PC}).

^{13}C NMR (100 MHz, $CDCl_3$, ppm) $\delta = 153.2$ (C_q , C_{Ar}), 150.9 (C_q , C_{Ar}), 142.1 (C_q , C_{Ar}), 140.7 (C_q , C_{Ar}), 140.6 (C_q , C_{Ar}), 138.7 (C_q , C_{Ar}), 137.4 (+, CH, C_{Ar}), 134.2 (+, CH, C_{Ar}), 133.8 (+, CH, C_{Ar}), 132.2 (+, CH, C_{Ar}), 130.7 (+, CH, C_{Ar}), 130.2 (+, CH, C_{Ar}), 129.2 (+, 2C, CH, C_{Ar}), 126.8 (C_q , C_{Ar}), 122.8 (+, 2C, CH, C_{Ar}), 121.7 (+, CH, C_{Ar}), 35.3 (-, CH_2), 35.0 (-, CH_2), 32.9 (-, CH_2), 31.9 (-, CH_2).

MS (EI, 70 eV, 20 °C, %) $m/z = 390/392$ (8/8) $[M]^+$, $364/366/368$ (17/33/16) $[C_{16}H_{14}^{79}Br_2]^+$, $311/312$ (46/12) $[M-Br]^+$, $207/208/209$ (100/58/8) $[M-C_8H_7Br]^+$, $182/184$ (77/72) $[C_8H_7Br]^+$.

HRMS-EI (m/z): $[M]^+$, calc. for $C_{22}H_{19}^{79}BrN_2$, 390.0732; found: 390.2492.

IR (ATR, $\tilde{\nu}$) = 1050 (vs), 1034 (vs), 965 (m), 798 (m), 792 (m), 766 (m), 449 (vs), 442 (vs), 433 (vs), 418 (vs), 399 (vs), 390 (vs), 378 (vs) cm^{-1} .

4-((E)-Azo-2',6'-difluorophenyl)-16-bromo[2.2]paracyclophane (107)

To a solution of 4-amino-16-bromo[2,2]paracyclophane (268 mg, 890 μmol , 1.00 equiv.) in acetic acid (10 mL) nitrosobenzene (254 mg, 1.77 mmol, 2.00 equiv.) was added and the reaction mixture was stirred for 48 hours at room temperature. The reaction mixture was extracted with dichloromethane, washed with water and brine, dried over MgSO_4 , filtered, and concentrated

under reduced pressure. The crude product was purified via flash column chromatography on silica gel using cyclohexane/ethyl acetate 20:1, obtaining the title compound (166 mg, 388 μmol , 44%) as a orange solid.

R_f = 0.42 (cyclohexane/ethyl acetate 20:1)

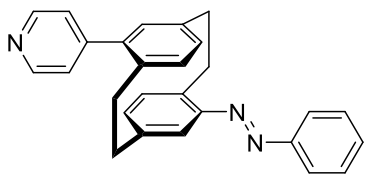
^1H NMR (400 MHz, CDCl_3 , ppm) δ = 7.30–7.22 (m, 2H, H_{Ar}), 7.06–6.97 (m, 2H, H_{Ar}), 6.59–6.54 (m, 3H, H_{Ar}), 6.45 (dd, J = 7.8, 1.8 Hz, 1H, H_{Ar}), 6.25 (d, J = 7.8 Hz, 1H, H_{Ar}), 4.10 (ddd, J = 13.1, 9.9, 3.5 Hz, 1H, H_{pc}), 3.45 (ddd, J = 13.0, 10.1, 2.5 Hz, 1H, H_{pc}), 3.19–2.95 (m, 4H, H_{pc}), 2.93–2.73 (m, 2H, H_{pc}).

^{13}C NMR (100 MHz, CDCl_3 , ppm) δ = 152.4 (C_q , C-F), 151.9 (C_q , C-F), 145.0 (C_q , C_{Ar}), 143.4 (C_q , C_{Ar}), 142.3 (C_q , C_{Ar}), 141.6 (C_q , C_{Ar}), 140.8 (C_q , C_{Ar}), 138.7 (C_q , C_{Ar}), 137.5 (+, CH, C_{Ar}), 134.3 (+, CH, C_{Ar}), 133.9 (+, CH, C_{Ar}), 133.1 (+, CH, C_{Ar}), 130.1 (+, CH, C_{Ar}), 129.7 (+, t, J = 10.0 Hz, CH, C_{Ar}), 126.8 (C_q , C_{Ar}), 121.0 (+, CH, C_{Ar}), 112.7–112.4 (+, m, 2C, CH, C_{Ar}), 35.3 (–, CH_2), 34.7 (–, CH_2), 32.8 (–, CH_2), 31.8 (–, CH_2).

MS (ESI, 70 eV, 20 $^\circ\text{C}$, %) m/z = 427/429 (21/20) $[\text{M}+\text{H}]^+$.

HRMS-ESI (m/z): $[\text{M}+\text{H}]^+$, calc. for $\text{C}_{22}\text{H}_{18}^{79}\text{BrF}_2\text{N}_2$, 427.0616; found: 427.0615.

IR (ATR, $\tilde{\nu}$) = 2927 (m), 1615 (w), 1587 (m), 1475 (vs), 1442 (m), 1435 (m), 1239 (s), 1024 (vs), 977 (w), 898 (m), 880 (w), 836 (m), 775 (vs), 734 (m), 710 (m), 669 (m), 654 (m), 514 (s), 487 (m), 475 (s) cm^{-1} .

4-(4'-Pyridinyl)-16-(E)-azophenyl[2.2]paracyclophane (108)

A vessel was charged with 4-azophenyl-16-bromo[2, 2]paracyclophane (245 mg, 670 μmol , 1.00 equiv.), pyridine-4-boronic acid (128 mg, 1.00 mmol, 1.70 equiv.), palladium-tetrakis(triphenylphosphine) (46.0 mg, 40 μmol , 0.06 equiv.), potassium phosphate (341 mg, 1.61

mmol, 2.50 equiv.), dioxane (8 mL) and water (2 mL). The mixture was heated under reflux for 16 h. Then the reaction mixture was then cooled to room temperature, extracted with ether (3 \times 30 mL), and the extracts were dried by MgSO_4 and evaporated under reduced pressure. The crude product was purified via flash column chromatography on silica gel using dichloromethane/ethyl acetate 4:1, obtaining the title compound (98.0 mg, 252 μmol , 40%) as an orange solid.

R_f = 0.5 (dichloromethane /ethyl acetate 1:1)

^1H NMR (400 MHz, CDCl_3 , ppm) δ = 8.73 (d, J = 5.1 Hz, 2H, H_{Py}), 8.03–7.95 (m, 2H, H_{Ar}), 7.58 (dd, J = 8.3, 6.6 Hz, 2H, H_{Ar}), 7.54–7.49 (m, 1H, H_{Ar}), 7.45–7.41 (m, 2H, H_{Py}), 6.81 (d, J = 2.0 Hz, 1H, H_{Ar}), 6.73–6.63 (m, 3H, H_{Ar}), 6.53–6.45 (m, 2H, H_{Ar}), 4.37–4.26 (m, 1H, H_{pc}), 3.40 (ddd, J = 13.7, 10.1, 3.9 Hz, 1H, H_{pc}), 3.25 (dd, J = 9.1, 5.4 Hz, 2H, H_{pc}), 3.10–2.98 (m, 2H, H_{pc}), 2.92 (ddd, J = 14.1, 10.4, 3.9 Hz, 1H, H_{pc}), 2.72 (ddd, J = 13.8, 10.1, 4.3 Hz, 1H, H_{pc}).

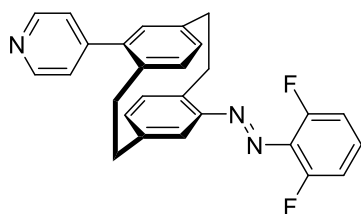
^{13}C NMR (100 MHz, CDCl_3 , ppm) δ = 153.2 (C_q , C_{Ar}), 151.0 (C_q , C_{Ar}), 150.1 (+, CH, 2C, C_{Py}), 148.6 (C_q , C_{Py}), 141.1 (+, CH, C_{Ar}), 141.0 (+, CH, C_{Ar}), 140.7 (+, CH, C_{Ar}), 139.6 (+, CH, C_{Ar}), 136.9 (+, CH, C_{Ar}), 135.1 (+, CH, C_{Ar}), 134.0 (+, CH, C_{Ar}), 132.9 (+, CH, C_{Ar}), 132.1 (+, CH, C_{Ar}), 131.9 (+, CH, C_{Ar}), 130.8 (+, CH, C_{Ar}), 129.2 (+, CH, 2C, C_{Ar}), 124.6 (+, CH, 2C, C_{Ar}), 122.9 (+, CH, 2C, C_{Py}), 121.8 (+, CH, C_{Ar}), 35.5 (–, CH_2), 34.4 (–, CH_2), 33.4 (–, CH_2), 32.1 (–, CH_2).

MS (ESI, 70 eV, 20 °C, %) m/z = 389/390 (81/23) $[\text{M}]^+$, 285 (28) $[\text{M}-\text{C}_6\text{H}_5\text{N}_2]^+$, 311/312 (46/12) $[\text{M}-\text{Br}]^+$, 207/208 (100/63) $[\text{M}-\text{C}_{13}\text{H}_{11}\text{N}]^+$, 181/182 (24/56) $[\text{C}_{13}\text{H}_{12}\text{N}]^+$.

HRMS-ESI (m/z): $[\text{M}]^+$, calc. for $\text{C}_{27}\text{H}_{23}\text{N}_3$, 389.1892; found: 389.3588.

IR (ATR, $\tilde{\nu}$) = 1047 (vs), 973 (m), 795 (m), 441 (vs), 432 (vs), 391 (vs), 380 (vs) cm^{-1} .

4-(4'-Pyridinyl)-16-((*E*)-azo-2',6'-difluorophenyl)[2.2]paracyclophane (109)



A vessel was charged with 4-((*E*)-Azo-2',6'-difluorophenyl)-16-bromo[2.2]paracyclophane (160 mg, 370 μmol , 1.00 equiv.), pyridine-4-boric acid (71.0 mg, 580 μmol , 1.50 equiv.), palladium-tetrakis(triphenylphosphine) (23.0 mg, 2.00 μmol , 0.05 equiv.), potassium phosphate (188 mg, 890 μmol , 2.50 equiv.), dioxane (6 mL)

and water (3 mL). The mixture was heated under reflux for 16 h. Then the reaction mixture was then cooled to room temperature, extracted with ether (3 \times 20 mL), and the extracts were dried by MgSO_4 and evaporated under reduced pressure. The crude product was purified via flash column chromatography on silica gel using dichloromethane /ethyl acetate 4:1, obtaining the title compound (49.2 mg, 116 μmol , 31%) as an orange solid.

R_f = 0.48 (dichloromethane /ethyl acetate 1:1)

^1H NMR (400 MHz, CDCl_3 , ppm) δ = 8.68–8.60 (m, 2H, H_{Py}), 7.38–7.34 (m, 2H, H_{Py}), 7.33–7.23 (m, 1H, H_{Ar}), 7.09–6.98 (m, 2H, H_{Ar}), 6.71 (d, J = 1.7 Hz, 1H, H_{Ar}), 6.67–6.61 (m, 3H, H_{Ar}), 6.53 (dd, J = 7.8, 1.9 Hz, 1H, H_{Ar}), 6.45 (d, J = 7.8 Hz, 1H, H_{Ar}), 4.17 (ddd, J = 13.0, 9.5, 3.7 Hz, 1H, H_{PC}), 3.34 (ddd, J = 13.7, 10.1, 3.9 Hz, 1H, H_{PC}), 3.18–3.08 (m, 2H, H_{PC}), 3.01–2.90 (m, 2H, H_{PC}), 2.85 (ddd, J = 14.1, 10.4, 3.9 Hz, 1H, H_{PC}), 2.64 (ddd, J = 13.8, 10.1, 4.3 Hz, 1H, H_{PC}).

^{13}C NMR (100 MHz, CDCl_3 , ppm) δ = 157.2 (C_q , d, $J_{\text{C-F}}$ = 4.4 Hz, C-F), 154.6 (C_q , d, $J_{\text{C-F}}$ = 4.4 Hz, C-F), 151.9 (C_q , C_{Ar}), 150.2 (+, 2C, C_{Py}), 148.6 (C_q , C_{Py}), 142.0 (C_q , C_{Ar}), 141.2 (C_q , C_{Ar}), 140.9 (C_q , C_{Ar}), 139.5

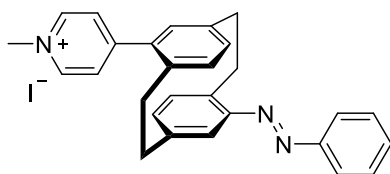
(C_q, C_{Ar}), 136.8 (C_q, C_{Ar}), 135.4 (C_q, C_{Ar}), 135.2 (+, CH, C_{Ar}), 134.1 (+, CH, C_{Ar}), 133.9 (+, CH, C_{Ar}), 132.2 (+, CH, C_{Ar}), 131.8 (+, CH, C_{Ar}), 129.8 (+, t, *J* = 10.0 Hz, CH, C_{Ar}), 124.5 (+, 2C, C_{Py}), 121.1 (+, CH, C_{Ar}), 112.7–112.4 (+, m, 2C, CH, C_{Ar}), 35.2 (–, CH₂), 34.4 (–, CH₂), 33.4 (–, CH₂), 32.0 (–, CH₂).

MS (ESI, 70 eV, 20 °C, %) *m/z* = 426/427(72/20) [M+H]⁺.

HRMS-ESI (*m/z*): [M+H]⁺, calc. for C₂₇H₂₂F₂N₃, 426.1777; found: 426.1775.

IR (ATR, $\tilde{\nu}$) = 3053 (vw), 3024 (vw), 2925 (w), 2850 (w), 1613 (w), 1591 (s), 1540 (w), 1475 (m), 1451 (w), 1436 (m), 1414 (w), 1400 (w), 1307 (vw), 1278 (w), 1238 (w), 1217 (w), 1191 (s), 1159 (w), 1137 (w), 1118 (s), 1095 (w), 1068 (w), 1023 (s), 1011 (m), 992 (m), 979 (w), 945 (w), 912 (w), 899 (w), 878 (w), 858 (w), 844 (w), 829 (m), 781 (s), 748 (m), 735 (w), 718 (vs), 694 (vs), 669 (w), 653 (m), 620 (m), 577 (w), 538 (vs), 506 (s), 482 (s), 458 (m), 445 (m), 387 (w) cm⁻¹.

4-(*N*-Methyl-4'-pyridinium)-16-(*E*)-azophenyl[2.2]paracyclophane iodide (AzoMVCP, 103)



4-(4'-Pyridinyl)-16-(*E*)-azophenyl[2,2]paracyclophane (159 mg, 408 μ mol, 1.00 equiv.) dissolved in acetonitrile 6 mL, then methyl iodide (300 μ L) was added. The mixture was stirred at 40 °C for 16 h excluded of the light. The solvent was removed under reduced pressure

to give a residue and then recrystallized from methanol to obtain 4-(*N*-methyl-4'-pyridinium)-16-(*E*)-azophenyl[2.2]paracyclophane iodide (132 mg, 248 μ mol, 61%) as an orange solid.

¹H NMR (400 MHz, DMSO-d₆, ppm) δ = 9.04 (d, *J* = 6.4 Hz, 2H, *H*_{Py}), 8.32–8.27 (m, 2H, *H*_{Py}), 8.02–7.94 (m, 2H, *H*_{Ar}), 7.71–7.55 (m, 3H, *H*_{Ar}), 7.08 (d, *J* = 1.8 Hz, 1H, *H*_{Ar}), 7.03 (d, *J* = 7.9 Hz, 1H, *H*_{Ar}), 6.75 (d, *J* = 2.0 Hz, 1H, *H*_{Ar}), 6.65 (d, *J* = 7.7 Hz, 1H, *H*_{Ar}), 6.58 (dd, *J* = 7.9, 1.9 Hz, 1H, *H*_{Ar}), 6.50 (dd, *J* = 7.8, 1.8 Hz, 1H, *H*_{Ar}), 4.41 (s, 3H, CH₃), 4.23–4.13 (m, 1H, *H*_{pc}), 3.33–3.27 (m, 2H, *H*_{pc}), 3.24–3.08 (m, *J* = 19.3, 10.4, 5.2 Hz, 3H, *H*_{pc}), 2.96 (ddd, *J* = 13.9, 10.2, 4.0 Hz, 1H, *H*_{pc}), 2.71–2.60 (m, 1H, *H*_{pc}).

¹³C NMR (100 MHz, DMSO-d₆, ppm) δ = 155.5 (C_q, C_{Py}), 153.2 (C_q, C_{Ar}), 150.9 (C_q, C_{Ar}), 145.9 (+, CH, 2C, C_{Py}), 144.3 (C_q, C_{Ar}), 141.4 (C_q, C_{Ar}), 141.3 (C_q, C_{Ar}), 138.6 (C_q, C_{Ar}), 137.0 (C_q, C_{Ar}), 136.0 (+, CH, C_{Ar}), 134.8 (+, CH, C_{Ar}), 133.8 (+, CH, C_{Ar}), 133.5 (+, CH, C_{Ar}), 133.1 (+, CH, C_{Ar}), 131.6 (+, CH, C_{Ar}), 130.0 (+, CH, 2C, C_{Ar}), 127.9 (+, CH, 2C, C_{Ar}), 123.0 (+, CH, 2C, C_{Py}), 121.9 (+, CH, C_{Ar}), 47.6 (+, CH₃), 35.2 (–, CH₂), 34.3 (–, CH₂), 33.3 (–, CH₂), 31.7 (–, CH₂).

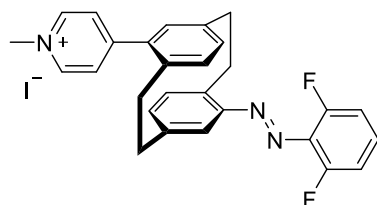
MS (ESI, 70 eV, 20 °C, %) *m/z* = 404/405 (100/30) [M]⁺.

HRMS-ESI (*m/z*): [M]⁺, calc. for C₂₇H₂₃N₃, 404.2122; found: 404.2118.

IR (ATR, $\tilde{\nu}$) = 3026 (m), 2961 (w), 2942 (m), 2928 (m), 2851 (m), 1635 (vs), 1585 (m), 1561 (m), 1548 (m), 1509 (m), 1479 (m), 1466 (m), 1451 (vs), 1439 (vs), 1402 (m), 1322 (m), 1288 (m), 1198 (vs), 1143 (vs), 1122 (s), 1094 (m), 1069 (s), 1043 (m), 914 (m), 901 (m), 878 (m), 861 (s), 847 (vs), 802 (m), 773

(vs), 739 (s), 727 (s), 690 (vs), 667 (s), 647 (vs), 620 (m), 585 (m), 555 (s), 531 (s), 510 (vs), 484 (vs), 459 (s), 446 (vs), 429 (s), 412 (m), 402 (m), 391 (s), 381 (m) cm^{-1} .

4-(*N*-Methyl-4'-pyridinium)-16-((*E*)-azo-2',6'-difluorophenyl)[2.2]paracyclophane iodide (AzoFMVCP, 104)



4-(4'-Pyridinyl)-16-((*E*)-azo-2',6'-difluorophenyl)[2.2]paracyclophane (60.0 mg, 142 μmol , 1.00 equiv.) dissolved in acetonitrile 5 mL, then methyl iodide (100 μL) was added. The mixture was stirred at 40 $^{\circ}\text{C}$ for 16 h, excluding the light. The solvent was removed under reduced pressure to give a residue and then recrystallized from methanol to

obtain 4-(*N*-methyl-4'-pyridinium)-16-((*E*)-Azo-2',6'-difluorophenyl)[2.2]paracyclophane iodide (38.0 mg, 67.0 μmol , 47%) as an orange solid.

^1H NMR (400 MHz, CDCl_3 , ppm) δ = 9.19 (d, J = 6.3 Hz, 2H, H_{Py}), 8.05 (d, J = 6.9 Hz, 2H, H_{Py}), 7.29 (tt, J = 8.4, 5.9 Hz, 1H, H_{Ar}), 7.03 (t, J = 8.6 Hz, 2H, H_{Ar}), 6.83–6.73 (m, 2H, H_{Ar}), 6.68–6.58 (m, 3H, H_{Ar}), 6.50 (d, J = 7.8 Hz, 1H, H_{Ar}), 4.64 (s, 3H, CH_3), 4.17–4.08 (m, 1H, H_{pc}), 3.29 (ddd, J = 13.9, 9.5, 4.3 Hz, 1H, H_{pc}), 3.20–3.11 (m, 2H, H_{pc}), 3.07–2.95 (m, 2H, H_{pc}), 2.90–2.75 (m, 2H, H_{pc}).

^{13}C NMR (100 MHz, CDCl_3 , ppm) δ = 157.2 (C_{q} , d, $J_{\text{C-F}}$ = 5.2 Hz, C-F), 154.6 (C_{q} , d, $J_{\text{C-F}}$ = 5.2 Hz, C-F), 156.9 (C_{q} , C_{Py}), 151.9 (C_{q} , C_{Ar}), 145.3 (+, CH, 2C, C_{Py}), 142.2 (C_{q} , C_{Ar}), 142.0 (C_{q} , C_{Ar}), 140.9 (C_{q} , C_{Ar}), 139.9 (C_{q} , C_{Ar}), 138.0 (C_{q} , C_{Ar}), 136.0 (+, CH, 2C, C_{Ar}), 134.3 (+, CH, C_{Ar}), 134.2 (+, CH, C_{Ar}), 134.0 (+, CH, C_{Ar}), 132.8 (+, CH, C_{Ar}), 130.1 (+, t, J = 10.0 Hz, CH, C_{Ar}), 128.1 (+, CH, 2C, C_{Py}), 121.4, 112.7–112.5 (+, m, 2C, CH, C_{Ar}), 48.9 (+, CH_3), 35.0 (–, CH_2), 34.8 (–, CH_2), 33.4 (–, CH_2), 31.9 (–, CH_2).

MS (ESI, 70 eV, 20 $^{\circ}\text{C}$, %) m/z = 440/441 (100/29) $[\text{M}]^+$.

HRMS-ESI (m/z): $[\text{M}]^+$, calc. for $\text{C}_{28}\text{H}_{24}\text{F}_2\text{N}_3$, 440.1933; found: 440.1916.

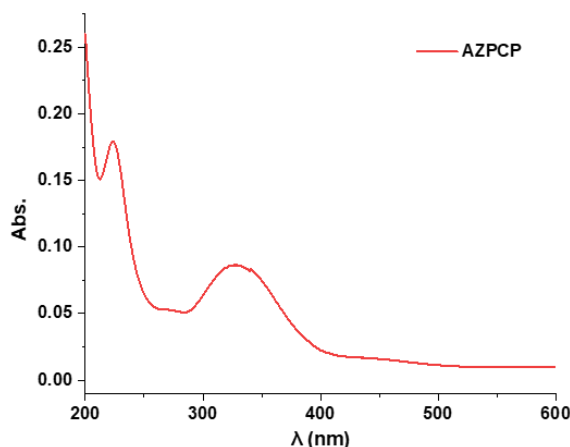


Figure 96. UV-Vis absorption spectra of AzoMVCP (10 μM) in water.

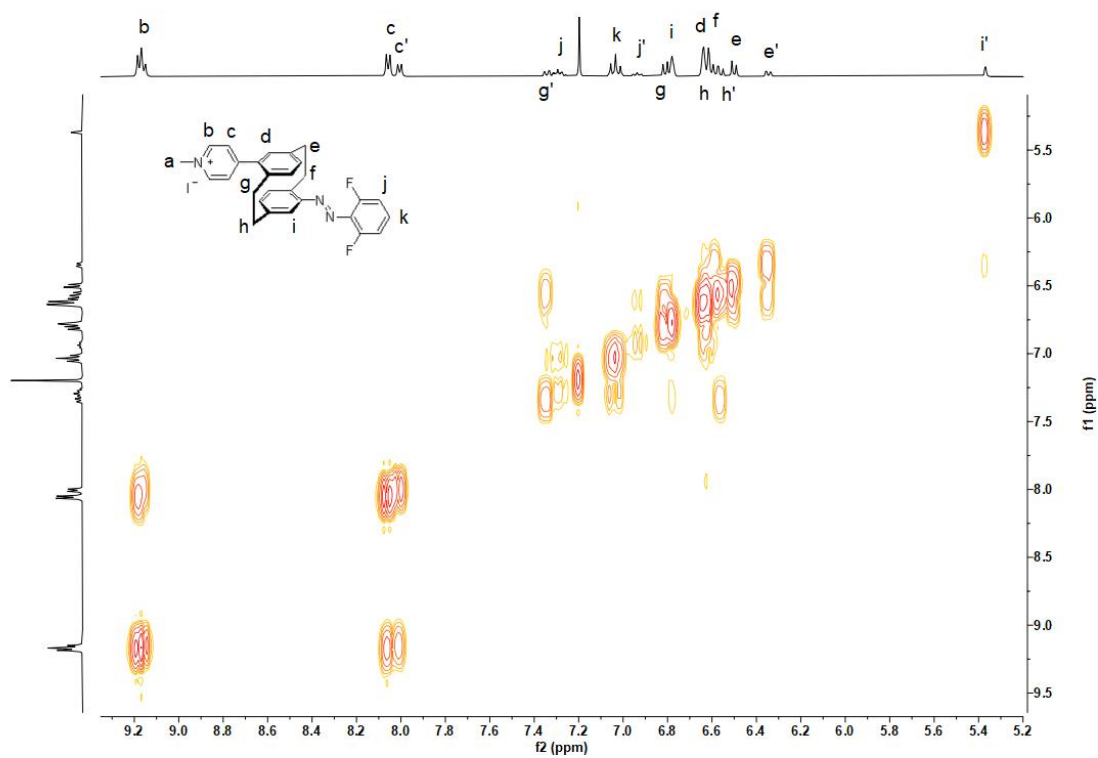
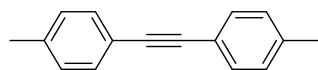


Figure 97. 2D ^1H - ^1H COSY spectrum of AzoFMPCP after irradiation.

5.4 Supramolecular Skeleton and Cage based on [2.2]Paracyclophane derivatives

4,4'-dimethyltolan (123)



Bis(triphenylphosphin)palladium(II)-dichlorid (48.0 mg, 68.0 μmol , 1.00 mol%), copper(I) iodide (26.0 mg, 138 μmol , 2.00 mol%), 4-iodotoluene (1.65 g, 7.58 mmol, 1.10 equiv.) and 4-ethynyltoluene (800 mg, 6.89 mmol, 1.00 equiv.) were reacted in a degassed solution of 15 mL dry THF with triethylamine (3.00 mL, 21.6 mmol, 3.10 equiv.) under argon at room temperature. After the complete conversion of the starting material was determined, the reaction mixture was filtered through a pad of silica gel with cyclohexane as solvent. The solvent was removed under reduced pressure and the crude product was purified by flash column chromatography on silica gel using cyclophane to obtain the title compound (815 mg, 3.95 mmol, 57%) as a white solid.

$R_f = 0.45$ (cyclophane)

$^1\text{H NMR}$ (400 MHz, CDCl_3 , ppm) $\delta = 7.46\text{--}7.38$ (m, 4H, H_{Ar}), 7.15 (d, $J = 7.9$ Hz, 4H, H_{Ar}), 2.37 (s, 6H, CH_3).

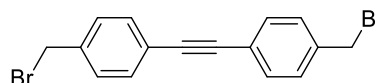
$^{13}\text{C NMR}$ (100 MHz, CDCl_3 , ppm) $\delta = 138.2$ (C_q , 2C, C_{Ar}), 131.5 (+, 4C, C_{Ar}), 129.1 (+, 4C, C_{Ar}), 120.4 (C_q , 2C, C_{Ar}), 88.9 (C_q , 2C, $\text{C}\equiv\text{C}$), 21.5 (+, 2C, CH_3).

MS (EI, 70 eV, 20 $^\circ\text{C}$, %) $m/z = 207/208$ (39/6) $[\text{M}+\text{H}]^+$.

HRMS-EI (m/z): $[\text{M}+\text{H}]^+$ calc. for $\text{C}_{16}\text{H}_{14}$, 207.1169; found: 207.1161.

IR (ATR, $\tilde{\nu}$) = 1513 (vs), 1439 (w), 1408 (w), 1183 (w), 1122 (w), 1034 (w), 1018 (w), 839 (w), 812 (vs), 755 (w), 739 (w), 705 (w), 513 (vs), 469 (m) cm^{-1} .

4,4'-bis(bromomethyl)tolan (112)



4,4'-Dimethyltolan (624 mg, 3.03 mmol, 1.00 equiv.) and *N*-bromosuccinimide (1.35 mg, 7.57 mmol, 2.50 equiv.) were dissolved in 1,2-dichloroethane (25 mL), and to this mixture 2,2'-azobis(2-ethylpropionitrile) (10.0 mg, 60.9 μmol , 0.02 equiv.) was added. The reaction mixture was heated under reflux at 85 $^\circ\text{C}$ for 15 min and the next portion of 2,2'-azobis(2-ethylpropionitrile) (10.0 mg, 60.9 μmol , 0.02 equiv.) was added and the reaction mixture was heated at 85 $^\circ\text{C}$ for a further 15 min. After cooling to room temperature, the reaction mixture was kept at 5 $^\circ\text{C}$ for 2 h and the precipitate was filtered off and washed with a small amount of 1,2-dichloroethane. The solvent was removed under reduced pressure and the crude product was purified by flash column chromatography on silica gel using cyclophane to obtain the title compound (202 mg, 555 μmol , 18%) as white solid.

$R_f = 0.5$ (cyclophane)

^1H NMR (400 MHz, CDCl_3 , ppm) $\delta = 7.54\text{--}7.45$ (m, 4H, H_{Ar}), $7.45\text{--}7.33$ (m, 4H, H_{Ar}), 4.50 (s, 4H, CH_2).

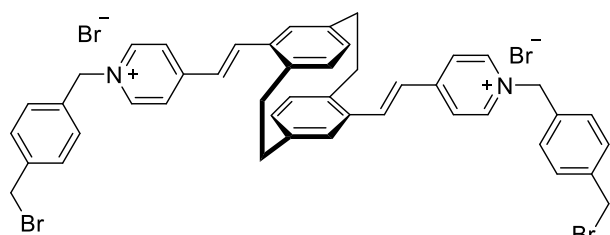
^{13}C NMR (100 MHz, CDCl_3 , ppm) $\delta = 138.0$ (C_q , 2C, C_{Ar}), 132.0 (+, 4C, C_{Ar}), 129.1 (+, 4C, C_{Ar}), 123.2 (C_q , 2C, C_{Ar}), 89.7 (C_q , 2C, $\text{C}\equiv\text{C}$), 33.0 (–, 2C, CH_2).

MS (ESI, 70 eV, 20 °C, %) $m/z = 364$ (1) $[\text{M}]^+$, $205/206$ (100/29) $[\text{M}+\text{H}-\text{Br}_2]^+$, $284/286$ (11/12) $[\text{M}-\text{Br}]^+$.

HRMS-ESI (m/z): $[\text{M}]^+$ calc. for $\text{C}_{16}\text{H}_{12}^{79}\text{Br}_2$, 363.9285; found: 364.0753.

IR (ATR, $\tilde{\nu}$) = 3060 (w), 3047 (w), 3026 (w), 2969 (w), 1701 (m), 1677 (m), 1656 (w), 1649 (w), 1639 (w), 1630 (w), 1608 (w), 1513 (m), 1436 (w), 1411 (m), 1367 (w), 1357 (w), 1222 (s), 1194 (s), 1181 (m), 1128 (w), 1088 (m), 834 (vs), 819 (s), 771 (s), 730 (m), 592 (vs), 537 (m), 520 (s), 482 (m), 472 (s), 436 (w), 428 (m), 408 (m), 388 (w) cm^{-1} .

4,16-(4,4'-((*E,E*)-bis(ethene-2,1-diyl))bis(*N*-(4-(bromomethyl)benzyl)pyridinium))[2.2]paracyclopane dibromide (115)



1,4-Bis(bromomethyl)benzene (726 mg, 2.75 mmol, 5.00 equiv.) and 4,16-di((*E*)-4'-pyridylvinyl)[2.2]paracyclopane (100 mg, 241 μmol , 1.00 equiv.) were suspended into a 1:2 mixture solution of dichloromethane and acetonitrile

(24 mL) and heated under reflux at 90 °C under argon. After refluxing for 64 h, the reaction mixture was cooled down to room temperature and the yellow precipitate was collected by filtration and washed with dichloromethane (40 mL) and methanol (10 mL) to yield the title compound (162 mg, 172 μmol , 71%) as a yellow solid.

^1H NMR (400 MHz, DMSO-d_6 , ppm) $\delta = 9.15\text{--}9.06$ (m, 4H, H_{Py}), 8.43 (m, 4H, H_{Py}), 8.03 (d, $J = 16.0$ Hz, 2H, $\text{CH}=\text{CH}$), $7.76\text{--}7.52$ (m, 8H, H_{Ar}), 7.32 (d, $J = 16.0$ Hz, 2H, $\text{CH}=\text{CH}$), 7.00 (s, 2H, H_{Ar}), $6.63\text{--}6.47$ (m, 4H, H_{Ar}), $5.86\text{--}5.75$ (m, 4H, CH_2), 4.80 (s, 4H, CH_2), $3.87\text{--}3.72$ (m, 2H, H_{PC}), $3.18\text{--}3.06$ (m, 2H, H_{PC}), $3.05\text{--}2.92$ (m, 4H, H_{PC}).

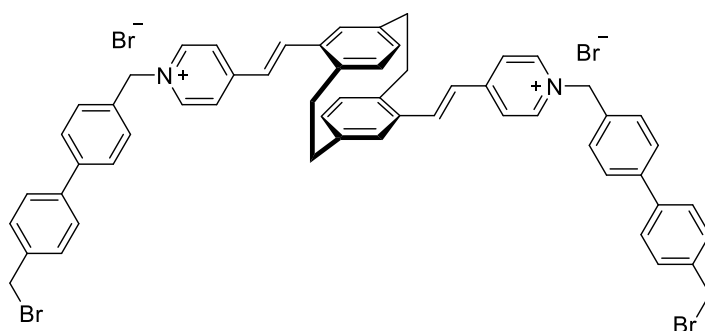
^{13}C NMR (125 MHz, DMSO-d_6 , ppm) $\delta = 154.1$ (C_q , 2C, C_{Ar}), 144.7 (+, 4C, C_{Py}), 141.5 (C_q , 2C, C_{Ar}), 140.3 (C_q , 2C, C_{Ar}), 139.5 (+, 2C, $\text{CH}=\text{CH}$), 139.2 (C_q , 2C, C_{Ar}), 136.0 (C_q , 2C, C_{Ar}), 135.3 (C_q , 2C, C_{Ar}), 134.3 (+, 2C, C_{Ar}), 131.5 (+, 2C, C_{Ar}), 130.1 (+, 4C, C_{Ar}), 129.4 (+, 4C, C_{Ar}), 128.9 (+, 2C, C_{Ar}), 127.6 (+, 2C, C_{Ar}), 124.9 (+, 2C, C_{Ar}), 124.3 (+, 2C, $\text{CH}=\text{CH}$), 62.8 (–, 2C, CH_2), 46.0 (–, 2C, CH_2), 34.6 (–, 2C, CH_2), 33.0 (–, 2C, CH_2).

MS (ESI, 70 eV, 20 °C, %) $m/z = 391/392$ (100/47), $[\text{M}]^{2+}$.

HRMS-ESI (m/z): $[\text{M}]^{2+}$, calc. for $\text{C}_{46}\text{H}_{42}^{79}\text{Br}_2\text{N}_2$, 391.0842/ 390.0852/ 391.5859/ 392.0832 (100/51/50/49); found: 391.0850/ 390.0858/ 391.5864/ 392.0840 (100/49/47/45).

IR (ATR, $\tilde{\nu}$) = 1636 (s), 1608 (vs), 1585 (s), 1510 (s), 1159 (s), 966 (s), 880 (vs), 826 (m), 789 (m), 762 (m), 657 (m), 629 (m), 579 (m), 524 (vs), 506 (vs), 487 (m), 472 (s), 458 (m), 446 (m) cm^{-1} .

4,16-(4,4'-((*E,E*)-diylbis(ethene-2,1-diyl))bis(*N*-((4'-(bromomethyl)-[1,1'-biphenyl]-4-yl)methyl)pyridinium))[2.2]paracyclophane dibromide (116)



4,4'-Bis-(bromomethyl)-biphenyl (246 mg, 723 μmol , 3.00 equiv.) and 4,16-vinyl-4'-pyridine[2.2]paracyclophane (100 mg, 241 μmol , 1.00 equiv.) were suspended into a 1:2 mixture solution of dichloromethane and acetonitrile (24 mL) and heated under reflux at 90 $^{\circ}\text{C}$ under argon. After refluxing

for 48 h, the reaction mixture was cooled down to room temperature and the yellow precipitate was collected by filtration and washed with dichloromethane (30 mL) and methanol (10 mL) to yield the title compound (191 mg, 174 μmol , 72%) as a yellow solid.

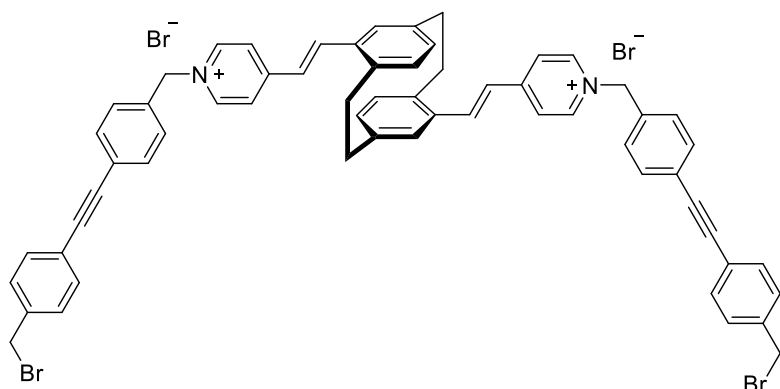
^1H NMR (400 MHz, DMSO- d_6 , ppm) δ = 9.14 (d, J = 6.8 Hz, 4H, H_{Py}), 8.45 (d, J = 6.8 Hz, 4H, H_{Py}), 8.03 (d, J = 16.0 Hz, 2H, CH=CH), 7.84–7.74 (m, 4H, H_{Ar}), 7.74–7.62 (m, 8H, H_{Ar}), 7.60–7.53 (m, 2H, H_{Ar}), 7.42 (d, J = 8.1 Hz, 2H, H_{Ar}), 7.32 (d, J = 16.0 Hz, 2H, CH=CH), 7.00 (d, J = 1.8 Hz, 2H, H_{Ar}), 6.64–6.51 (m, 4H, H_{Ar}), 5.84 (s, 4H, CH_2), 4.77 (s, 4H, CH_2), 3.85–3.75 (m, 2H), 3.17–2.92 (m, 6H).

MS (ESI, 70 eV, 20 $^{\circ}\text{C}$, %) m/z = 467/468 (100/63), $[\text{M}]^{2+}$.

HRMS-ESI (m/z): $[\text{M}]^{2+}$, calc. for $\text{C}_{58}\text{H}_{50}^{79}\text{Br}_2\text{N}_2$, 467.1155/ 467.6172/ 466.1165/ 468.1145 (100/63/51/49); found: 467.1155/ 467.6171/ 466.1165/ 468.1145 (100/63/50/46).

IR (ATR, $\tilde{\nu}$) = 3393 (w), 3386 (w), 3376 (w), 3369 (w), 3354 (w), 3340 (w), 3332 (w), 3024 (w), 3013 (w), 3000 (w), 2938 (w), 2928 (w), 1636 (s), 1606 (vs), 1585 (s), 1558 (m), 1513 (m), 1499 (m), 1483 (w), 1463 (m), 1400 (w), 1337 (w), 1320 (m), 1204 (s), 1154 (s), 1004 (w), 965 (s), 880 (s), 790 (vs), 735 (m), 714 (m), 686 (w), 656 (m), 628 (m), 601 (m), 585 (m), 569 (m), 540 (m), 514 (vs), 504 (vs), 492 (vs), 483 (vs), 452 (s), 439 (s), 431 (s), 426 (s), 412 (s), 404 (s), 397 (s), 387 (s) cm^{-1} .

4,16-(4,4'-((*E,E*)-diylbis(ethene-2,1-diyl))bis(1-(4-((4-(bromomethyl)phenyl)ethynyl)benzyl)pyridinium))[2.2]paracyclophane dibromide (117)



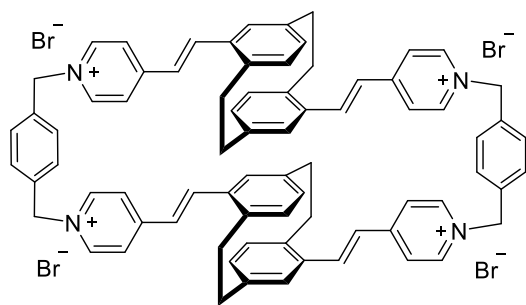
1,2-Bis(4-(bromomethyl)phenyl)ethyne (132 mg, 362 μmol , 1.00 equiv.) and 4,16-vinyl-4'-pyridine[2.2]paracyclophane (50.0 mg, 121 μmol , 1.00 equiv.) were suspended into a 1:2 mixture solution of dichloromethane and

acetonitrile (24 mL) and heated under reflux at 90 °C under argon. After refluxing for 48 h, the reaction mixture was cooled down to room temperature and the yellow precipitate was collected by filtration and washed with dichloromethane (30 mL) and methanol (10 mL) to yield the title compound (74.0 mg, 64.8 mmol, 54%) as a yellow solid.

MS (ESI, 70 eV, 20 °C, %) m/z = 467/468 (100/63), $[\text{M}]^{2+}$.

HRMS-ESI (m/z): $[\text{M}]^{2+}$, calc. for $\text{C}_{62}\text{H}_{50}^{79}\text{Br}_2\text{N}_2$, 491.1155/ 491.6172/ 492.1145 (100/67/48); found: 491.1244/ 467.6261/ 492.1233.

PCPBOX-1 (118)



A solution of **115** (47.0 mg, 49.9 μmol , 1.00 equiv.), 4,16-di-((*E*)-4'-pyridylvinyl[2.2]paracyclophane (21.0 mg, 50.0 μmol , 1.00 equiv.), and tetra-*n*-butylammonium iodide (4.00 mg, 10.0 μmol , 0.20 equiv.) in dry acetonitrile (100 mL) was heated under reflux at 90 °C for 3 days. After cooling to room temperature, the solvent was concentrated under vacuum to 20 mL. Then purified by C18 reverse

HPLC on a linear gradient from 5% to 95% MeCN with 0.1% aqueous TFA in diH_2O with 0.1% aqueous TFA and with a flow rate of 10 mL/min at 25 °C to yield light yellow solid (1.12 mg, 1%).

Collection of operating periods: 10 min to 12 min.

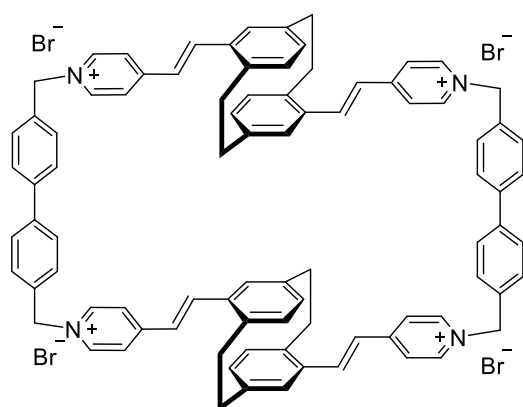
^1H NMR (400 MHz, CD_3OD , ppm) δ = 8.89 (d, J = 6.6 Hz, 8H, H_{Py}), 8.10 (d, J = 6.5 Hz, 8H, H_{Py}), 7.81–7.69 (m, 12H, $\text{CH}=\text{CH}$, H_{Ar}), 7.02 (d, J = 16.1 Hz, 4H, H_{Ar}), 6.72 (s, 4H, H_{Ar}), 6.37 (t, J = 5.0 Hz, 4H, H_{Ar}), 6.24 (dd, J = 7.8, 6.2 Hz, 4H, H_{Ar}), 5.73 (s, 8H, CH_2), 3.55–3.45 (m, 4H, H_{PC}), 2.94–2.72 (m, 12H, H_{PC}).

HRMS-ESI (m/z): $[\text{M}]^{4+}$, calc. for $\text{C}_{76}\text{H}_{68}\text{N}_4$, 259.1356/ 259.3864/ 259.6372 (100/82/33); found: 259.1354/ 259.3862/ 259.6370 (73/59/25). $[\text{M}+\text{Br}]^{3+}$, calc. for $\text{C}_{76}\text{H}_{68}^{79}\text{BrN}_4$, 371.8204/ 372.4864; found: 371.8198/ 372.4859.

PCPBOX•4PF₆

Part of the solid **PCPBOX-1** was added to a solution of amine hexafluorophosphate consisting of NH₄PF₆ (106 mg) and H₂O (30 mL), stirred for 2h and the resulting precipitate was filtered, followed by washing with H₂O (2 × 5 mL) and dried in vacuo to yield PCPBOX•4PF₆.

¹H NMR (400 MHz, CD₃CN, ppm) δ = 8.61 (d, *J* = 6.5 Hz, 8H, *H*_{Py}), 7.90 (d, *J* = 6.6 Hz, 8H, *H*_{Py}), 7.61–7.50 (m, 12H, CH=CH, *H*_{Ar}), 6.87 (d, *J* = 16.0 Hz, 4H, *H*_{Ar}), 6.61 (d, *J* = 6.7 Hz, 4H, *H*_{Ar}), 6.28 (d, *J* = 7.7 Hz, 4H, *H*_{Ar}), 6.18 (dd, *J* = 7.8, 3.0 Hz, 4H, *H*_{Ar}), 5.56 (s, 8H, CH₂), 3.37 (d, *J* = 12.6 Hz, 4H, *H*_{PC}), 2.87–2.77 (s, 4H, *H*_{PC}), 2.76–2.64 (d, *J* = 8.7 Hz, 8H, *H*_{PC}).

PCPBOX-2 (119)

HRMS-ESI (*m/z*): [*M*]⁴⁺, calc. for C₈₈H₇₆N₄, 297.1512/297.4021; found: 297.151/297.402/297.653/297.904.

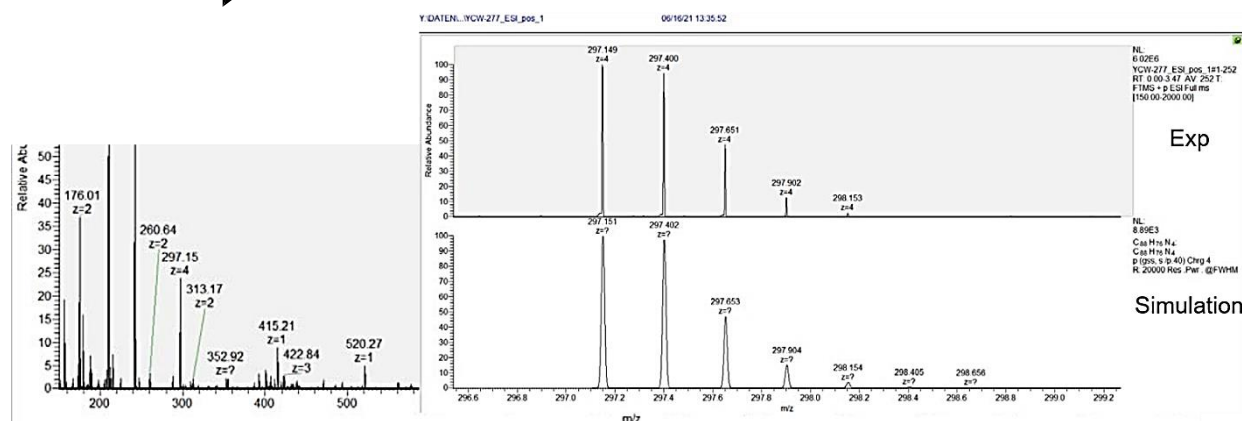
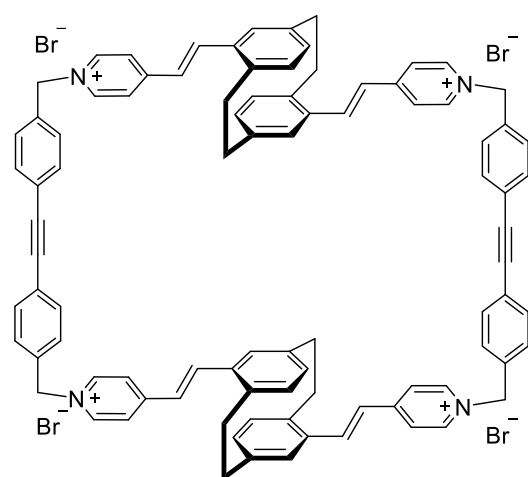


Figure 98. ESI mass spectra of **PCPBOX-2**. Results provided by Dr. Partick Weis.

PCPBOX-3 (120)

HRMS-ESI (m/z): $[M]^{4+}$, calc. for $C_{92}H_{76}N_4$, 309.1512/309.4021; found: 309.15/ 309.40/ 309.65/ 309.90.

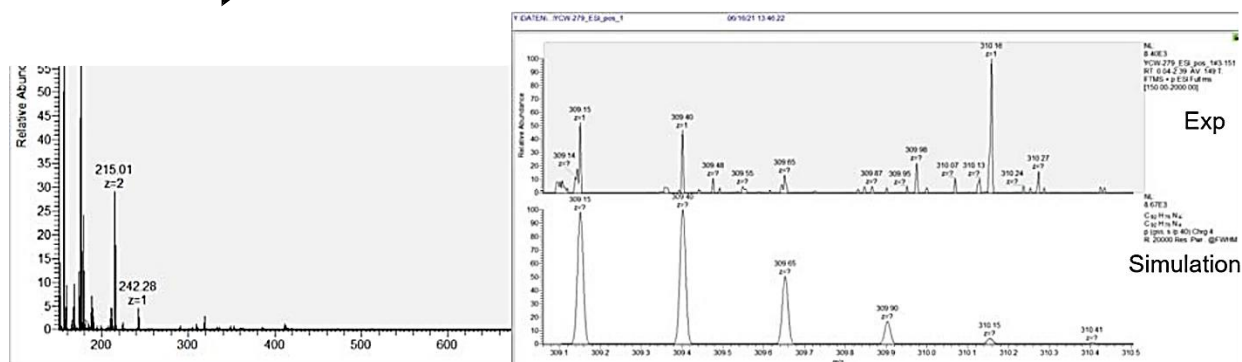
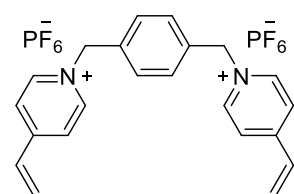


Figure 99. ESI mass spectra of PCPBOX-3. Results provided by Dr. Partick Weis.

1,1'-(1,4-phenylenebis(methylene))bis(4-vinylpyridinium) hexafluorophosphate (124)

1,4-Bis(bromomethyl)benzene (500 mg, 1.89 mmol, 1.00 equiv.) and 4-vinylpyridine (497 mg, 4.74 mmol, 0.50 mL, 2.50 equiv.) were dissolved in dry acetonitrile (13 mL) and stirred at 80 °C for 5 days. The reaction mixture was brought to room temperature and excess NH_4Cl was added to precipitate a solid.

The precipitate was filtered off and washed with acetone and dichloromethane to remove the tetrabutylammonium salt. The solid was dried and dissolved in water, then reprecipitated as its salt by adding NH_4PF_6 solution. Multiple washes removed the excess NH_4PF_6 with water to yield the pure title compound (1.07 g, 1.76 mmol, 93%) as a light yellow solid.

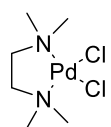
1H NMR (400 MHz, DMSO- d_6 , ppm) δ = 9.12–9.06 (m, 4H, H_{Py}), 8.24 (d, J = 6.8 Hz, 4H, H_{Py}), 7.58 (s, 4H, H_{Ar}), 7.00 (dd, J = 17.6, 10.9 Hz, 2H, $CH=CH_2$), 6.60 (d, J = 17.6 Hz, 2H, CH_2), 6.02 (d, J = 10.9 Hz, 2H, $CH=CH_2$), 5.77 (s, 4H, $CH=CH_2$).

^{13}C NMR (100 MHz, DMSO- d_6 , ppm) δ = 153.4 (C_q , 2C, C_{Py}), 145.3 (+, 4C, C_{Py}), 135.9(+, 2C, $CH=CH_2$), 132.8 (C_q , 2C, C_{Ar}), 129.9 (+, 4C, C_{Ar}), 128.6 (–, 2C, $CH=CH_2$), 125.2 (+, 4C, C_{Py}), 62.5 (–, 2C, CH_2).

HRMS-ESI (m/z): $[M]^{2+}$, calc. for $C_{22}H_{22}N_2$, 157.0886/ 157.5903 (100/24); found: 157.0886/ 157.5902 (100/24). $[M+PF_6]^+$, calc. for $C_{22}H_{22}F_6N_2P$, 459.1420; found: 459.1418.

IR (ATR, $\tilde{\nu}$) = 1640 (w), 1469 (w), 1164 (vw), 826 (vs), 776 (m), 739 (w), 728 (w), 555 (vs), 514 (w), 467 (w), 426 (w), 419 (vw), 411 (vw), 402 (w), 388 (w) cm^{-1} .

Dichloro-(N,N,N',N'-tetramethylethylenediamine)palladium(II) (*cis*-(tmen)PdCl₂, 126)



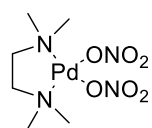
Palladium(II) chloride (200 mg, 1.13 mmol, 1.00 equiv.) was suspended in acetone (5 mL) and tetramethylethylenediamine(tmeda, 168 μ L, 1.13 mmol, 1.00 equiv.) was added. The suspension was stirred at room temperature for 24 h. Then filtered, and washed with water, acetone, and diethyl ether to yield yellow solid (281 mg, 957 μ mol, 84%).

1H NMR (400 MHz, DMSO-d₆, ppm) δ = 2.73 (s, 4H, CH₂), 2.65 (s, 12H, CH₃).

^{13}C NMR (100 MHz, DMSO-D₆, ppm) δ = 62.2 (–, 2C, CH₂), 51.0 (+, 4C, CH₃).

IR (ATR, $\tilde{\nu}$) = 1466 (s), 1438 (w), 1125 (w), 1045 (m), 1009 (s), 953 (s), 807 (vs), 772 (s), 506 (m) cm^{-1} .

Dinitro-(N,N,N',N'-tetramethylethylenediamine)palladium(II) (*cis*-(tmen)Pd(ONO₂)₂, 114)

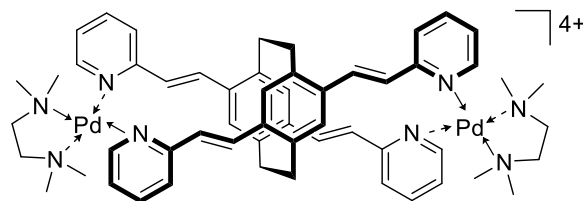


Pd(tmeda)Cl₂ (150 mg, 511 μ mol, 1.00 equiv.) was suspended in 15 mL of water. With exclusion from light AgNO₃ (174 mg, 1.02 mmol, 2.00 equiv.) was added and stirred at room temperature for 16 h. The resulting suspension was then filtered and the filtrate was concentrated in vacuo to yield a yellow solid (165 mg, 476 μ mol, 93%).

1H NMR (400 MHz, D₂O, ppm) δ = 2.89 (s, 4H, CH₂), 2.68 (s, 12H, CH₃).

^{13}C NMR (100 MHz, D₂O, ppm) δ = 63.0 (–, 2C, CH₂), 50.3 (+, 4C, CH₃).

PCPCage (127)



In a vessel 4,7,12,15-tetra-((*E*)-vinyl-2'-pyridyl)[2.2]paracyclophane (100 mg, 161 μ mol, 1.00 equiv.) was dissolved in 12 mL of methanol. To this stirred and gently warmed solution was added *cis*-(tmen)Pd(ONO₂)₂ (112 mg, 322 μ mol, 2.00 equiv.)

dissolved in 12 mL of distilled water. Then the mixture was stirred at 60 °C for 12 h.

Mass spectrometry was detected after anion exchange, replacing nitro with iodide ions.

HRMS-ESI (m/z): $[M]^{4+}$, calc. for $C_{56}H_{68}N_8Pd_2$, 266.59/ 266.84; found: 266.59/ 266.84. $[M+I]^{3+}$, calc. for $C_{56}H_{68}N_8Pd_2I$, 397.76/ 398.09; found: 397.76/ 398.09. $[M+2I]^{2+}$, calc. for $C_{56}H_{68}N_8Pd_2I_2$, 660.09/ 660.59; found: 660.09/ 660.59. $[M+3I]^{2+}$, calc. for $C_{56}H_{68}N_8Pd_2I_3$, 1447.08/ 1448.08; found: 1447.08/ 1448.08.

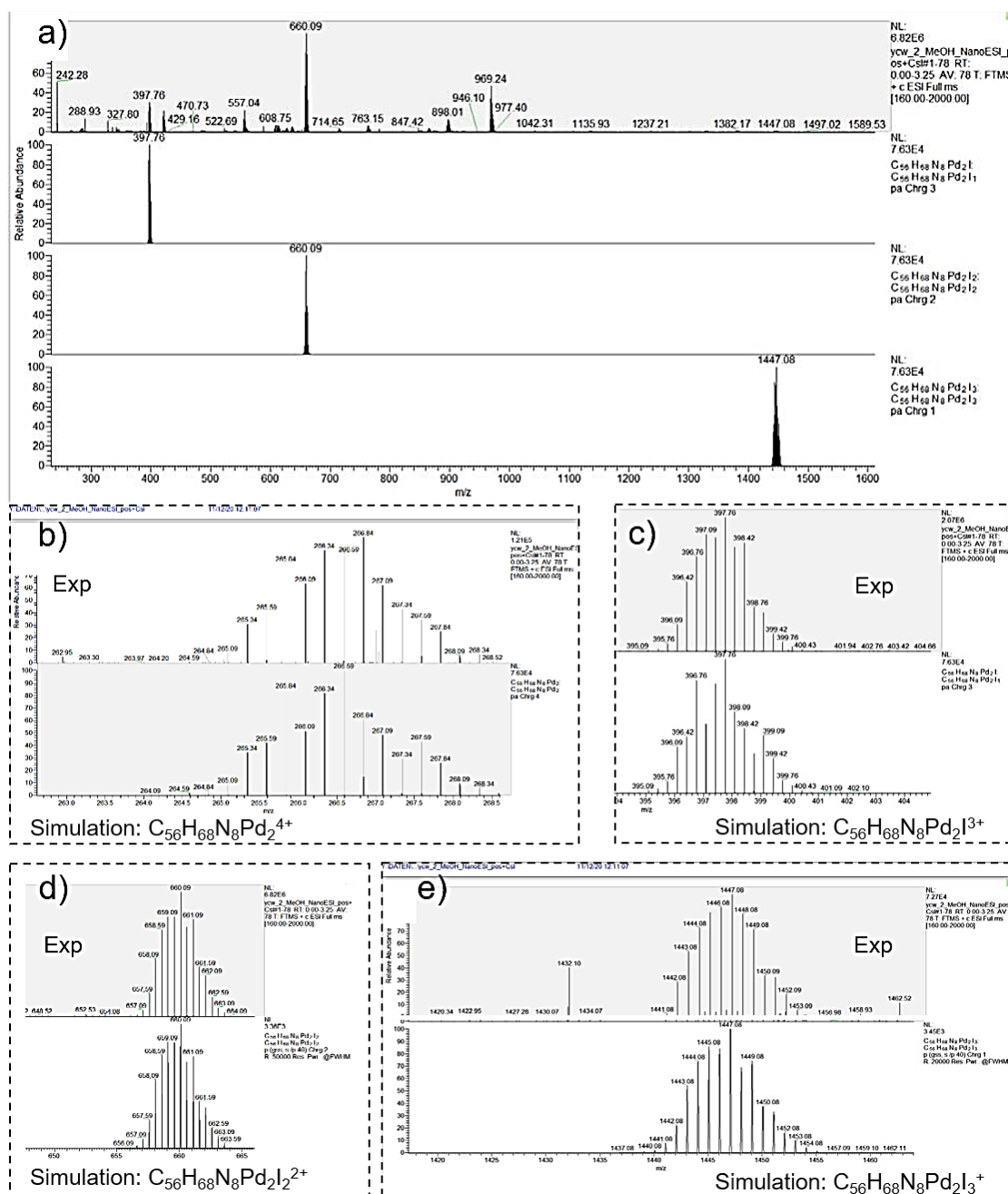


Figure 100. ESI mass spectra of PCPCage. (a) the peaks of $C_{56}H_{68}N_8Pd_2^{4+}$, (b) the peaks of $C_{56}H_{68}N_8Pd_2I^{3+}$, (c) the peaks of $C_{56}H_{68}N_8Pd_2I_2^{2+}$, (d) the peaks of $C_{56}H_{68}N_8Pd_2I_3^{2+}$. Results provided by Dr. Partick Weis.

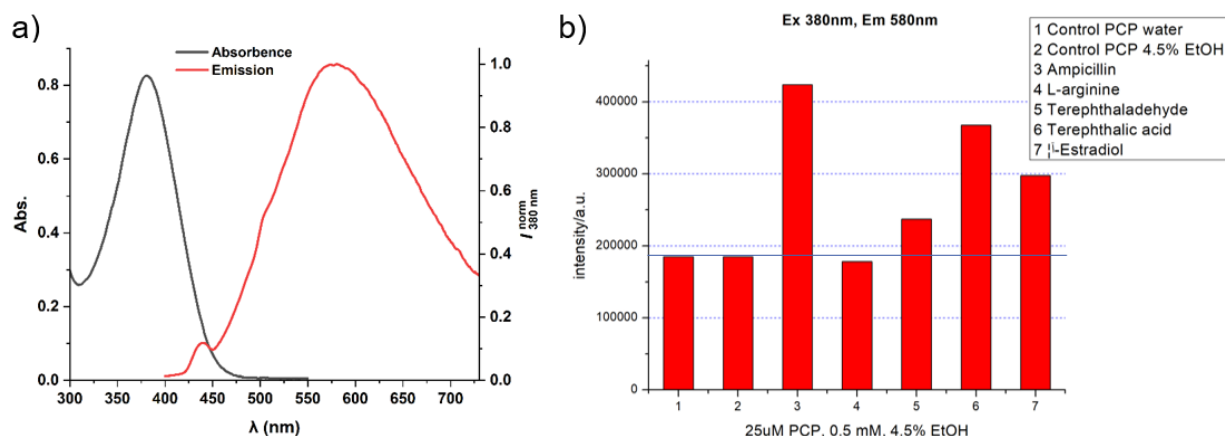
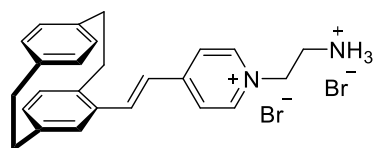
PCPBox-1 (118)

Figure 101. (a) Absorbance and fluorescence spectrum of **PCPBox-1** (25 μM) in water. (b) Fluorescence change in **PCPBox-1** solution (25 μM) with adding of samples (0.5 mM).

4-(*N*-(2-Ammonioethyl)-4'-pyridinium-(*E*)-vinyl)[2.2]paracyclophane bromide (128)

A solution of a mixture of 4-(*rac*)-4'-pyridylvinyl[2.2]paracyclophane (100 mg, 321 μmol , 1.00 equiv.) and 2-bromoethylamine hydrobromide (79.0 mg, 385 μmol , 1.20 equiv.) in EtOH (10 mL) was heated at 100 $^{\circ}\text{C}$ for 36 h. After the solution was cooled to 21 $^{\circ}\text{C}$, the precipitate was filtered off, washed with EtOH (3 \times 10 mL), and dried in air to yield the title compound as a yellow solid (85.0 mg, 165 μmol , 51%).

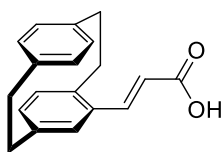
^1H NMR (400 MHz, DMSO- d_6 , ppm) δ = 8.92 (d, J = 6.7 Hz, 2H, H_{Py}), 8.45 (d, J = 6.5 Hz, 2H, H_{Py}), 8.06–7.96 (m, 4H, CH_3 , CH=CH), 7.33 (d, J = 16.1 Hz, 1H, CH=CH), 6.96 (d, J = 1.8 Hz, 1H, H_{Ar}), 6.66 (dd, J = 7.9, 1.7 Hz, 1H, H_{Ar}), 6.58 (d, J = 11.5 Hz, 3H, H_{Ar}), 6.48–6.38 (m, 2H, H_{Ar}), 4.78 (t, J = 5.7 Hz, 2H, CH_2), 3.84–3.74 (m, 1H, H_{PC}), 3.53 (t, J = 5.7 Hz, 2H, CH_2), 3.19–2.95 (m, 5H, H_{PC}), 2.95–2.85 (m, 2H, H_{PC}).

^{13}C NMR (100 MHz, DMSO- d_6 , ppm) δ = 159.1 (C_q , C_{Py}), 150.0 (+, 2C, C_{Py}), 146.5 (C_q , C_{Ar}), 145.5 (+, CH, C_{Ar}), 144.3 (C_q , C_{Ar}), 144.3 (+, CH, C_{Ar}), 144.1 (C_q , C_{Ar}), 140.5 (+, CH, C_{Ar}), 140.5 (+, CH, C_{Ar}), 140.0 (+, CH, C_{Ar}), 138.4 (+, CH, C_{Ar}), 138.3 (+, CH C_{Ar}), 136.8 (+, CH C_{Ar}), 136.2 (+, CH, C_{Ar}), 135.3 (+, CH, C_{Ar}), 129.3 (+, 2C, C_{Py}), 128.6 (+, CH, C_{Ar}), 62.1 (–, CH_2), 40.0 (–, CH_2), 40.0 (–, CH_2), 39.8 (–, CH_2), 38.4 (–, CH_2), 38.4 (–, CH_2).

MS (ESI, 70 eV, 20 $^{\circ}\text{C}$, %) m/z = 355/356 (100/27) [$\text{M}-\text{HBr}$] $^+$.

HRMS-ESI (m/z): [$\text{M}-\text{HBr}$] $^+$ calc. for $\text{C}_{25}\text{H}_{27}\text{N}_2$, 355.2169; found: 355.2161.

IR (ATR, $\tilde{\nu}$) = 2951 (w), 2925 (m), 2891 (w), 2854 (m), 2813 (w), 2800 (w), 2775 (w), 2713 (w), 2615 (w), 1643 (s), 1613 (vs), 1587 (m), 1517 (m), 1493 (m), 1483 (w), 1473 (w), 1439 (w), 1187 (s), 1174 (m), 1145 (m), 982 (m), 916 (w), 895 (w), 839 (m), 800 (m), 717 (s), 581 (w), 518 (s), 448 (w) cm^{-1} .

4-(E)-[2.2]paracyclophanyl acrylic acid (129)

Malonic acid (528 mg, 5.08 mmol, 1.20 equiv.), followed by formyl[2.2]paracyclophane (1.00 g, 4.23 mmol, 1.00 equiv.), pyridine (20 mL) and 3 drops of piperidine. The reaction was stirred and heated at 100 °C for 3 h. The reaction mixture was allowed to reach room temperature. The solvent was removed

under reduced pressure and the crude product was purified by flash column chromatography on silica gel using dichloromethane /methanol 20:1 to obtain the title compound (591 mg, 2.12 mmol, 50%) as white solid.

$R_f = 0.25$ (dichloromethane/methanol 20/1)

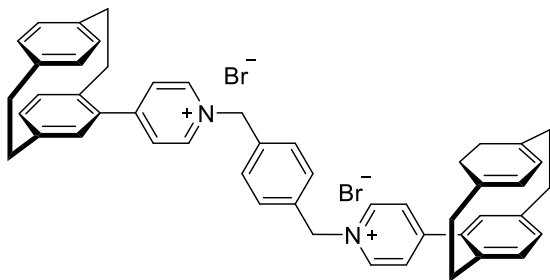
$^1\text{H NMR}$ (400 MHz, CDCl_3 , ppm) $\delta = 7.91$ (d, $J = 15.8$ Hz, 1H, CH=CH), 6.73 (d, $J = 1.9$ Hz, 1H, H_{Ar}), 6.63–6.50 (m, 5H, H_{Ar}), 6.44–6.40 (m, 1H, H_{Ar}), 6.30 (d, $J = 1.9$ Hz, 1H, CH=CH), 3.67–3.56 (m, 1H, H_{PC}), 3.26–2.84 (m, 7H, H_{PC}).

$^{13}\text{C NMR}$ (100 MHz, CDCl_3 , ppm) $\delta = 172.0$ (C_q , C_{Ar}), 144.7 (+, CH, CH=CH), 141.1 (C_q , C_{Ar}), 140.5 (C_q , C_{Ar}), 139.4 (C_q , C_{Ar}), 139.2 (C_q , C_{Ar}), 135.3 (+, CH, C_{Ar}), 135.0 (+, CH, C_{Ar}), 134.3 (C_q , C_{Ar}), 133.2 (+, CH, C_{Ar}), 133.0 (+, CH, C_{Ar}), 131.8 (+, CH, C_{Ar}), 131.4 (+, CH, C_{Ar}), 130.7 (+, CH, C_{Ar}), 116.9 (+, CH, CH=CH) 35.4 (–, CH_2), 35.2 (–, CH_2), 35.2 (–, CH_2), 33.8 (–, CH_2).

MS (ESI, 70 eV, 20 °C, %) $m/z = 278$ [M] $^+$, 104/105 (100/28) [C_8H_8] $^+$.

HRMS-ESI (m/z): [M] $^+$ calc. for $\text{C}_{19}\text{H}_{18}\text{O}_2$, 278.1307; found: 278.2538.

IR (ATR, $\tilde{\nu}$) = 2951 (w), 2924 (m), 2890 (w), 2850 (w), 2816 (w), 1683 (vs), 1623 (s), 1589 (m), 1414 (s), 1316 (m), 1295 (s), 1283 (s), 1245 (m), 1214 (s), 1184 (m), 1159 (m), 1143 (m), 1102 (w), 1082 (w), 976 (s), 939 (m), 918 (m), 901 (s), 881 (s), 866 (s), 798 (s), 772 (w), 747 (m), 718 (s), 690 (m), 683 (m), 642 (s), 599 (s), 581 (m), 548 (m), 535 (m), 518 (s), 506 (s), 483 (s), 459 (m), 446 (w), 433 (s), 425 (s), 409 (w), 398 (w), 377 (m) cm^{-1} .

Bis(4-(1,1'-(1,4-phenylenedi(methylene))-4'-pyridinium)[2.2]paracyclophane) bromide (130)

1,4-Bis(bromomethyl)benzene (379 mg, 1.44 mmol, 1.00 equiv.) and (*rac*)-4-pyridyl[2.2]paracyclophane (410 mg, 1.44 mmol, 1.00 equiv.) were dissolved in dry acetonitrile (12 mL) and stirred at 80 °C for 2 days. The reaction mixture was brought to room temperature. The solvent was removed under reduced pressure and the

crude product was purified by flash column chromatography on silica gel using dichloromethane /methanol 5:1 to obtain the title compound (163 mg, 195 μmol , 14%) as a light yellow solid.

$R_f = 0.1$ (dichloromethane /methanol 5/1)

^1H NMR (400 MHz, MeOD, ppm) δ = 9.10–9.06 (m, 4H, H_{Py}), 8.26–8.19 (m, 4H, H_{Py}), 7.76 (s, 4H, H_{Ar}), 6.87 (d, J = 1.6 Hz, 2H, H_{Ar}), 6.82–6.73 (m, 4H, H_{Ar}), 6.70–6.65 (m, 4H, H_{Ar}), 6.61 (dd, J = 8.0, 2.0 Hz, 2H, H_{Ar}), 6.44 (dd, J = 8.1, 2.0 Hz, 2H, H_{Ar}), 5.94 (s, 4H, CH_2), 3.42 (ddd, J = 13.6, 10.0, 3.5 Hz, 2H, H_{PC}), 3.15 (tdd, J = 13.7, 7.3, 4.4 Hz, 10H, H_{PC}), 2.96 (ddd, J = 13.4, 10.1, 3.3 Hz, 2H, H_{PC}), 2.65 (ddd, J = 13.8, 9.9, 5.3 Hz, 2H, H_{PC}).

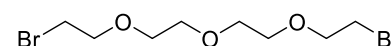
^{13}C NMR (100 MHz, MeOD, ppm) δ = 157.6 (C_q , 2C, C_{Py}), 144.3 (+, 4C, C_{Py}), 141.2 (C_q , 2C, C_{Ar}), 139.8 (C_q , 2C, C_{Ar}), 139.0 (C_q , 2C, C_{Ar}), 138.5 (C_q , 2C, C_{Ar}), 136.9 (+, 2C, C_{Ar}), 136.1 (+, 2C, C_{Ar}), 135.7 (C_q , 2C, C_{Ar}), 135.1 (C_q , 2C, C_{Ar}), 133.3 (+, 2C, C_{Ar}), 132.7 (+, 2C, C_{Ar}), 132.5 (+, 2C, C_{Ar}), 131.8 (C_q , 2C, C_{Ar}), 130.2 (+, 4C, C_{Ar}), 129.4 (+, 2C, C_{Ar}), 128.1 (+, 4C, C_{Py}), 62.8 (–, 2C, CH_2), 34.7 (–, 2C, CH_2), 34.6 (–, 2C, CH_2), 34.4 (–, 2C, CH_2), 33.5 (–, 2C, CH_2).

MS (ESI, 70 eV, 20 °C, %) m/z = 337/338 (100/55) $[\text{M}]^{2+}$, 753/755 (9/9) $[\text{M}-\text{Br}]^+$.

HRMS-ESI (m/z): $[\text{M}]^{2+}$ calc. for $\text{C}_{50}\text{H}_{46}\text{N}_2$, 337.1925/337.6842; found: 337.1823/337.6839. $[\text{M}+\text{Br}]^+$ calc. for $\text{C}_{50}\text{H}_{46}\text{N}_2^{79}\text{Br}$, 753.2839; found: 753.2836.

IR (ATR, $\tilde{\nu}$) = 3395 (m), 3387 (m), 3349 (w), 2922 (w), 1633 (vs), 1510 (m), 1502 (w), 1449 (m), 1213 (w), 1169 (m), 1156 (s), 854 (s), 803 (s), 772 (s), 734 (m), 718 (s), 704 (m), 683 (w), 664 (m), 640 (s), 618 (s), 591 (s), 574 (s), 558 (vs), 516 (vs), 503 (vs), 483 (vs), 446 (vs), 438 (vs), 429 (vs), 405 (vs), 398 (vs), 390 (vs), 382 (vs) cm^{-1} .

1-Bromo-2-(2-(2-(2-bromoethoxy)ethoxy)ethoxy)ethane (131)

 100 mL Dichloromethane was cooled to -78 °C using a mixture of dry ice/isopropanol. Under stirring NBS (4.89 g, 28.0 mmol, 2.50 equiv.) and triphenylphosphine (6.42 g, 28.0 mmol, 2.20 equiv.) were added. After 10 min, tetraethylene glycol (2.14 g, 1.90 mL, 11.0 mmol, 1.00 equiv.) was added, the solution was stirred for 16 h and the temperature was slowly increased to room temperature. The solvent was removed under reduced pressure and the crude product was purified by flash column chromatography on silica gel using cyclohexane/ethyl acetate 4:1 to obtain the title compound (2.94 g, 9.19 mmol, 83%) as light yellow liquid.

R_f = 0.45 (cyclohexane/ethyl acetate 4:1)

^1H NMR (400 MHz, CDCl_3 , ppm) δ = 3.82 (t, J = 6.3 Hz, 4H, CH_2), 3.68 (s, 8H, CH_2), 3.48 (t, J = 6.3 Hz, 4H, CH_2).

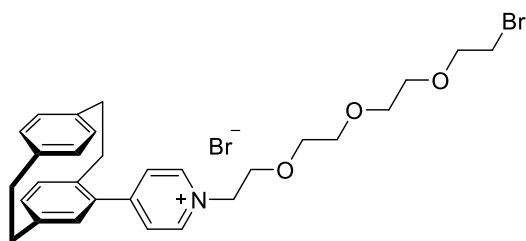
^{13}C NMR (100 MHz, CDCl_3 , ppm) δ = 71.2 (–, 2C, CH_2), 70.7 (–, 2C, CH_2), 70.6 (–, 2C, CH_2), 30.4 (–, 2C, CH_2).

MS (EI, 70 eV, 20 °C, %) m/z = 322/320/318 (49/100/52) $[\text{M}+\text{H}]^+$.

HRMS-EI (m/z): $[\text{M}+\text{H}]^+$ calc. for $\text{C}_8\text{H}_{17}^{79}\text{Br}_2\text{O}_3$, 320.9519/318.9539; found: 320.9515, 318.9536.

IR (ATR, $\tilde{\nu}$) = 2864 (m), 1350 (m), 1276 (s), 1101 (vs), 1040 (s), 1020 (s), 997 (s), 953 (m), 933 (m), 909 (m), 878 (m), 824 (w), 664 (m), 571 (s), 527 (w) cm^{-1} .

4-(2-(2-(2-(2-bromoethoxy)ethoxy)ethoxy)ethyl)pyridinium[2.2]paracyclophane bromide (132)



4-Pyridyl[2.2]paracyclophane (143 mg, 501 μmol , 1.00 equiv.) was added to a stirred solution of 1,11-dibromo-3,6,9-trioxaundecane (192 mg, 600 μmol , 1.20 equiv.) in refluxing acetonitrile (10 mL) contained in a vessel. After 3 h of heating, the mixture was left under

stirring for 16 h at room temperature. The solvent was removed under reduced pressure and the crude product was purified by flash column chromatography on silica gel using cyclohexane/ethyl acetate 4:1 to obtain the title compound (95.0 mg, 157 μmol , 31%) as a light yellow liquid.

R_f = 0.4 (dichloromethane/methanol 10:1)

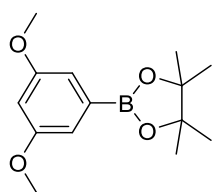
^1H NMR (400 MHz, CDCl_3 , ppm) δ = 9.56 (d, J = 6.2 Hz, 2H, H_{Py}), 7.99 (d, J = 6.1 Hz, 2H, H_{Py}), 6.69 (d, J = 4.4 Hz, 3H, H_{Ar}), 6.64 (dd, J = 7.8, 1.8 Hz, 1H, H_{Ar}), 6.58 (dd, J = 8.0, 1.9 Hz, 2H, H_{Ar}), 6.40 (dd, J = 8.0, 1.9 Hz, 1H, H_{Ar}), 5.24 (t, J = 4.2 Hz, 2H, CH_2), 4.14 (t, J = 4.6 Hz, 2H, CH_2), 3.80 (t, J = 5.9 Hz, 2H, CH_2), 3.75–3.68 (m, 2H, CH_2), 3.67–3.56 (m, 6H, CH_2), 3.46 (t, J = 5.9 Hz, 2H, CH_2), 3.31 (ddd, J = 13.7, 10.0, 3.6 Hz, 1H, H_{PC}), 3.24–3.05 (m, 5H, H_{PC}), 2.97 (ddd, J = 13.8, 10.1, 3.7 Hz, 1H, H_{PC}), 2.71 (ddd, J = 14.0, 9.9, 4.9 Hz, 1H, H_{PC}).

^{13}C NMR (100 MHz, CDCl_3 , ppm) δ = 157.1 (C_q , C_{Py}), 145.4 (+, 2C, C_{Py}), 141.3 (C_q , C_{Ar}), 139.8 (C_q , C_{Ar}), 139.0 (C_q , C_{Ar}), 138.2 (C_q , C_{Ar}), 137.1 (+, C_{Ar}), 136.3 (+, C_{Ar}), 135.7 (C_q , C_{Ar}), 133.6 (+, C_{Ar}), 132.9 (+, C_{Ar}), 132.5 (+, C_{Ar}), 132.0 (+, C_{Ar}), 129.8 (+, C_{Ar}), 127.3 (+, 2C, C_{Py}), 71.1 (–, CH_2), 70.6 (–, CH_2), 70.5 (–, CH_2), 70.3 (–, 2C, CH_2), 69.7 (–, CH_2), 60.4 (–, CH_2), 35.4 (–, CH_2), 35.2 (–, CH_2), 35.1 (–, CH_2), 34.0 (–, CH_2), 30.9 (–, CH_2).

MS (ESI, 70 eV, 20 $^\circ\text{C}$, %) m/z = 524/526 (99/100) $[\text{M}]^+$.

HRMS-ESI (m/z): $[\text{M}]^+$ calc. for $\text{C}_{29}\text{H}_{35}^{79}\text{BrNO}_3$, 524.1795; found: 524.1774.

IR (ATR, $\tilde{\nu}$) = 3422 (w), 3417 (w), 3408 (w), 3401 (w), 3383 (w), 3373 (w), 3359 (w), 3350 (w), 2924 (s), 2859 (m), 1635 (vs), 1513 (m), 1455 (m), 1349 (w), 1289 (w), 1279 (w), 1214 (w), 1181 (m), 1108 (vs), 1095 (vs), 1040 (m), 916 (w), 854 (s), 817 (w), 799 (m), 720 (m), 640 (m), 584 (w), 565 (m), 544 (w), 535 (w), 528 (w), 516 (m), 496 (w), 486 (m) cm^{-1} .

2-(3,5-dimethoxyphenyl)-4,4,5,5-tetramethyl-1,3,2 dioxaborolane (133)

1-Brom-3,5-dimethoxybenzol (1.00 g, 4.60 mmol, 1.00 equiv.), bis(pinacolato)diboron (1.40 g, 5.50 mmol, 1.20 equiv.), [1,1'-bis(diphenylphosphine)-ferrocene] dichloropalladium (II) (337 mg, 421 μ mol, 0.09 equiv.), and potassium acetate (903 mg, 9.20 mmol, 2.00 equiv.) were dissolved in degassed DMF (20 ml) under argon atmosphere. The reaction mixture was stirred and heated at 100 °C for 16 h.

After cooling to room temperature, the reaction mixture was added to water and then extracted with hexane. The organic layers were combined and washed with water and brine, then dried with $MgSO_4$ and evaporated under reduced pressure to give the desired product to yield a black solid (985 mg, 3.73 mmol, 81%).

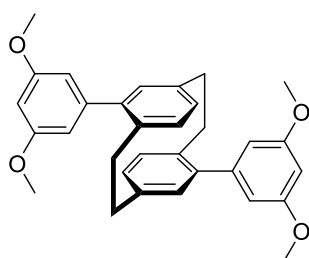
1H NMR (400 MHz, $CDCl_3$, ppm) δ = 6.95 (d, J = 2.4 Hz, 2H, H_{Ar}), 6.57 (t, J = 2.4 Hz, 1H, H_{Ar}), 3.81 (s, 6H, CH_3), 1.34 (s, 12H, CH_3).

^{13}C NMR (100 MHz, $CDCl_3$, ppm) δ = 160.4 (C_q , 2C, C_{Py}), 111.6 (+, 2C, C_{Ar}), 104.5 (+, C_{Ar}), 83.9 (C_q , 2C), 55.4 (+, 2C, CH_3), 24.9 (+, 4C, CH_3).

MS (ESI, 70 eV, 20 °C, %) m/z = 265/264/266 (100/24/15) $[M+H]^+$.

HRMS-ESI (m/z): $[M+H]^+$, calc. for $C_{14}H_{22}BO_4$, 265.1606; found: 265.1603.

IR (ATR, $\tilde{\nu}$) = 2975 (w), 2935 (w), 1587 (s), 1482 (w), 1448 (s), 1418 (s), 1390 (m), 1367 (vs), 1323 (vs), 1307 (vs), 1282 (m), 1269 (m), 1247 (w), 1217 (w), 1200 (vs), 1149 (vs), 1102 (s), 1062 (vs), 1043 (vs), 990 (w), 966 (s), 926 (s), 898 (s), 868 (w), 844 (vs), 832 (vs), 769 (w), 732 (m), 720 (s), 704 (vs), 671 (m), 657 (w), 612 (w), 579 (w), 534 (m), 503 (m), 477 (m), 438 (w), 426 (w), 401 (w) cm^{-1} .

4,16-Bis(3,5-dimethoxyphenyl)[2.2]paracyclophane (134)

A vessel was charged with 4,16-dibromo[2, 2]paracyclophane (400 mg, 1.10 mmol, 1.00 equiv.), 2-(3,5-dimethoxyphenyl)-4,4,5,5-tetramethyl-1,3,2-dioxaborolane (640 mg, 2.42 mmol, 2.20 equiv.), palladium-tetrakis(triphenylphosphine) (76.0 mg, 66 μ mol, 0.06 equiv.), potassium phosphate (560 mg, 2.64 mmol, 2.40 equiv.), dioxane (16.0 mL) and water (8 mL) under argon. The mixture was heated under reflux for 16 h. Then the

reaction mixture was cooled to room temperature, extracted with dichloromethane (3×50 mL), the extracts were dried with $MgSO_4$. The resulting crude product was purified by flash column chromatography on silica gel using cyclohexane/ dichloromethane 10:1 to yield a white solid (145 mg, 239 μ mol, 27%).

R_f = 0.37 (cyclohexane/ethyl acetate 10:1)

1H NMR (400 MHz, $CDCl_3$, ppm): δ = 6.70–6.59 (m, 10H, H_{Ar}), 6.50 (t, J = 2.2 Hz, 2H, H_{Ar}), 3.89 (s, 12H, CH_3), 3.54–3.43 (m, 2H, H_{PC}), 3.07–2.96 (m, 2H, H_{PC}), 2.85 (t, J = 7.2 Hz, 4H, H_{PC}).

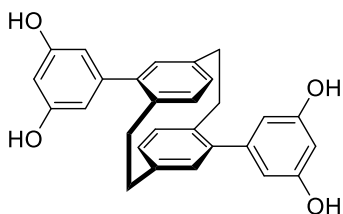
^{13}C NMR (100 MHz, CDCl_3 , ppm): $\delta = 160.8$ (C_q , 4C, C_{Ar}), 143.5 (C_q , 2C, C_{Ar}), 141.9 (C_q , 2C, C_{Ar}), 139.9 (C_q , 2C, C_{Ar}), 136.9 (C_q , 2C, C_{Ar}), 134.8 (+, 2C, C_{Ar}), 132.2 (+, 2C, C_{Ar}), 129.5 (+, 2C, C_{Ar}), 108.1 (+, 4C, C_{Ar}), 98.5 (+, 2C, C_{Ar}), 55.5(+, 4C, CH_3), 34.8 (-, 2C, CH_2), 33.9 (-, 2C, CH_2).

MS (ESI, 70 eV, 20 °C, %) $m/z = 481$ (28) $[\text{M}+\text{H}]^+$, 282 (100) $[\text{M}-\text{C}_{10}\text{H}_{14}\text{O}_4]^+$.

HRMS-ESI (m/z): $[\text{M}+\text{H}]^+$, calc. for $\text{C}_{32}\text{H}_{32}\text{O}_4$, 481.2373; found: 481.2374.

IR (ATR, $\tilde{\nu}$) = 2927 (m), 1587 (vs), 1451 (vs), 1422 (s), 1400 (m), 1346 (m), 1200 (vs), 1150 (vs), 1062 (vs), 1037 (vs), 924 (m), 882 (w), 850 (s), 832 (vs), 795 (s), 737 (m), 713 (s), 690 (s), 667 (s), 656 (m), 616 (m), 535 (m), 507 (s), 466 (m), 455 (w), 450 (w), 432 (m), 412 (m), 398 (w), 378 (w) cm^{-1} .

4,16-Bis(3,5-dihydroxyphenyl)[2, 2]paracyclophane (135)



4,16-Bis-(3,5-dimethoxyphenyl)[2.2]paracyclophane (122 mg, 250 μmol , 1.00 equiv.) was diluted in dichloromethane (4.00 mL) and added 1.0 M dichloromethane solution of boron tribromide (1.90 mL, 1.75 mmol, 3.50 equiv.) under argon and ice cooling. The mixture was stirred at room temperature for 3.5 h. The reaction mixture was added to cooled water

under ice-cooling and extracted with dichloromethane. The combined organic layers were washed with water and brine, dried over MgSO_4 , and concentrated under reduced pressure. The resulting residue was purified by flash column chromatography on silica gel using dichloromethane/methanol 20/1 to yield a white solid (35.8 mg, 84 μmol , 34%).

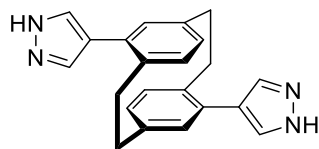
$R_f = 0.21$ (dichloromethane/methanol 20:1)

^1H NMR (400 MHz, DMSO-d_6 , ppm) $\delta = 9.29$ (s, 4H, OH), 6.61–6.53 (m, 4H, H_{Ar}), 6.49 (dd, $J = 7.8, 1.8$ Hz, 2H, H_{Ar}), 6.36 (d, $J = 2.2$ Hz, 4H, H_{Ar}), 6.23 (t, $J = 2.2$ Hz, 2H, H_{Ar}), 3.41–3.33 (m, 2H, H_{Ar}), 2.95 (ddd, $J = 13.4, 9.8, 4.3$ Hz, 2H, H_{PC}), 2.82 (ddd, $J = 13.8, 9.8, 4.0$ Hz, 2H, H_{PC}), 2.74–2.63 (m, 2H, H_{PC}).

^{13}C NMR (100 MHz, DMSO-d_6 , ppm) $\delta = 158.8$ (C_q , 4C, C_{Ar}), 143.3 (C_q , 2C, C_{Ar}), 142.4 (C_q , 2C, C_{Ar}), 139.7 (C_q , 2C, C_{Ar}), 136.7 (C_q , 2C, C_{Ar}), 135.0 (+, 2C, C_{Ar}), 132.2 (+, 2C, C_{Ar}), 129.3 (+, 2C, C_{Ar}), 108.1 (+, 4C, C_{Ar}), 101.7 (+, 2C, C_{Ar}), 34.7 (-, 2C, CH_2), 33.8 (-, 2C, CH_2).

HRMS-ESI (m/z): $[\text{M}+\text{H}]^+$, calc. for $\text{C}_{28}\text{H}_{25}\text{O}_4$, 425.1748; found: 425.1748.

IR (ATR, $\tilde{\nu}$) = 3318 (m), 3312 (m), 3301 (m), 3293 (m), 3288 (m), 3278 (m), 3271 (m), 3257 (m), 2932 (w), 1629 (w), 1587 (s), 1468 (w), 1452 (w), 1408 (w), 1339 (w), 1300 (m), 1221 (w), 1198 (m), 1156 (vs), 1105 (w), 1064 (w), 999 (vs), 960 (w), 948 (w), 846 (m), 829 (vs), 800 (m), 735 (m), 713 (m), 690 (s), 666 (m), 647 (m), 622 (m), 611 (m), 579 (m), 569 (m), 547 (m), 531 (m), 518 (s), 475 (m), 463 (m), 452 (m), 435 (m), 422 (m), 397 (m), 382 (m) cm^{-1} .

4,16-(4,4'-dipyrazole)[2,2]paracyclophane (136)

A vessel was charged with 4,16-dibromo[2, 2]paracyclophane (732 mg, 2.00 mmol, 1.00 equiv.), 4-(4,4,5,5-tetramethyl-1,3,2-dioxaborolan-2-yl)-1H-pyrazole (970 mg, 5.00 mmol, 3.50 equiv.), palladium-tetrakis(triphenylphosphine) (139 mg, 120 μ mol, 0.06 equiv.), potassium phosphate (1.06 g, 5.00 mmol, 2.50 equiv.), dioxane (16 mL) and water (8 mL) under argon. The mixture was heated under reflux for 16 h. The reaction mixture was then cooled to room temperature, and extracted with dichloromethane (3×50 mL), the extracts were dried with $MgSO_4$ and evaporated under reduced pressure. The resulting residue was purified by flash column chromatography on silica gel using dichloromethane/methanol 20:1 to 15:1 to yield a white solid (148 mg, 434 μ mol, 22%).

$R_f = 0.20$ (dichloromethane/methanol 15:1)

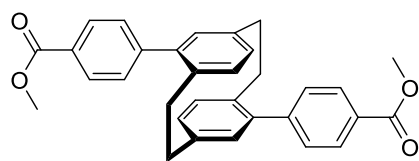
1H NMR (400 MHz, DMSO- d_6 , ppm) $\delta = 12.94$ (s, 2H, NH), 8.07–7.60 (m, 4H, H_{Ar}), 6.57 (t, $J = 9.0$ Hz, 2H, H_{Ar}), 6.50 (d, $J = 1.9$ Hz, 2H, H_{Ar}), 6.39 (dd, $J = 7.7, 1.9$ Hz, 2H, H_{Ar}), 3.61–3.44 (m, 2H, H_{PC}), 2.95–2.77 (m, 4H, H_{PC}), 2.64 (m, 2H, H_{PC}).

^{13}C NMR (100 MHz, DMSO- d_6 , ppm) $\delta = 140.3$ (C_q , 2C, C_{Ar}), 137.5 (C_q , 2C, C_{Ar}), 135.4 (+, 2C, C_{Ar}), 133.2 (+, 2C, C_{Ar}), 132.8 (+, 4C, C_{Ar}), 130.8 (C_q , 2C, C_{Ar}), 129.5 (+, 2C, C_{Ar}), 123.4 (C_q , 2C, C_{Ar}), 33.9 (–, 2C, CH_2), 33.6 (–, 2C, CH_2).

MS (EI, 70 eV, 20 $^\circ C$, %) $m/z = 341$ (45) $[M+H]^+$, 136/137/138 (100/75/44) $[M-C_{10}H_{14}O_4]^+$.

HRMS-EI (m/z): $[M+H]^+$, calc. for $C_{22}H_{20}N_4$, 341.1761; found: 341.2155.

IR (ATR, $\tilde{\nu}$) = 3111 (m), 2922 (vs), 2891 (s), 2849 (s), 2830 (s), 2748 (m), 1371 (m), 1145 (s), 1034 (s), 977 (m), 958 (s), 945 (vs), 863 (vs), 823 (vs), 735 (s), 714 (vs), 669 (vs), 629 (s), 497 (vs) cm^{-1} .

Dimethyl-4,4'-(4,16-[2.2]paracyclophanyl) dibenzoate (137)

A vessels was respectively charged with 4,16-dibromo[2,2]paracyclophane (1.10 g, 3.00 mmol, 1.00 equiv.), 4-methoxycarbonyl phenylboronic (2.67 g, 15.0 mmol, 5.00 equiv.), tetra(triphenylphosphine)palladium(0) (208 mg, 180 μ mol, 0.06 equiv.), potassium carbonate (3.18 g, 15.0 mmol, 5.00 equiv.), dioxane (16 mL) and water (8 mL) under argon. The mixture was heated under reflux for 16 h. The reaction mixture was then cooled to room temperature, and extracted with dichloromethane (3×40 mL). All of the extracts were dried with $MgSO_4$ and evaporated under reduced pressure. The resulting residue was purified by flash column chromatography on silica gel using cyclohexane/dichloromethane 1:1 to yield a light pale-yellow solid (1.05 mg, 2.20 mmol, 36.7%).

$R_f = 0.38$ (cyclohexane/ethyl acetate 20:1)

^1H NMR (400 MHz, CDCl_3 , ppm) δ = 8.17–8.01 (m, 4H, H_{Ar}), 7.76–7.59 (m, 4H, H_{Ar}), 6.84 (d, J = 7.8 Hz, 2H, H_{Ar}), 6.75 (d, J = 1.8 Hz, 2H, H_{Ar}), 6.50 (dd, J = 7.8, 1.8 Hz, 2H, H_{Ar}), 3.98 (s, 6H, CH_3), 3.32–3.28 (m, 2H, H_{PC}), 3.08 (ddd, J = 13.6, 9.9, 4.6 Hz, 2H, H_{PC}), 2.88 (ddd, J = 13.8, 10.0, 4.0 Hz, 2H, H_{PC}), 2.75–2.54 (m, 2H, H_{PC}).

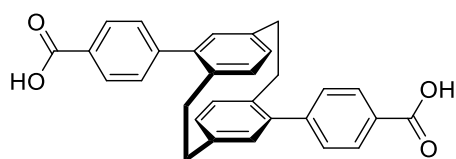
^{13}C NMR (100 MHz, CDCl_3 , ppm) δ = 167.1 (C_q , 2C, COO), 145.7 (C_q , 2C, C_{Ar}), 141.1 (C_q , 2C, C_{Ar}), 140.0 (C_q , 2C, C_{Ar}), 137.1 (C_q , 2C, C_{Ar}), 135.0 (+, 2C, C_{Ar}), 132.3 (+, 2C, C_{Ar}), 129.9 (+, 4C, C_{Ar}), 129.8 (+, 2C, C_{Ar}), 129.7 (+, 4C, C_{Ar}), 128.6 (C_q , 2C, C_{Ar}), 52.2 (+, 2C, CH_3), 34.7 (–, 2C, CH_2), 33.8 (–, 2C, CH_2).

MS (ESI, 70 eV, 20 °C, %) m/z = 477(35) $[\text{M}+\text{H}]^+$, 282/283(100/19) $[\text{M}-\text{C}_{10}\text{H}_{10}\text{O}_4]^+$, 223(23) $[\text{C}_{15}\text{H}_{11}\text{O}_2]^+$.

HRMS-ESI (m/z): $[\text{M}+\text{H}]^+$, calc. for $\text{C}_{32}\text{H}_{28}\text{O}_4$, 477.2060; found: 477.2055.

IR (ATR, $\tilde{\nu}$) = 2918 (m), 1714 (vs), 1604 (s), 1432 (m), 1272 (vs), 1188 (m), 1174 (s), 1115 (s), 1099 (vs), 1017 (s), 984 (m), 966 (m), 914 (s), 901 (m), 857 (vs), 843 (vs), 819 (s), 776 (vs), 731 (vs), 710 (vs), 687 (s), 660 (vs), 649 (s), 632 (m), 567 (s), 526 (m), 486 (vs), 446 (m), 384 (m) cm^{-1} .

4.4'-(4,16-[2.2]Paracyclophanyl) dibenzoic acid (138)



A 100 mL flask was charged with dimethyl 4.4'-(4,16-[2.2]paracyclophanyl) dibenzoate (920 mg, 1.93 mmol, 1.00 equiv.), 2 mL H_2O_2 solution, 2 M NaOH solution (50 mL) and 1,4-dioxane (50 mL). Then the reaction mixture was stirred at r.t.

for 5 h. The reaction mixture was acidified to pH~3 with 1 M HCl and then extracted with dichloromethane (3 \times 50 mL). The extracts were dried with MgSO_4 and evaporated under reduced pressure. The product was dried in the oven to a yield a white solid (882 mg, 1.97 mmol, 98%).

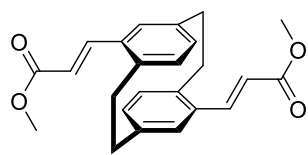
^1H NMR (400 MHz, $\text{DMSO}-d_6$, ppm) δ = 8.17–8.01 (m, 4H, H_{Ar}), 7.76–7.59 (m, 4H, H_{Ar}), 6.84 (d, J = 7.8 Hz, 2H, H_{Ar}), 6.75 (d, J = 1.8 Hz, 2H, H_{Ar}), 6.50 (dd, J = 7.8, 1.8 Hz, 2H, H_{Ar}), 3.32–3.28 (m, 2H, H_{PC}), 3.08 (ddd, J = 13.6, 9.9, 4.6 Hz, 2H, H_{PC}), 2.88 (ddd, J = 13.8, 10.0, 4.0 Hz, 2H, H_{PC}), 2.75–2.54 (m, 2H, H_{PC}).

^{13}C NMR (101 MHz, $\text{DMSO}-d_6$, ppm) δ = 167.8 (C_q , 2C, COO), 145.5 (C_q , 2C, C_{Ar}), 140.9 (C_q , 2C, C_{Ar}), 140.0 (C_q , 2C, C_{Ar}), 137.3 (C_q , 2C, C_{Ar}), 135.5 (+, 2C, C_{Ar}), 132.5 (+, 2C, C_{Ar}), 130.2 (+, 8C, C_{Ar}), 130.0 (+, 2C, C_{Ar}), 129.6 (C_q , 2C, C_{Ar}), 34.5 (–, 2C, CH_2), 33.7 (–, 2C, CH_2).

MS (ESI, 70 eV, 20 °C, %) m/z = 449 (5) $[\text{M}+\text{H}]^+$.

HRMS-ESI (m/z): $[\text{M}+\text{H}]^+$, calc. for $\text{C}_{30}\text{H}_{25}\text{O}_4$, 449.1747; found: 449.1740.

IR (ATR, $\tilde{\nu}$) = 2952 (w), 2941 (w), 2921 (w), 2893 (w), 2850 (w), 2669 (w), 2550 (w), 1674 (vs), 1605 (s), 1565 (w), 1424 (s), 1397 (w), 1319 (s), 1295 (vs), 1288 (vs), 1255 (m), 1181 (m), 1126 (m), 1112 (m), 1102 (w), 1016 (w), 943 (m), 915 (w), 870 (s), 844 (w), 809 (m), 781 (s), 738 (w), 720 (m), 687 (w), 657 (w), 551 (m), 482 (m) cm^{-1} .

Dimethyl-4,4'-(4,16-[2.2]paracyclophanyl) diacrylate (139)

A vessel was charged with 4,16-dibromo [2.2]paracyclophane (1.05 g, 2.87 mmol, 1.00 equiv.), methyl acrylate (1.24 g, 14.34 mmol, 5.00 equiv.), palladium acetate (32.0 mg, 143 μ mol, 0.05 equiv.), tetrapropylammonium bromide (1.91 g, 7.17 mmol, 2.50 equiv.), potassium carbonate (1.98 g, 14.34 mmol, 5.00 equiv.), and DMF (24 mL) under argon. The reaction mixture was heated at 100 °C for 16 hours. Then the reaction was cooled to room temperature, diluted with dichloromethane, and washed with brine. The organic layer was dried with Na₂SO₄ and concentrated. The residual liquid was precipitated with hexanes and collected by filtration. The resulting residue was purified by flash column chromatography on silica gel using cyclohexane/ethyl acetate 8:1 to yield a light yellow solid (45.0 mg, 120 μ mol, 4%).

R_f = 0.33 (dichloromethane)

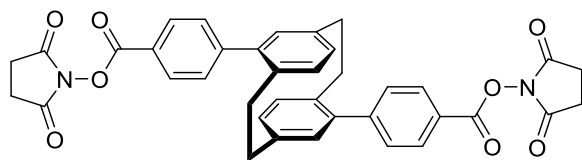
¹H NMR (400 MHz, CDCl₃, ppm) δ = 7.67 (d, J = 15.9 Hz, 2H, CH=CH), 6.70 (d, J = 1.9 Hz, 2H, H_{Ar}), 6.58–6.45 (m, 4H, H_{Ar}), 6.12 (d, J = 15.9 Hz, 2H, CH=CH), 3.77 (s, 6H, CH₃), 3.62–3.50 (m, 2H, H_{PC}), 3.11 (m, 2H, H_{PC}), 2.88–2.76 (m, 4H, H_{PC}).

¹³C NMR (100 MHz, CDCl₃, ppm) δ = 167.7 (C_q, 2C, COO), 141.5 (+, 2C, CH=CH), 140.3 (C_q, 2C, C_{Ar}), 139.9 (C_q, 2C, C_{Ar}), 135.3 (+, 2C, C_{Ar}), 134.6 (C_q, 2C, C_{Ar}), 134.2 (+, 2C, C_{Ar}), 128.7 (+, 2C, C_{Ar}), 117.8 (+, 2C, CH=CH), 51.7 (+, 2C, CH₃), 34.5 (–, 2C, CH₂), 33.7 (–, 2C, CH₂).

MS (ESI, 70 eV, 20 °C, %) m/z = 377/378 (100/25) [M+H]⁺.

HRMS-ESI (m/z): [M+H]⁺, calc. for C₂₄H₂₄O₄, 377.1747; found: 377.1777.

IR (ATR, $\tilde{\nu}$) = 2922 (m), 1704 (vs), 1625 (s), 1589 (m), 1431 (s), 1317 (s), 1271 (vs), 1224 (s), 1191 (vs), 1170 (vs), 1163 (vs), 1105 (m), 1035 (s), 1018 (s), 979 (vs), 959 (m), 911 (m), 878 (m), 866 (s), 858 (s), 837 (m), 795 (m), 783 (m), 748 (s), 703 (s), 684 (m), 646 (m), 599 (m), 584 (m), 482 (s), 404 (m) cm⁻¹.

Bis(2,5-dioxopyrrolidin-1-yl)-4,4'-(4,16-[2.2]paracyclophanyl) dibenzoate (140)

In an oven-dried flask, 4,4'-(4,16-[2.2]paracyclophane)dibenzoic acid (448 mg, 1.00 mmol, 1.00 equiv.) was dissolved in 20 mL of dry DMF and *N*-hydroxysuccinimide (253 mg, 2.20 mmol, 2.20 equiv.), EDC (422 mg, 2.20 mmol, 2.20 equiv.) was added while stirring at ice bath under argon. Then the mixture was stirred at room temperature for 16 hours. After solvent removal, the residue was dissolved in ethyl acetate and washed with Na₂CO₃ and NaCl solution. The organic phase was collected and evaporated under reduced pressure to yield a white solid (595 mg, 926 μ mol, 92%).

^1H NMR (400 MHz, DMSO- d_6 , ppm) δ = 8.26–8.21 (m, 4H, H_{Ar}), 7.88–7.82 (m, 4H, H_{Ar}), 6.90 (d, J = 7.8 Hz, 2H, H_{Ar}), 6.82 (d, J = 1.8 Hz, 2H, H_{Ar}), 6.55 (dd, J = 7.7, 1.8 Hz, 2H, H_{Ar}), 3.39–3.32 (m, 2H, H_{PC}), 3.11 (ddd, J = 13.8, 10.0, 4.6 Hz, 2H, H_{PC}), 2.95–2.88 (m, J = 16.4 Hz, 10H, H_{PC} , CH_2), 2.70–2.61 (m, 2H, H_{PC}).

^{13}C NMR (100 MHz, DMSO- d_6 , ppm) δ = 170.4 (C_q , 4C, COO), 161.8 (C_q , 2C, COO), 147.5 (C_q , 2C, C_{Ar}), 140.1 (C_q , 2C, C_{Ar}), 139.8 (C_q , 2C, C_{Ar}), 137.1 (C_q , 2C, C_{Ar}), 135.2 (+, 2C, C_{Ar}), 132.1 (+, 2C, C_{Ar}), 130.6 (+, 4C, C_{Ar}), 130.4 (+, 4C, C_{Ar}), 130.0 (+, 2C, C_{Ar}), 122.7 (C_q , 2C, C_{Ar}), 34.0 (–, 2C, CH_2), 33.2 (–, 2C, CH_2), 25.6 (–, 4C, CH_2).

MS (ESI, 70 eV, 20 °C, %) m/z = 681(44) $[\text{M}+\text{K}]^+$, 291(100) $[\text{C}_{17}\text{H}_9\text{NO}_4]^+$, 293(98) $[\text{C}_{17}\text{H}_{11}\text{NO}_4]^+$.

HRMS-ESI (m/z): $[\text{M}+\text{K}]^+$, calc. for $\text{C}_{38}\text{H}_{30}\text{KN}_2\text{O}_8$, 681.1634; found: 681.4193.

IR (ATR, $\tilde{\nu}$) = 2931 (w), 1772 (s), 1735 (vs), 1667 (w), 1604 (m), 1565 (w), 1425 (w), 1395 (w), 1364 (w), 1251 (w), 1232 (s), 1207 (vs), 1069 (s), 1047 (m), 1023 (w), 990 (vs), 956 (w), 914 (w), 856 (m), 836 (m), 810 (w), 765 (w), 732 (w), 720 (w), 701 (m), 647 (s), 605 (m), 575 (w), 564 (w), 524 (w), 504 (w), 480 (w), 426 (w), 398 (w), 387 (w) cm^{-1} .

5.5 Crystallographic Data

5.5.1 Crystallographic Data solved by Dr. Martin Nieger

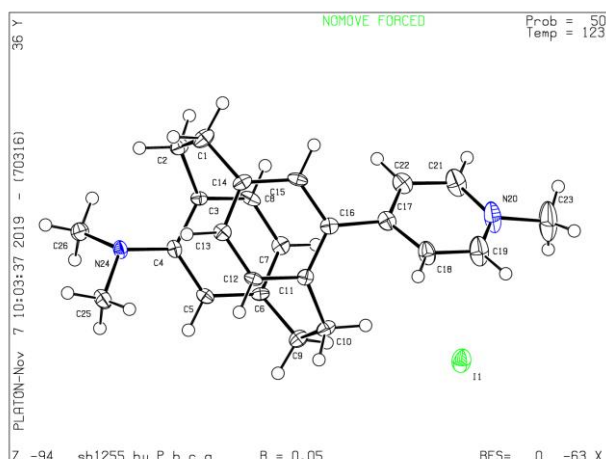
Crystal structures in this section were measured and solved by Dr. Martin Nieger at the University of Helsinki.

Table 6. Overview of the numbering and sample code of crystals.

Entry	Compound		Oxidation (V)
1	<i>(rac)</i> -4-(4'-pyridylvinyl)[2.2]paracyclophane	56	SB1304_HY
2	4-Pyridinium-16-(<i>N,N</i> -dimethylamino)-[2.2]paracyclophane iodide (pAMPCP)	94	SB1255_HY
3	4-(<i>N</i> -Methyl-4'-pyridinium)-16-(<i>E</i>)-Azophenyl- [2.2]paracyclophane iodide (AzoMVCP)	103	YCW97

SB1255_HY

YCW-38

methylpyridin-1-ium is slightly disordered

4-(4³-(dimethylamino)-1,4(1,4)-dibenzenacyclohexaphane-1²-yl)-1-methylpyridin-1-ium iodide – SB1255_HY

Crystal data

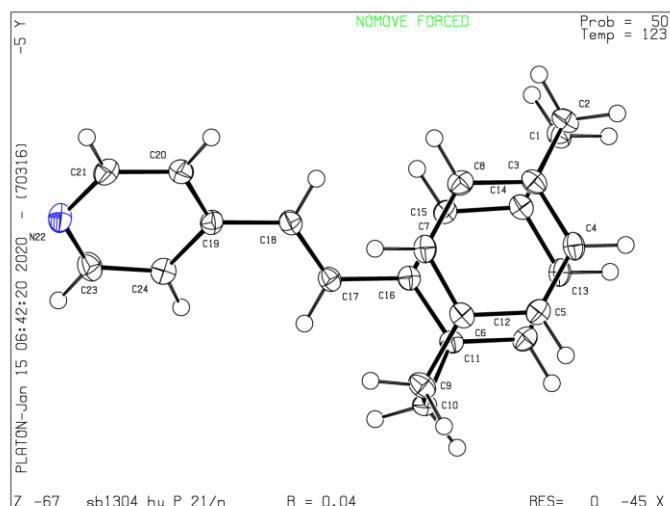
$C_{24}H_{27}N_2^+I^-$	$D_x = 1.530 \text{ Mg m}^{-3}$
$M_r = 470.37$	Cu $K\alpha$ radiation, $\lambda = 1.54178 \text{ \AA}$
Orthorhombic, <i>Pbca</i> (<i>no. 61</i>)	Cell parameters from 9968 reflections
$a = 8.0686 (4) \text{ \AA}$	$\theta = 3.8\text{--}72.1^\circ$
$b = 10.9948 (5) \text{ \AA}$	$\mu = 12.38 \text{ mm}^{-1}$
$c = 46.050 (2) \text{ \AA}$	$T = 123 \text{ K}$
$V = 4085.2 (3) \text{ \AA}^3$	Plates, yellow
$Z = 8$	$0.18 \times 0.12 \times 0.04 \text{ mm}$
$F(000) = 1904$	

Data collection

Bruker D8 VENTURE diffractometer with PhotonII CPAD detector	3979 reflections with $I > 2\sigma(I)$
Radiation source: INCOATEC microfocus sealed tube	$R_{\text{int}} = 0.026$
rotation in ϕ and ω , 0.5° , shutterless scans	$\theta_{\text{max}} = 72.2^\circ$, $\theta_{\text{min}} = 3.8^\circ$
Absorption correction: SADABS (Sheldrick, 2014) multi-scan	$h = -9 \rightarrow 9$
$T_{\text{min}} = 0.354$, $T_{\text{max}} = 0.623$	$k = -13 \rightarrow 12$
21854 measured reflections	$l = -56 \rightarrow 51$
4009 independent reflections	

Refinement

Refinement on F^2	Primary atom site location: dual
Least-squares matrix: full	Secondary atom site location: difference Fourier map
$R[F^2 > 2\sigma(F^2)] = 0.050$	Hydrogen site location: mixed
$wR(F^2) = 0.116$	H-atom parameters constrained
$S = 1.29$	$w = \frac{1}{[\sigma^2(F_o^2) + 33.150P]}$ where $P = (F_o^2 + 2F_c^2)/3$
4009 reflections	$(\Delta/\sigma)_{\text{max}} = 0.003$
247 parameters	$\Delta_{\text{max}} = 1.13 \text{ e \AA}^{-3}$
0 restraints	$\Delta_{\text{min}} = -1.26 \text{ e \AA}^{-3}$



SB1304_HY

YCW-164

(E)-4-(2-(1,4-dibenzenacyclohexaphane-1²-yl)vinyl)pyridine – SB1304_HY**Crystal data**

$C_{23}H_{21}N$	$F(000) = 664$
$M_r = 311.41$	$D_x = 1.295 \text{ Mg m}^{-3}$
Monoclinic, $P2_1/n$ (<i>no.14</i>)	Cu $K\alpha$ radiation, $\lambda = 1.54178 \text{ \AA}$
$a = 9.1926$ (8) \AA	Cell parameters from 9758 reflections
$b = 7.7306$ (6) \AA	$\theta = 6.9\text{--}72.2^\circ$
$c = 22.8689$ (19) \AA	$\mu = 0.56 \text{ mm}^{-1}$
$\beta = 100.571$ (2) $^\circ$	$T = 123 \text{ K}$
$V = 1597.6$ (2) \AA^3	Blocks, colourless
$Z = 4$	$0.36 \times 0.24 \times 0.12 \text{ mm}$

Data collection

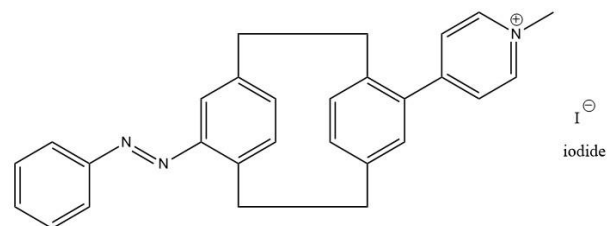
Bruker D8 VENTURE diffractometer with PhotonII CPAD detector	3088 reflections with $I > 2\sigma(I)$
Radiation source: INCOATEC microfocuss sealed tube	$R_{\text{int}} = 0.028$
rotation in ϕ and ω , 1° , shutterless scans	$\theta_{\text{max}} = 72.3^\circ$, $\theta_{\text{min}} = 3.9^\circ$
Absorption correction: multi-scan SADABS (Sheldrick, 2014)	$h = -11 \rightarrow 11$
$T_{\text{min}} = 0.838$, $T_{\text{max}} = 0.915$	$k = -9 \rightarrow 9$
26702 measured reflections	$l = -28 \rightarrow 28$
3140 independent reflections	

Refinement

Refinement on F^2	Primary atom site location: dual
Least-squares matrix: full	Secondary atom site location: difference Fourier map
$R[F^2 > 2\sigma(F^2)] = 0.040$	Hydrogen site location: difference Fourier map
$wR(F^2) = 0.103$	H-atom parameters constrained
$S = 1.04$	$w = \frac{1}{[\sigma^2(F_o^2) + (0.0464P)^2 + 0.8253P]}$ where $P = (F_o^2 + 2F_c^2)/3$
3140 reflections	$(\Delta/\sigma)_{\text{max}} = 0.001$
217 parameters	$\Delta_{\text{max}} = 0.26 \text{ e \AA}^{-3}$
0 restraints	$\Delta_{\text{min}} = -0.25 \text{ e \AA}^{-3}$

YCW97

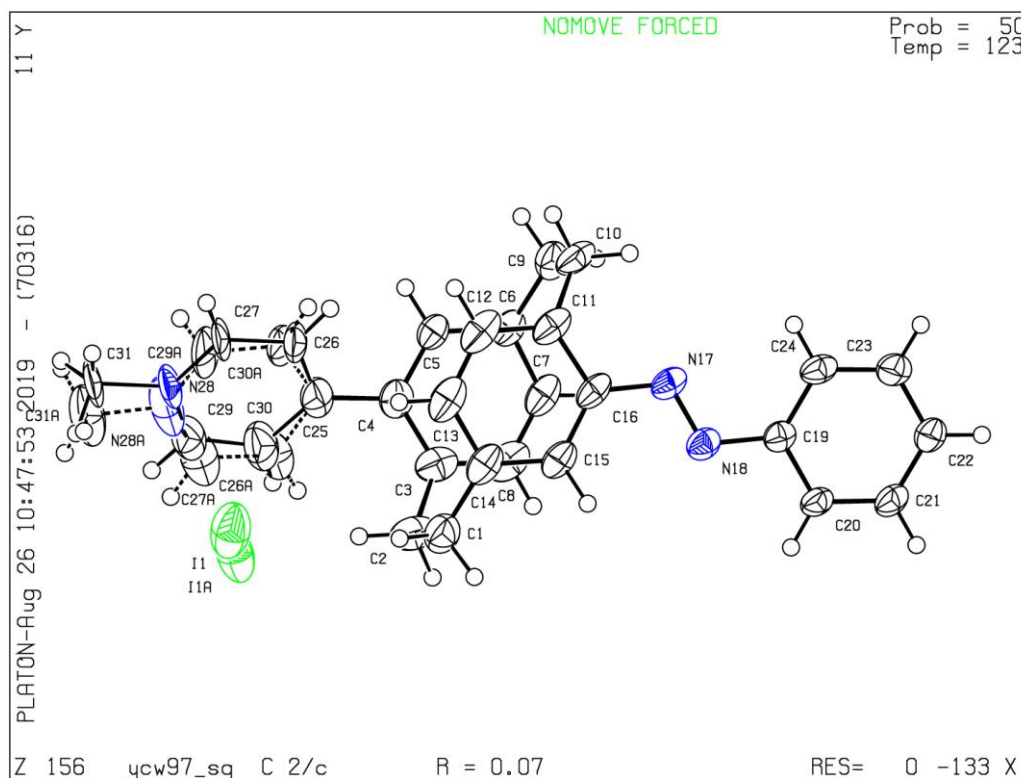
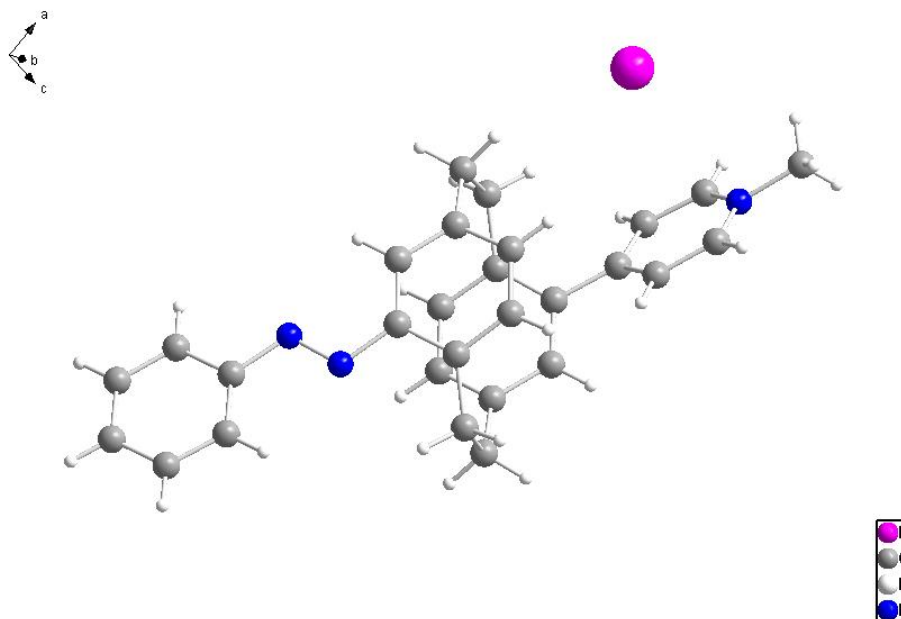
SB1255_HY_YCW97



structural proposal differs from suggestion

(*E*)-1-methyl-4-(4³-(phenyldiazenyl)-1,4(1,4)-dibenzenacyclohexane-1²-yl)pyridin-1-ium

in 2 voids 76 e- per void squeezed out (acetonitrile or dichloromethane)



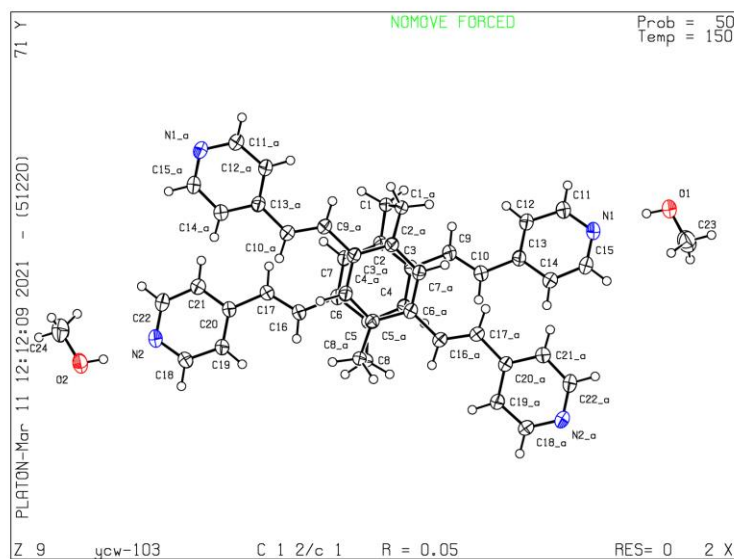
5.5.2 Crystallographic Data solved by Dr. Olaf Fuhr

Crystal structures in this section were measured and solved by Dr. Olaf Fuhr at the Institute of Nanotechnology (INT) at the Karlsruhe Institute of Technology.

Table 7. Overview of the numbering and sample code of crystals.

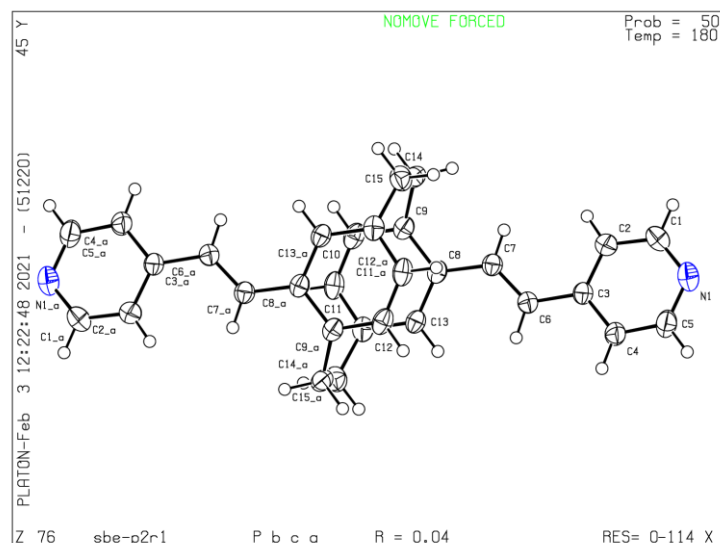
Entry	Compound		Oxidation (V)
1	4,7,12,15-Tetra-(4'-pyridyl-(E)-vinyl)[2.2]paracyclophane	91	YCW-106
2	4,16-Di-((E)-vinyl-4'-pyridyl)[2.2]paracyclophane	85	SBe-P2R1

4,7,12,15-Tetra-(4'-pyridyl-(E)-vinyl)[2.2]paracyclophane (91)_YCW-106



Crystal data and structure refinement for YCW-103.

Identification code	YCW-103
Empirical formula	C ₄₈ H ₅₂ N ₄ O ₄
Formula weight	748.93
Temperature/K	150.0
Crystal system	monoclinic
Space group	C2/c
a/Å	13.9463(4)
b/Å	20.2162(7)
c/Å	14.8817(4)
α/°	90
β/°	108.919(2)
γ/°	90
Volume/Å ³	3969.1(2)
Z	4
ρ _{calc} /cm ³	1.253
μ/mm ⁻¹	0.405
F(000)	1600.0
Crystal size/mm ³	0.16 × 0.14 × 0.12
Radiation	GaKα (λ = 1.34143)
2θ range for data collection/°	6.96 to 124.998
Index ranges	-15 ≤ h ≤ 18, -24 ≤ k ≤ 26, -19 ≤ l ≤ 10
Reflections collected	28257
Independent reflections	4795 [R _{int} = 0.0361, R _{sigma} = 0.0139]
Data/restraints/parameters	4795/0/257
Goodness-of-fit on F ²	1.039
Final R indexes [I ≥ 2σ (I)]	R ₁ = 0.0540, wR ₂ = 0.1451
Final R indexes [all data]	R ₁ = 0.0582, wR ₂ = 0.1487
Largest diff. peak/hole / e Å ⁻³	0.38/-0.39

4,16-Di-((*E*)-4'-pyridylvinyl[2.2]paracyclophane (85)_ SBe-P2R1**Crystal data and structure refinement for SBe-P2R1.**

Identification code	SBe-P2R1
Empirical formula	C ₃₀ H ₂₆ N ₂
Formula weight	414.53
Temperature/K	180.0
Crystal system	orthorhombic
Space group	Pbca
a/Å	11.4371(3)
b/Å	7.5642(2)
c/Å	24.9819(9)
α /°	90
β /°	90
γ /°	90
Volume/Å ³	2161.25(11)
Z	4
$\rho_{\text{calc}}/\text{cm}^3$	1.274
μ/mm^{-1}	0.365
F(000)	880.0
Crystal size/mm ³	0.14 × 0.12 × 0.02
Radiation	GaK α (λ = 1.34143)
2 θ range for data collection/°	12.33 to 124.974
Index ranges	-10 ≤ h ≤ 15, -10 ≤ k ≤ 8, -32 ≤ l ≤ 32
Reflections collected	26131
Independent reflections	2420 [R _{int} = 0.0223, R _{sigma} = 0.0079]
Data/restraints/parameters	2420/0/145
Goodness-of-fit on F ²	1.036
Final R indexes [I ≥ 2 σ (I)]	R ₁ = 0.0411, wR ₂ = 0.1087
Final R indexes [all data]	R ₁ = 0.0447, wR ₂ = 0.1112
Largest diff. peak/hole / e Å ⁻³	0.19/-0.18

5.6 Additional data

Data can be found on <https://suprabank.org/>.

Table 8. Comparison of experimentally obtained binding constants ($\log K_a$) for CB7 and CB8 complexes, corresponding to **Figure 32**.

Literature guests	detection method	CB7	CB8	Ref.
MPCP (38)	FL, water	< 4	13.52 ± 0.13	
MVCP (50)	FL, water	5.01 ± 0.01	12.97 ± 0.02	
DMPCP (51)	FL, water	< 4	15.06 ± 0.20	
DMVCP (52)	FL, water	4.67 ± 0.05	14.54 ± 0.11	
63a	NMR, buffer ^[a]	12.63 ± 0.1	8.91 ± 0.09	[148]
	Abs, water		9.43 ± 0.09	[149]
	FL, water,	14.23 ± 0.22		[150]
63b	ITC, water	10.4 ± 0.2	6.8 ± 0.2	[124]
63c	NMR, buffer ^[a]	12.23 ± 0.1	10.99 ± 0.11	[119c]
63d	NMR, buffer ^[a]	13.38 ± 0.11	10.34 ± 0.12	[102]
63e	NMR, buffer ^[a]	12.83 ± 0.10	12.23 ± 0.10	[102]
63f	NMR, buffer ^[a]	11.94 ± 0.10	9.15 ± 0.13	[102]
63g	NMR, buffer ^[a]	11.08 ± 0.11	9.49 ± 0.11	[102]
63h	NMR, buffer ^[a]	11.85 ± 0.10	11.45 ± 0.11	[102]
63i	NMR, buffer ^[a]	11.51 ± 0.11	11.04 ± 0.12	[102]
63j	NMR, buffer ^[a]	11.04 ± 0.12	9.11 ± 0.10	[102]
63k	NMR, buffer ^[a]	11.77 ± 0.11	9.0 ± 0.13	[102]
63l	NMR, buffer ^[a]	12.3 ± 0.09	9.3 ± 0.11	[102]
64a	NMR, buffer ^[a]	4.4 ± 0.07	11.64 ± 0.11	[102]
	FL, water		12.92 ± 0.02	[34]
64b	NMR, buffer ^[a]	6.08 ± 0.07	11.11 ± 0.12	[102]
64c	NMR, buffer ^[a]	4.81 ± 0.07	11.05 ± 0.11	[102]
65a	ITC, water	6.8 ± 0.2	6.6 ± 0.2	[124]
65b	ITC, water	7.1 ± 0.2	7.2 ± 0.2	[124]
65c	NMR, buffer ^[a]	11.90 ± 0.11	12.43 ± 0.12	[102]
65d	NMR, buffer ^[a]	15.28 ± 0.09	12.30 ± 0.13	[102]
65e	NMR, buffer ^[a]	11.11 ± 0.10	11.92 ± 0.12	[102]
65f	NMR, buffer ^[a]	15.28 ± 0.09	13.11 ± 0.10	[102]
66a	ITC, water	9.4 ± 0.2	6.6 ± 0.2	[124]
66b	ABS, water		9.84 ± 0.09	[149]
	ITC, water	12.38 ± 0.15		[150]
66c	ABS, water		9.91 ± 0.09	[149]
	ITC, water	12.61 ± 0.11		[150]
67a	ABS, water	7.85 ± 0.09	9.79 ± 0.09	[149]
67b	ABS, water	8.83 ± 0.09	7.73 ± 0.09	[149]
68a	FL, water	5.67 ± 0.07	9.79 ± 0.08	[151]
68b	FL, water	5.77 ± 0.07	8.3 ± 0.09	[151]
69a ^[d]	ITC, water		8.36 ± 0.2	[152]
	FL, water	5.93 ± 0.2		[153]
69b ^[d]	ITC, water		8.51 ± 0.2	[152]
	FL, water	6.68 ± 0.2		[153]
70 ^[d]	FL, water	6.28 ± 0.2	8.87 ± 0.2	[152]
71	ABS, water	5.16 ± 0.04	10.56 ± 0.09	[154]
72a	FL, water		8.19 ± 0.09	[155]
	ITC, water	7.05 ± 0.07		[151]
72b	FL, water		7.97 ± 0.09	[155]
	FL, water	4.77 ± 0.08		[124]
72c	ITC, water	< 3	8.04 ± 0.09	[151]
72d	ITC, water	< 3	6.15 ± 0.07	[151]
73	ITC, water	< 3	5.28 ± 0.09	[151]

74 ^[d]	ITC, complex ^[b]	5.52 ± 0.2	< 4	[156]
75a	ITC, complex ^[b]	5.58 ± 0.02	3.44 ± 0.03	[156]
75b	ITC, complex ^[b]	7.13 ± 0.01	4.20 ± 0.2	[156]
75c	ITC, complex ^[b]	7.32 ± 0.12	5.77 ± 0.01	[156]
76	ITC, complex ^[b]	7.29 ± 0.05	7.48 ± 0.04	[156]
77a	ITC, buffer ^[c]	6.82 ± 0.01	5.91 ± 0.02	[157]
77b	ITC, buffer ^[c]	7.15 ± 0.03	6.86 ± 0.08	[157]

[a] Data measured in 50 mM deuterated sodium acetate buffer, pH 4.7. [b] hydrochloric acid, pH 6.0. [c] 10 mM sodium phosphate, pH 7.0. [d] Typical errors are 0.2 in $\log K_a$ that are not referred in literature.

Table 9. Values collected during a literature survey on the entropic ($-\Delta S_{\text{exp}}$) and enthalpic (ΔH_{exp}) contributions for CB8 with high ($K_a > 10^6 \text{ M}^{-1}$), and low ($K_a < 10^6 \text{ M}^{-1}$) binders in solution, corresponding to **Figure 32**.

Literature guests	T (°C)	$\log K_a$	ΔH_{exp} (kcal mol ⁻¹)	$-\Delta S_{\text{exp}}$ (kcal mol ⁻¹)	Ref
63b	25	6.8 ± 0.2	-8.1 ± 0.4	-1.2 ± 0.8	[124]
65a	25	6.6 ± 0.2	-7.8 ± 0.4	-1.2 ± 0.8	[124]
65b	25	7.2 ± 0.2	-7.7 ± 0.4	-2.3 ± 0.8	[124]
66a	25	6.6 ± 0.2	-13.1 ± 0.4	-4.2 ± 0.8	[124]
68a	25	9.79 ± 0.08	-9.8 ± 0.5	-3.5 ± 0.6	[151]
68b	25	8.30 ± 0.09	-8.3 ± 0.5	-3.0 ± 0.6	[151]
69a	25	8.36 ± 0.2	-10.9 ± 0.4	0.5 ± 0.8	[152]
69b	25	8.51 ± 0.2	-12.3 ± 0.4	-0.7 ± 0.8	[152]
70	25	8.87 ± 0.2	-11.4 ± 0.4	0.7 ± 0.8	[152]
72a	25	8.19 ± 0.09	-9.0 ± 0.5	-1.0 ± 0.6	[151]
72c	25	8.04 ± 0.08	-9.7 ± 0.5	-1.3 ± 0.6	[151]
72d	25	6.15 ± 0.07	-7.1 ± 0.5	-1.2 ± 0.6	[151]
73	25	5.28 ± 0.09	-11.0 ± 0.5	3.8 ± 0.6	[151]
74	25	3.04 ± 0.2	-8.4 ± 0.4	4.3 ± 0.8	[156]
75a	25	3.44 ± 0.03	-5.0 ± 0.2	0.3 ± 0.3	[156]
75b	25	4.20 ± 0.2	-8.8 ± 0.4	3.1 ± 0.8	[156]
75c	25	5.77 ± 0.01	-9.5 ± 0.1	1.6 ± 0.1	[156]
76	25	7.48 ± 0.2	-8.8 ± 0.5	-1.4 ± 0.4	[156]
77a	27	5.93 ± 0.02	-3.7 ± 0.3	-4.5 ± 0.2	[157]
77b	27	6.86 ± 0.08	-5.6 ± 0.3	-3.8 ± 0.3	[157]
77c	27	6.86 ± 0.08	-5.6 ± 0.1	-3.8 ± 0.1	[157]
78a	25	5.58 ± 0.01	-3.5 ± 0.1	-4.1 ± 0.2	[158]
78b	25	6.02 ± 0.03	-5.4 ± 0.1	-2.7 ± 0.2	[158]
78c	25	6.68 ± 0.01	-8.5 ± 0.1	-0.6 ± 0.1	[158]
78d	25	6.44 ± 0.02	-9.2 ± 0.1	0.5 ± 0.1	[158]
78e	25	6.16 ± 0.01	-7.4 ± 0.1	-1.0 ± 0.2	[158]
78f	25	6.02 ± 0.02	-6.6 ± 0.1	-1.6 ± 0.2	[158]
79a	27	8.14 ± 0.02	-15.5 ± 0.4	4.3 ± 0.2	[159]
79b	27	4.47 ± 0.09	-9.5 ± 0.1	3.4 ± 0.1	[159]
79c	27	5.51 ± 0.07	-14.1 ± 0.5	6.5 ± 0.1	[159]
79d	27	6.70 ± 0.07	-15.5 ± 0.1	6.3 ± 0.2	[159]
79e	27	6.16 ± 0.04	-16.1 ± 0.2	7.7 ± 0.2	[159]
79f	27	6.54 ± 0.06	-16.1 ± 0.2	7.2 ± 0.1	[159]

[a] Data measured in hydrochloric acid, pH 6.0. [b] 50 mM Sodium acetate buffer. [c] 10 mM phosphate buffer, pH 7.0. [d] Typical errors are 0.2 in $\log K_a$, 0.4 kcal mol⁻¹ in ΔH and ΔG , and 0.8 kcal mol⁻¹ in $-\Delta S$ that are not referred in literature.

6 List of Abbreviations

δ	Chemical shift
λ	Wavelength
λ_{ex}	Excitation wavelength
ε	Molar attenuation coefficient
ΔH	Enthalpy
ΔS	Entropy
ΔG	Gibbs free energy
μg	Microgram
μL	Microliter
μmol	Micromole
μM	Micromolar
\AA	Angstrom
Abs	Absorption of a photon
ABA	Associative binding assays
Ar	Angstrom
Ala	Alanine
aq.	Aqueous
a.u.	Arbitrary unit
BC	Berberine chloride
Bu	Butyl
calc.	Calculated
cat.	Catalyst
conc.	Concentration
CB6	Cucurbit[6]urils
CB7	Cucurbit[7]urils
CB8	Cucurbit[8]urils
CB10	Cucurbit[10]urils
CB14	Cucurbit[14]urils
CB n	Cucurbit[n]urils
CD	Circular dichroism
CIP	Cahn-Ingold-Prelog
CT	Charge transfer

CVD	Chemical vapor deposition
CPL	Circularly polarized luminescence
d	Day
D	Dye
DBA	Direct binding assay
D ₂ O	Deuterium oxide
DCM	Dichloromethane
<i>de novo</i>	New
DFT	Density functional calculation
DMF	Dimethylformamide
DMSO	Dimethyl sulfoxide
DOX	Doxorubicin
dppf	1,1'-bis(diphenylphosphino)ferrocene
<i>ee</i>	Enantiomeric excess (% <i>ee</i>)
<i>e.g.</i>	<i>Exemplari gratia</i> , for example
equiv.	Equivalents
<i>et al.</i>	<i>Et alii</i> (and others)
<i>etc.</i>	<i>Et cetera</i> , and so forth
eq.	Equation
EI	Electron ionization
ESI	Electrospray ionization
FDCD	Fluorescence-detected circular dichroism
FL	Fluorescence
FRET	Fluorescence resonance energy transfer
g	Gram
G	Guest
GC	Gas chromatography
GDA	Guest displacement assays
h	Hour
H	Host
H ₂ O ₂	Hydrogen peroxide
HPLC	High performance liquid chromatography
HRMS	High resolution mass spectrometry
Hz	Hertz

<i>i.e.</i> ,	<i>Id est</i> , that is to say
I_{norm}	Normalized intensity
IC	Internal conversion
IDA	Indicator displacement assay
ITC	Isothermal titration calorimetry
IR	Infrared
ISC	Intersystem crossing
IUPAC	International union of pure and applied chemistry
J	Coupling constant
K	Kelvin
K_a	Association constant
K_{rel}	Competition release rates
L	Liter
LDA	Lithium diisopropylamide
Leu	Leucine
Lys	Lysine
$\log K_a$	Logarithm of association constant
<i>m</i>	<i>meta</i>
M	Mole
m	Multiplet
MeOH	Methanol
Mem	Memantine
mg	Milligram
mL	Millilitre
mM	Millimolar
MRI	Magnetic resonance imaging
mol	Molar
<i>n</i> BuLi	<i>N</i> -butyllithium
nm	Nanometer
MOF	Metal organic framework
NBS	<i>N</i> -bromosuccinimide
NMR	Nuclear magnetic resonance
NOESY	Nuclear overhauser enhancement and exchange spectroscopy
MS	Mass spectrometry

<i>o</i>	<i>ortho</i>
<i>p</i>	<i>para</i>
P	Phosphorescent
PB	Phosphate buffer
PBS	Phosphate buffered saline
PC	Packing coefficient
PCP	[2.2]paracyclophane
pH	Potential of hydrogen
Phe	Phenylalanine
PL	Photoluminescence
PTZ	Phenothiazine
ppm	Parts per million
Py	Pyridyl
q	Quartet
<i>R/R_p</i>	Right-handed (clockwise) stereodescriptor
r.t.	Room temperature
<i>rac</i>	Racemic
s	Seconds
s	Singlet
S ₁	First excited singlet state
<i>S/S_p</i>	Left-handed (clockwise) stereodescriptor
sat.	Saturated
SEM	Scanning electron microscopy
t	Triplet
T	Temperature
T ₁	First excited triplet state
^t Bu	<i>tert</i> -butyl
TFA	Trifluoroacetic acid
THF	Tetrahydrofuran
TLC	Thin layer chromatography
Tyr	Tyrosine
UV	Ultraviolet
UV-Vis	Ultraviolet-visible
vs	Very strong

vw	Very weak
VR	Vibrational relaxation
w	Weak
W	Watt
wt%	Weight percent

7 Bibliography

- [1] B. L. Feringa, *Angew. Chem. Int. Ed.* **2017**, *56*, 11060-11078.
- [2] D. J. Cram, in *Cyclophanes*, Academic Press, **1983**, pp. 1-21.
- [3] H. Hopf, *Angew. Chem. Int. Ed.* **2008**, *47*, 9808-9812.
- [4] C. Brown, A. Farthing, *Nature* **1949**, *164*, 915-916.
- [5] D. J. Cram, H. Steinberg, *J. Am. Chem. Soc.* **1951**, *73*, 5691-5704.
- [6] K. L. Noble, H. Hopf, M. Jones Jr, S. L. Kammula, *Angewandte Chemie International Edition in English* **1978**, *17*, 602-602.
- [7] B. S. Moore, J. L. Chen, G. M. Patterson, R. E. Moore, L. S. Brinen, Y. Kato, J. Clardy, *J. Am. Chem. Soc.* **1990**, *112*, 4061-4063.
- [8] B. Odell, M. V. Reddington, A. M. Slawin, N. Spencer, J. F. Stoddart, D. J. Williams, *Angewandte Chemie International Edition in English* **1988**, *27*, 1547-1550.
- [9] R. Boyd, *Tetrahedron* **1966**, *22*, 119-122.
- [10] D. J. Cram, N. L. Allinger, H. Steinberg, *J. Am. Chem. Soc.* **1954**, *76*, 6132-6141.
- [11] H. Hope, J. Bernstein, K. Trueblood, *Acta Crystallographica Section B: Structural Crystallography and Crystal Chemistry* **1972**, *28*, 1733-1743.
- [12] D. J. Cram, J. M. Cram, *Container molecules and their guests*, Royal Society of Chemistry, **1997**.
- [13] M. Szwarc, *The Journal of Chemical Physics* **1948**, *16*, 128-136.
- [14] H. Winberg, F. Fawcett, W. Mochel, C. Theobald, *J. Am. Chem. Soc.* **1960**, *82*, 1428-1435.
- [15] H.-F. Chow, K.-H. Low, K. Y. Wong, *Synlett* **2005**, *2005*, 2130-2134.
- [16] F. Vögtle, L. Schunder, *Chem. Ber.* **1969**, *102*, 2677-2683.
- [17] T. Otsubo, V. Boekelheide, *Tetrahedron Lett.* **1975**, *16*, 3881-3884.
- [18] M. Montanari, A. Bugana, A. K. Sharma, D. Pasini, *Org. Biomol. Chem.* **2011**, *9*, 5018-5020.
- [19] F. Vögtle, P. Neumann, *Tetrahedron Lett.* **1969**, *10*, 5329-5334.
- [20] R. S. Cahn, C. Ingold, V. Prelog, *Angewandte Chemie International Edition in English* **1966**, *5*, 385-415.
- [21] P. Mata, A. M. Lobo, C. Marshall, A. P. Johnson, *Journal of Chemical Information and Computer Sciences* **1994**, *34*, 491-504.
- [22] H. J. Reich, D. J. Cram, *J. Am. Chem. Soc.* **1969**, *91*, 3527-3533.
- [23] Y. L. Yeh, W. F. Gorham, *The Journal of Organic Chemistry* **1969**, *34*, 2366-2370.
- [24] H. J. Reich, D. J. Cram, *J. Am. Chem. Soc.* **1969**, *91*, 3517-3526.
- [25] O. R. David, *Tetrahedron* **2012**, *68*, 8977-8993.
- [26] A. Pelter, B. Mootoo, A. Maxwell, A. Reid, *Tetrahedron Lett.* **2001**, *42*, 8391-8394.

- [27] D. J. Cram, J. M. Cram, *Acc. Chem. Res.* **1971**, *4*, 204-213.
- [28] M. Stöbбе, O. Reiser, R. Näder, A. de Meijere, *Chem. Ber.* **1987**, *120*, 1667-1674.
- [29] Z. Hassan, E. Spuling, D. M. Knoll, S. Bräse, *Angew. Chem. Int. Ed.* **2020**, *59*, 2156-2170.
- [30] aS. E. Gibson, J. D. Knight, *Org. Biomol. Chem.* **2003**, *1*, 1256-1269; bJ. Paradies, *Synthesis* **2011**, *2011*, 3749-3766; cZ. Hassan, E. Spuling, D. M. Knoll, J. Lahann, S. Bräse, *Chem. Soc. Rev.* **2018**, *47*, 6947-6963.
- [31] aK. C. K. Cheng, M. A. Bedolla-Pantoja, Y. K. Kim, J. V. Gregory, F. Xie, A. de France, C. Hussal, K. Sun, N. L. Abbott, J. Lahann, *Science* **2018**, *362*, 804-808; bH. Y. Chen, J. Lahann, *Langmuir* **2011**, *27*, 34-48; cY. Elkasabi, J. Lahann, *Macromol. Rapid Commun.* **2009**, *30*, 57-63.
- [32] V. Rozenberg, E. Sergeeva, H. Hopf, *Modern cyclophane chemistry* **2004**, 435-462.
- [33] aE. Elacqua, M. Gregor, *Angew. Chem., Int. Ed. Engl.* **2019**, *58*, 9527-9532; bY. Morisaki, Y. Chujo, *Angew. Chem., Int. Ed. Engl.* **2006**, *45*, 6430-6437; cY. Morisaki, Y. Chujo, *Bull. Chem. Soc. Jpn.* **2009**, *82*, 1070-1082; dY. Morisaki, Y. Chujo, *Macromolecules* **2003**, *36*, 9319-9324; eG. P. Bartholomew, G. C. Bazan, *Acc. Chem. Res.* **2001**, *34*, 30-39; fM. Hasegawa, K. Kobayakawa, H. Matsuzawa, T. Nishinaga, T. Hirose, K. Sako, Y. Mazaki, *Chem. Eur. J.* **2017**, *23*, 3267-3271.
- [34] S. Sinn, E. Spuling, S. Bräse, F. Biedermann, *Chem. Sci.* **2019**, *10*, 6584-6593.
- [35] Z. Hassan, S. Bräse, *Chem. Eur. J.* **2021**, *27*, 15021-15027.
- [36] Z. Hassan, E. Spuling, D. M. Knoll, S. Bräse, *Angew. Chem., Int. Ed.* **2020**, *59*, 2156-2170.
- [37] Z. Hassan, E. Spuling, D. M. Knoll, J. Lahann, S. Bräse, *Chem. Soc. Rev.* **2018**, *47*, 6947-6963.
- [38] aS. Dahmen, S. Bräse, *J. Am. Chem. Soc.* **2002**, *124*, 5940-5941; bN. Hermanns, S. Dahmen, C. Bolm, S. Bräse, *Angew. Chem.* **2002**, *114*, 3844-3846.
- [39] C. Zippel, Z. Hassan, A. Q. Parsa, J. Hohmann, S. Bräse, *Adv. Synth. Catal.* **2021**, *363*, 2861-2865.
- [40] D. Varadharajan, K. Nayani, C. Zippel, E. Spuling, K. C. Cheng, S. Sarangarajan, S. Roh, J. Kim, V. Trouillet, S. Bräse, *Adv. Mater.* **2022**, *34*, 2108386.
- [41] aY. Morisaki, Y. Chujo, *Macromolecules* **2003**, *36*, 9319-9324; bY. Morisaki, Y. Chujo, *Angew. Chem. Int. Ed.* **2006**, *45*, 6430-6437; cE. Elacqua, M. Gregor, *Angew. Chem. Int. Ed.* **2019**, *58*, 9527-9532.
- [42] aG. S. Papaefstathiou, T. Frišćić, L. R. MacGillivray, *J. Am. Chem. Soc.* **2005**, *127*, 14160-14161; bW. Gong, H. Xie, K. B. Idrees, F. A. Son, Z. Chen, F. Sha, Y. Liu, Y. Cui, O. K. Farha, *J. Am. Chem. Soc.* **2022**, *144*, 1826-1834; cX. Xue, J. Wang, Q. Zhu, Y. Xue, H. Liu, *Dalton Transactions* **2021**, *50*, 1374-1383.
- [43] J. H. Burroughes, D. D. Bradley, A. Brown, R. Marks, K. Mackay, R. H. Friend, P. L. Burns, A. B. Holmes, *nature* **1990**, *347*, 539-541.
- [44] U. H. Bunz, *Chem. Rev.* **2000**, *100*, 1605-1644.
- [45] H. Hopf, R. Gleiter, *Modern cyclophane chemistry*, John Wiley & Sons, **2006**.
- [46] aM. Gon, H. Kozuka, Y. Morisaki, Y. Chujo, *Asian Journal of Organic Chemistry* **2016**, *5*, 353-359; bM. Gon, Y. Morisaki, Y. Chujo, *Journal of Materials Chemistry C* **2015**, *3*, 521-529; cM. Hasegawa, Y. Ishida, H. Sasaki, S. Ishioka, K. Usui, N. Hara, M. Kitahara, Y. Imai, Y. Mazaki, *Chem. Eur. J.* **2021**, *27*, 16225-16231.
- [47] K. J. Weiland, N. Münch, W. Gschwind, D. Häussinger, M. Mayor, *Helv. Chim. Acta* **2019**, *102*, e1800205.

- [48] aD. J. Cram, *Angewandte Chemie International Edition in English* **1988**, *27*, 1009-1020; bC. J. Pedersen, *Angewandte Chemie International Edition in English* **1988**, *27*, 1021-1027; cJ. M. Lehn, *Angewandte Chemie International Edition in English* **1988**, *27*, 89-112.
- [49] P. Pfeiffer, *Organische Molekülverbindungen, Vol. 11*, F. Enke, **1927**.
- [50] J.-M. Lehn, *Science* **1993**, *260*, 1762-1763.
- [51] aH. J. Schneider, *Angew. Chem. Int. Ed.* **2009**, *48*, 3924-3977; bF. Biedermann, H.-J. r. Schneider, *Chem. Rev.* **2016**, *116*, 5216-5300.
- [52] aD. B. Amabilino, D. K. Smith, J. W. Steed, *Chem. Soc. Rev.* **2017**, *46*, 2404-2420; bW.-C. Geng, J. L. Sessler, D.-S. Guo, *Chem. Soc. Rev.* **2020**, *49*, 2303-2315; cD. A. Uhlenheuer, K. Petkau, L. Brunsveld, *Chem. Soc. Rev.* **2010**, *39*, 2817-2826; dM. J. Webber, R. Langer, *Chem. Soc. Rev.* **2017**, *46*, 6600-6620; eM. J. Webber, E. A. Appel, E. Meijer, R. Langer, *Nature materials* **2016**, *15*, 13-26.
- [53] aJ. P. Sauvage, *Angew. Chem. Int. Ed.* **2017**, *56*, 11080-11093; bJ. F. Stoddart, *Angew. Chem. Int. Ed.* **2017**, *56*, 11094-11125.
- [54] E. R. Kay, D. A. Leigh, F. Zerbetto, *Angew. Chem. Int. Ed.* **2007**, *46*, 72-191.
- [55] L. Brunsveld, B. J. Folmer, E. W. Meijer, R. P. Sijbesma, *Chem. Rev.* **2001**, *101*, 4071-4098.
- [56] Q. Wang, J. L. Mynar, M. Yoshida, E. Lee, M. Lee, K. Okuro, K. Kinbara, T. Aida, *Nature* **2010**, *463*, 339-343.
- [57] aM. Fujita, D. Oguro, M. Miyazawa, H. Oka, K. Yamaguchi, K. Ogura, *Nature* **1995**, *378*, 469-471; bM. Yoshizawa, J. K. Klosterman, M. Fujita, *Angew. Chem. Int. Ed.* **2009**, *48*, 3418-3438.
- [58] H.-J. Schneider, A. K. Yatsimirsky, *Chem. Soc. Rev.* **2008**, *37*, 263-277.
- [59] aJ. Wankar, N. G. Kotla, S. Gera, S. Rasala, A. Pandit, Y. A. Rochev, *Adv. Funct. Mater.* **2020**, *30*, 1909049; bA. S. Braegelman, M. J. Webber, *Theranostics* **2019**, *9*, 3017.
- [60] aM. C.-L. Yeung, V. W.-W. Yam, *Chem. Soc. Rev.* **2015**, *44*, 4192-4202; bS. K. Sahoo, D. Sharma, R. K. Bera, G. Crisponi, J. F. Callan, *Chem. Soc. Rev.* **2012**, *41*, 7195-7227.
- [61] aF. L. Dickert, A. Haunschild, *Adv. Mater.* **1993**, *5*, 887-895; bA. Karmakar, P. Samanta, A. V. Desai, S. K. Ghosh, *Acc. Chem. Res.* **2017**, *50*, 2457-2469.
- [62] aX. Yang, D. Yuan, J. Hou, A. C. Sedgwick, S. Xu, T. D. James, L. Wang, *Coord. Chem. Rev.* **2021**, *428*, 213609; bY. Takashima, A. Harada, *Journal of Inclusion Phenomena and Macrocyclic Chemistry* **2017**, *88*, 85-104.
- [63] R. Behrend, E. Meyer, F. Rusche, *Justus Liebigs Annalen der Chemie* **1905**, *339*, 1-37.
- [64] W. Freeman, W. Mock, N. Shih, *J. Am. Chem. Soc.* **1981**, *103*, 7367-7368.
- [65] aJ. Kim, I.-S. Jung, S.-Y. Kim, E. Lee, J.-K. Kang, S. Sakamoto, K. Yamaguchi, K. Kim, *J. Am. Chem. Soc.* **2000**, *122*, 540-541; bA. Day, A. P. Arnold, R. J. Blanch, B. Snushall, *The Journal of organic chemistry* **2001**, *66*, 8094-8100.
- [66] X. J. Cheng, L. L. Liang, K. Chen, N. N. Ji, X. Xiao, J. X. Zhang, Y. Q. Zhang, S. F. Xue, Q. J. Zhu, X. L. Ni, *Angew. Chem.* **2013**, *125*, 7393-7396.
- [67] W. H. Huang, P. Y. Zavalij, L. Isaacs, *Angew. Chem. Int. Ed.* **2007**, *46*, 7425-7427.
- [68] aH. Cong, X. L. Ni, X. Xiao, Y. Huang, Q.-J. Zhu, S.-F. Xue, Z. Tao, L. F. Lindoy, G. Wei, *Org. Biomol. Chem.* **2016**, *14*, 4335-4364; bS. Zhang, Z. Domínguez, K. I. Assaf, M. Nilam, T. Thiele, U. Pischel, U. Schedler, W.

- M. Nau, A. Hennig, *Chem. Sci.* **2018**, *9*, 8575-8581; cJ. Lagona, P. Mukhopadhyay, S. Chakrabarti, L. Isaacs, *Angew. Chem. Int. Ed.* **2005**, *44*, 4844-4870.
- [69] aP. Germain, J. Letoffe, M. Merlin, H. Buschmann, *Thermochim. Acta* **1998**, *315*, 87-92; bJ. W. Lee, S. Samal, N. Selvapalam, H.-J. Kim, K. Kim, *Acc. Chem. Res.* **2003**, *36*, 621-630.
- [70] M. A. Rankin, B. D. Wagner, *Supramol. Chem.* **2004**, *16*, 513-519.
- [71] J. Mohanty, W. M. Nau, *Angew. Chem.* **2005**, *117*, 3816-3820.
- [72] F. Biedermann, O. A. Scherman, *The Journal of Physical Chemistry B* **2012**, *116*, 2842-2849.
- [73] C. Márquez, R. R. Hudgins, W. M. Nau, *J. Am. Chem. Soc.* **2004**, *126*, 5806-5816.
- [74] aW. L. Mock, N. Y. Shih, *The Journal of Organic Chemistry* **1986**, *51*, 4440-4446; bK. I. Assaf, W. M. Nau, *Chem. Soc. Rev.* **2015**, *44*, 394-418.
- [75] S. Mecozzi, J. Rebek, Julius, *Chem. Eur. J.* **1998**, *4*, 1016-1022.
- [76] W. M. Nau, M. Florea, K. I. Assaf, *Isr. J. Chem.* **2011**, *51*, 559-577.
- [77] aF. Biedermann, M. Vendruscolo, O. A. Scherman, A. De Simone, W. M. Nau, *J. Am. Chem. Soc.* **2013**, *135*, 14879-14888; bF. Biedermann, V. D. Uzunova, O. A. Scherman, W. M. Nau, A. De Simone, *J. Am. Chem. Soc.* **2012**, *134*, 15318-15323; cF. Biedermann, W. M. Nau, H. J. Schneider, *Angew. Chem. Int. Ed.* **2014**, *53*, 11158-11171.
- [78] S. J. C. Lee, J. W. Lee, H. H. Lee, J. Seo, D. H. Noh, Y. H. Ko, K. Kim, H. I. Kim, *The Journal of Physical Chemistry B* **2013**, *117*, 8855-8864.
- [79] aS. J. Barrow, S. Kasera, M. J. Rowland, J. Del Barrio, O. A. Scherman, *Chem. Rev.* **2015**, *115*, 12320-12406; bS. Sinn, F. Biedermann, *Isr. J. Chem.* **2018**, *58*, 357-412.
- [80] aS. Li, Y. Gao, Y. Ding, A. Xu, H. Tan, *Chin. Chem. Lett.* **2021**, *32*, 313-318; bM. Li, S. Kim, A. Lee, A. Shrinidhi, Y. H. Ko, H. G. Lim, H. H. Kim, K. B. Bae, K. M. Park, K. Kim, *ACS applied materials & interfaces* **2019**, *11*, 43920-43927; cY. H. Liu, Y. M. Zhang, H. J. Yu, Y. Liu, *Angew. Chem. Int. Ed.* **2021**, *60*, 3870-3880.
- [81] aJ. Liu, Y. Lan, Z. Yu, C. S. Tan, R. M. Parker, C. Abell, O. A. Scherman, *Acc. Chem. Res.* **2017**, *50*, 208-217; bR.-H. Gao, Y. Huang, K. Chen, Z. Tao, *Coord. Chem. Rev.* **2021**, *437*, 213741; cX. D. Zhang, K. Chen, W. Y. Sun, *Chem. Eur. J.* **2021**, *27*, 5107-5119.
- [82] M. Wiemann, P. Jonkheijm, *Isr. J. Chem.* **2018**, *58*, 314-325.
- [83] V. D. Uzunova, C. Cullinane, K. Brix, W. M. Nau, A. I. Day, *Org. Biomol. Chem.* **2010**, *8*, 2037-2042.
- [84] M. Li, A. Lee, K. L. Kim, J. Murray, A. Shrinidhi, G. Sung, K. M. Park, K. Kim, *Angew. Chem.* **2018**, *130*, 2142-2147.
- [85] L. Cao, G. Hettiarachchi, V. Briken, L. Isaacs, *Angew. Chem. Int. Ed.* **2013**, *52*, 12033-12037.
- [86] S. K. Samanta, J. Quigley, B. Vinciguerra, V. Briken, L. Isaacs, *J. Am. Chem. Soc.* **2017**, *139*, 9066-9074.
- [87] C. Sun, H. Zhang, S. Li, X. Zhang, Q. Cheng, Y. Ding, L.-H. Wang, R. Wang, *ACS applied materials & interfaces* **2018**, *10*, 25090-25098.
- [88] W. L. Mock, T. A. Irra, J. P. Wepsiec, M. Adhya, *The Journal of Organic Chemistry* **1989**, *54*, 5302-5308.
- [89] K. Reddy, T. d. S. Cavallini, G. J.-F. Demets, L. Silva, *New J. Chem.* **2014**, *38*, 2262-2264.

- [90] C. Yang, T. Mori, Y. Origane, Y. H. Ko, N. Selvapalam, K. Kim, Y. Inoue, *J. Am. Chem. Soc.* **2008**, *130*, 8574-8575.
- [91] aR.-C. Mutihac, A. A. Bunaciu, H.-J. Buschmann, L. Mutihac, *Journal of Inclusion Phenomena and Macrocyclic Chemistry* **2020**, *98*, 137-148; bR. Pinalli, A. Pedrini, E. Dalcanale, *Chem. Soc. Rev.* **2018**, *47*, 7006-7026; cM. A. Beatty, F. Hof, *Chem. Soc. Rev.* **2021**, *50*, 4812-4832.
- [92] H. Nie, Z. Wei, X.-L. Ni, Y. Liu, *Chem. Rev.* **2022**.
- [93] aS. L. Wiskur, H. Ait-Haddou, J. J. Lavigne, E. V. Anslyn, *Acc. Chem. Res.* **2001**, *34*, 963-972; bB. T. Nguyen, E. V. Anslyn, *Coord. Chem. Rev.* **2006**, *250*, 3118-3127; cA. C. Sedgwick, J. T. Brewster, T. Wu, X. Feng, S. D. Bull, X. Qian, J. L. Sessler, T. D. James, E. V. Anslyn, X. Sun, *Chem. Soc. Rev.* **2021**, *50*, 9-38; dH. H. Jo, C.-Y. Lin, E. V. Anslyn, *Acc. Chem. Res.* **2014**, *47*, 2212-2221.
- [94] M. Florea, W. M. Nau, *Angew. Chem.* **2011**, *123*, 9510-9514.
- [95] J. Vázquez, P. Remón, R. N. Dsouza, A. I. Lazar, J. F. Arteaga, W. M. Nau, U. Pischel, *Chem. Eur. J.* **2014**, *20*, 9897-9901.
- [96] H. D. Nguyen, D. T. Dang, J. L. Van Dongen, L. Brunsveld, *Angew. Chem.* **2010**, *122*, 907-910.
- [97] aS. Sinn, J. Krämer, F. Biedermann, *Chem. Commun.* **2020**, *56*, 6620-6623; bA. Prabodh, S. Sinn, L. Grimm, Z. Miskolczy, M. Megyesi, L. Biczók, S. Bräse, F. Biedermann, *Chem. Commun.* **2020**, *56*, 12327-12330.
- [98] aF. Biedermann, D. Hathazi, W. M. Nau, *Chem. Commun.* **2015**, *51*, 4977-4980; bY. Ling, W. Wang, A. E. Kaifer, *Chem. Commun.* **2007**, 610-612.
- [99] aH. Kessler, M. Gehrke, C. Griesinger, *Angew. Chem.* **1988**, *100*, 507-554; bS. Sun, R. Zhang, S. Andersson, J. Pan, D. Zou, B. Åkermark, L. Sun, *The Journal of Physical Chemistry B* **2007**, *111*, 13357-13363; cJ. Hu, Y. Cheng, Q. Wu, L. Zhao, T. Xu, *The Journal of Physical Chemistry B* **2009**, *113*, 10650-10659; dY. Cohen, L. Avram, L. Frish, *Angew. Chem. Int. Ed.* **2005**, *44*, 520-554.
- [100] aM. W. Freyer, E. A. Lewis, *Methods in cell biology* **2008**, *84*, 79-113; bA. Saboury, *Journal of the Iranian Chemical Society* **2006**, *3*, 1-21; cF. P. Schmidtchen, *Supramolecular chemistry: from molecules to nanomaterials* **2012**.
- [101] C. A. Schalley, *Analytical methods in supramolecular chemistry, Vol. 1*, John Wiley & Sons, **2012**.
- [102] D. Sigwalt, M. Sekutor, L. Cao, P. Y. Zavalij, J. Hostas, H. Ajani, P. Hobza, K. Mlinaric-Majerski, R. Glaser, L. Isaacs, *J. Am. Chem. Soc.* **2017**, *139*, 3249-3258.
- [103] J. R. Lakowicz, *Principles of fluorescence spectroscopy*, Springer, **2006**.
- [104] aD. F. Swinehart, *J. Chem. Educ.* **1962**, *39*, 333; bW. Mäntele, E. Deniz, *Vol. 173*, Elsevier, **2017**, pp. 965-968.
- [105] C. M. Marian, *Wiley Interdisciplinary Reviews: Computational Molecular Science* **2012**, *2*, 187-203.
- [106] S. Hotta, *Mathematical Physical Chemistry: Practical and Intuitive Methodology*, Springer Nature, **2020**.
- [107] L. You, D. Zha, E. V. Anslyn, *Chem. Rev.* **2015**, *115*, 7840-7892.
- [108] M. M. Pierce, C. Raman, B. T. Nall, *Methods* **1999**, *19*, 213-221.
- [109] W. B. Turnbull, A. H. Daranas, *J. Am. Chem. Soc.* **2003**, *125*, 14859-14866.
- [110] aK. Yan, M. Fujita, *Science* **2015**, *350*, 1165-1166; bH. Sunohara, K. Koyamada, H. Takezawa, M. Fujita, *Chem. Commun.* **2021**, *57*, 9300-9302.

- [111] B. Huang, L. Mao, X. Shi, H.-B. Yang, *Chem. Sci.* **2021**, *12*, 13648-13663.
- [112] C. Bravin, E. Badetti, F. A. Scaramuzzo, G. Licini, C. Zonta, *J. Am. Chem. Soc.* **2017**, *139*, 6456-6460.
- [113] aV. Martí-Centelles, R. L. Spicer, P. J. Lusby, *Chem. Sci.* **2020**, *11*, 3236-3240; bR. Küng, T. Pausch, D. Rasch, R. Göstl, B. M. Schmidt, *Angew. Chem. Int. Ed.* **2021**, *60*, 13626-13630.
- [114] aK. Cai, M. C. Lipke, Z. Liu, J. Nelson, T. Cheng, Y. Shi, C. Cheng, D. Shen, J.-M. Han, S. Vemuri, *Nature communications* **2018**, *9*, 1-8; bX.-Y. Chen, D. Shen, K. Cai, Y. Jiao, H. Wu, B. Song, L. Zhang, Y. Tan, Y. Wang, Y. Feng, *J. Am. Chem. Soc.* **2020**, *142*, 20152-20160.
- [115] aJ. Anhäuser, R. Puttreddy, L. Glanz, A. Schneider, M. Engeser, K. Rissanen, A. Lützen, *Chem. Eur. J.* **2019**, *25*, 12294-12297; bJ. Anhäuser, R. Puttreddy, Y. Lorenz, A. Schneider, M. Engeser, K. Rissanen, A. Lützen, *Organic Chemistry Frontiers* **2019**, *6*, 1226-1235; cG. Meyer-Eppler, F. Topić, G. Schnakenburg, K. Rissanen, A. Lützen, *Eur. J. Inorg. Chem.* **2014**, *2014*, 2495-2501.
- [116] D. R. Martir, L. Delforce, D. B. Cordes, A. M. Slawin, S. L. Warriner, D. Jacquemin, E. Zysman-Colman, *Inorganic Chemistry Frontiers* **2020**, *7*, 232-238.
- [117] H.-J. Schneider, P. Agrawal, A. K. Yatsimirsky, *Chem. Soc. Rev.* **2013**, *42*, 6777-6800.
- [118] aJ. Kornhuber, G. Quack, *Neuroscience letters* **1995**, *195*, 137-139; bN. Rifai, A. R. Horvath, C. T. Wittwer, J. Park, *Principles and applications of molecular diagnostics*, Elsevier, **2018**.
- [119] aJ. Murray, K. Kim, T. Ogoshi, W. Yao, B. C. Gibb, *Chem. Soc. Rev.* **2017**, *46*, 2479-2496; bD. Ma, P. Y. Zavalij, L. Isaacs, *The Journal of organic chemistry* **2010**, *75*, 4786-4795; cS. Liu, C. Ruspic, P. Mukhopadhyay, S. Chakrabarti, P. Y. Zavalij, L. Isaacs, *J. Am. Chem. Soc.* **2005**, *127*, 15959-15967.
- [120] C. J. Friedmann, S. Ay, S. Bräse, *The Journal of Organic Chemistry* **2010**, *75*, 4612-4614.
- [121] L. Bondarenko, I. Dix, H. Hinrichs, H. Hopf, *Synthesis* **2004**, *2004*, 2751-2759.
- [122] aC. Braun, E. Spuling, N. B. Heine, M. Cakici, M. Nieger, S. Bräse, *Adv. Synth. Catal.* **2016**, *358*, 1664-1670; bM. N. Mungalpara, P. G. Plieger, G. J. Rowlands, *Adv. Synth. Catal.* **2021**, *363*, 1069-1080; cC. Braun, M. Nieger, W. R. Thiel, S. Bräse, *Chem. Eur. J.* **2017**, *23*, 15474-15483.
- [123] E. Keszei, *ChemTexts* **2016**, *2*, 1-2.
- [124] L. M. Grimm, S. Spicher, B. Tkachenko, P. R. Schreiner, S. Grimme, F. Biedermann, *Chem. Eur. J.* **2022**, e202200529.
- [125] H. He, M. A. Mortellaro, M. J. Leiner, R. J. Fraatz, J. K. Tusa, *J. Am. Chem. Soc.* **2003**, *125*, 1468-1469.
- [126] aM. V. Rekharsky, T. Mori, C. Yang, Y. H. Ko, N. Selvapalam, H. Kim, D. Sobransingh, A. E. Kaifer, S. Liu, L. Isaacs, *Proc. Natl. Acad. Sci. U.S.A.* **2007**, *104*, 20737-20742; bM. Šekutor, K. Molčanov, L. Cao, L. Isaacs, R. Glaser, K. Mlinarić-Majerski, *Eur. J. Org. Chem.* **2014**, *2014*, 2533-2542.
- [127] aG. A. Hembury, V. V. Borovkov, Y. Inoue, *Chem. Rev.* **2008**, *108*, 1-73; bM. Liu, L. Zhang, T. Wang, *Chem. Rev.* **2015**, *115*, 7304-7397; cY. Li, C. Liu, X. Bai, F. Tian, G. Hu, J. Sun, *Angew. Chem. Int. Ed.* **2020**, *59*, 3486-3490.
- [128] aN. Berova, L. Di Bari, G. Pescitelli, *Chem. Soc. Rev.* **2007**, *36*, 914-931; bL. You, J. S. Berman, E. V. Anslyn, *Nature chemistry* **2011**, *3*, 943-948.
- [129] aL.-J. Chen, H.-B. Yang, M. Shionoya, *Chem. Soc. Rev.* **2017**, *46*, 2555-2576; bL.-L. Wang, Z. Chen, W.-E. Liu, H. Ke, S.-H. Wang, W. Jiang, *J. Am. Chem. Soc.* **2017**, *139*, 8436-8439.

- [130] S. He, F. Biedermann, N. Vankova, L. Zhechkov, T. Heine, R. E. Hoffman, A. De Simone, T. T. Duignan, W. M. Nau, *Nat. Chem.* **2018**, *10*, 1252-1257.
- [131] aS. Rösel, J. Becker, W. D. Allen, P. R. Schreiner, *J. Am. Chem. Soc.* **2018**, *140*, 14421-14432; bM. M. Quesada Moreno, P. Pinacho, C. Pérez, M. Šekutor, P. R. Schreiner, M. Schnell, *Chem. Eur. J.* **2020**, *26*, 10817-10825.
- [132] N. A. Fokina, B. A. Tkachenko, A. Merz, M. Serafin, J. E. P. Dahl, R. M. K. Carlson, A. A. Fokin, P. R. Schreiner, *Eur. J. Org. Chem.* **2007**, 4738-4745.
- [133] K. Yazaki, L. Catti, M. Yoshizawa, *Chem. Commun.* **2018**, *54*, 3195-3206.
- [134] B. König, B. Knieriem, A. D. Meijere, *Chem. Ber.* **1993**, *126*, 1643-1650.
- [135] D. Kurandina, M. Parasram, V. Gevorgyan, *Angew. Chem. Int. Ed.* **2017**, *56*, 14212-14216.
- [136] aB. König, S. Ramm, P. Bubenitschek, P. G. Jones, H. Hopf, B. Knieriem, A. D. Meijere, *Chem. Ber.* **1994**, *127*, 2263-2266; bH. F. Bettinger, R. Einholz, A. Göttler, M. Junge, M.-S. Sättele, A. Schnepf, C. Schrenk, S. Schundelmeier, B. Speiser, *Organic Chemistry Frontiers* **2017**, *4*, 853-860.
- [137] B. Qu, Y. Ma, Q. Ma, X. Liu, F. He, C. Song, *The Journal of Organic Chemistry* **2009**, *74*, 6867-6869.
- [138] K. P. Jayasundera, D. N. Kusmus, L. Deuilhé, L. Etheridge, Z. Farrow, D. J. Lun, G. Kaur, G. J. Rowlands, *Org. Biomol. Chem.* **2016**, *14*, 10848-10860.
- [139] aH. B. Cheng, S. Zhang, J. Qi, X. J. Liang, J. Yoon, *Adv. Mater.* **2021**, *33*, 2007290; bJ. del Barrio, P. N. Horton, D. Lairez, G. O. Lloyd, C. Toprakcioglu, O. A. Scherman, *J. Am. Chem. Soc.* **2013**, *135*, 11760-11763; cG. S. Hartley, *Nature* **1937**, *140*, 281-281.
- [140] aL. Zhu, H. Yan, X.-J. Wang, Y. Zhao, *The Journal of Organic Chemistry* **2012**, *77*, 10168-10175; bJ. Zhao, Y. M. Zhang, H. L. Sun, X. Y. Chang, Y. Liu, *Chem. Eur. J.* **2014**, *20*, 15108-15115; cJ. Wu, L. Isaacs, *Chem. Eur. J.* **2009**, *15*, 11675-11680.
- [141] E. Pazos, P. Novo, C. Peinador, A. E. Kaifer, M. D. García, *Angew. Chem. Int. Ed.* **2019**, *58*, 403-416.
- [142] aA. Walczak, G. Kurpik, A. R. Stefankiewicz, *International journal of molecular sciences* **2020**, *21*, 6171; bH. Xu, Y. Gou, J. Ye, Z.-l. Xu, Z. Wang, *J. Solid State Chem.* **2016**, *237*, 323-329.
- [143] X. Zhao, J. Zhou, S. Wang, L. Tan, M. Li, H. Li, C. Yi, *ACS Applied Energy Materials* **2021**, *4*, 6903-6911.
- [144] aD. M. Knoll, Karlsruhe Institut für Technologie (KIT) **2020**; bR. Bär, Karlsruhe Institut für Technologie (KIT) **2020**; cE. Spuling, Karlsruhe Institut für Technologie (KIT) **2019**; dC. Braun, Karlsruhe Institut für Technologie (KIT) **2017**.
- [145] F. Vögtle, P. Neumann, *Tetrahedron Lett.* **1969**, *60*, 5329-5334.
- [146] R. S. Cahn, C. Ingold, V. Prelog, *Angew. Chem. Int. Ed.* **1966**, *5*, 385-415.
- [147] C. Braun, S. Bräse, L. L. Schafer, *Eur. J. Org. Chem.* **2017**, *2017*, 1760-1764.
- [148] L. Cao, M. Šekutor, P. Y. Zavalij, K. Mlinarić-Majerski, R. Glaser, L. Isaacs, *Angew. Chem.* **2014**, *126*, 1006-1011.
- [149] P. Ferreira, B. Ventura, A. Barbieri, J. P. Da Silva, C. A. Laia, A. J. Parola, N. Basílio, *Chem. Eur. J.* **2019**, *25*, 3477-3482.
- [150] S. Moghaddam, C. Yang, M. Rekharsky, Y. H. Ko, K. Kim, Y. Inoue, M. K. Gilson, *J. Am. Chem. Soc.* **2011**, *133*, 3570-3581.

- [151] A. I. Lazar, F. Biedermann, K. R. Mustafina, K. I. Assaf, A. Hennig, W. M. Nau, *J. Am. Chem. Soc.* **2016**, *138*, 13022-13029.
- [152] M. A. Romero, J. A. González-Delgado, J. Mendoza, J. F. Arteaga, N. Basilio, U. Pischel, *Isr. J. Chem.* **2018**, *58*, 487-492.
- [153] M. A. Romero, N. Basílio, A. J. Moro, M. Domingues, J. A. González-Delgado, J. F. Arteaga, U. Pischel, *Chem. Eur. J.* **2017**, *23*, 13105-13111.
- [154] I. Neira, C. Peinador, M. D. García, *Org. Lett.* **2022**.
- [155] J. K. S. Sinn, F. Biedermann, *Chem. Commun* **2020**, *56*, 6620-6623.
- [156] D.-S. Guo, V. D. Uzunova, K. I. Assaf, A. I. Lazar, Y. Liu, W. M. Nau, *Supramol. Chem.* **2016**, *28*, 384-395.
- [157] G. A. Vincil, A. R. Urbach, *Supramol. Chem.* **2008**, *20*, 681-687.
- [158] Y. H. Ko, Y. Kim, H. Kim, K. Kim, *Chem. Asian. J.* **2011**, *6*, 652-657.
- [159] L. C. Smith, D. G. Leach, B. E. Blaylock, O. A. Ali, A. R. Urbach, *J. Am. Chem. Soc.* **2015**, *137*, 3663-3669.

8 Acknowledgments

The Nobel laureate D. J. Cram went from the earliest synthesis of [2.2]paracyclophane and then to winning the Nobel Prize for supramolecules, while my journey, firstly to supramolecules and afterwards to the synthesis of [2.2]paracyclophane, to the present, feels like exploring the mysteries of supramolecules and [2.2]paracyclophane in the footsteps of the D. J. Cram.

And all this is thanks to my PhD supervisors, Prof. Dr. Stefan Bräse and Dr. Frank Biedermann. They were the ones who accepted me as a PhD student and were able to carry out my research on my topic under the laboratory conditions they provided. Stefan often supervises my projects in synthesis and provides me with all kinds of help and advice at IOC. I have great admiration for Stefan because he is always hard working and a more kind person. There is a Chinese idiom that says, "Once a teacher, always a father", and to me Stefan is more like a father than a mentor. I feel warm and welcomed in this place at KIT where I am far from my family. Frank, on the other hand, is more like a brother than a tutor, and can give students patient guidance and detailed explanations. I have only been in his lab for two months at INT, but I have felt that he is humored and meticulous in his work. So many thanks to him for guidance on the Host-Guest Systems project and I always believed in and admired his insights in research. There is another I would like to thank, Dr. Zahid Hassan, for his assistance with my experiments during my four years in the group as subgroup leader. Zahid has been very supportive and encouraging in my project and in my life, and he has also helped me to complete this thesis.

I would like to thank Dr. Zhen Zhang specially for all his help with my life and work when I first came to the lab, and for giving me guidance and encouragement when I was overwhelmed. I feel very fortunate that they were so generous in helping me when I needed help, include colleagues Dr. Eduard Spuling, Dr. Christoph Zippel, Nicolai Rosenbaum, Johannes Karcher, Susanne Kirchner, who have since left, and Xuemin Gan, Xujun Qu, Yuting Li, Dr. Salma Begum, Dr. Mareen Stahlberger, Lisa Schmidt, Lukas Langer, Jens Hohmann who are still helping hands for me. They have helped me a lot with daily laboratory equipment and chemicals *etc.* A huge thanks to Dr. Nicole Jung, Dr. Christin Bednarek, Christinane Lampert, and Janine Bolz, who manage the whole group keep running.

I am also grateful to my colleagues in the Biedermann's group at INT, Dr. Changming Hu, Dr. Rui Kang, Dr. Amrutha Prabodh, Dr. Laura Grimm, and Joana Krämer, and additional Sebastian Spicher, who provided much guidance and assistance during my experiments. Their help was essential to the completion of my thesis.

In addition, I want to acknowledge the impeccable work of Dr. Olaf Fuhr for crystal structure analyses at KIT, Dr. Martin Nieger for crystal structure analyses at the University of Helsinki, Dr. Andreas Rapp and Tanja Ohmer-Scherrerr for NMR spectroscopy, Dr. Norbert Foitzik, Lara Hirsch, Angelika Mösle and Karolin Kohnle for mass spectrometry and IR. All of them helped very kindly by analyzing all compound and without whom my results and thesis would not have been possible.

In addition, I would like to thank my colleagues, Dr. Patrick Hodapp, Dr. Christoph Schissler, Dr. Robin Bär, Dr. Stephan Münch, Dr. Yuling Hu, Sarah Al Muthafer, Hannes Kühner, Anna-Lena, Simon Oßwald, Steffen Otterbach, Henrik Tappert, Jasmin Seibert, Céline Leonhardt, who have provided me with other assistance in the laboratory. And my friends, Dr. Junbo Wang, Dr. Minting Hao, Dr. Ziwei Pang, Dr. Yemao Lu, Dr. Zengwen Li, Dr. Chunting Zhong, Si Chen, Tingting Ruan, who have helped me in life.

Finally, I would like to thank the China Scholarship Council (CSC) for providing me with this opportunity to study for a PhD, which has allowed me to see more and meet more people and learn more about the world and life, “It is better to travel ten thousand miles than to read ten thousand books.” In particular, I would like to thank my parents and relatives for their concern and care for me far from thousands of miles away. Special thanks to my fiancée Leilei Zhao, whose relentless support and love have given me more courage and confidence over the past four years. went through the two years of inseparable laughter together at the Masters and the four years spent on the other side of the world, we are growing and facing hardships and believing that we can embrace a wonderful future together.